

**THE BEHAVIOUR OF ULTRA-HIGH-PERFORMANCE CONCRETE IN  
PRECAST CONCRETE BRIDGE DECK CONNECTIONS**

by

Heather Lindsay Stefaniuk

A Thesis submitted to the Faculty of Graduate Studies of  
The University of Manitoba  
in partial fulfillment of the requirements of the degree of

MASTER OF SCIENCE

Department of Civil Engineering  
University of Manitoba  
Winnipeg, Manitoba



## Abstract

This thesis studies the behaviour of ultra-high-performance concrete (UHPC) in the precast concrete bridge deck connections. The experimental program consisted of shear pocket push-out testing and full-scale bridge deck testing. The main objective was to study the UHPC performance in the shear pocket and joint connections. All specimens were statically loaded until failure.

The push-out test specimens consisted of two small 45 MPa concrete slabs on either side of a built-up steel section, joined together by shear studs and UHPC shear pockets. There were three 6-stud specimens, two 3-stud specimens and two 0-stud specimens. The 6-stud specimens reached ultimate loads of 2642 kN, 2892 kN, and 3045 kN. The 3-stud specimens reached ultimate loads of 1445 kN and 1674 kN. The 0-stud specimens reached ultimate loads of 4.91 kN and 3.44 kN. The failure modes for the 6-stud and 3-stud specimens were stud failure or concrete crushing, while the 0-stud specimens failed when the UHPC and steel section surface debonded. The push-out specimens were instrumented with LVDTs, pi-gauges and strain gauges to collect data on the displacements, debonding, and shear stud strains throughout testing.

The bridge deck testing included a full panel deck (FPD) and jointed panel deck (JPD). The FPD was cast monolithically with regular strength concrete and had UHPC shear pocket connections to the steel support girders. The JPD was cast as two half-size regular strength panels connected together with a UHPC joint, and connected to the steel support girders with UHPC shear pockets. The FPD and JPD reached ultimate loads of 1926 kN and 1878 kN, respectively. Both decks failed by concrete punching under the load point. The bridge decks were instrumented with LVDTs, pi-gauges, and strain gauges to collect data on the deflections, crack widths, steel strains, concrete strains, and shear stud strains throughout testing.

The experimental results implied the number and length of the studs in the shear pockets may be reduced. The better performance of the FPD also indicated the circular pockets were superior and the use of UHPC in precast deck connections does not significantly improve the overall performance.



## **Acknowledgements**

I would like to thank my advisor Dr. Dagmar Svecova for her immense support and assistance over the course of this graduate degree and thesis project.

I would like to acknowledge and thank the following individuals and groups for their guidance: Dr. Ali Semendary, Dr. Dimos Polyzois, Dr. Hugues Vogel and my advisory committee consisting of Dr. Aftab Mufti, Dr. Baidar Bakht and Dr. Emile Shehata.

Thank you to Dr. Chad Klowak and the technical staff at the University of Manitoba W.R. McQuade Structural Laboratory for your immense contributions and assistance in executing the experimental program.

I would also like to recognize and thank the following firms, Manitoba Infrastructure for the research project and financial support; LafargeHolcim Ltd. for casting the precast bridge deck panels, supplying the Ductal UHPC and reinforcing steel bars; and Falcon Machinery Ltd. for the shear stud welding.

---



---

# Table of Contents

---



---

<b>Chapter 1 Introduction</b>	<b>1</b>
1.1 Background .....	1
1.2 Project Background.....	2
1.3 Research Objectives.....	2
1.4 Project Scope .....	3
<b>Chapter 2 Literature Review</b>	<b>4</b>
2.1 Introduction.....	4
2.2 Shear Pockets .....	4
2.2.1 Test Methods.....	5
2.2.2 Joints .....	8
2.2.3 Test Methods.....	9
2.3 Precast Concrete Bridges .....	12
<b>Chapter 3 Research Program</b>	<b>16</b>
3.1 Introduction.....	16
3.2 Material Testing .....	17
3.2.1 Concrete Testing .....	17
3.2.2 Shear Stud Testing .....	19
3.3 Shear Pocket Experiments .....	21
3.3.1 Naming Convention .....	21
3.3.2 Slab and Shear Pocket Details .....	22
3.3.3 Test Method and Setup .....	30
3.3.3.1 Load Apparatus and Test Details.....	30
3.3.3.2 Instrumentation Details and Layout.....	31
3.4 Bridge Deck Experiments .....	34
3.4.1 Naming Convention.....	34
3.4.2 Material Testing .....	34
3.4.3 Pre-Cast Deck Panel Details .....	35
3.4.4 Connection Details.....	39

3.4.4.1 Haunches .....	41
3.4.4.2 Shear Pockets .....	42
3.4.4.3 Deck Joint .....	46
3.4.5 Test Method and Setup .....	48
3.4.5.1 Load Apparatus Details .....	48
3.4.5.2 Instrumentation Details and Layout.....	49
<b>Chapter 4 Experimental Results and Analysis</b>	<b>57</b>
4.1 Introduction.....	57
4.2 Material Testing .....	57
4.2.1 Shear Pocket Concrete .....	57
4.2.2 Bridge Deck Concrete.....	58
4.2.3 Steel Shear Studs.....	64
4.3 Shear Pocket Specimens .....	68
4.3.1 Experimental Failure Modes .....	69
4.3.2 Displacement and Debonding Behaviours.....	71
4.3.3 Shear Stud Performance.....	89
4.4 Bridge Decks.....	101
4.4.1 PUNCH Program Analysis .....	101
4.4.2 Experimental Failure Modes.....	102
4.4.3 Cracking Patterns .....	103
4.4.4 Load Deflection Behaviours .....	119
4.4.5 Joint Performance .....	129
4.4.6 Shear Stud Performance.....	138
<b>Chapter 5 Conclusions</b>	<b>145</b>
5.1 Shear Pocket Specimens .....	145
5.2 Bridge Decks.....	146
5.3 Future Research .....	148
<b>References</b>	<b>149</b>
<b>Appendix A: Shop Drawings</b>	<b>150</b>
<b>Appendix B: PUNCH Program Analysis</b>	<b>154</b>

---

## List of Tables

---

Table 3.1 Research program specimen details.....	17
Table 3.2 Shear Pocket Concrete Cast Details.....	28
Table 3.3 Bridge Deck Concrete Cast Details .....	34
Table 4.1 RC Slab Strengths.....	57
Table 4.2 UHPC Shear Pocket Compressive Strengths on Test Day .....	58
Table 4.3 Regular Concrete Compression Cylinder Testing .....	59
Table 4.4 UHPC Deck Connection Compressive Strength Test Results.....	60
Table 4.5 UHPC Deck Connection Tensile Strength Test Results.....	62
Table 4.6 Shear Stud Shear Strength Test Results.....	64
Table 4.7 Shear Stud Tensile Strength Test Results .....	66
Table 4.8 Push-Out Test Failure Modes .....	70
Table 4.9 SP6-1 LVDT Results .....	73
Table 4.10 SP6-2 LVDT Results .....	73
Table 4.11 SP6-3 LVDT Results .....	73
Table 4.12 SP3-1 LVDT Results .....	77
Table 4.13 SP3-2 LVDT Results .....	78
Table 4.14 SP6 and SP3 Result Comparison.....	80
Table 4.15 SP6-1 Pi-Gauge Results.....	82
Table 4.16 SP6-2 Pi-Gauge Results.....	82
Table 4.17 SP6-3 Pi-Gauge Results.....	83
Table 4.18 SP3-1 Pi-Gauge Results.....	85
Table 4.19 SP3-2 Pi-Gauge Results.....	85
Table 4.20 SP6-1A Strain Gauge Results .....	90
Table 4.21 SP6-1B Strain Gauge Results .....	91
Table 4.22 SP6-2A Strain Gauge Results .....	92
Table 4.23 SP6-2B Strain Gauge Results .....	92
Table 4.24 SP6-3A Strain Gauge Results .....	93
Table 4.25 SP6-3B Strain Gauge Results .....	94

---

Table 4.26 SP3-1A Strain Gauge Results .....	97
Table 4.27 SP3-1B Strain Gauge Results .....	97
Table 4.28 SP3-2A Strain Gauge Results .....	98
Table 4.29 SP3-2B Strain Gauge Results .....	98
Table 4.30 Push-Out Test Results Summary .....	101
Table 4.31 Pi-gauge measurements for FPD and JPD during testing.....	116
Table 4.32 FPD Centerline Longitudinal Deflection Results .....	123
Table 4.33 JPD Centerline Longitudinal Deflection Results.....	124
Table 4.34 FPD Transverse Deflection Results.....	124
Table 4.35 JPD Transverse Deflection Results.....	125
Table 4.36 FPD and JPD Concrete Strain Gauge Results .....	130
Table 4.37 FPD Internal Strain Gauge Results .....	131
Table 4.38 JPD South Panel Internal Strain Gauge Results .....	132
Table 4.39 JPD North Panel Internal Strain Gauge Results .....	133
Table 4.40 FPD Shear Stud Strain Results for Shear Pockets P1 and P3.....	141
Table 4.41 FPD Shear Stud Strain Results for Shear Pockets P2 and P4.....	142
Table B.1 Initial PUNCH Analysis (1/2).....	154
Table B.2 Initial PUNCH Analysis (2/2).....	155
Table B.3 Final PUNCH Analysis (1/2) .....	156
Table B.4 Final PUNCH Analysis (2/2) .....	157

## List of Figures

---

Figure 2.1 Typical push-off test specimens. ....	5
Figure 2.2 Typical push-out test specimens.....	7
Figure 2.3 Typical Joint Shapes.....	9
Figure 2.4 Typical Push-Off Joint Specimens .....	10
Figure 3.1 (a) Test Mark Industries CM-3000-DIR test machine; (b) Compression cylinder test setup; (c) Splitting tension cylinder test setup. ....	18
Figure 3.2 Shear stud shear test setup: (a) side view, and (b) isometric view.....	19
Figure 3.3 Shear stud test equipment: (a) side view, (b) end view, and (c) during testing.....	20
Figure 3.4 Shear stud direct tension test setup: (a) side view, and (b) instrumented stud.....	21
Figure 3.5 Push-out shear pocket test setup.....	22
Figure 3.6 Shear pocket slab dimensions and reinforcement. ....	23
Figure 3.7 Shear pocket dimensions. ....	23
Figure 3.8 Shear pockets with 6-stud groupings (SP6).....	24
Figure 3.9 Shear pockets with 3-stud groupings (SP3).....	25
Figure 3.10 (a) Shear pocket blockout, (b) Threaded lifting loop concrete insert, (c) Shear pocket slab formwork with reinforcement and blockout placed. ....	26
Figure 3.11 Smooth finished shear pocket slabs.....	26
Figure 3.12 Push-out test specimen UHPC shear pocket casting: (a) slab placement; (b) UHPC cast formwork; and (c) UHPC haunch post-casting.....	27
Figure 3.13 Built-up steel support beam for push-out test specimens.....	29
Figure 3.14 (a) Push-out test setup and MTS machine; (b) push-out test; (c) side view of test setup. ....	31
Figure 3.15 Shear stud strain instrumentation. ....	32
Figure 3.16 Strain gauge application. ....	32
Figure 3.17 Push-out test instrumentation. ....	33
Figure 3.18 Push-out test instrumentation: (a) LVDTs, (b) LVDTs and pi-gauge.....	33
Figure 3.19 JPD half panel formwork, shear pocket blockouts and reinforcement.....	35
Figure 3.20 JPD half panel concrete casting and vibrating. ....	36
Figure 3.21 Finished JPD half panel.....	36

---

Figure 3.22 Bridge deck and support girder setup. ....	37
Figure 3.23 End diaphragm details. ....	38
Figure 3.24 Girder details. ....	39
Figure 3.25 UHPC casting of JPD. ....	40
Figure 3.26 Deck joint formwork. ....	40
Figure 3.27 Precast deck placement for 50 mm haunch. ....	41
Figure 3.28 The bridge deck haunch construction: (a) EVA foam installation; (b) placing FPD. ....	41
Figure 3.29 Bridge deck JPD shear pocket layout. ....	42
Figure 3.30 Bridge deck JPD shear pocket layout. ....	43
Figure 3.31 FPD shear pocket layout. ....	44
Figure 3.32 JPD shear pocket layout. ....	45
Figure 3.33 JPD transverse deck joint dimensions and reinforcement details. ....	46
Figure 3.34 JPD transverse deck joint details showing only the 10M hooked rebar of the joint. ....	47
Figure 3.35 JPD transverse deck joint. ....	47
Figure 3.36 Load plate location. ....	48
Figure 3.37 Load setup for deck testing: (a) overall test setup, (b) close-up of load cell and load plate. ....	49
Figure 3.38 LVDT setup for JPD and FPD. ....	50
Figure 3.39 Pi-gauge locations for JPD and FPD. ....	51
Figure 3.40 Concrete strain gauge locations. ....	52
Figure 3.41 (a) CSG 1 and LVDT 4, (b) CSG 3 and LVDT 7. ....	52
Figure 3.42 JPD internal rebar strain gauge instrumentation. ....	53
Figure 3.43 FPD internal rebar strain gauge instrumentation. ....	54
Figure 3.44 FPD shear stud strain gauge locations. ....	56
Figure 4.1 Bridge deck RC compressive strength development. ....	59
Figure 4.2 Bridge deck connection UHPC compressive strength development. ....	61
Figure 4.3 Bridge deck connection UHPC tensile strength development. ....	62
Figure 4.4 Compression cylinders after testing: (a) and (b) are RC, and (c) to (e) are UHPC. ....	63
Figure 4.5 Shear stud shear tests displacement development. ....	64
Figure 4.6 Shear stud shear failure. ....	65
Figure 4.7 Elongation of the shear studs during direct tension testing. ....	66

Figure 4.8 Shear stud tension failure. ....	67
Figure 4.9 Stress-strain curves for shear stud TS2: (a) full data set; (b) 0.2% offset method for shear stud yield strength and modulus of elasticity. ....	67
Figure 4.10 SP6-2A stud shearing failure: (a) UHPC haunch with studs still inside, and (b) close-up on bottom left shear stud base.....	70
Figure 4.11 SP6-3A concrete crushing failure.....	71
Figure 4.12 SP6-1 vertical displacement development.....	75
Figure 4.13 SP6-2 vertical displacement development.....	76
Figure 4.14 SP6-3 vertical displacement development.....	76
Figure 4.15 SP3-1 vertical displacement development.....	79
Figure 4.16 P3-2 vertical displacement development.....	79
Figure 4.17 Shear pocket specimen rotation.....	81
Figure 4.18 UHPC and steel debonding for specimens (a) SP6-1, (b) SP6-2, and (c) SP6-3. ....	84
Figure 4.19 UHPC and steel debonding for specimens (a) SP3-1, and (b) SP3-2.....	86
Figure 4.20 Pi-gauge profiles at 60% of the ultimate load for all SP6 and SP3 specimens. ....	87
Figure 4.21 Pi-gauge profiles at the ultimate load for all SP6 and SP3 specimens.....	87
Figure 4.22 SP6-1 shear stud strain development for (a) specimen A, and (b) specimen B. ....	91
Figure 4.23 SP6-2 shear stud strain development for (a) specimen A, and (b) specimen B. ....	95
Figure 4.24 SP6-3 shear stud strain development for (a) specimen A, and (b) specimen B. ....	96
Figure 4.25 SP3-1 shear stud strain development for (a) specimen A, and (b) specimen B. ....	99
Figure 4.26 SP3-2 shear stud strain development for (a) specimen A, and (b) specimen B. ....	99
Figure 4.27 Failure crack along longitudinal centerline for FPD and JPD.....	103
Figure 4.28 Crack development at 200 kN and 400 kN during bridge deck testing.....	105
Figure 4.29 Crack development at 600 kN and 800 kN during bridge deck testing.....	106
Figure 4.30 Crack development at 1000 kN and 1200 kN during bridge deck testing.....	107
Figure 4.31 Crack development at 1400 kN during bridge deck testing and post-failure cracking. .....	108
Figure 4.32 Post-failure load plate punch shape in bridge deck surface: (a) JPD with load plate; (b) FPD after load plate removed. ....	109
Figure 4.33 FPD failure crack after chiselling away loose pieces of concrete (north half of deck). .....	110

Figure 4.34 JPD failure crack after chiselling away loose pieces of concrete (south panel).....	110
Figure 4.35 JPD demolition setup with concrete water saw.....	111
Figure 4.36 FPD cut section around load plate: (a) northern face adjacent to load plate edge (looking south), and (b) opposite face of section (looking north). .....	112
Figure 4.37 FPD deck section of south half (looking south). .....	112
Figure 4.38 JPD cut section around load plate: (a) southern joint-panel interface adjacent to load plate edge (looking south), and (b) opposite face of section south side of load plate (looking north). .....	113
Figure 4.39 JPD deck section of north panel, cut through UHP joint (opposite cut of Figure 4.38(a), looking north).....	113
Figure 4.40 South corners of the north JPD section from Figure 4.39: (a) south-west corner, and (b) south-east corner. ....	114
Figure 4.41 Close-up photographs at the deck center post-testing of (a) FPD, and (b) JPD.....	117
Figure 4.42 Crack width development during bridge deck testing.....	118
Figure 4.43 FPD longitudinal centerline deflection development during testing. ....	120
Figure 4.44 FPD transverse deflection development during testing.....	120
Figure 4.45 JPD longitudinal centerline deflection development during testing.....	121
Figure 4.46 JPD transverse deflection development during testing. ....	121
Figure 4.47 FPD centerline longitudinal deflection profiles during testing. ....	127
Figure 4.48 JPD centerline longitudinal deflection profiles during testing.....	128
Figure 4.49 Concrete strain development during bridge deck testing. ....	130
Figure 4.50 FPD internal reinforcing bar strains at deck center. ....	133
Figure 4.51 JPD strain development of 10M hooked bars on (a) bottom of west bars, (b) bottom of east bars, (c) bottom of center bars, and (d) top of center bars. ....	134
Figure 4.52 JPD strain profiles for the center top internal strain gauges.....	136
Figure 4.53 JPD strain profiles for the center bottom internal strain gauges. ....	136
Figure 4.54 JPD strain profiles for easternmost and westernmost internal strain gauges. ....	137
Figure 4.55 Expected shear stud behaviour and deck deflection.....	138
Figure 4.56 FPD shear stud strain development during testing for shear pockets (a) P1, (b) P3, (c) P2, and (d) P4.....	139
Figure 4.57 Arching action and load resistance.....	140

---

Figure 4.58 FPD 1400 kN cracking and shear stud behaviour. ....	141
Figure 4.59 FPD P1 shear stud strain development versus the SP3-2 shear strain development. .....	143

## Abbreviations and Acronyms

---

---

AASHTO	American Association of State Highway Transportation Officials
ABC	Accelerated Bridge Construction
ASTM	American Society for Testing and Materials
c/c	Center-to-center
CHBDC	Canadian Highway Bridge Design Code
CIP	Cast-in-place
DAQ	Data acquisition system
EVA	Ethyl-vinyl Acetate
FPD	Full Panel Deck
h:d	height-to-diameter ratio
HPC	High-Performance Concrete
JPD	Joint Panel Deck
LVDT	Linear Variable Displacement Transducer
MI	Manitoba Infrastructure
o/c	On center
RC	Regular strength Portland cement concrete
Rebar	Reinforcing steel bars
SG	Strain Gauge
SP	Shear Pocket / Shear Key
TYP	Typical
UHPC	Ultra High-Performance Concrete

---

# Chapter 1 Introduction

---

## 1.1 Background

Today, technological innovation and advancement are anything but *novel* practice in our ever demanding and progressive world. There is an expectation that we continually challenge the status quo.

The exponential growth of some technologies is surpassing Moore's Law, which indicates we can expect the pace of technological advancements (processor speed and power) of computers to double every two-years. That timeline has been challenged and is now assessed as doubling every 18 months.

As we ride this continuum, with the goal of exponential technological growth, engineers are critical to this pursuit and are called upon to be pro-active, innovative and responsive to the increased demand to create better materials, faster methods, and more efficient solutions with consideration of financial constraints.

This research program was conceived with the understanding and need to identify solutions to impact the performance of using pre-cast bridge deck connections with ultra-high-performance concrete, a material that is becoming widely used, but still somewhat uncharted to its greatest potential and application. Bridge construction is an area of constant research and engineering advancement. Projects concerning main artery roads, highways and bridges typically require rapid construction and minimal road closure to prevent rerouting traffic and straining other major thoroughfares.

It is becoming increasingly common for projects to use prefabricated bridge deck components in order to accelerate the on-site construction work; known as Accelerated Bridge Construction

(ABC). ABC allows for the concrete casting to be completed in concrete plants, where there are fewer conditional variants, fewer safety concerns, and less disruption to traffic.

Prefabricating concrete panels brings a new set of challenges to bridge design because the bridge deck is no longer a homogenous cast-in-place slab, but individual precast panels that must now be connected to each other and to the support girders. The main design focus of precast bridge deck slab connections is to create monolithic behaviour along the full bridge deck.

## 1.2 Project Background

The consulting engineering firm Stantec Consulting was awarded the design of a bridge in Eden Lake, Manitoba for the Manitoba Infrastructure project in 2016. The precast bridge decks were designed to have UHPC deck joints and shear pocket connections cast on-site. Manitoba Infrastructure requested comparative testing of precast bridge decks with UHPC connected precast bridge decks to a control specimen without a UHPC joint. The control specimen simulates a cast-in-place bridge deck, comparing typical bridge construction performance to prefabricated ABC methods.

The bridge decks cast for this research have the same design and reinforcement layouts as the Eden Lake bridge. This design also governs the dimensions of the small-scale experiments also conducted in the research.

## 1.3 Research Objectives

This research aims to analyze the behaviour of composite bridge decks with precast concrete panels and UHPC connections. The experiments were conducted to study the performance and load transfer between regular strength precast concrete slabs through a UHPC joint, and the impact of varying numbers of shear studs in UHPC shear pockets.

## 1.4 Project Scope

The scope of this research includes material testing, small-scale shear pocket specimens, and the full-size bridge deck testing. The push-out test method was used to test shear pockets, allowing for two specimens to be tested at one time. Fourteen shear pocket specimens were tested; 6 specimens contained groupings of 6 shear studs, 4 specimens contained groupings of 3 shear studs, and 4 specimens contained zero shear studs. The full-sized bridge deck testing involved two static punching tests to failure.

Material testing was completed on concrete compression and tension cylinders, steel reinforcing bars, and shear studs. Each material test had 3 specimens tested to ensure statistic reliability. The concrete testing was completed to ensure compressive and tensile strength developed appropriately for the scheduled experimental tests. The steel rebar and studs were tested to confirm material's strength.

---

## Chapter 2 Literature Review

---

### 2.1 Introduction

The following chapter summarizes recent research in the bridge deck field with a focus on precast concrete bridges and their connections. Since the focus of this research project is precast concrete bridge deck connections and composite concrete and steel bridge deck systems, a literature review was conducted in the areas of composite precast concrete bridge deck systems, the panel-to-panel joints, and the shear connections to the supporting girders.

### 2.2 Shear Pockets

When a composite bridge deck system is constructed, there are specific connections required to ensure the loads transfer properly through the deck slabs down to the supporting girders. Concrete bridge decks are commonly cast separately from the supporting girders due to constructability reasons, such as the span length and what the bridge spans (roads, body of water, valley, etc.). The connection between the concrete bridge deck and its supporting girders, whether concrete or steel, is called a shear key connection. For precast concrete bridge decks this connection is also referred to as a shear pocket since the concrete deck is cast with blockouts (hence the term pocket) to allow the connection to the support girder to be cast on site. The connection to the support girders is designed to resist any lateral loading the bridge may be subjected to from vibrations or wind that causes shearing forces to the connection.

In research shear pockets are tested in small-scale experiments and as part of bridge deck systems. There have been different methods developed to test the connection in pure shear loading and combined loading. There are advantages to both because within a bridge system the governing

forces will likely never be from shear loading, however optimizing the shear performance of the connection is invaluable to ensuring its long-term durability.

### 2.2.1 Test Methods

There are two common small-scale methods to test concrete shear pockets: push-off and push-out experiments. A third method is pull-out specimens; however, these will not be discussed in this research. The push-off tests can be used to test shear connections between concrete shear pockets and either a steel or concrete supporting member. Figure 2.1 shows two simplified sketches of typical test setups for the push-off experiments. Please note there would be reinforcement in the concrete specimens, however for simplicity it is not shown in any of the figures in this chapter. The figures also do not show any of the loading, stabilizing or levelling mechanisms that these tests require.

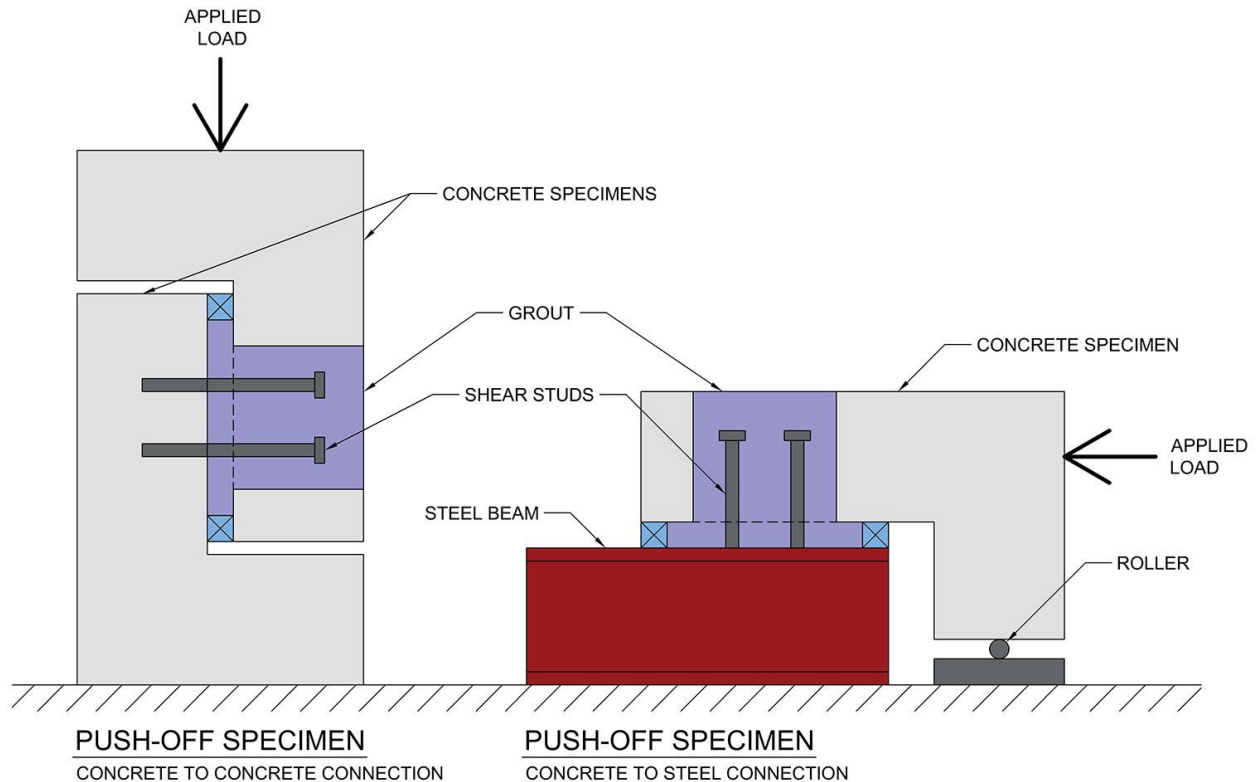


Figure 2.1 Typical push-off test specimens.

The “L” shaped concrete specimens are cast with blockouts for the shear pocket connection. For concrete-to-concrete connections, another “L” shape is cast with the shear studs embedded, whereas with the concrete-to-steel connection, the shear studs are welded onto the flange of the steel beam. The assembly may be tested in the vertical position, as shown, or horizontally in a similar manner to the concrete-to-steel connection. The applied loads cause shearing forces on the grouted shear stud connection. The objective is to observe if the connection fails through stud shearing from its support structure, or if the failure will be due to concrete crushing.

Two typical push-out test setups are shown in Figure 2.2. Small concrete slabs with shear pocket blockouts are cast, and then mounted vertically and cast against the steel section around the shear stud groupings. The shear studs are welded to the flange of the steel section. This type of test utilizes two connections within the same setup, which has the benefits and setbacks in comparison to the push-off tests. This setup allows double the amount of connections to be tested, however care must be taken to minimize the construction discrepancies between sides to ensure the loading is as equal as possible on each connection. As seen in Figure 2.2, the column may either be 90° vertical or slightly angled. The vertical specimens are only subjected to shear forces, similar to the push-off tests. The angled specimens subject the shear pocket connection to shear and tension forces. The angled push-out method is less common since it is more difficult to construct. The steel section must be custom made and the flange angles must be equal. The requirements for all the angled pieces create greater risk of discrepancies between concrete specimens and the accuracy of the stud angles; the studs would still be welded at 90° to the flange, which would be challenging if they are welded after the support section is fabricated.

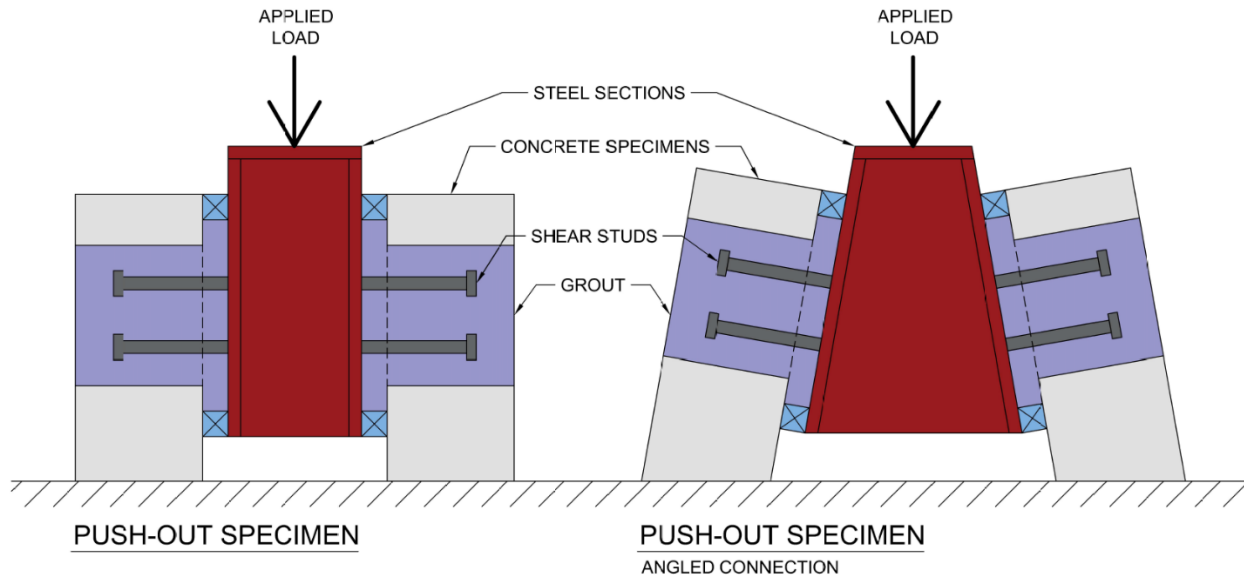


Figure 2.2 Typical push-out test specimens.

Kim et al. (2013) tested push-out specimens of varying concrete slab thicknesses and stud lengths to analyze the experimental strength and durability requirements with a shear pocket of 180 MPa UHPC [1]. The capacities seen in the results were adequate, with values greater than those seen through code equations of AASHTO 2010 and the Eurocode-4. Their results suggested that the greater the height-to-diameter ( $h:d$ ) ratios of the studs and the greater the stud's concrete cover, the greater durability. The ductility the longer studs afforded the specimens resulted in less cracking compared to the specimens with lower  $h:d$  and decreased concrete cover to the studs. This concept is understood in reinforced concrete design, as the use of fewer steel reinforcing bars at smaller spacing leads to less cracking than larger reinforcing bars with greater spacing.

The arrangement of the shear studs also has an effect on the strength and durability performance of the shear connection. Spremic et al. (2013) conducted push-out testing to investigate the behaviour of five different 4-stud layouts and the effects of reducing the stud spacing below the allowed minimum of five times the stud diameter ( $5d$ ) in the direction of loading [2]. The shear studs had a diameter of 16 mm, which would require a spacing of 80 mm in the load direction.

The shear pocket fill material was regular strength grout concrete with compressive strengths of 32 MPa or 40 MPa. The stud groupings tested were a rectangle, straight line parallel to the load direction, straight line perpendicular to the load direction, a horizontal diamond shape, and square with spacing less than 5d parallel to the load direction. The specimens with studs in a straight line had the lowest average shear resistance with 340 kN for the 32 MPa concrete specimens and 369 kN for the 40 MPa concrete specimens. This stud layout also caused significant bending of the studs with increasing severity of bending along the line of studs due to the distance from the load point. The rectangular stud groupings, perpendicular stud line and horizontal diamond stud groupings resulted in similar shear resistances around approximately 375 kN with concrete specimens of 40 MPa. The specimens with the square stud layouts had stud spacing of 45 mm, nearly half the minimum 5d and the shear pocket fill was 32 MPa. These specimens performed the best with average shear strengths of 376 kN and 384 kN for specimens without additional shear pocket reinforcement, and those with rebar across the pocket.

### **2.2.2 Joints**

With precast concrete decks, it is essential there is a strong connection between the panels to achieve composite behaviour. The panel-to-panel joints are different than expansion and control joints, because these are sealed joints that transfer load between panels. A major design component is reducing the cracking and debonding around the joint to lessen road runoff ingress that will corrode the steel reinforcement.

There are many different joint designs currently used, from the joint shape to the reinforcement. The most common joint shapes are female-female joints, female-male joints, and joints with a wide opening at the top of the deck that tapers to a narrow opening at the bottom face [Figure 2.3]. The joint reinforcement has wide variability in its design. The precast panels often have reinforcement

protruding out of the panels to be cast within the joint, and the rebar may be straight, hooked or a complete “U” back into the panel. Joints typically contain transverse reinforcement that is tied to the longitudinal rebar once the panels are placed. It is also common to use post-tensioning across the bridge deck joint to reduce cracking. Figure 2.3 includes some examples of the joint reinforcement: the wide opening joint includes hooked rebar and transverse bars; the female-female joint includes “U” shaped rebar with transverse bars; and the female-male joint shows only straight spliced bars and no transverse bars. The wide opening style of joint is commonly plugged with ethylene-vinyl acetate (EVA) foam to close the joint to avoid additional formwork requirements on site.

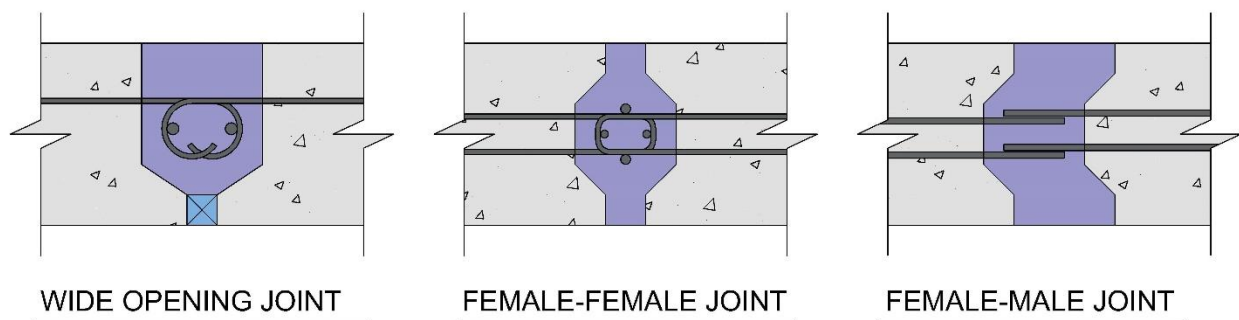


Figure 2.3 Typical Joint Shapes

### 2.2.3 Test Methods

Similar to the shear pocket connections, the joints may be tested in small-scale experiments or as part of a full bridge deck system. The concrete-to-concrete push-off test specimens may be designed to test joint shapes in shear; rather than the full blockout, the inside of the “L” shaped specimens is formed to cast the desired joint shape for testing [see Figure 2.4].

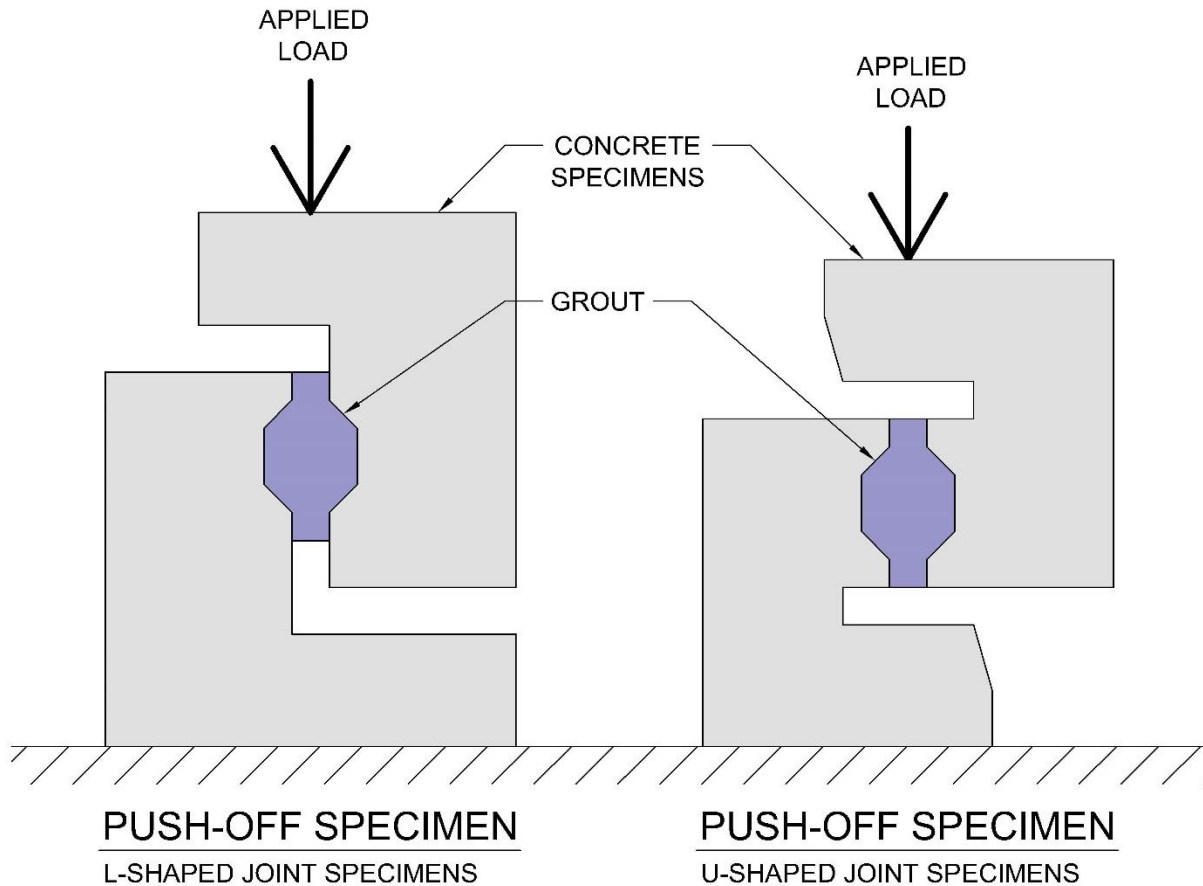


Figure 2.4 Typical Push-Off Joint Specimens

In 2010, S. Porter and J. Julander tested four different types of bridge deck joints to compare the shear behaviours and performances with regular strength 34.5 MPa joint fill grout [3]. The tested joint configurations consisted of the four of the following shapes each: wide opening joint shape, the female-female joint shape, the female-female joint shape with post-tensioning, and a shape in between the wide opening and female-female shapes that was un-reinforced. The wide opening joint had plates welded to shear studs that were cast into the concrete specimens along the tapered face with plates, and the joint contained a transverse rod that was fillet welded to each plate to connect the two specimens. For 10 out of the 12 specimens tested, they cast the push-off specimens in the “L” shape and the last two were cast in the “U” shape. The “U” shaped test specimens

allowed more realistic results since a 45° shear crack was allowed to form and propagate through the concrete. It was found to be advantageous to have the extra clearance on all sides of the joint. The results indicated the welded connection specimens deflected the most under the shear loading with deflections between 1 mm and 1.4 mm, but had the second greatest resistance with an average of 623 kN/m. The post-tensioned specimens had the greatest shear load resistance at 720 kN/m with deflections below 0.6 mm.

Porter and Julander (2012) completed experiments with small 914 mm x 457 mm x 222 mm concrete slab elements joined together to form a single specimen [4]. They tested the same joints as their push-off test specimens mentioned above with the addition of female-female joints with 610 mm and 914 mm long post-tensioned curved bolts installed across the joint, and a plate welded to the concrete specimen rebar rather than shear studs. The joints were also filled with 34.5 MPa grout. The longer post-tensioned curved bolt connection performed the best, followed by the plate welded rebar and the post-tensioned joint. However, the greatest capacity was only half the theoretical value of a monolithic bridge deck. The high strengths of UHPC fill not only increase the strength capacity of the bridge deck joint connection, but is also a durable material that resists cracking due to the steel fibers in the mix [5].

The governing design factor for bridge deck joints may not depend on the UHPC's strength and performance. In July 2011, an aging and cracked three-span concrete T-beam bridge spanning the Whiteman Creek in southern Ontario was replaced by a single-span pre-cast concrete bridge deck utilizing the strength of UHPC in the deck connections to the supporting steel girders [6]. The bridge deck consists of two rows of eight concrete panels supported by five steel girders. A longitudinal joint along the bridge centerline connects the short-edges of the deck panels, and transverse joints run between the long-edges of the deck panels; all female-female shaped joints.

The transverse joints were minimized due to the strength benefits of UHPC, measuring 200 mm at the widest point in the center, with a top opening of 160 mm, bottom opening of 10 mm. Conversely, since the longitudinal joint is directly over the center girder, integrating the panel-to-panel reinforcement and the shear studs welded to the girder flange, the joint was required to be 400 mm at its widest and has top and bottom openings of 350 mm. The capacity of the UHPC may have allowed for an even smaller transverse joint, but the space had to fit reinforcement and allow proper development lengths. Therefore, despite the strength advantages of the UHPC, the joint details and design can often be governed by requirements of other components and/or the constructability of the bridge.

### 2.3 Precast Concrete Bridges

Concrete is the most common material used for bridge deck design. The ability to shape the concrete with formwork makes it a superior material for its compressive and flexural strength, and the ability to create aesthetically pleasing bridge designs. Concrete bridge decks are typically either cast monolithically as T-beams or box girder bridges, which integrates the support system into the deck slabs, or are mounted to steel girders. If a composite concrete-steel bridge is cast-in-place the concrete deck will be cast integrally to the top flange of the girders around the shear studs. Precast bridge decks must be cast to the girders through the shear pockets, as discussed. To fully integrate the decks to the girders the decks are placed with a small gap on top of the flange to cast a concrete haunch along the girder extents. The haunch is cast through the shear pocket blockouts. The EVA foam is commonly used in the field to seal the haunch for casting and avoid complicated formwork.

It is well known that while concrete is strong in compression, it is much weaker in tension. Steel is strong in both compression and tension, therefore, its use in bridge deck systems allows greater

tensile resistance. The challenge in designing steel supported concrete deck bridges is the differing behaviour of the materials and connecting them to perform as one system. The flange of a steel girder is smooth, which does not allow for a strong bond to concrete. Therefore, to strengthen the bond steel studs are typically welded to the top flange of the steel girders. The steel studs are cast within the shear pocket fill and a concrete haunch that extends the length of the girder the concrete deck to connect the two components.

Precasting concrete bridge panels also removes the component from the critical path of the construction schedule, alleviating resource and personnel pressures. Basic small-span bridge replacement typically takes four to six months, however with ABC technologies this timeline can be reduced to under a week [6]. Depending on the design requirements, pre-cast bridge deck components typically use regular strength concrete with a compressive strength between 35 to 65 MPa at 28-days. UHPC can reach 100 MPa at 3-day compressive strength and typically ranges between 125 to 175 MPa at 28-day compressive strength, more than doubling that of RC. The impressive strength of UHPC significantly improves the overall strength and performance of pre-cast deck connections, which otherwise are typically considered the weakest link. The strength increase allows the shear pockets and deck joints to be smaller in size, minimizing the volume of UHPC required to be poured on site, compared to connections with RC, and its cost.

To reduce the amount of formwork required on site, bridge deck panels may be designed such that the panel joints are overtop of the steel girders, effectively using the girder flange as the formwork. This design feature was used in the Whiteman Creek Bridge since the longitudinal joints connect the concrete panels to each other and to the girders. Since the bottom opening of the transverse joint was only 10 mm, it was blocked with EVA foam for casting UHPC, also eliminating the need for formwork [6].

Another critical design component is reducing cracking and debonding at the connection interfaces to lessen the ingress of road run-off that could cause corrosion of the steel reinforcing bars. Precast bridge decks will be weakest at the concrete interfaces due to the cold concrete-to-concrete bond. The bond is strengthened by roughening concrete surfaces inside the shear pocket blockouts and the joint faces of the precast panels. Two common methods are treating the required faces of the formwork with a retarding agent to prevent the smooth finish, or sand-blasting the concrete surface after casting. The use of higher-strength concrete aids in strengthening interface bonds and reducing cracking, transforming these connections to one of the strongest design components.

In ABC the joints and shear pockets are the only concrete connection components cast on site. The concrete used as the joint and shear pocket fill is either the same strength as the concrete panels or of higher strength. The use of high-performance concrete (HPC) and UHPC as precast concrete deck connection fill material is being researched at institutions around the globe as its superiority is being widely recognized.

In 2015, David Amorim completed research that involved testing precast bridge decks with UHPC transverse joints in negative bending [7]. The experimental program consisted of completing fatigue and static testing of two full-scale bridge decks. Both bridge decks were constructed from three prestressed precast concrete panels of 6007 mm wide x 2415 mm long x 250 mm deep, connected by transverse joints filled with UHPC for a full length of 7295 mm. The panels were prestressed with six 7-wire low relaxation strands in the transverse direction. The joint had a 25 mm opening at the bottom that tapered up to a width of 176 mm. The bottom of the joint was plugged with EVA foam for casting the UHPC. The bridge deck was supported by two built-up steel girders spaced at 3251 mm c/c. The concrete deck panels were connected to the girders via the shear pocket and 50 mm haunch cast with UHPC. There were two different sizes of rectangular

shear pockets and each pocket contained six shear studs welded with a stud gun onto the top flange of the girders. The shear studs used had a diameter of 19 mm and a length of 178 mm.

In order to achieve negative bending, the deck was loaded with a hydraulic jack from below. The first deck was tested statically to failure in the center of the middle panel, and then in partial fatigue adjacent to the joint of the west panel. The second deck had the same fatigue test location, completed first, followed by a static test to failure from the mirrored location adjacent to the east panel joint. The static testing resulted in punching failures, as expected, with adequate load transfer across the joints. For the static test adjacent to the panel-to-panel joint, the observed cracking on the top surface of the deck protruded equally as far into the panel across the joint as the panel where the load plate was located. The UHPC joint had numerous cracks across the surface. The fatigue testing resulted in shear stud failure, where the shear studs ripped off the girder flanges. The fatigue testing was halted once this occurred and a punching failure was not achieved. The conclusions of this thesis research project were to increase the size and/or number of shear studs within the shear pockets due to the fatigue testing results.

---

## Chapter 3 Research Program

---

### 3.1 Introduction

Concrete is a brittle material that is strong in compression and weak in tension. There are many different mix designs available, depending on the application of the concrete and the conditions it will be exposed to during its lifespan. On the other hand, since steel is a metal forged into shapes, a ductile material and is very strong in tension. Reinforced concrete elements combine the compression strength of concrete and tensile strength of steel to resist applied loads. Though these behaviours are well known in engineering design, in research it is important to test the materials individually to ensure the quality and strength criteria to validate the experimental results.

There were two types of concrete used in this research, regular strength Portland cement concrete (RC) with a 28-day compressive strength of 45 MPa and UHPC with a 3-day compressive strength of 100 MPa. The shear pocket slabs and bridge deck slabs were cast with RC, and the corresponding shear pockets and deck joints are cast with UHPC. All concrete specimens are reinforced with 400 MPa black steel bars.

Shear pockets are designed to not only connect the concrete deck slab to the steel support girders, but also to resist the shear forces that are transferred between the deck and girders from live and environmental loading. There are many different designs for the shear pocket shape, and the shear stud arrangement. The shear pockets in the small-scale specimens and the bridge decks are rectangular with a taper on two opposing faces.

The bridge deck joints are strictly to transfer loads between the deck panels and are not designed as expansion or control joints. The behaviours and result data will be compared between a homogenous control bridge deck and a two-panel jointed bridge deck.

The research program specimen numbers and test methods are summarized in Table 3.1. The scope of work includes material testing (concrete, UHPC and steel), shear pocket push-out tests, and full-scale bridge deck testing.

Table 3.1 Research program specimen details.

<b>Specimen/Material</b>	<b>Test Method</b>	<b>Details</b>	<b>No. Samples</b>
Regular Strength Concrete and UHPC	Compression	Cylinders	3 per day of testing
	Splitting tension	Cylinders	3 per day of testing
Shear Studs	Shear	2 shear planes along stud	3
	Tension	Stud welded onto base plate	5
Shear Pockets	Push-out	6 shear studs	6
	Push-out	3 shear studs	4
	Push-out	0 shear studs	4
Bridge Decks	Static loading	No deck joint (control)	1
	Static loading	UHPC deck joint	1

## 3.2 Material Testing

### 3.2.1 Concrete Testing

Compression and tension concrete cylinders were cast during each concrete pour to test the strength development leading up to the experimental specimen testing. For each test day three cylinders were cast for statistical accuracy. Typically, three extra cylinders were cast for each test type in the event any significant outliers resulted and additional specimen(s) required re-testing.

The compression cylinders were cast in two different sizes, 102 x 203 mm for RC and 76 x 152 mm for UHPC. The compression cylinders were cast and tested according to the standard ASTM C39/C39M-18 Standard Test Method for Compressive Strength of Cylindrical Concrete Specimens [8]. The cylinders were loaded at a rate of 182 kg/s (400 lbs/s) until compression failure. Similarly, the tension cylinders were cast in two different sizes, 152 x 305 mm for RC and 76 x 152 mm for UHPC. The tension cylinders were cast and tested according to the standard ASTM C496/C496M-17 Standard Test Method for Splitting Tensile Strength of Cylindrical Concrete Specimens [9]. The cylinders were loaded at a rate of 91 kg/s (200 lbs/s) until tensile failure.

The compression testing machine at the University of Manitoba is a Test Mark Industries CM-3000-DIR with a capacity of 1334 kN (300,000 lbs) and was used to test the compression and tension cylinders.

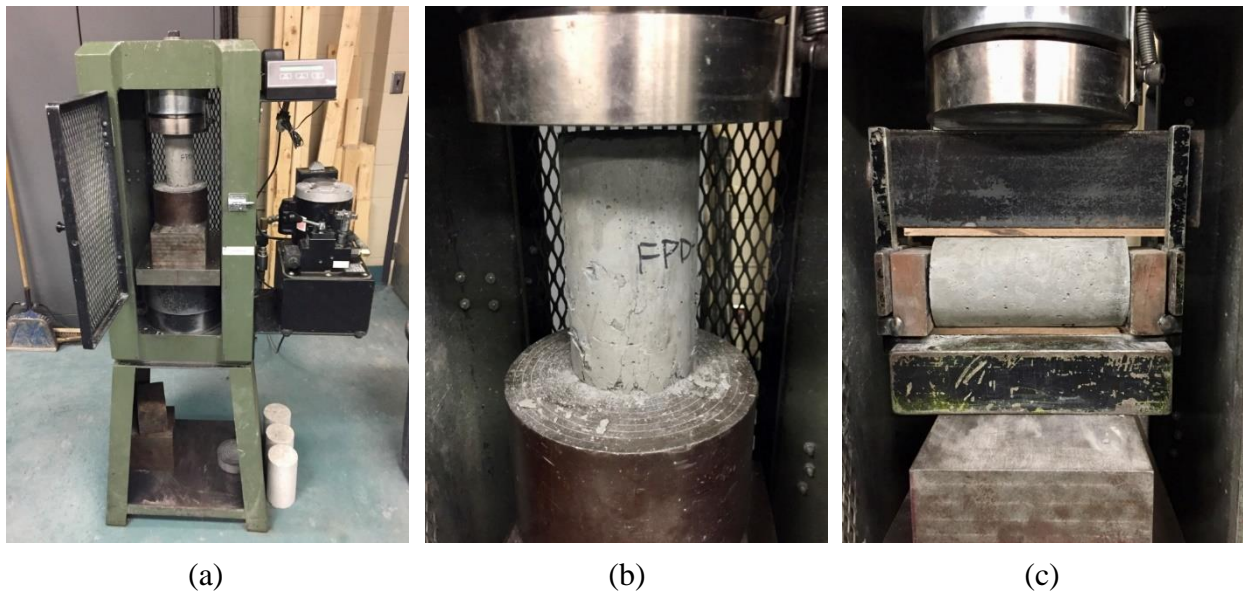


Figure 3.1 (a) Test Mark Industries CM-3000-DIR test machine; (b) Compression cylinder test setup; (c) Splitting tension cylinder test setup.

### 3.2.2 Shear Stud Testing

The push-out testing subjects the shear studs to direct shear since the load was applied directly perpendicular to the studs. However, during the bridge deck testing, the shear pockets were a small component in a whole system resisting the loading, therefore, the shear pockets were subjected to a combination of flexure, shear, compression and tension. The shear studs were tested to failure in both shear and tension to observe their behaviour during testing, and to confirm the ultimate strengths.

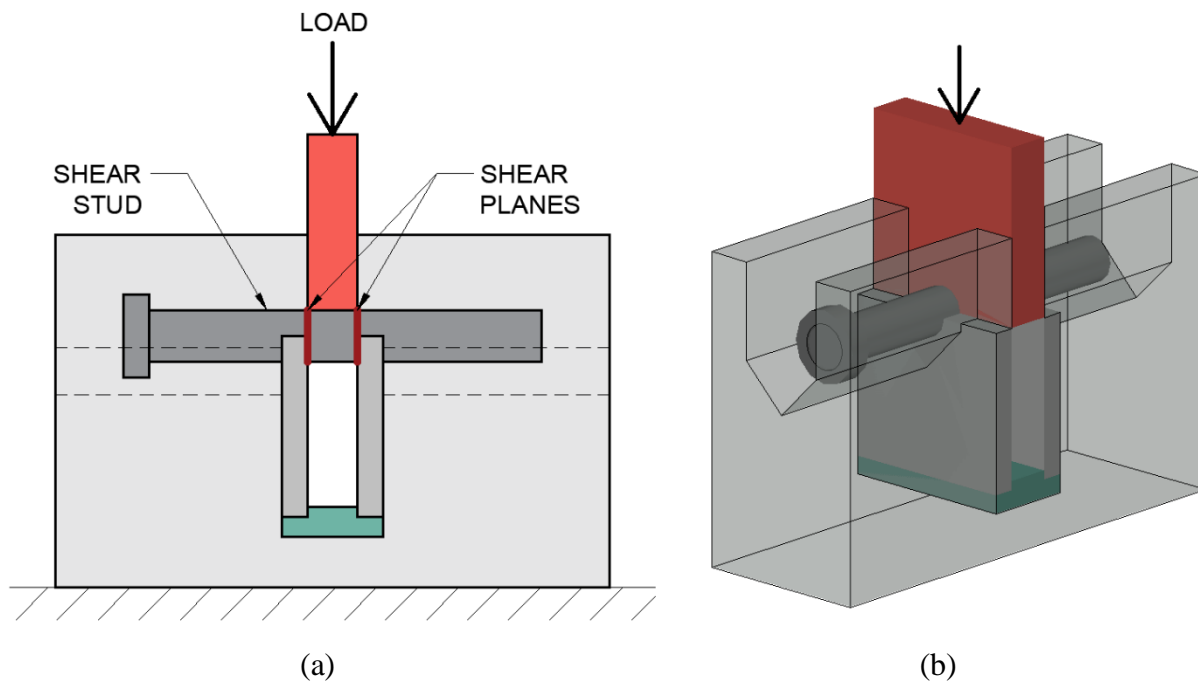


Figure 3.2 Shear stud shear test setup: (a) side view, and (b) isometric view.

The shear test involved shearing off a section in the center of the shear stud. A slotted steel support block is used to secure the head and end of the shear stud, and the load is applied downwards on a plate that is aligned with the slot in the steel block. The load is applied until failure of the stud. The shear stud was not instrumented for this test since the shear capacity of the studs could be determined with the load data and the stud's cross-sectional area. The test setup creates two

shearing planes along the stud. Figure 3.2 and Figure 3.3 show the direct shear test setup. The shear studs are fixed at each end with bolts that are tied across the steel block; however, to simplify the figure, these restraints are not shown but can be seen in the photographs.

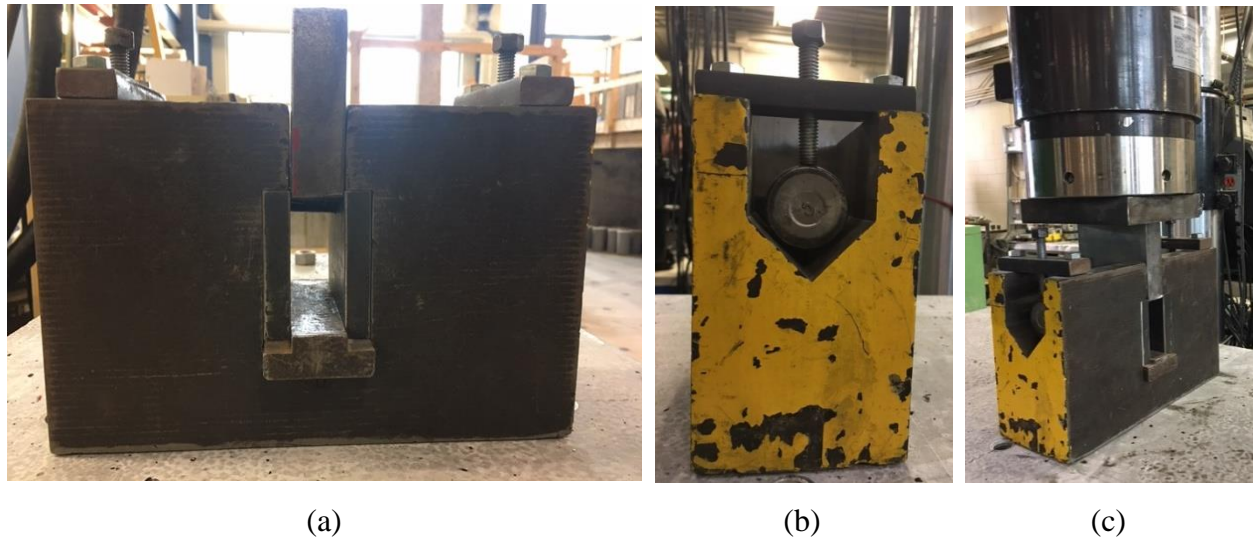


Figure 3.3 Shear stud test equipment: (a) side view, (b) end view, and (c) during testing.

The tension test was a slightly more complicated setup. The shear stud was welded onto a small steel base plate with a weld strong enough to resist failure during the tension testing. The steel plate was then fixed to the strong floor, and the head of the stud was clamped to the MTS testing machine. The MTS testing machine pulled upwards on the stud, creating tensile forces along the stud, until its failure. The MTS machine is typically for larger specimen tests; however, its capacity was required to fail the shear studs. Long threaded rods were used to secure the load cell to the top plate that supported the clamp, pictured in Figure 3.4. Long threaded rods were also used to secure the base plate to the strong floor.

The shear studs were instrumented with two 6 mm, 350  $\Omega$  strain gauges that were glued to opposite sides approximately 10 mm from the base of the stud. A 50 mm extensometer was also zip-tied to the stud to measure the stretching that occurred during testing. Upon necking, prior to the stud

failure, the extensometer was removed to avoid damage since the top half of the shear stud pops off. In the test results, the shear studs will be numbered with a prefix denoting the type of test; “SS” for the shear test of the studs and “TS” for the tension test of the studs.

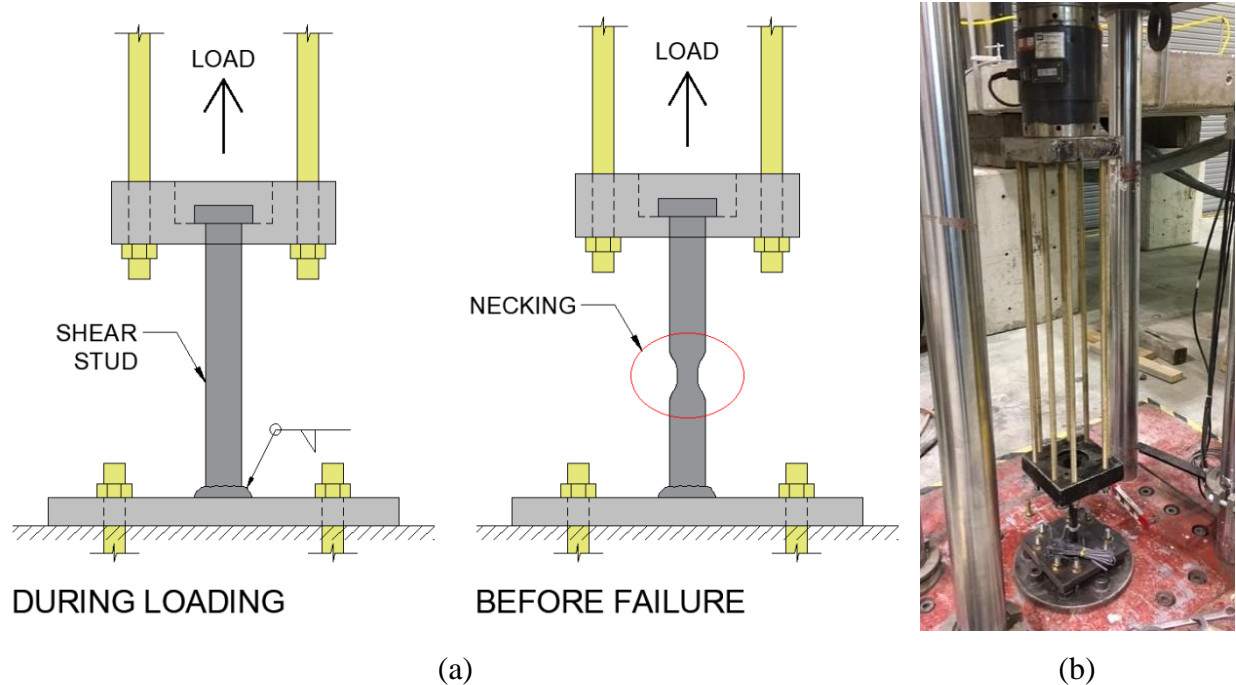


Figure 3.4 Shear stud direct tension test setup: (a) side view, and (b) instrumented stud.

### 3.3 Shear Pocket Experiments

#### 3.3.1 Naming Convention

The naming convention chosen for the shear pocket slabs considers the amount of steel studs present in each pocket and the test number. Since the push-out test method was used, there are two shear pocket slabs per specimen, which are differentiated by an A or B.

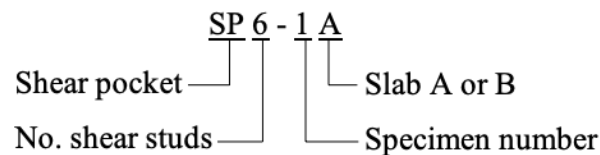


Figure 3.5 shows the push-out test setup with 6-stud layout specimens. The 3-stud specimens had one row of 3 studs, which can be seen later in Figure 3.9.

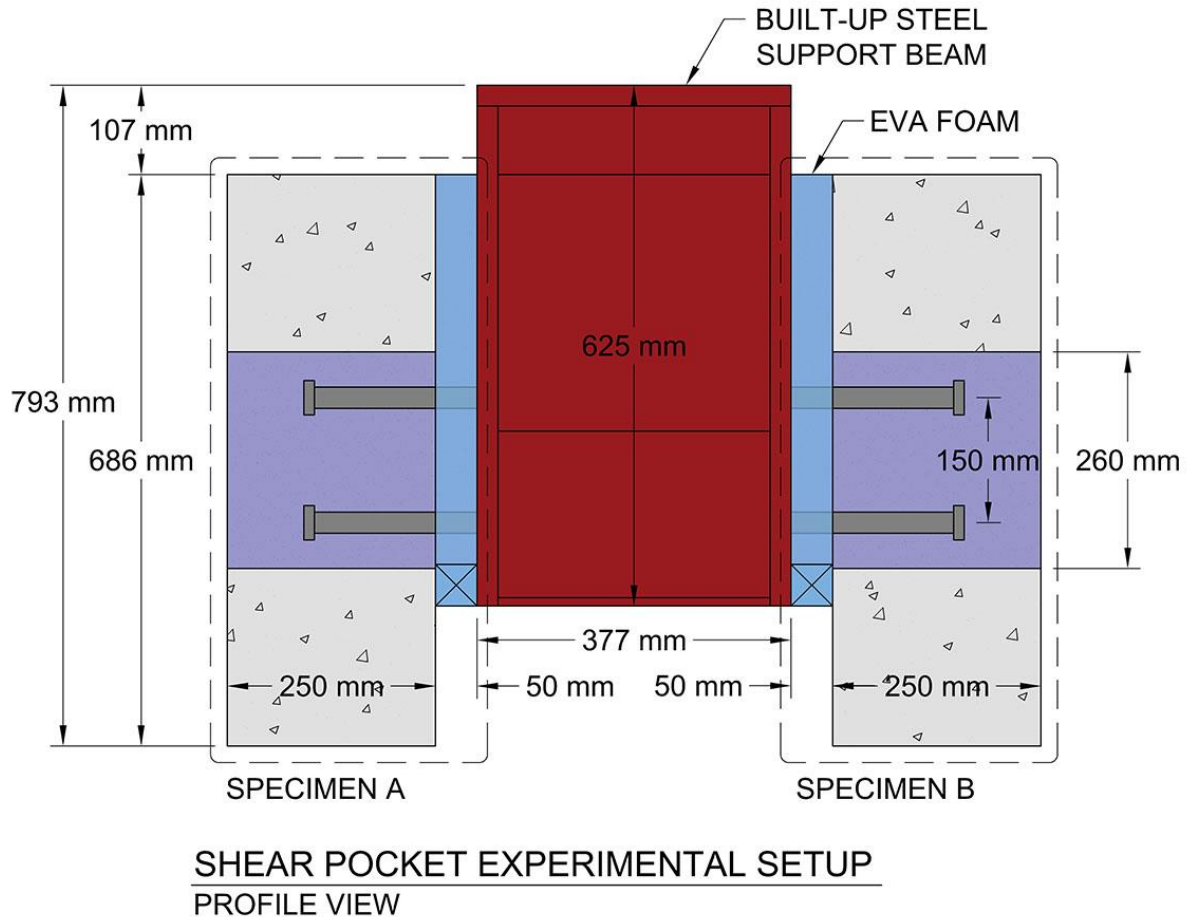


Figure 3.5 Push-out shear pocket test setup.

### 3.3.2 Slab and Shear Pocket Details

The shear pocket specimens consist of a small slab with a shear pocket blockouts. These slabs contain steel rebar reinforcement in the tensile zone, consisting of one layer of transverse and longitudinal 15M bars [Figure 3.6]. The slabs measure 686 x 608 mm and are 250 mm thick. The slab thickness is the same as the thickness of the full-size bridge decks to allow result comparison. The shear pocket is the full depth of the slab and measures 310 x 260 mm with a taper downwards

to 290 x 260 mm [Figure 3.7]. The shear pocket details were also designed to match those of the bridge decks.

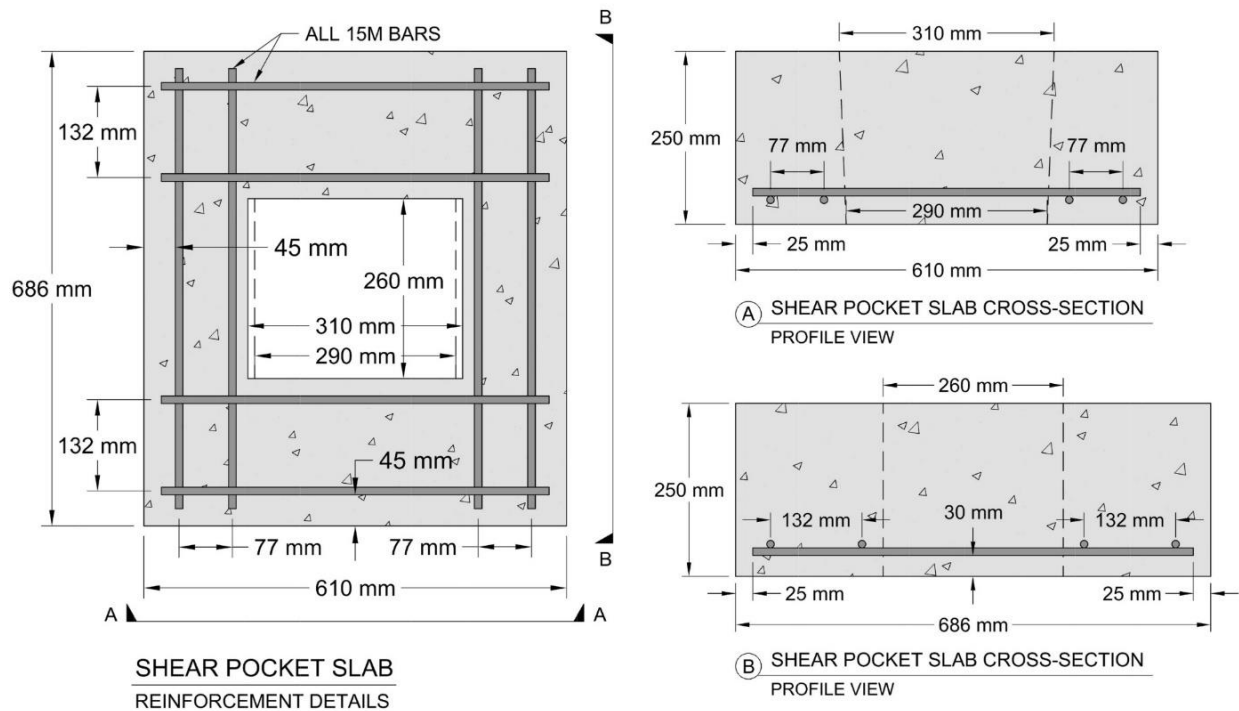


Figure 3.6 Shear pocket slab dimensions and reinforcement.

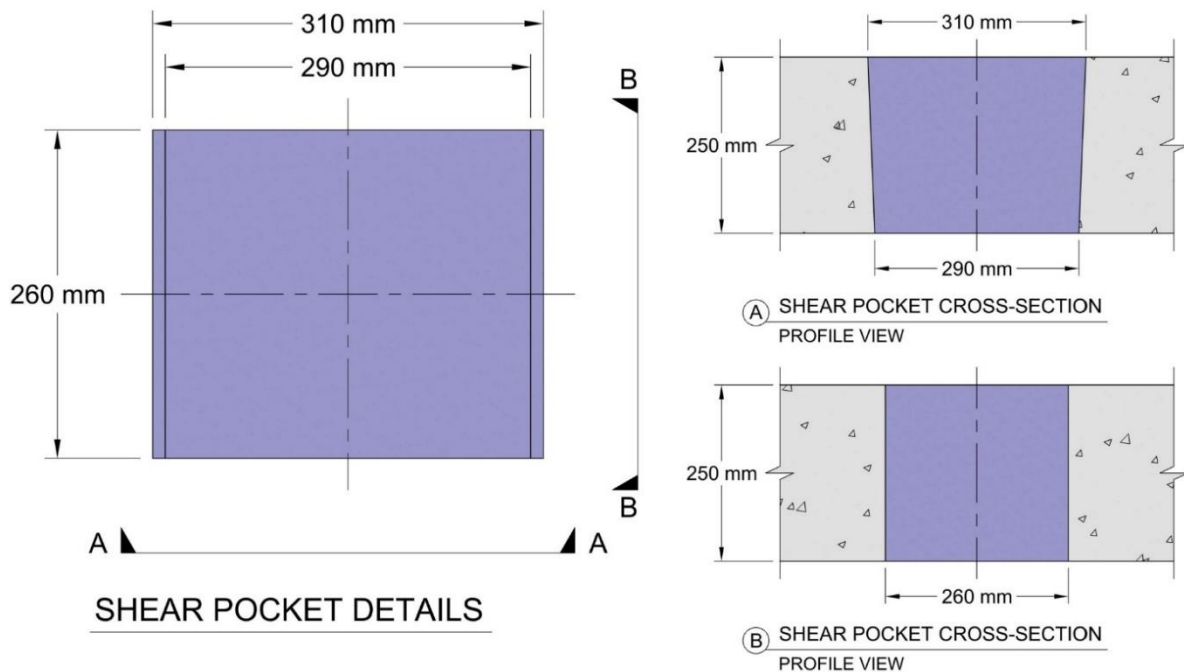


Figure 3.7 Shear pocket dimensions.

The 6-stud specimens had 2 rows of 3 shear studs, and the 3-stud specimens had 1 row of 3 shear studs [see Figure 3.8]. Therefore, when the push-out specimens were loaded, the force went through the row(s) of 3 studs [see Figure 3.9]. The 0-stud specimens had no additional reinforcement, simply UHPC within the pockets and haunches.

The construction of the shear pocket slabs was straightforward. The formwork was built of plywood and the shear pocket blockouts were built of layers of dense insulation foam glued together and cut to the required taper, as seen in image (a) of Figure 3.10. The sides of the blockouts were coated with a retarder to create a rough surface during concrete curing. The resulting roughness of the hardened concrete provided a better bond surface for the UHPC cast to fill the shear pocket. The same surface preparation is used for the slabs and Eden Lake Bridge.

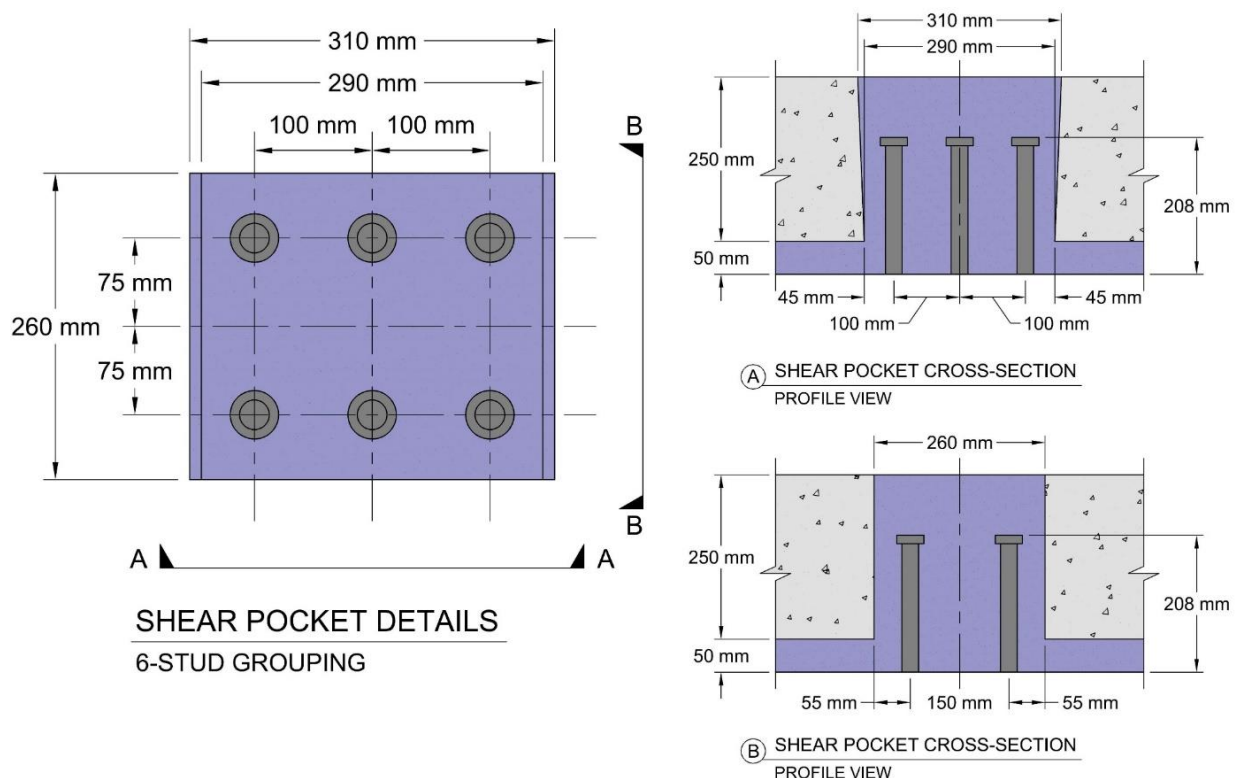


Figure 3.8 Shear pockets with 6-stud groupings (SP6).

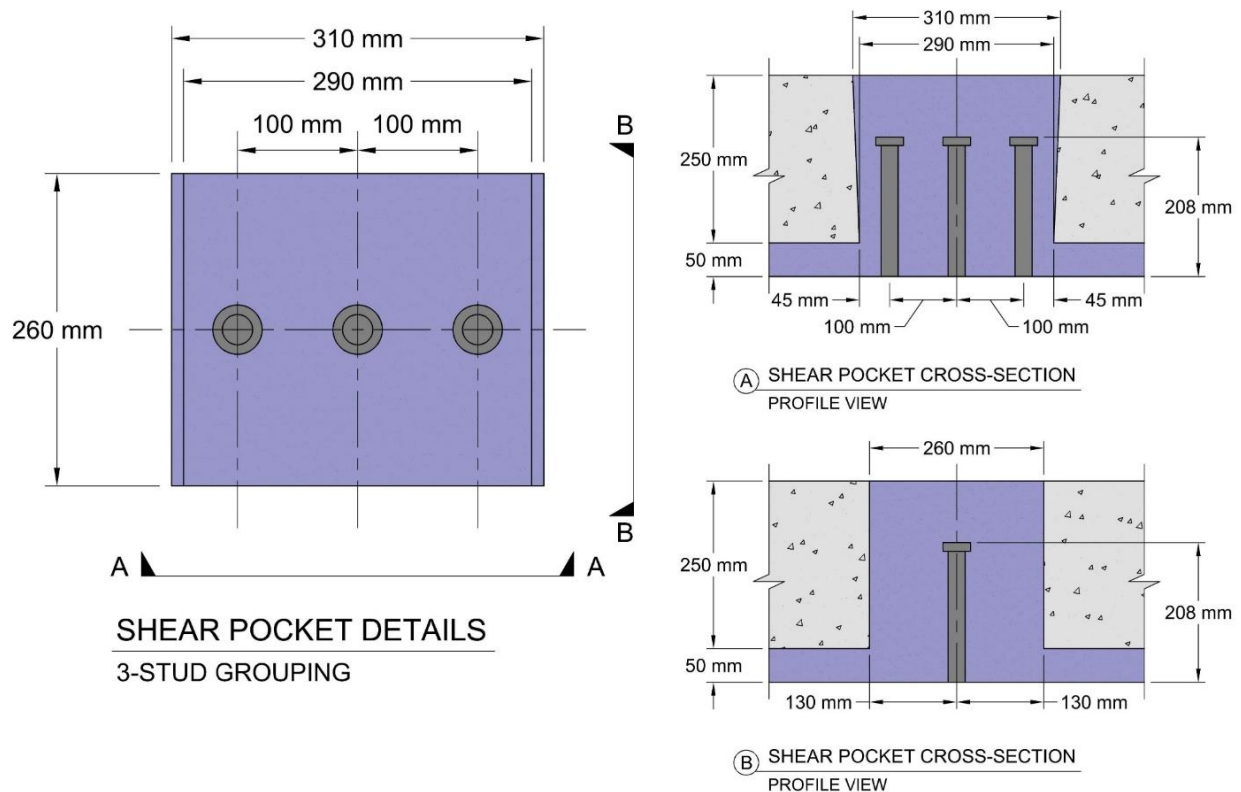


Figure 3.9 Shear pockets with 3-stud groupings (SP3).

Plastic chairs were used to support the layers of rebar to a clear cover of 30 mm. Since the specimens are experimental and not subject to potential water ingress, the rebar cover is not a critical detail in the design. In order to lift and place the shear pocket slabs during the experimental testing, threaded lifting loops were cast in the top and bottom faces of the slab; two per face [see images (b) and (c) of Figure 3.10]. Threaded eyebolts were screwed into the lifting hardware to move the slabs and/or experimental setup with the laboratory's overhead crane.

The formwork allowed for six shear pocket slabs to be cast at a time. The concrete for the slabs was ordered and shipped to the laboratory in a concrete truck from LafargeHolcim Ltd. (LafargeHolcim). The shear pocket foam blockouts were glued into place in the formwork, however, during placing and concrete vibrating they were weighed down to ensure no movement occurred. Once sufficiently vibrated, the concrete was finished to a smooth surface.

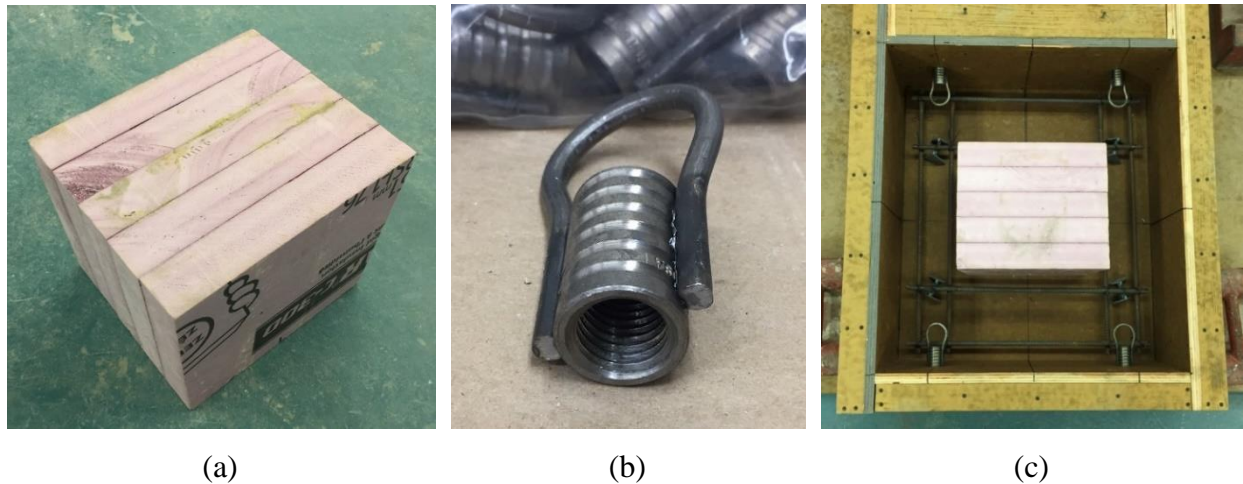


Figure 3.10 (a) Shear pocket blockout, (b) Threaded lifting loop concrete insert, (c) Shear pocket slab formwork with reinforcement and blockout placed.

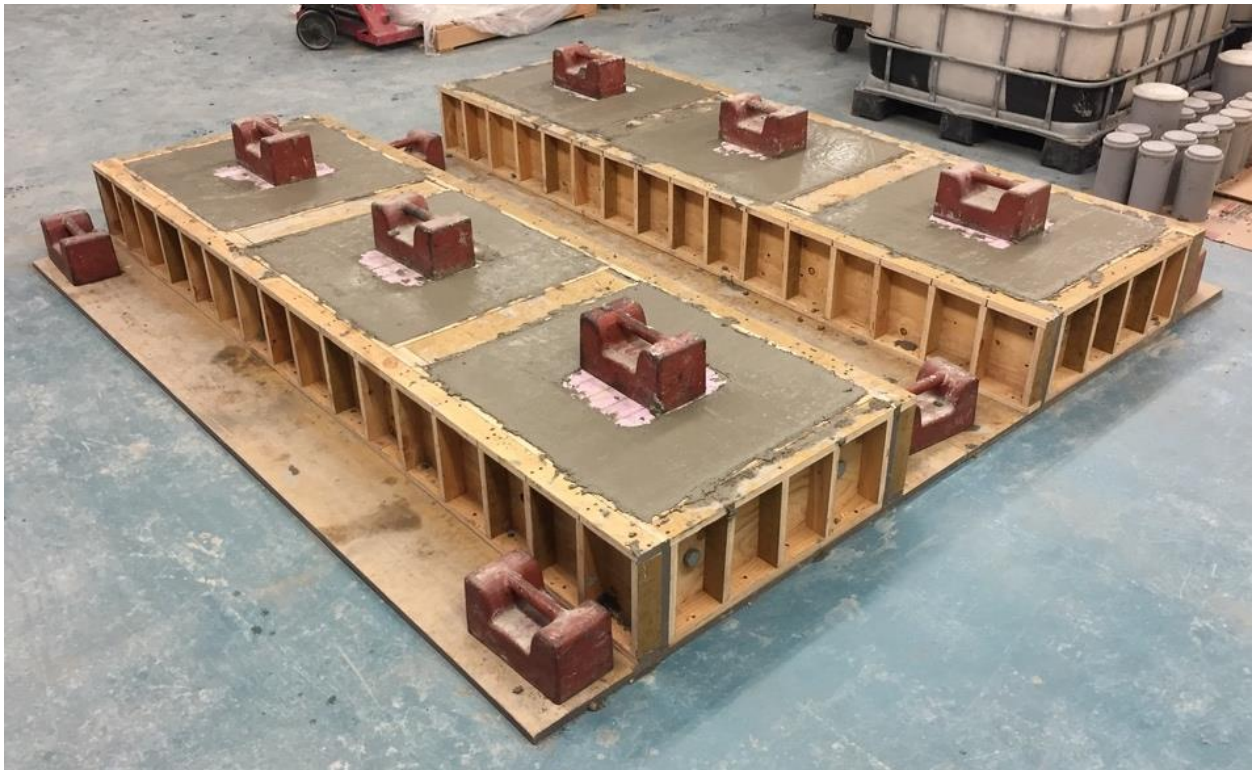


Figure 3.11 Smooth finished shear pocket slabs.

The shear pocket slabs were cast with 3 different concrete pours. The 6 shear pocket slabs for the 6-stud layout were cast in the first batch on December 19, 2017. The 4 shear pocket slabs for the 3-stud layout, and first 2 of the stud-free specimens were cast in the second batch on February 8,

2018. The third batch on October 25, 2018 cast the remaining 2 shear pocket slabs for the stud-free specimens, and 4 additional slabs to be used as needed.

Once the test date was set for the push-out tests, the push-out test specimens could be assembled through the casting of the UHPC shear pockets. The gap for the haunch, between the built-up steel beam and the shear pocket slabs, was created by gluing EVA foam to the flange of the beam. The slabs were then placed on either side and tension rods were tightened to secure the slabs during casting and curing, as seen in Figure 3.12(b).

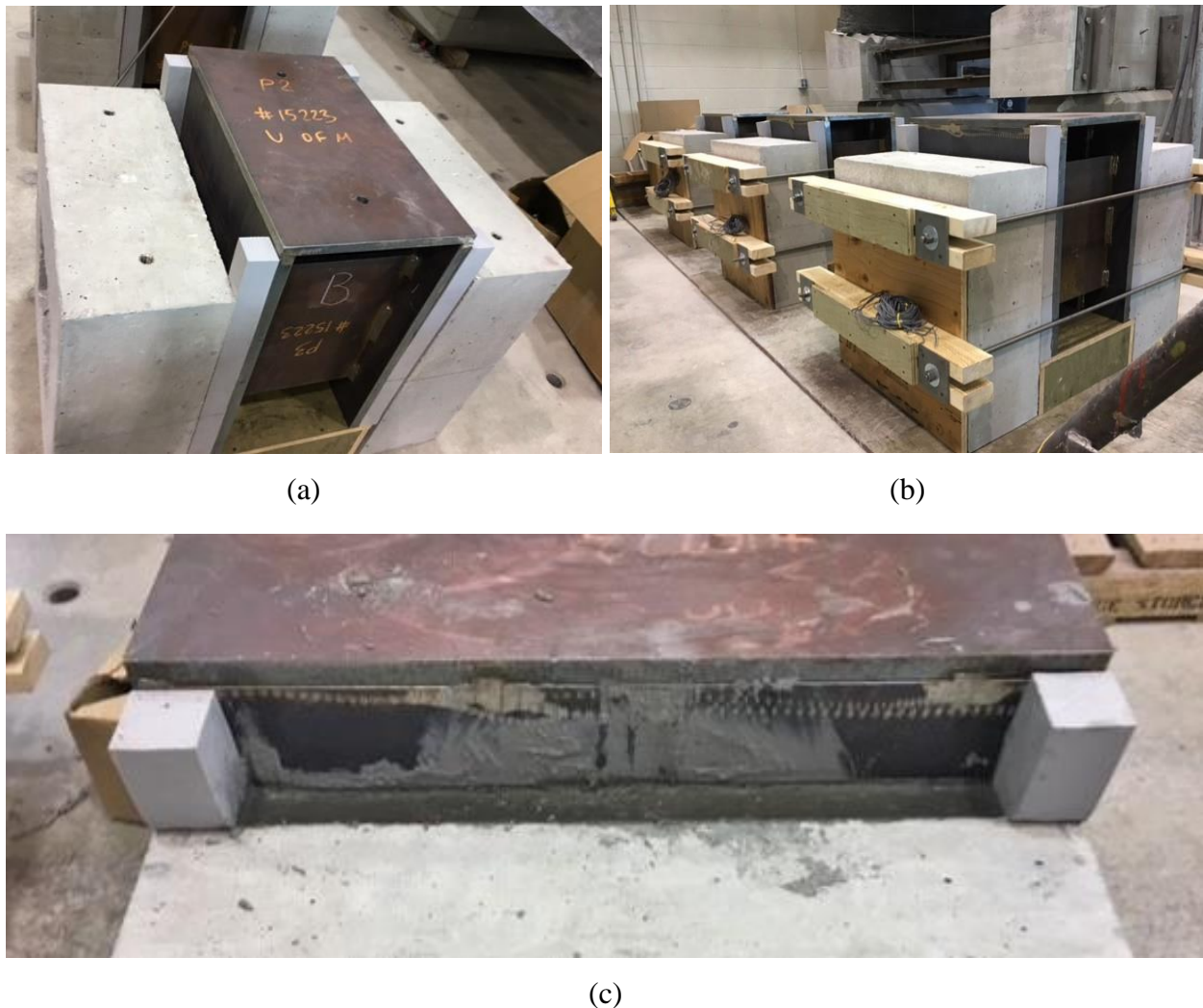


Figure 3.12 Push-out test specimen UHPC shear pocket casting: (a) slab placement; (b) UHPC cast formwork; and (c) UHPC haunch post-casting.

The UHPC was poured down into the shear pocket blockout from the haunch opening between the steel beam and shear pocket slab until it was level with the top of the shear pocket slab [see Figure 3.12(c)]. Since UHPC does not have large aggregates like regular concrete, there was no concern of air pockets forming around the shear studs. After the UHPC casting, the specimens were covered with plastic sheeting for protection during curing.

Minimal cylinders were cast for the shear pocket concrete and UHPC as a more extensive batch of cylinders were cast for the bridge decks, discussed below. The shear pocket slabs had compression cylinders cast for 28-day strength and test day (3 per day per batch). The strength development of the RC slab was not a priority; therefore, it was sufficient to verify the strength at 28-days and on test day. The UHPC shear pockets had compression cylinders cast to verify the strength on test day. Table 3.2 summarizes the casting of the shear pocket specimens and material test specimens.

Table 3.2 Shear Pocket Concrete Cast Details

Concrete Pour Date	Specimens Cast	Type of Concrete	Test Cylinders	
			Compression	Tension
19-Dec-2017	SP6-1A, SP6-1B, SP6-2A, SP6-2B, SP6-3A, SP6-3B	RC	15	3
08-Feb-2018	SP3-1A, SP3-1B, SP3-2A, SP3-2B SP0-1A, SP0-1B,	RC	15	3
25-Oct-2018	SP0-2A, SP0-2B, 4 additional shear pocket slabs	RC	12	3
17-Oct-2018	SP6-1, 2, and 3 Shear Pockets	UHPC	6	0
25-Nov-2018	SP3-1, and 2 Shear Pockets	UHPC	6	0
11-Mar-2019	SP0-1, and 2 Shear Pockets	UHPC	6	0

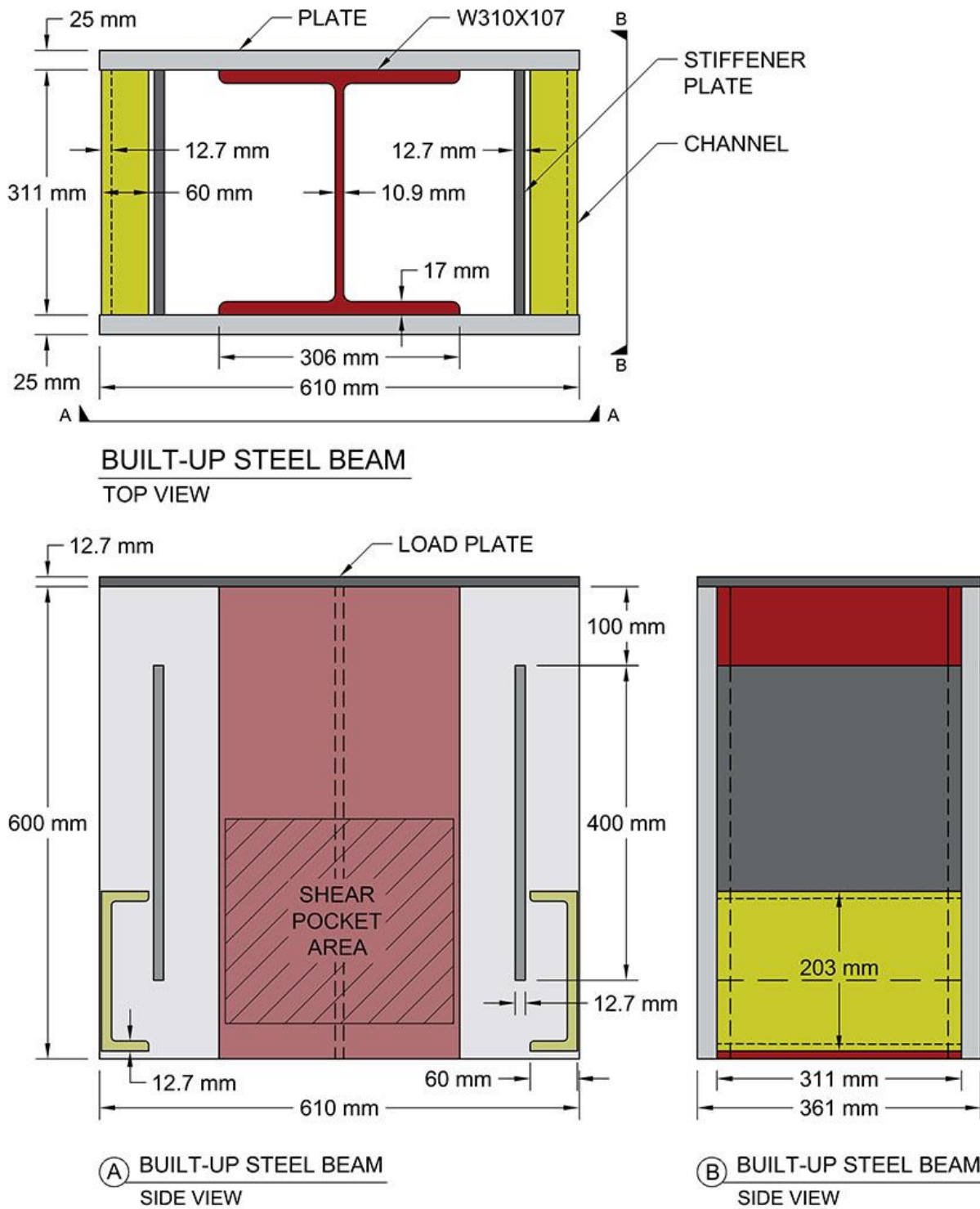


Figure 3.13 Built-up steel support beam for push-out test specimens.

A built-up steel beam was designed and constructed for the shear pocket slabs to be cast against, as seen in Figure 3.13. The push-out shear pocket test is setup for an axial load on the top of the steel section and it must resist buckling to allow the concrete and/or shear studs to fail first. The built-up steel beam for these push-out tests were comprised of a 600 mm tall W310x158 section and various plates welded together. The W310x158 section had 600 x 610 x 25 mm thick plate welded to each flange. The flange plates were previously shipped to Falcon Machinery to have the shear studs welded on with a stud gun. The use of a stud gun creates a better weld to the steel surface, rather than stick welding. Welding the plates with pre-installed shear studs cut down on the overall construction time for the built-up beams, since the W-sections had to be special ordered. Once the plates were welded onto the flanges of the W-section, a 25 mm thick loading plate was welded to the top of the built-up section. Stiffener plates (350 x 327 x 25.4 mm thick) were also welded between the flanges adjacent to the stud groupings location. During the first push-out test completed the steel buckled under loading. Therefore, a stiffener plate and channel were also welded between the flanges for added stiffness for the remaining six test setups.

### **3.3.3 Test Method and Setup**

#### **3.3.3.1 Load Apparatus and Test Details**

The push-out tests were performed in a hydraulic testing machine equipped with a 5000 kN capacity closed loop servo-hydraulic machine. Two large 550 x 550 x 1000 mm tall concrete blocks were placed below the testing machine to elevate the test specimens off the floor, and reduce their distance from the actuator. The push-out test specimens were levelled with plaster filled bags and shims. Figure 3.14 shows the test setup and machine.

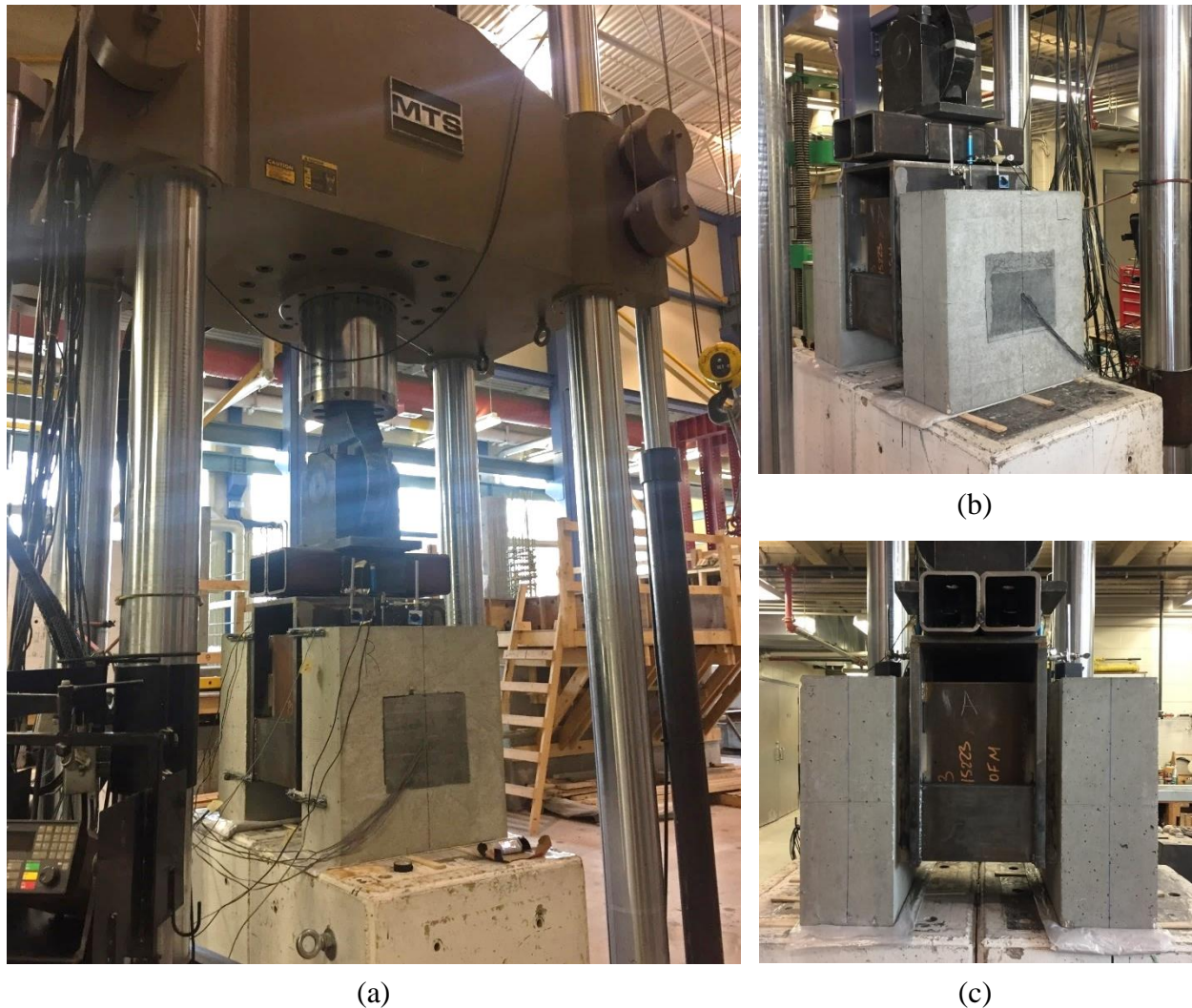


Figure 3.14 (a) Push-out test setup and MTS machine; (b) push-out test; (c) side view of test setup.

The shear pocket specimens were tested statically at a loading rate of 0.5 mm/min until failure. Each specimen had a trial run to 60 kN to ensure all equipment and instrumentation was working. Cracking was marked as the testing was in progress.

### 3.3.3.2 Instrumentation Details and Layout

Strain gauges were glued onto the top and bottom faces of the middle studs within the shear pockets to read the strains during testing. The 6-stud specimens had a set of strain gauges 10 mm from the base of both middle studs, and a set of strain gauges 10 mm from the head of the top middle stud.

Since the 3-stud specimens only had one row of studs, the middle studs were instrumented with a set of strain gauges 10 mm from the base and head of the stud. The strain gauges were placed at each end of the studs to understand how the shear forces develop along the full length of the stud and whether the stud length is adequate. Figure 3.15 shows the strain gauge locations and the nomenclature used in the results. The “LS”, “MS”, and “RS” refer to left stud, middle stud, and right stud, respectively; the 6-stud groupings are distinguished with a 1 or 2 for the row number. “ET”, “EB”, “HT” and “HB” refer to the locations of the strain gauges as end-top, end-bottom, head-top, and head-bottom.

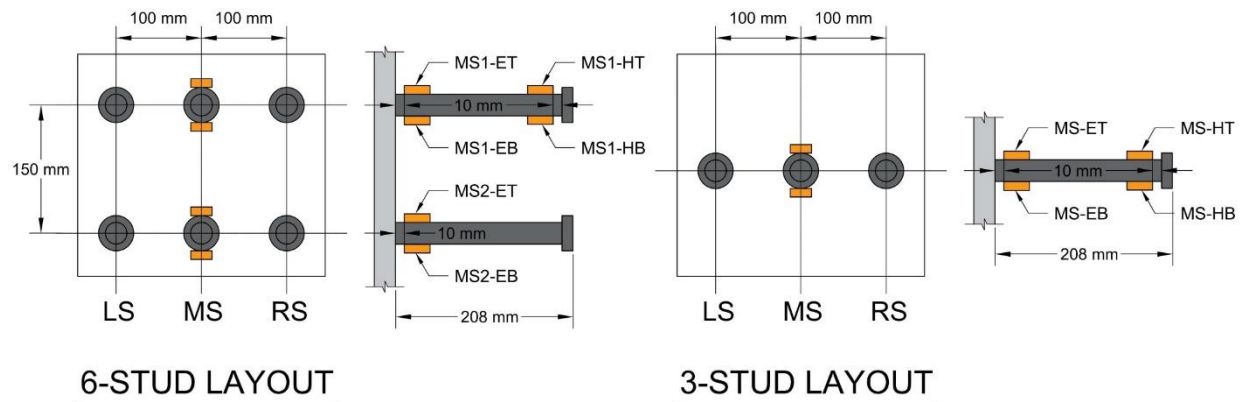


Figure 3.15 Shear stud strain instrumentation.



Figure 3.16 Strain gauge application.

LVDTs were used to measure the relative vertical displacement of the build-up beam during testing. Two LVDTs were glued to the exposed surface of the UHPC haunch of each slab specimen with one clamped to a mount on the steel and the other clamped to the mount on the RC surface. Four pi-gauges were installed on each test setup to measure the separation between the concrete and steel. The gauges were adhered to the steel flange and side of the concrete slab; one at the top and bottom of each shear pocket slab.

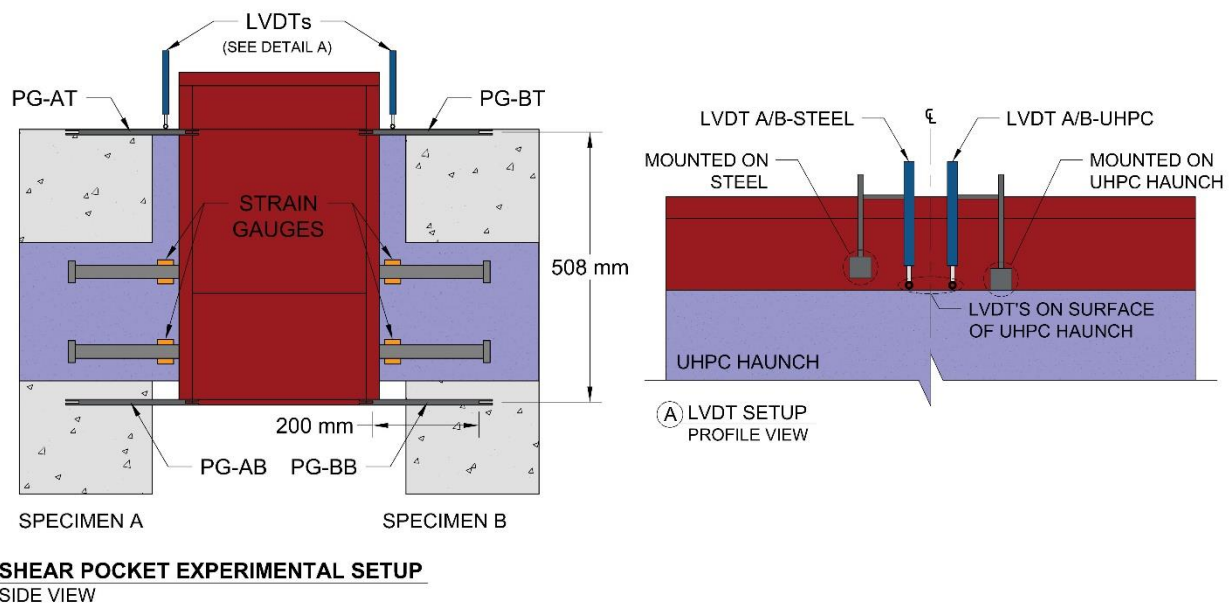


Figure 3.17 Push-out test instrumentation.

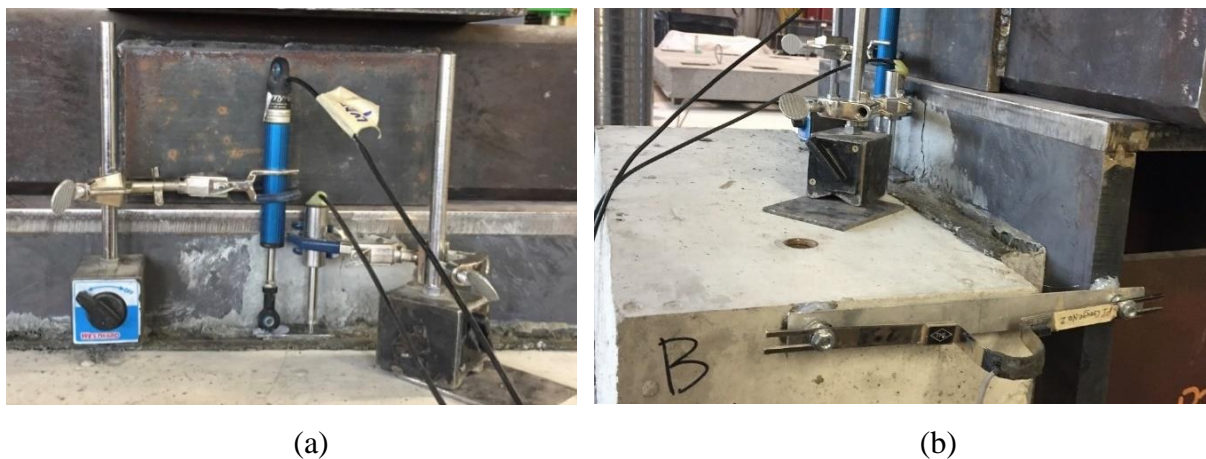


Figure 3.18 Push-out test instrumentation: (a) LVDTs, (b) LVDTs and pi-gauge.

## 3.4 Bridge Deck Experiments

### 3.4.1 Naming Convention

The control bridge deck will herein be referred to as the Full Panel Deck (FPD) since it was cast as one slab. The second bridge deck was constructed of two half-sized panels connected with a UHPC joint, and will therefore be called the Joint Panel Deck (JPD).

### 3.4.2 Material Testing

Table 3.3 summarizes the casting details for the bridge decks, including the material testing specimens, the deck panels, and the UHPC connections.

Table 3.3 Bridge Deck Concrete Cast Details

Concrete Pour Date	Concrete Batches	Specimen Cast	Type of Concrete	Test Cylinders	
				Compression	Tension
19-Mar-2018	1	FPD	RC	18	3
20-Mar-2018	1	Half Panel 1 (for JPD)	RC	18	3
23-Mar-2018	1	Half Panel 2 (for JPD)	RC	18	3
12-Apr-2019	3	JPD Connections	UHPC	36	24
13-Aug-2019	2	FPD Connections	UHPC	24	24

Concrete cylinders were cast for material testing to accompany each set of shear pocket slabs. Compression cylinders were cast for 7, 14, and 28-day strengths (3 per day). The UHPC compression cylinders were cast for 3, 7, 14, and test-day strengths; 28-day strength cylinders were cast for both decks, but they were used as the test-day strength cylinders since the bridge deck testing occurred near or prior to the UHPC 28-day age. For the JPD, tension cylinders were cast for 3, 7, and test-day strengths for 2 out of the 3 UHPC batches required to fill the deck

connections. For the other UHPC batch cast, tension cylinders were made for 3, 7, 14, and test-day strengths to observe the strength development on the same days as the compression tests. Based on the tensile strength results for the JPD, discussed later, both batches of UHPC mixed for the FPD had tension cylinders made for 3, 7, 14, and test-day strengths.

### 3.4.3 Pre-Cast Deck Panel Details

The FPD measured 4890 x 2965 x 250 mm thick, and after joining the panels for the JPD it had the same dimensions. The individual panels of the JPD measure 2380 x 2965 x 250 mm thick. The bridge decks were cast with 45 MPa RC at the LafargeHolcim Prestressed Concrete Plant in Winnipeg, Manitoba, and transported to the University of Manitoba for testing. Figure 3.19 through Figure 3.21 are photographs from the deck slab casting at the LafargeHolcim precast concrete plant.

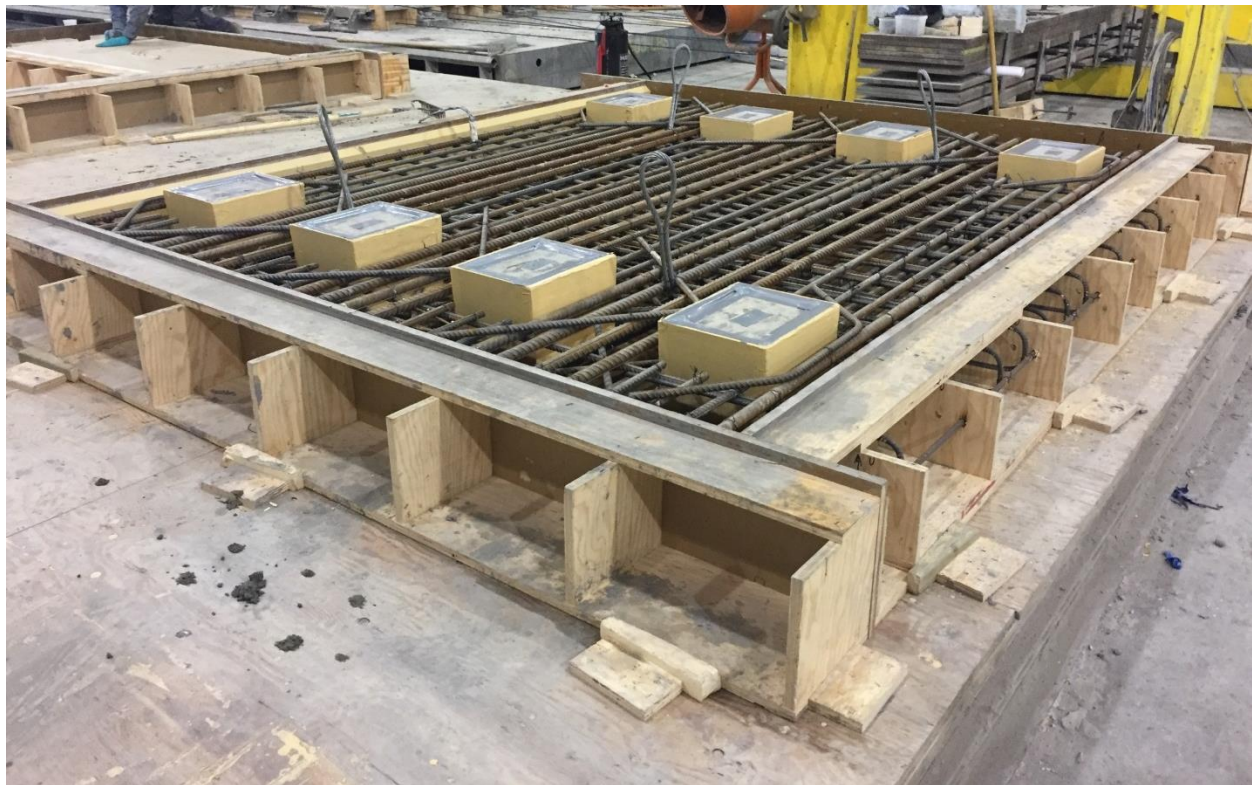


Figure 3.19 JPD half panel formwork, shear pocket blockouts and reinforcement.

The decks had bottom and top layers of reinforcement comprised of mainly 15M rebar and 20M and 25M bars in the transverse direction. The shear pocket blockouts had bent bars surrounding the openings for support. The shop drawings of the three slabs can be found in Appendix A.



Figure 3.20 JPD half panel concrete casting and vibrating.



Figure 3.21 Finished JPD half panel.

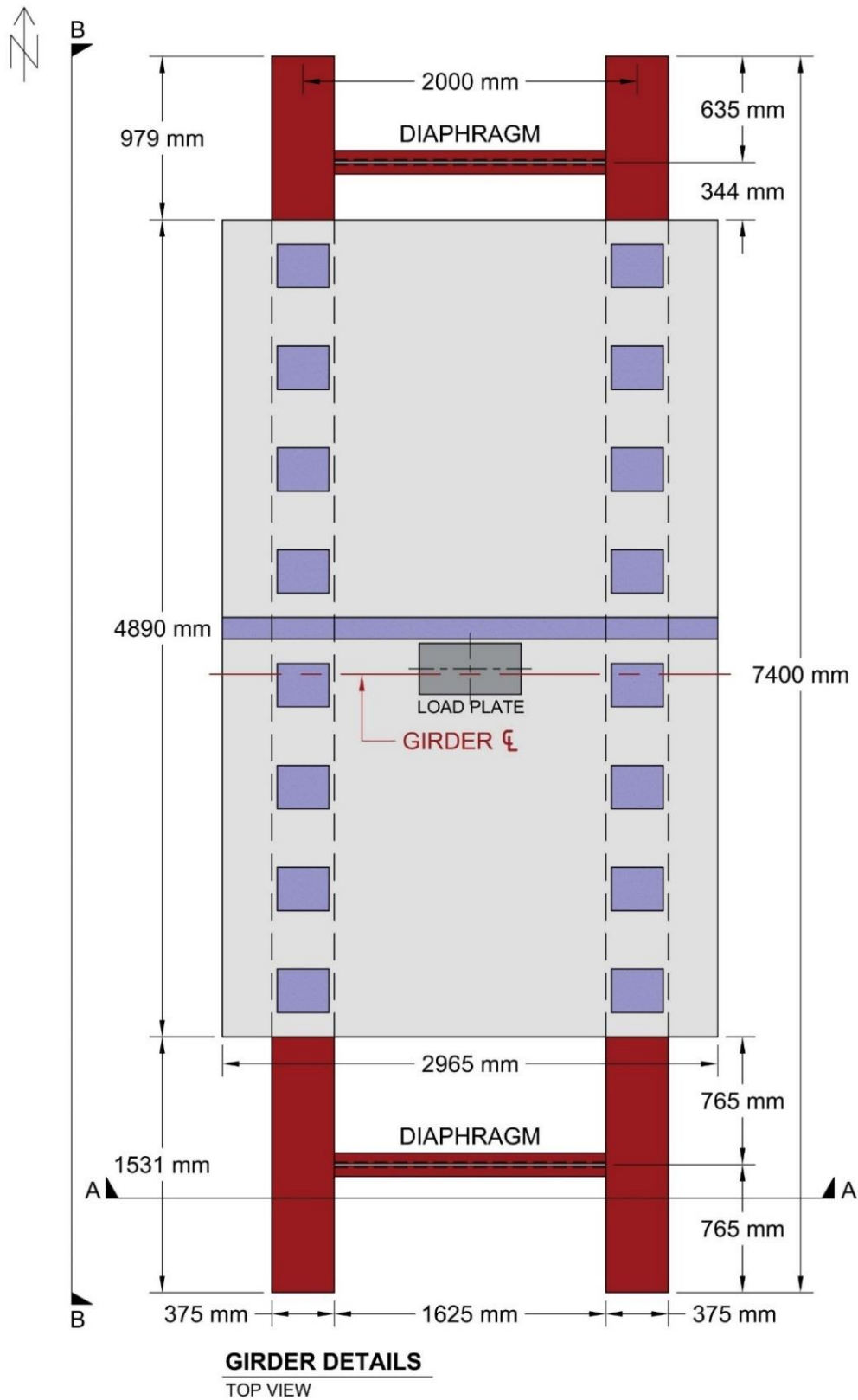


Figure 3.22 Bridge deck and support girder setup.



Two different sets of girders were used to allow preparation work on the second set of girders while the JPD was demobilized after testing. All four girders have stiffener plates between flanges on both sides of their webs and their locations vary from the outside to the inside of the girders. Since the stiffeners are not critical to the design or testing of these bridge decks, and to simplify the drawings, the only stiffeners shown are those at the ends and where the diaphragms attach. These stiffeners are seen in Figure 3.24 with distances to the ends of the girders and an annotation indicating the diaphragm attachment.

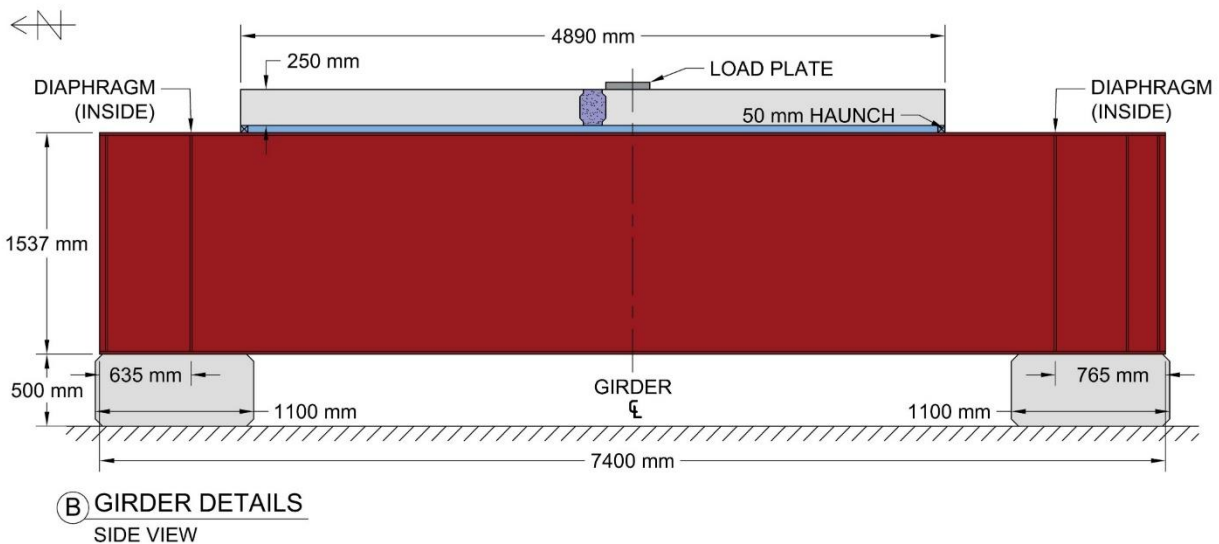


Figure 3.24 Girder details.

### 3.4.4 Connection Details

The UHPC connections were cast in the structural laboratory at the University of Manitoba. The Mix Systems, Inc. 0.59 m<sup>3</sup> (21 cubic feet) capacity paddle mixer was used to mix the UHPC. Once mixed, the UHPC was transferred into the large concrete crane bucket and the overhead crane lifted it to the bridge deck [see Figure 3.25]. The JPD's UHPC connections were cast on April 12, 2019, and the FPD's UHPC connections were cast on August 13, 2019.

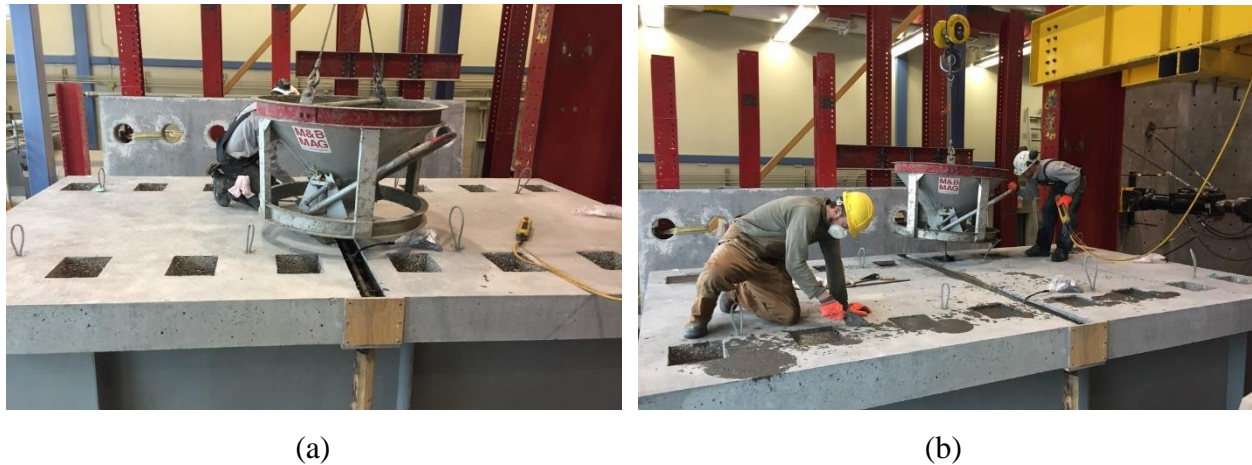


Figure 3.25 UHPC casting of JPD.



Figure 3.26 Deck joint formwork.

The only formwork required during casting the UHPC connections was for the joint of the JPD since the UHPC poured for shear pockets and haunch were contained by EVA foam glued to the top flange of the girders. A sheet of plywood was cut into pieces 254 mm wide to block the bottom and sides of the joint. Five 102 x 102 mm (4 x 4") posts were cut in 2 m lengths to hold up the plywood with screw jacks for a tight seal [see Figure 3.26].

### 3.4.4.1 Haunches

The Eden Lake bridge was designed with a 50 mm haunch between the top of the girder flanges and the bottom of the precast concrete decks. To achieve the haunch, EVA foam was glued to the edges of the girder flanges to contain the UHPC during the shear pocket casting. The EVA foam was 75 mm tall x 50 mm wide, allowing 25 mm of vertical compression to create a tight seal upon deck placement, preventing leakage of the wet UHPC during casting. As the EVA foam would not be able to support the deck slabs unaided, four nuts were welded along the centerline of both girder flanges and A325 bolts were screwed into the nuts until a height of 50 mm.

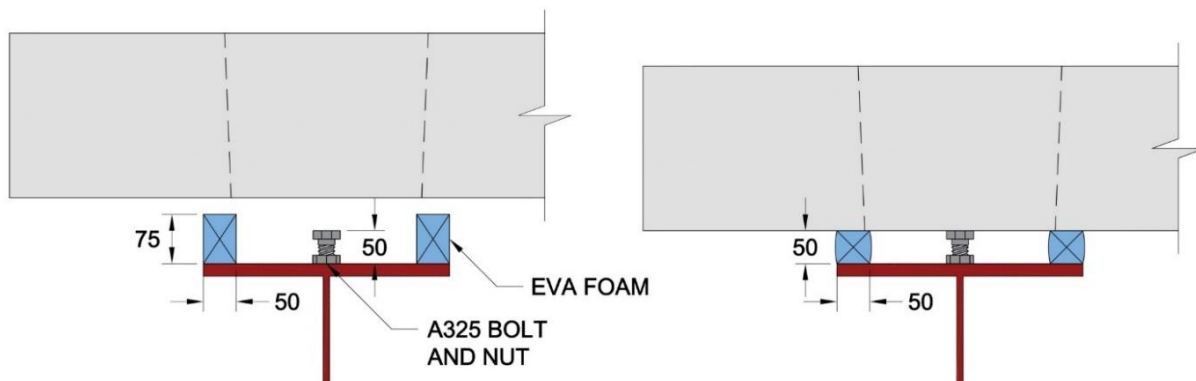


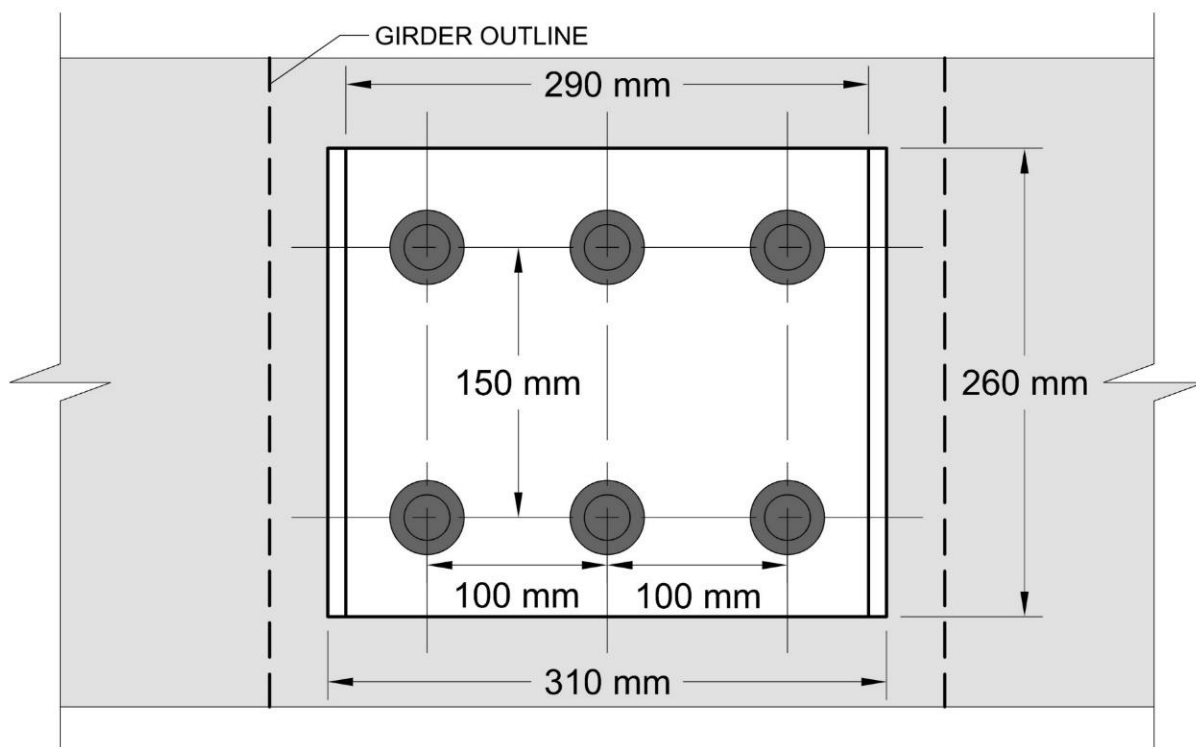
Figure 3.27 Precast deck placement for 50 mm haunch.



Figure 3.28 The bridge deck haunch construction: (a) EVA foam installation; (b) placing FPD.

### 3.4.4.2 Shear Pockets

As aforementioned, the shear pocket shape for the small-scale experimental specimens was chosen based on the design for the bridge deck's shear pockets. Therefore, the same sized shear pocket blockouts were used during deck casting of the JPD [see Figure 3.7]. The shear pockets were reinforced with 6 stud groupings; the same 6-stud layout as for the push-out shear pocket specimens seen in Figure 3.29.

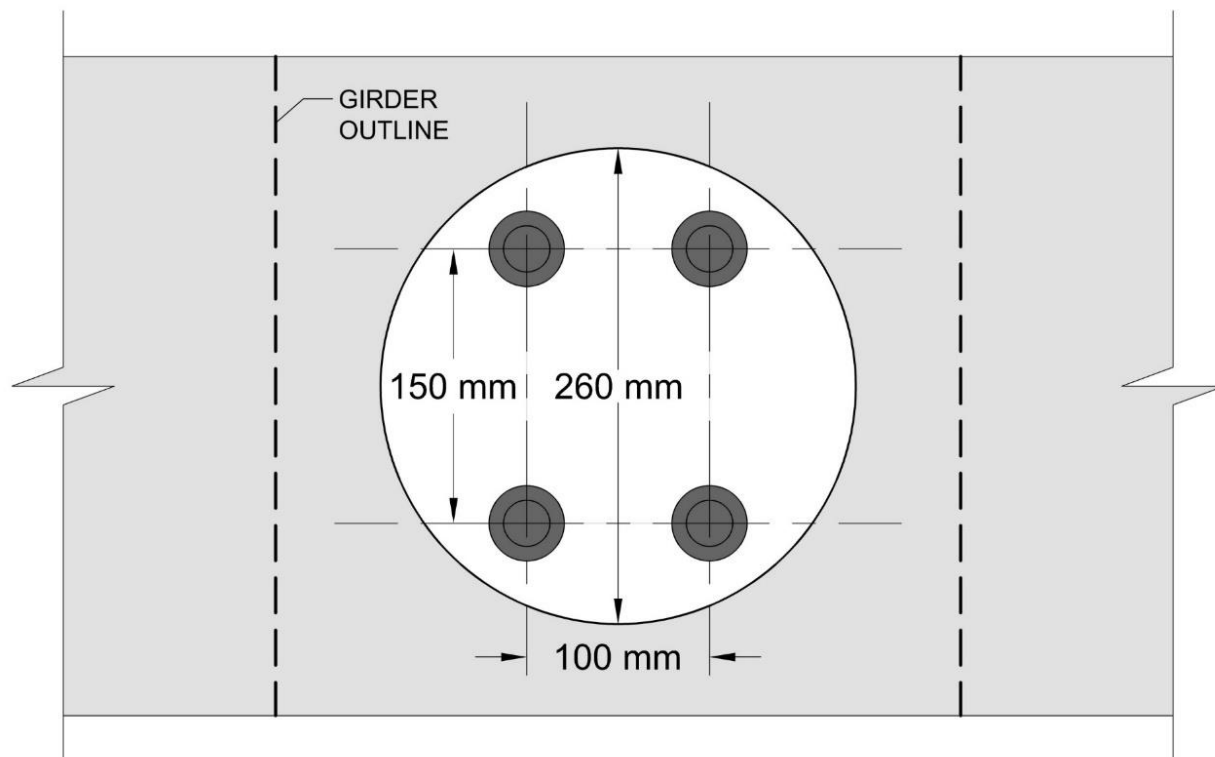


**SHEAR POCKET**  
TOP VIEW

Figure 3.29 Bridge deck JPD shear pocket layout.

Due to a misunderstanding with the shop drawings, the shear pockets were not blocked out during casting of the FPD. Di-Tech International was hired to cut shear pockets in the deck slab. For ease of cutting and cost, the pockets cut in the deck were circular. The spacing of the deck

reinforcement governed the shear pocket diameter. A circular shear pocket would not fit the same shear stud reinforcement; however, it was determined 4 shear studs could fit with the same stud and row spacing. Considering both factors, the shear pockets were cut to be the same width as the rectangular ones at 260 mm. Figure 3.30 shows the new pocket shape with the 4-shear stud grouping. Another noteworthy difference is since the shear pockets on the FPD were cut, the resulting surface was smooth, unlike the rectangular ones that were rough due to the retarding agent on the blockouts during casting; therefore, the bond strength between the UHPC and the RC would not be as strong as in the JPD shear pockets.



### CIRCULAR SHEAR POCKET

#### TOP VIEW

Figure 3.30 Bridge deck JPD shear pocket layout.

The full shear pocket layout details for the FPD and JPD can be seen in Figure 3.31 and Figure 3.32, respectively.

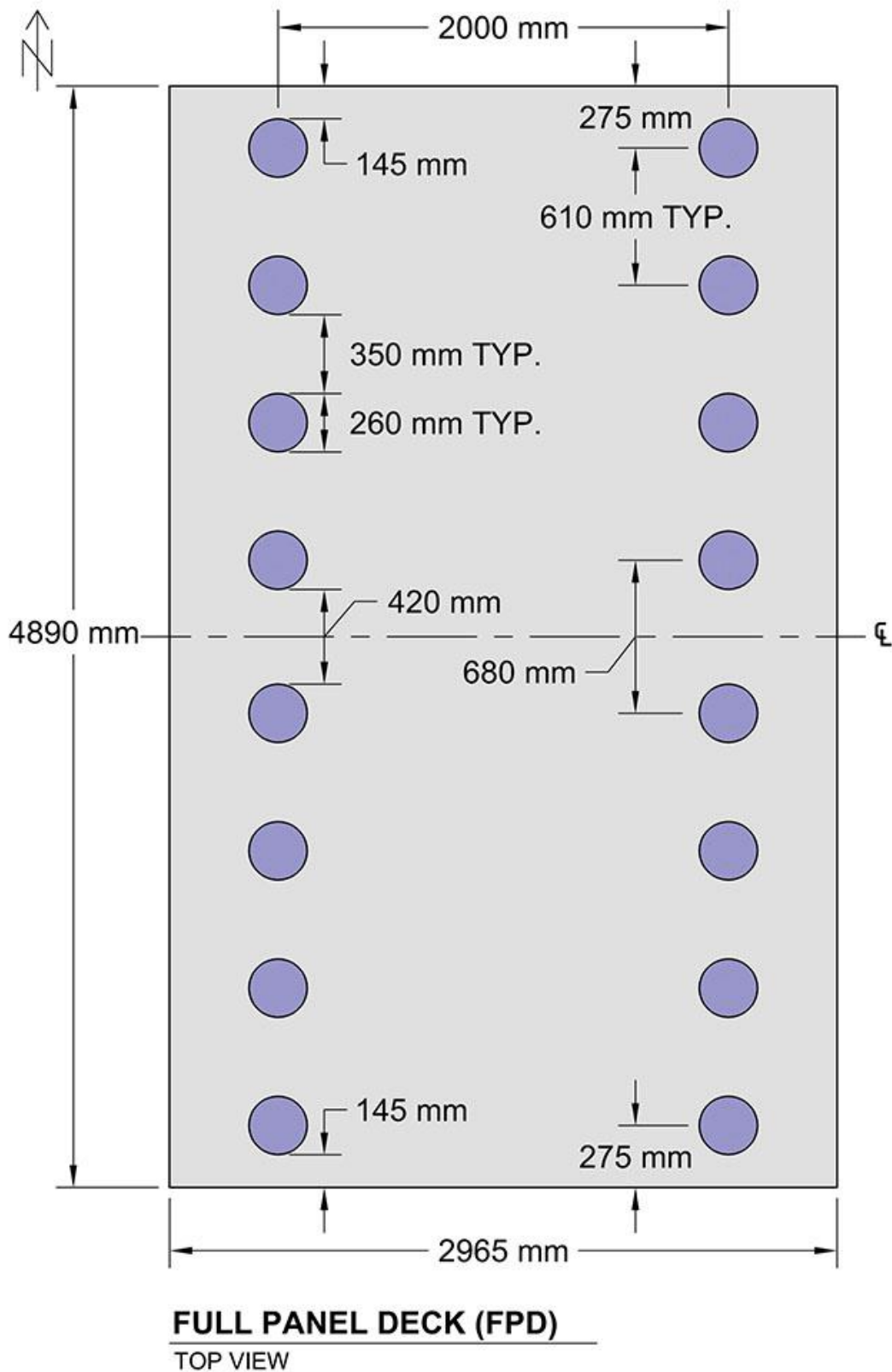


Figure 3.31 FPD shear pocket layout.





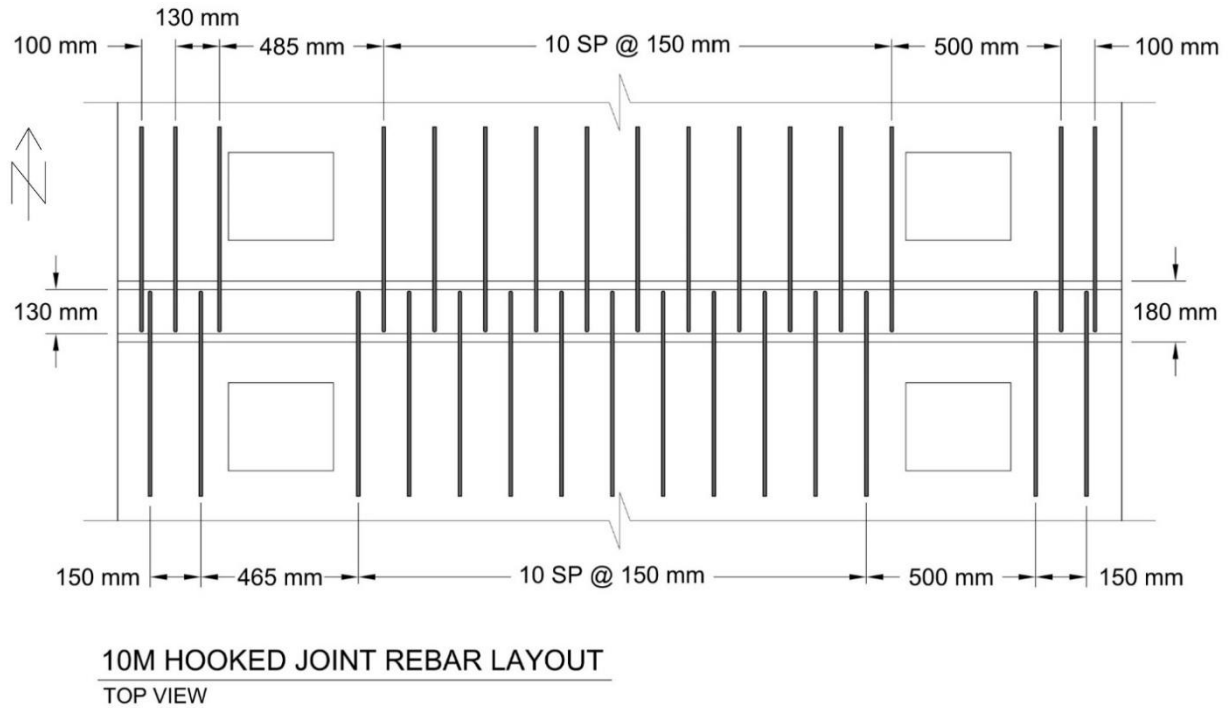


Figure 3.34 JPD transverse deck joint details showing only the 10M hooked rebar of the joint.

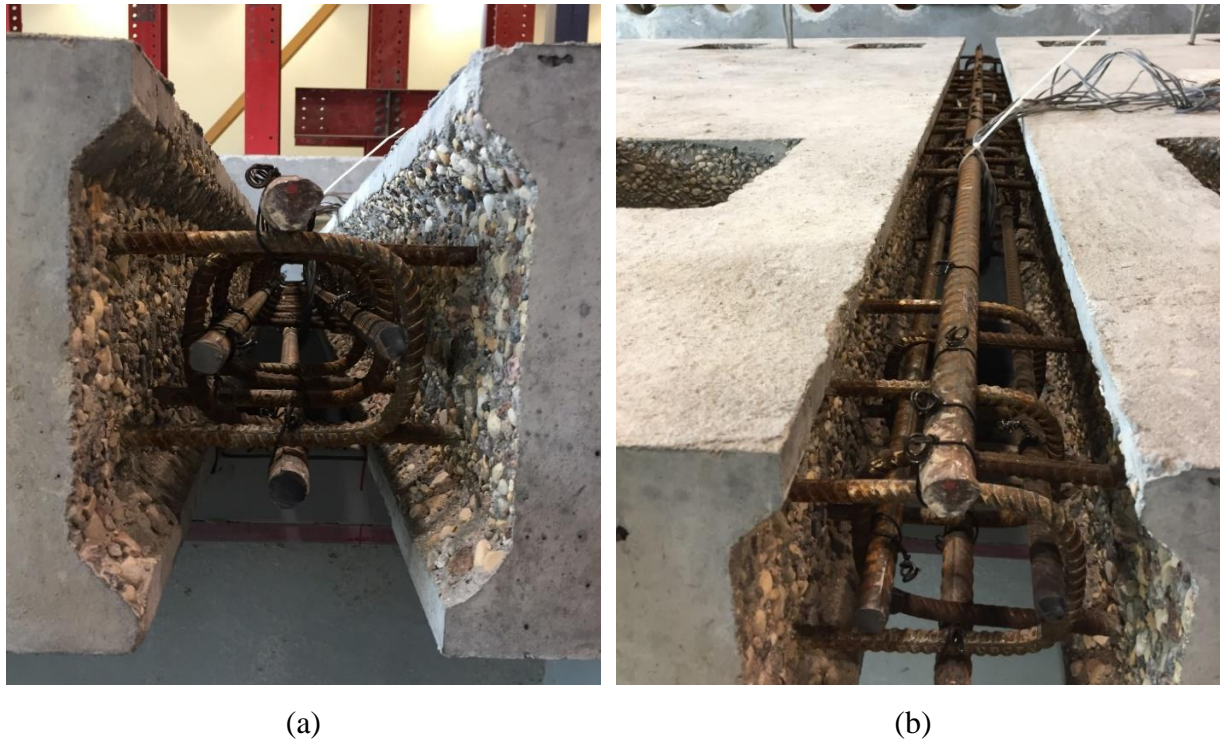


Figure 3.35 JPD transverse deck joint.

### 3.4.5 Test Method and Setup

#### 3.4.5.1 Load Apparatus Details

The main goal in the bridge deck testing was to understand how the load transfers across the UHPC deck-to-deck joint. Therefore, rather than place the load plate directly over the joint center, it was decided to place it adjacent to the joint interface. The load plate was aligned with the inner face of the joint, rather than the opening [Figure 3.36].

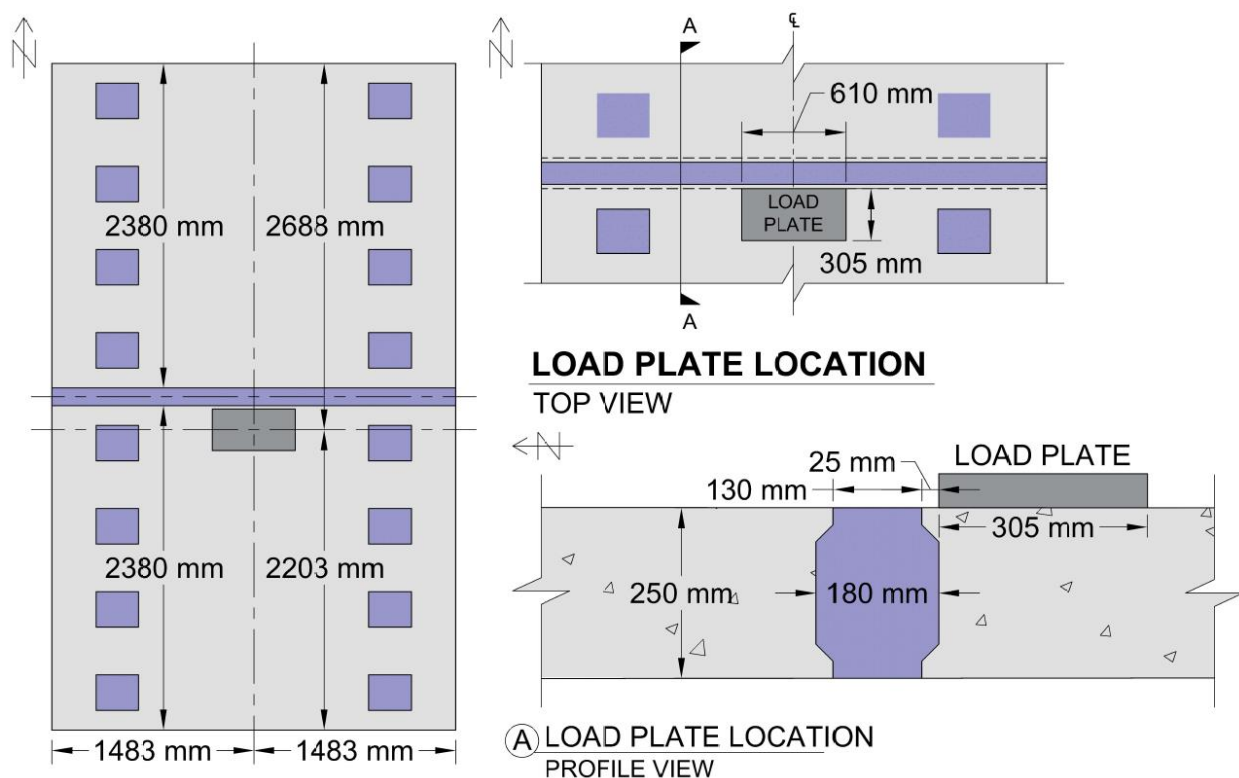


Figure 3.36 Load plate location.

The bridge decks were tested statically until punching failure occurred. The decks were loaded with a hand operated hydraulic jack, connected to a cylindrical spring piston with a capacity of 5000 kN. Once the first crack appeared the loading was paused every 200 kN to mark crack progressions until a load of 1400 kN for both decks. After this point the loading continued without interruption until complete failure. The load frame used consisted of two heavy duty W-section

steel columns with a beam across from which to mount the load cell. To secure the load frame for testing, each column had two 25 mm diameter bars prestressed at 3175 kgs to the strong floor.

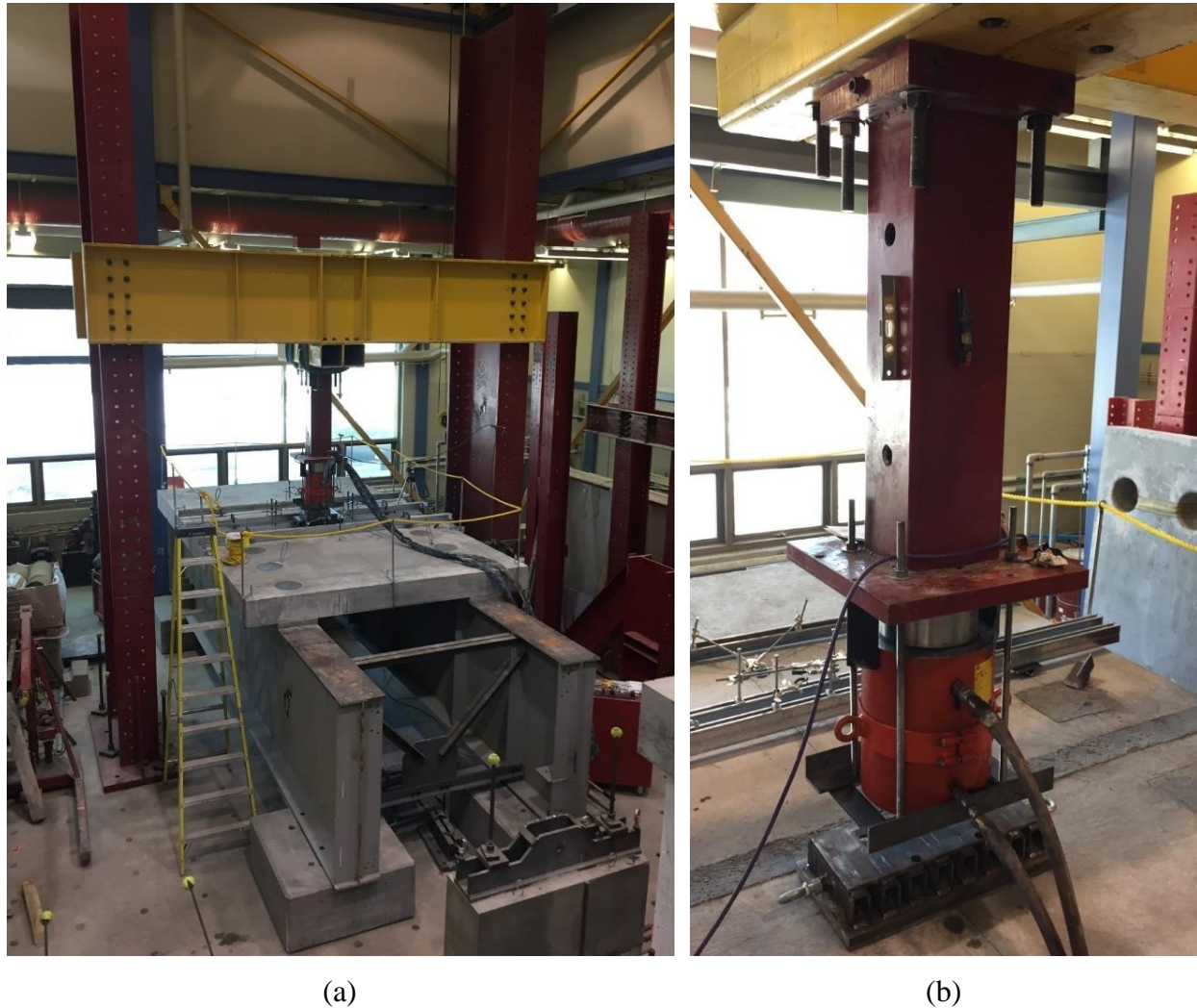


Figure 3.37 Load setup for deck testing: (a) overall test setup, (b) close-up of load cell and load plate.

#### 3.4.5.2 Instrumentation Details and Layout

All instrumentation locations were kept consistent between the JPD and FPD samples, despite no actual joint in the FPD, to allow for direct comparisons between the results. The deck displacements, crack development, concrete strains, internal strains on the joint rebar, and the

internal strains on the shear studs were measured during testing. All instrumentation wires were tied into a data acquisition system (DAQ).

LVDTs were placed along the bridge deck centerlines and two rows transversely along both joint-deck interfaces [see Figure 3.38]. Though the figure shows the JPD, the LVDT locations on the FPD are the same. The LVDTs were mounted to clamps attached to three channels placed transversely between LVDTs 1 and 2, along the joint centerline, and between LVDTs 9 and 10. For simplicity, this is not shown in Figure 3.38.

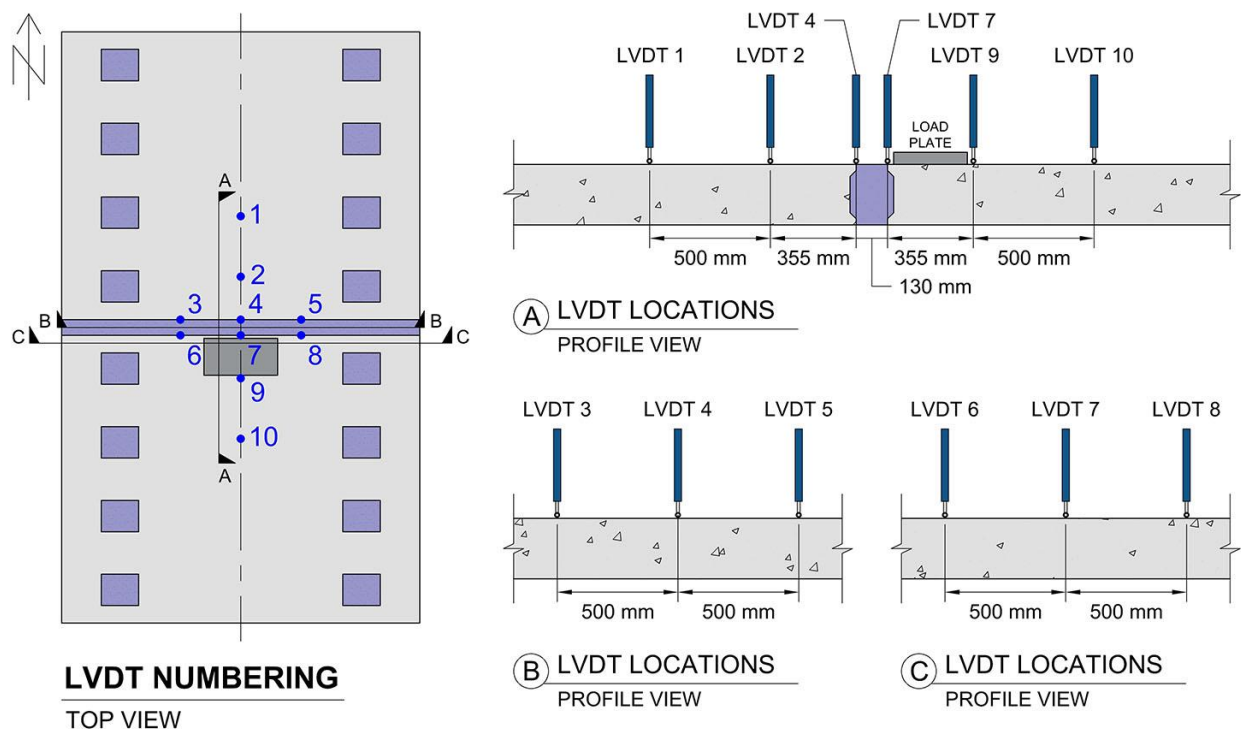


Figure 3.38 LVDT setup for JPD and FPD.

Pi-gauges were used to read the crack widths on the bottom of the bridge decks. Prior to testing, two pi-gauges were installed across the joint-deck interfaces on the JPD. Since the gauges were too long for both to fit on the centerline while intersecting the joint-deck interface, they were staggered 20 mm apart [see Figure 3.39]. The pi-gauges were installed at the same locations on the bottom of the FPD, even though there was no joint interface, in order to take comparable

readings to the JPD. On both decks a third pi-gauge was placed perpendicular to the first crack. The first crack on both decks occurred underneath the load plate, therefore the pi-gauges are in similar locations as shown in Figure 3.39. The pi-gauge nomenclature for the results section will herein refer to the gauge across the northern joint-deck interface as “PGN” and similarly the gauge across the southern joint-deck interface is “PGS”. The pi-gauges added at the first visible crack are referred to as “PGFC”.

Though the pi-gauge readings are labelled as crack widths, the JPD-PGN and PGS are measuring the separation across the deck-joint interface indicating if debonding occurred.

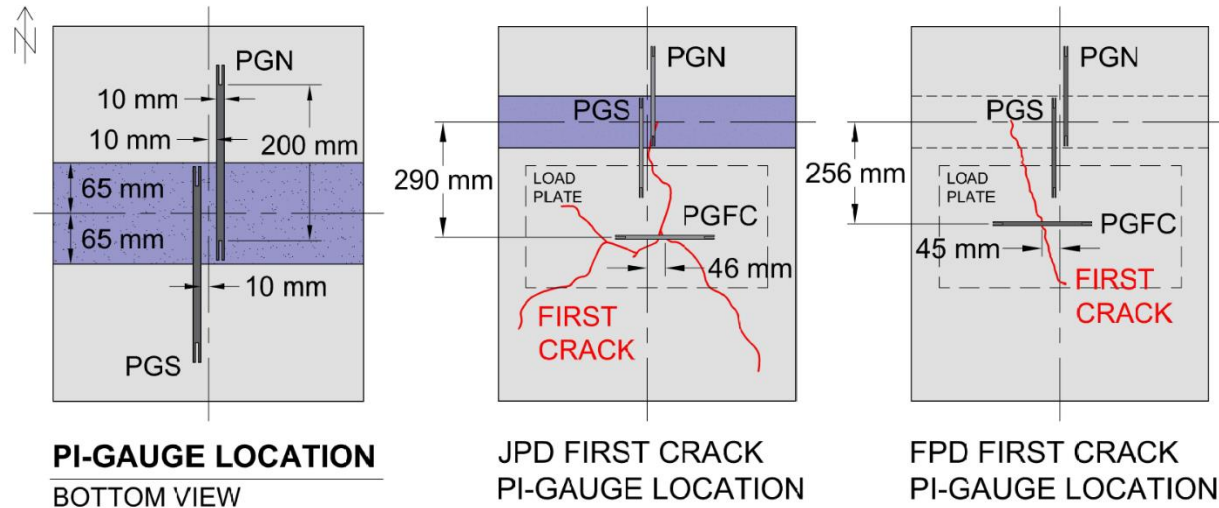


Figure 3.39 Pi-gauge locations for JPD and FPD.

The concrete strains were measured with three 200 mm long, 350  $\Omega$  strain gauges glued to the surface of each bridge deck. One gauge was placed 10 mm north of the deck joint, one in the middle of the joint, and one 10 mm south of the deck joint. The gauge locations were chosen to give insight into the strain transfer across joint and through the UHPC. The FPD locations were chosen the same, despite there being no UHPC joint present, to allow direct comparison in the shears at each location on the JPD. Since the LVDTs are along the deck centerline and joint-deck interfaces, the concrete strain gauges were offset from the centerline by 10 mm. Figure 3.40

illustrates the concrete gauge locations for both decks, including the LVDTs in proximity. The pictures in Figure 3.41 shows how close the instrumentation was in reality. The concrete strain gauges will be referred to as CSG-N, J, and S, as seen in Figure 3.40 referring to their locations of north panel, joint, and south panel, respectively.

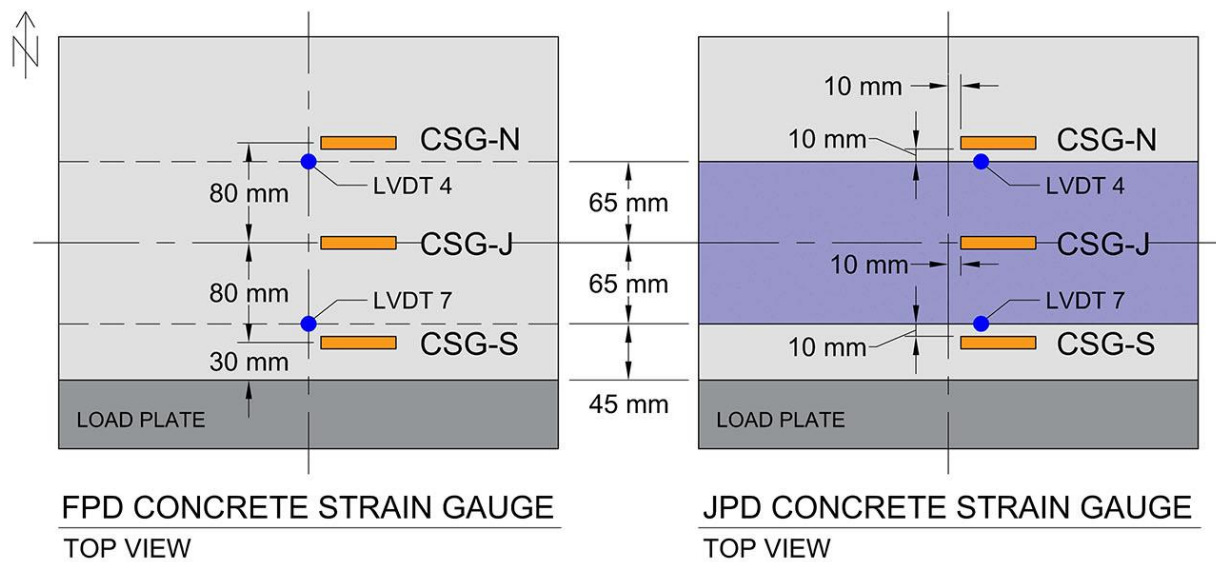


Figure 3.40 Concrete strain gauge locations.



Figure 3.41 (a) CSG 1 and LVDT 4, (b) CSG 3 and LVDT 7.

Prior to casting the JPD and FPD some of the rebar was instrumented with 6 mm long, 350  $\Omega$  strain gauges. The strain readings across the joint of the JPD were valuable to understanding the

transfer of load from the RC panel through the UHPC joint to the connected RC panel. Therefore, the three centermost 10M hooks from each JPD panel were instrumented. The gauges were installed 50 mm from the joint interface within the RC for both JPD panels, and 50 mm into the joint. The strain gauges in the RC panels were instrumented prior to the panel casting at LafargeHolcim, whereas the strain gauges within the joints were instrumented at the University of Manitoba prior to casting the UHPC joint. The middle 10M hook had gauges on the bottom face of the top and bottom of the hooked bar, and the bars on either side only had gauges on the bottom face of the bottom of the hooks [see Details A and B of Figure 3.42].

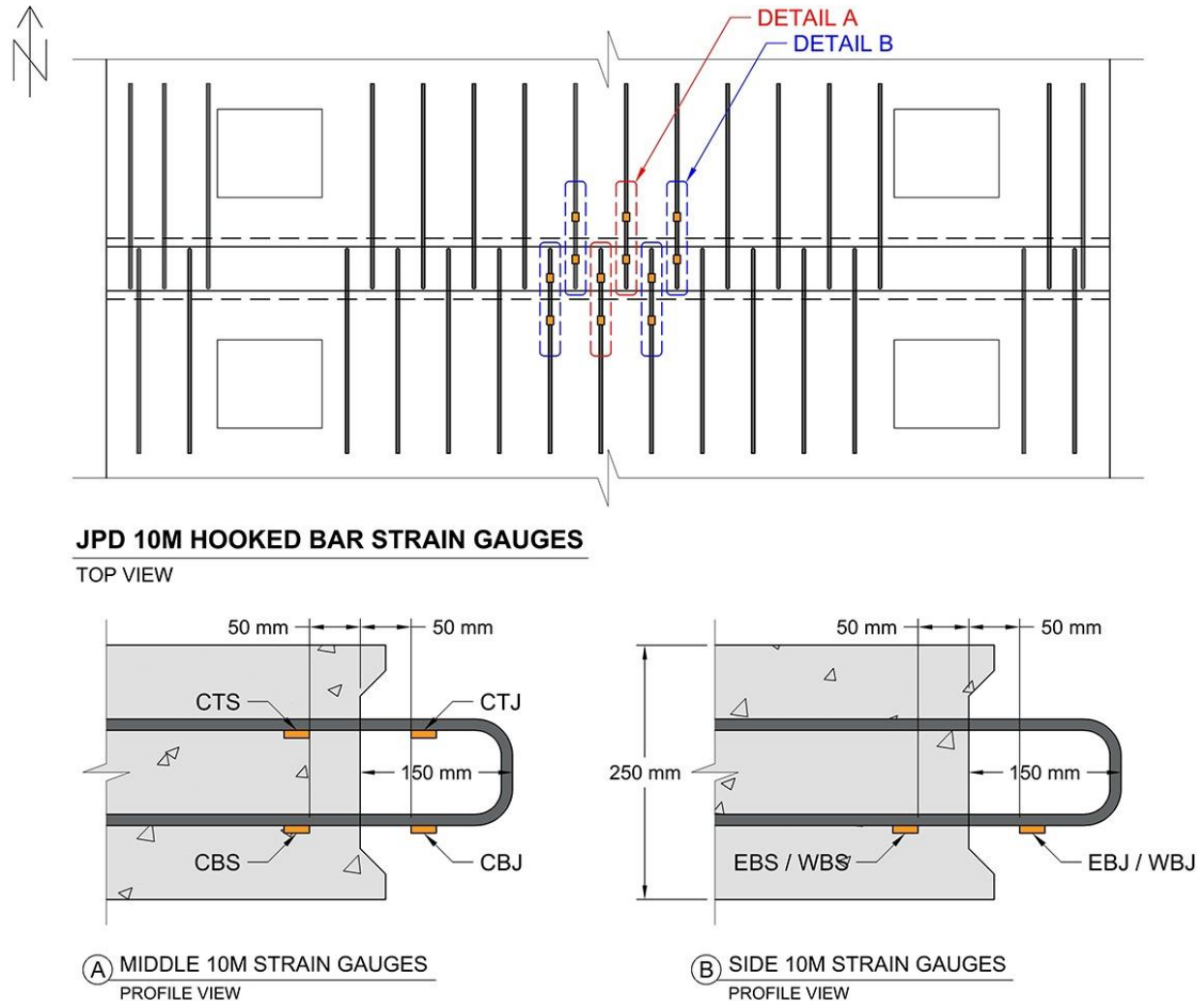


Figure 3.42 JPD internal rebar strain gauge instrumentation.

The 10M hooks located in the center of the FPD were instrumented with strain gauges similar to the JPD; however, since there was no UHPC joint, there was only one set of strain gauges glued to the bars [see Figure 3.43]. The two transverse 15M bars along the “joint” location were instrumented with strain gauges on the bottom face at the center of the bars in the FPD only.

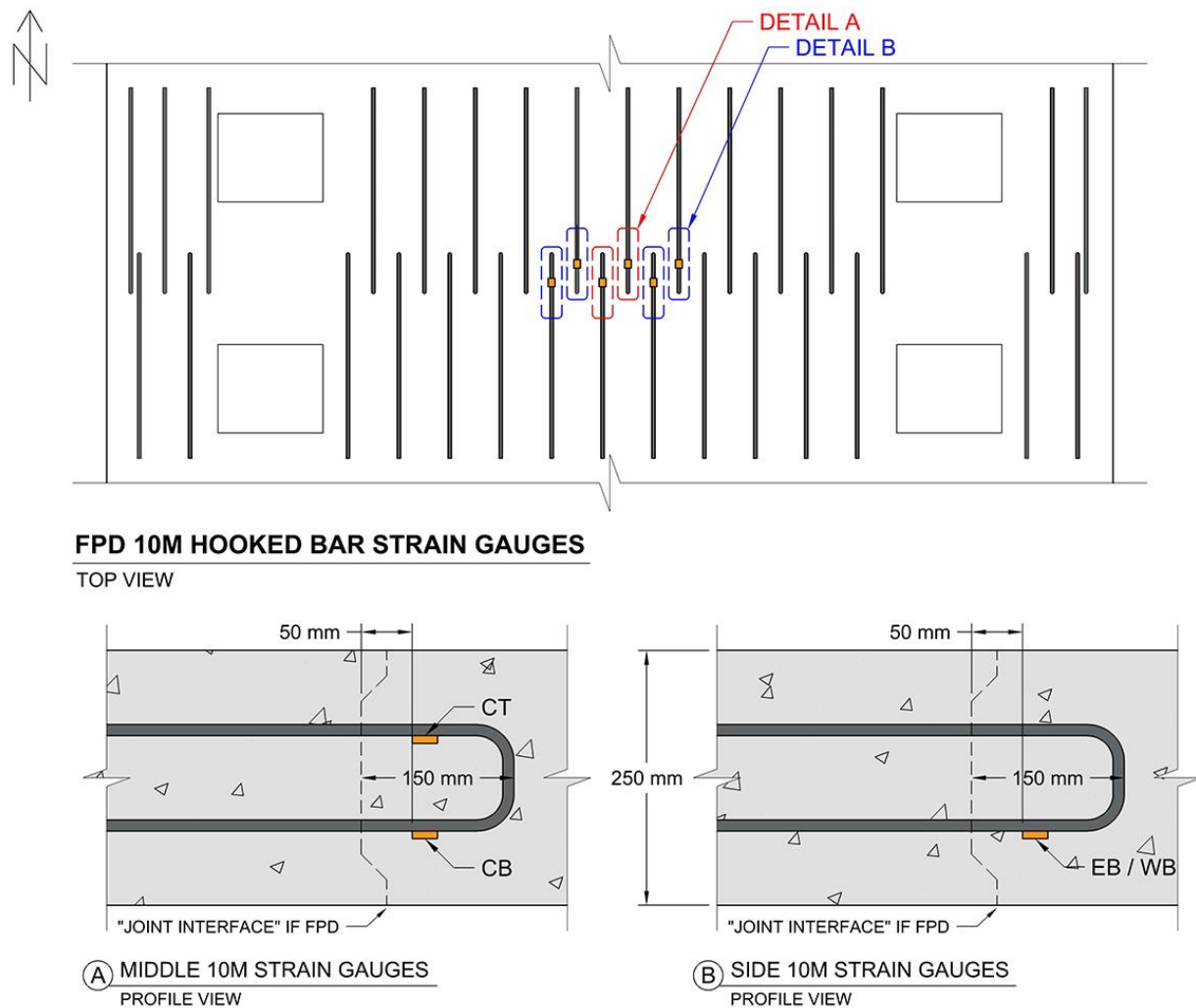


Figure 3.43 FPD internal rebar strain gauge instrumentation.

In the results section the gauges will be referred to by the nomenclature shown in Figure 3.42 and Figure 3.43. The center bars are designated with a “C” and the side bars with an “E” or “W” for east or west side to the center bar. The “T” refers to top of the 10M hook, while “B” refers to the bottom. Similarly, the “S” vs. “J” refers to whether the strain gauge is within the slab or the joint.

After casting, the bridge decks were stored outside at the LafargeHolcim plant, prior to being shipped to the University of Manitoba for testing. The strain gauge locations were labelled on the wire itself, and with a tag adhered to the end of the wire. Unfortunately, due to the exposure to weather, both sets of labels were faded and torn from the strain gauge wires for both bridges. Since the JPD was cast in two half panels, the joint rebar was still exposed and the strain gauge locations were determined; the top and bottom of each hooked reinforcing bar was tapped while the DAQ read the resulting strains. The joint strain gauges were instrumented prior to casting therefore the locations within the joints were known.

Despite efforts to determine the strain gauges exact locations within the FPD, it could not be done. The strain gauge wires were run to two separate exit points on the FPD deck; one contained the four strain gauge wires from the 10M hooks on the southern half of the deck centerline, and the other contained the remaining six strain gauge wires for the 10M hooks on the northern half of the deck and the 15M transverse bars. Therefore, it is at least known which strain gauges correspond to which half of the bridge deck, but not which reinforcing bar the strain gauge was reading. The strain gauges on the two 15M transverse bars could not be distinguished from the gauges on the 10M hooks either.

One wire out of each grouping was not working, therefore only three strain gauges from the South half and five from the North half of the FPD were tied into the DAQ during testing. The results present the data with arbitrary labelling for the general location within the FPD; N1, N2, N3, N4, and N5 for the northern half and S1, S2, and S3 for the southern half.

Select shear studs were also instrumented with 6 mm long, 350  $\Omega$  strain gauges. The four shear pockets closest to the bridge deck's center had each one gauge on each shear stud, for a total of 16 strain gauges. The gauges were adhered to the surface of the stud facing inwards towards the

loading point; the west girder had gauges on the east face of the studs and those on the east girder had gauges on the west face of the studs [see Figure 3.44]. The shear studs were instrumented in this manner to face the direction of the applied load.

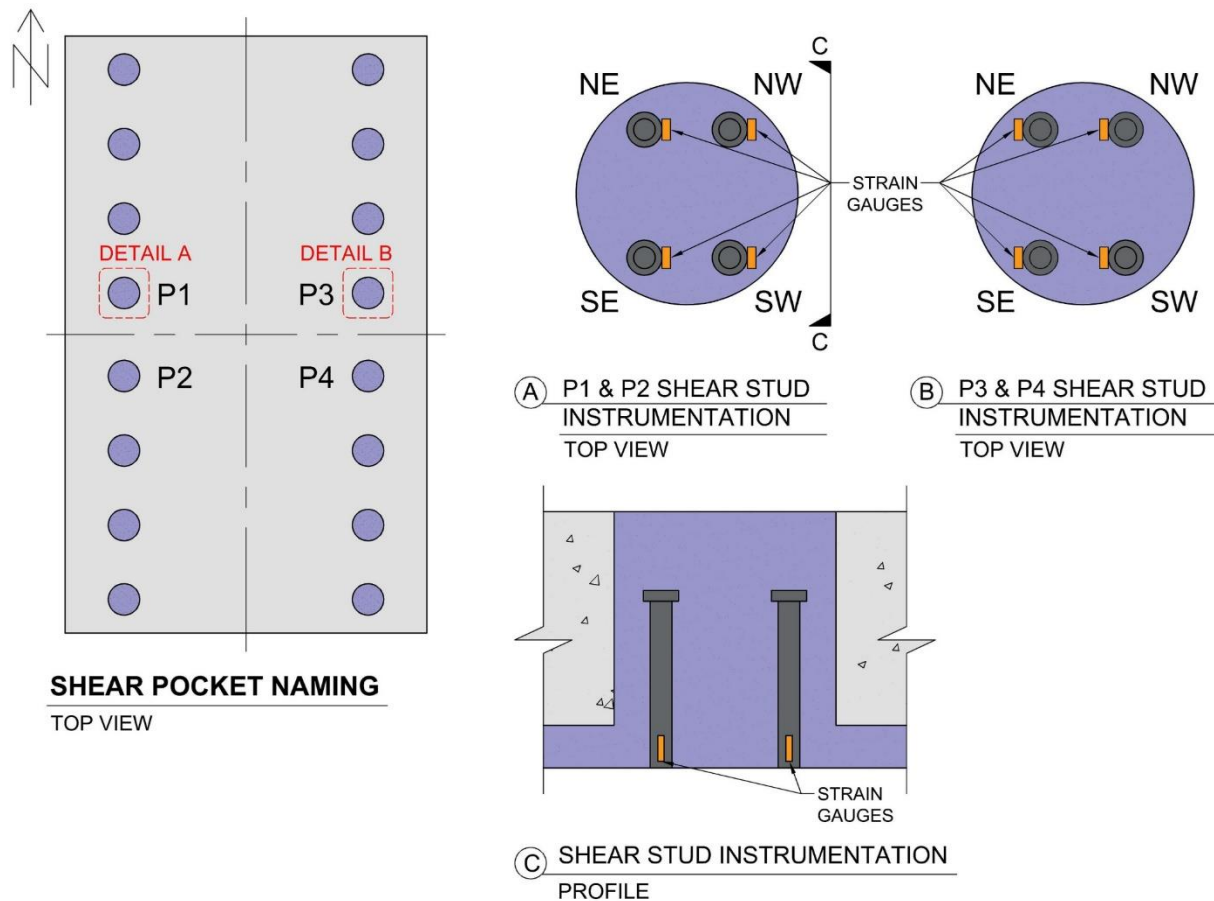


Figure 3.44 FPD shear stud strain gauge locations.

In the results section, the shear stud strain gauges will be referred to by their pocket nomenclature and the stud name, as seen in Figure 3.44. For example, the gauges of the studs in the shear pocket P1 will be P1NE, P1NW, P1SE, and P1SW.

## Chapter 4 Experimental Results and Analysis

### 4.1 Introduction

The experimental program test results are presented in graphical and tabular format. The shear pocket specimen results are compared to each other, and to the shear stud strains from the FPD bridge deck. The bridge deck results are analysed and compared to understand the capacity and performance differences between the full panel and UHPC jointed half panels. The results of the individual material testing are also discussed below.

### 4.2 Material Testing

#### 4.2.1 Shear Pocket Concrete

The strengths of the RC slabs and UHPC pockets within the shear pocket specimens are tabulated in this section. The compressive and tensile strengths of the RC slabs are reported in Table 4.1. The SP6 specimens averaged compressive strengths of 35.5 MPa at 28-days and 40 MPa on the respective test days. The SP3 specimens averaged greater compressive strengths of 53.6 MPa at 28-days and 57.84 MPa on the test days. The average tensile strength of the RC on the test days was 3.98 MPa and 3.15 MPa for the SP6 specimens and SP3 specimens, respectively. Unfortunately, the SP0 RC strength data is unavailable.

Table 4.1 RC Slab Strengths

Day	Compressive Strength (MPa)			Tensile Strength (MPa)		
	SP6	SP3	SP0	SP6	SP3	SP0
28	35.50	53.60	53.60	–	–	–
Test Day	40.00	57.84	<i>unavailable</i>	3.98	3.15	<i>unavailable</i>

The push-out tests were completed seven days after casting the UHPC shear pocket for the SP6 and SP3 specimens. The SP0 specimens were tested on day ten due to the availability of the laboratory equipment and support technicians, therefore the compressive strength is slightly greater than for the SP6 and SP3 specimens. The SP6 and SP3 specimens had similar strengths with average compressive strengths of 127.15 MPa and 121.15 MPa, respectively. Within the three extra days the SP0 specimen UHPC attained an average compressive strength of 146.92 MPa.

Table 4.2 UHPC Shear Pocket Compressive Strengths on Test Day

Specimen	Compressive Strength (MPa)	Average Compressive Strength (MPa)
SP6-1	125.0	126.43
SP6-2	125.5	
SP6-3	128.8	
SP3-1	120.2	121.15
SP3-2	122.1	
SP0-1	144.83	146.92
SP0-2	149.00	

#### 4.2.2 Bridge Deck Concrete

LafargeHolcim completed the tests at release, 3-day, 7-day, 14-day and 28-day strengths. The test-day cylinders were tested at the University of Manitoba on the same day as the bridge deck tests. The concrete order for bridge deck panels was for 45 MPa in compression at 28-day strength, however, the strength at 28-days was nearly double at 84.27 MPa, 81.17 MPa, and 84.30 MPa for the FPD, and the JPD North and South panels, respectively [see Table 4.3]. During the delay between casting the bridge deck panels and casting the UHPC connections to the support girders

for testing, the concrete strength decreased to 68.42 MPa, 68.06 MPa and 67.41 MPa for the JPD North panel, JPD South panel, and FPD, respectively. Table 4.3 has the results for the average of the compression cylinder tests.

Table 4.3 Regular Concrete Compression Cylinder Testing

Deck Panel	Compressive Strength (MPa)					Test-Day‡
	<i>Tested by LafargeHolcim*</i>					
	Release†	3-Day	7-Day	14-Day	28-Day	
FPD	37.30	53.53	62.77	79.00	<b>84.27</b>	67.41
JPD North	39.50	56.23	68.73	82.20	<b>84.30</b>	68.42
JPD South	36.00	57.00	66.33	72.83	<b>81.17</b>	68.06

\*LafargeHolcim water cured these cylinders, which is why they have a greater strength than the test-day.

†Release time was 16 hours after casting when the deck was removed from the formwork.

‡Test-day was at day 536 for the FPD, 423 for the JPD North panel, and 420 for the JPD-South panel.

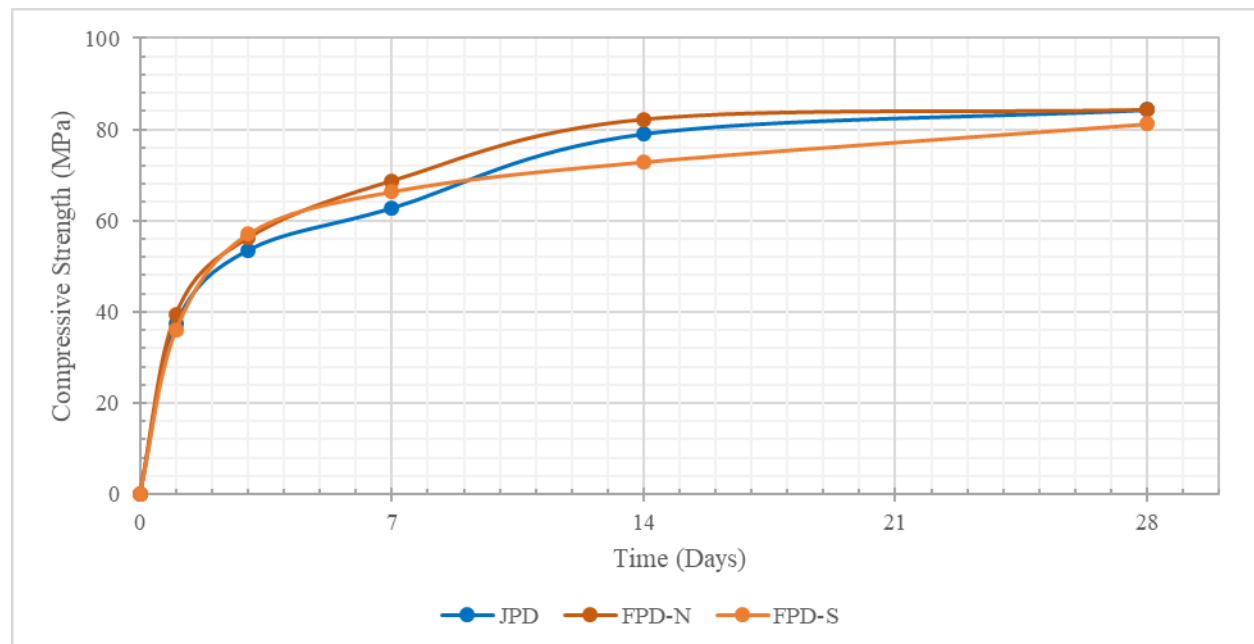


Figure 4.1 Bridge deck RC compressive strength development.

As aforementioned in Chapter 3, the UHPC connections of the JPD were cast with three batches and the FPD with two batches since it required less concrete. Concrete cylinders were cast for both compression and tension testing and the test data is presented in Table 4.4. The compression test results reveal a discrepancy between the strength of the UHPC cast for the JPD and the FPD. The results of the JPD compression cylinders had an average 3-day and 7-day compressive strengths of 105.49 MPa and 132.05 MPa, respectively. However, the FPD compression cylinders compressive strength results were significantly lower with an average 3-day and 7-day compressive strengths of 60.44 MPa and 72.34 MPa, respectively [Table 4.4].

Table 4.4 UHPC Deck Connection Compressive Strength Test Results

Day	Compressive Strength (MPa)						
	JPD UHPC Connections				FPD UHPC Connections		
	Batch 1	Batch 2	Batch 3	Average	Batch 1	Batch 2	Average
3	106.39	107.67	102.41	<b>105.49</b>	63.05	57.83	<b>60.44</b>
7	129.76	135.94	130.43	<b>132.05</b>	71.36	73.32	<b>72.34</b>
14	157.55	153.24	148.38	<b>153.05</b>	99.34	102.68	<b>101.01</b>
Test Day*	181.91	173.87	179.52	<b>178.43</b>	129.30	107.23	<b>118.26</b>

\*Test day for the JPD was at day 35, and day 24 for the FPD.

The UHPC cement was ordered in large quantities, since the research program included push-out testing and full-size deck testing, and was delivered on pallets with stacks of 340 kg canvas bags (five bags per pallet). The bulk bags would be advantageous on a construction site in which large batches of UHPC are cast, and all contents would be used within a short time frame. The shear pockets specimens were all cast prior to the bridge deck connections, therefore, the packaging protecting the UHPC canvas bags was opened. The delay in compressive strength development is

assumed to have resulted from the age of the UHPC cement and potential exposure to moisture. The second batch of the FPD demonstrates a slow strength increase, whereas the first batch appears to be increasing at a greater rate, approaching the expected compressive strengths with time [Figure 4.2].

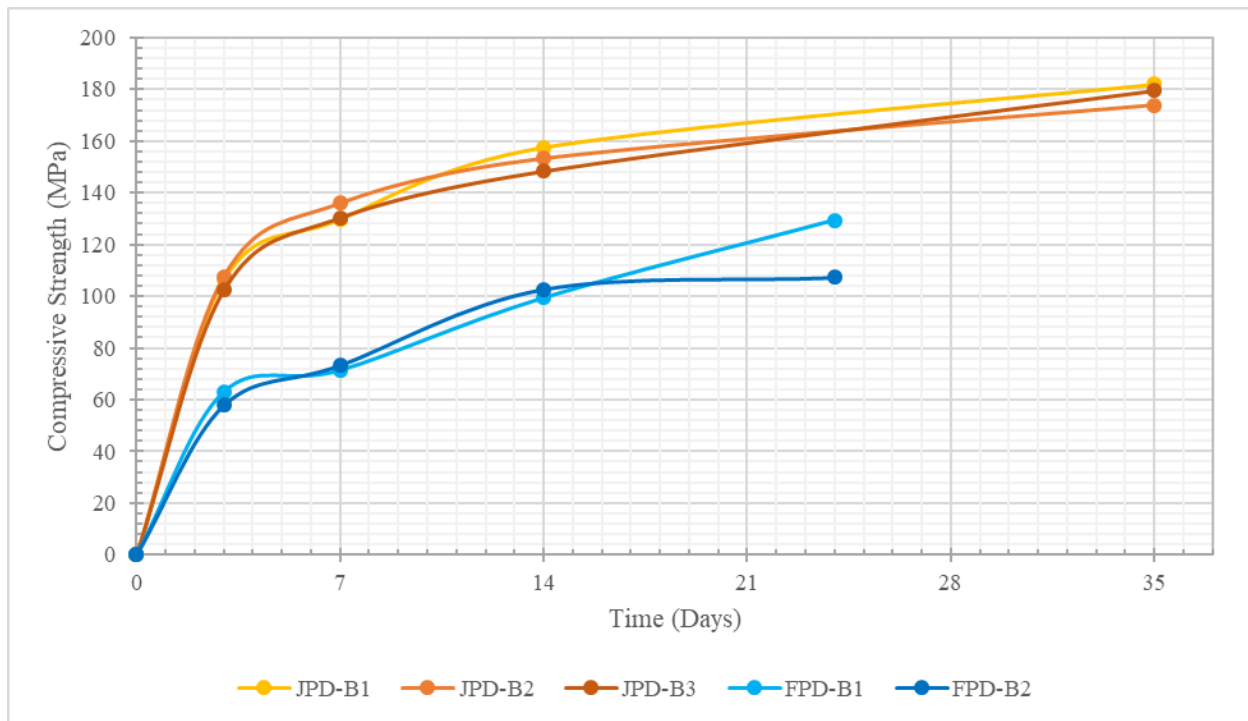


Figure 4.2 Bridge deck connection UHPC compressive strength development.

The UHPC tension cylinder results are seen in Table 4.5 and Figure 4.3. A high early tensile strength was seen in the first batch of the JPD UHPC of 28.29 MPa, compared to its 7-day strength of 22.10 MPa. There was also another peak at the 14-day strength of 29.1 MPa, which reduced to 27.38 MPa by the JPD test-day on day 35. The results from the other two batches of the JPD UHPC missed measuring the tensile strengths at these ages, and therefore added tension cylinders were cast for the FPD to observe if the JPD-UHPC-Batch 1 was an anomaly, or if the data would be replicated. Unfortunately, due to the UHPC cement issues discussed above, the tensile strengths

measured were low and any confirmation of the high early strength at 3-days could not be confirmed, nor denied.

Table 4.5 UHPC Deck Connection Tensile Strength Test Results

Day	Tensile Strength (MPa)						
	JPD UHPC Connections				FPD UHPC Connections		
	Batch 1	Batch 2	Batch 3	Average	Batch 1	Batch 2	Average
3	28.29	–	–	<b>28.29</b>	13.86	13.26	<b>13.56</b>
7	22.10	19.05	19.82	<b>20.33</b>	17.13	16.37	<b>16.75</b>
14	29.11	–	–	<b>29.11</b>	18.36	18.51	<b>18.43</b>
Test Day*	27.38	21.63	24.10	<b>24.37</b>	21.95	19.57	<b>20.76</b>

\*Test day for the JPD was at day 35, and day 24 for the FPD.

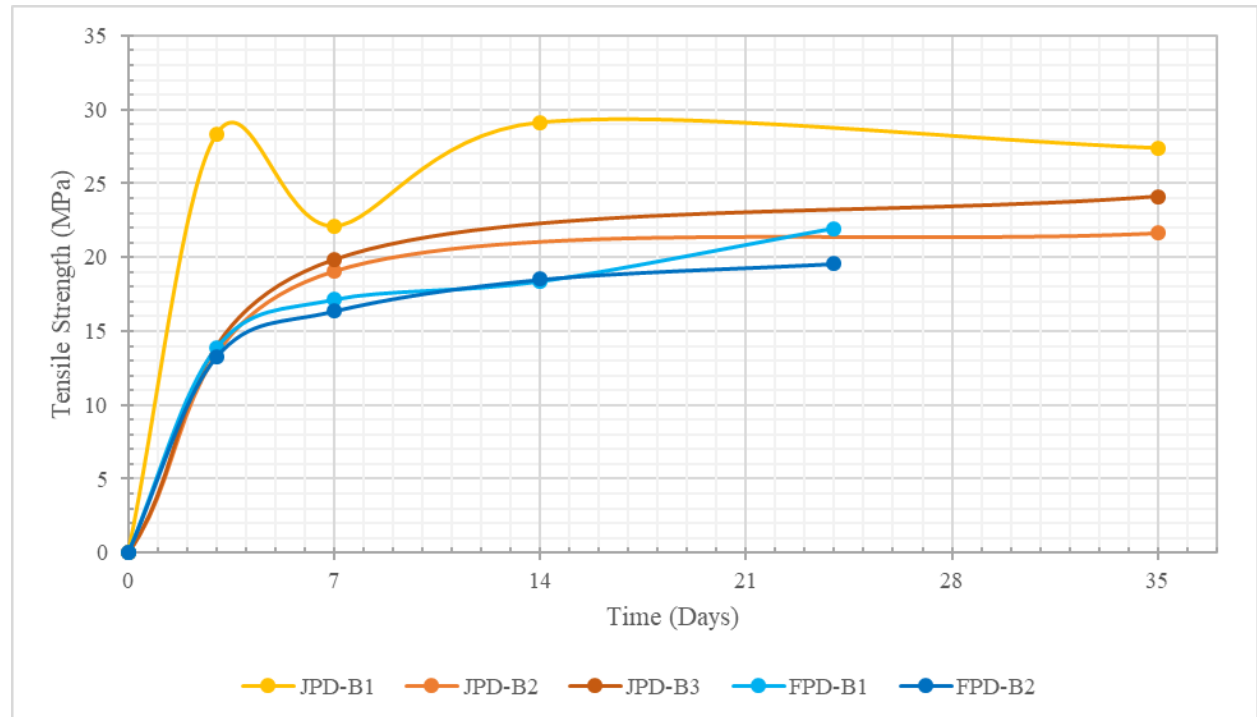


Figure 4.3 Bridge deck connection UHPC tensile strength development.

Figure 4.4 includes photographs of the RC and UHPC compression cylinders after testing. The first two photographs are of the same cylinder from the RC, and display a typical compression cylinder failure that would be defined as a Type 2 in the ASTM C39 compression cylinder test standard since there is one defined cone from one end and not from the other [8]. The UHPC cylinder failure is not as disruptive since the steel fibers hold the concrete together and prevent the cylinder from breaking apart. Photographs (c) and (d) are of different UHPC cylinder failures, and (e) is a close up on the cracking seen from another angle of the cylinder from (d).

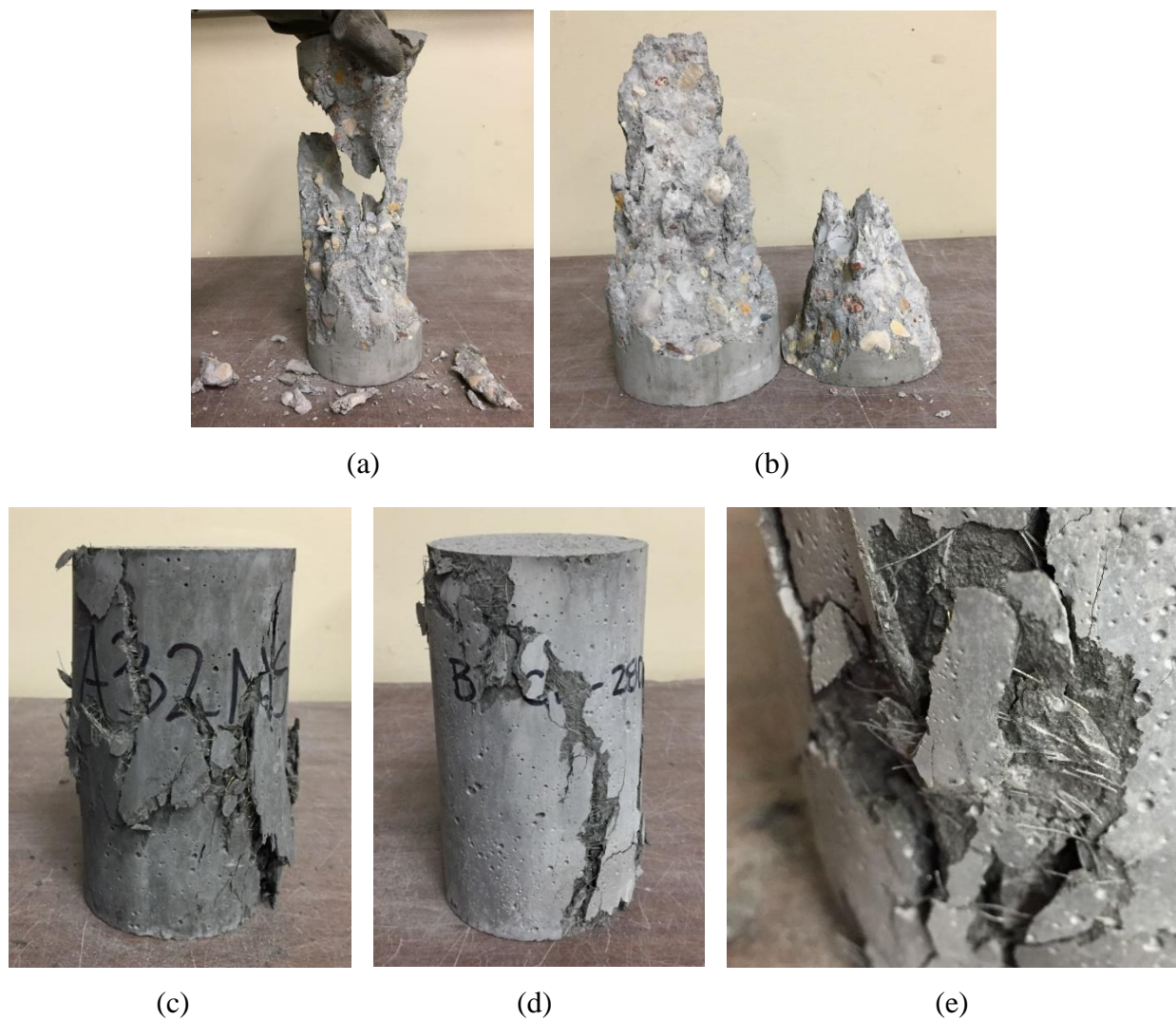


Figure 4.4 Compression cylinders after testing: (a) and (b) are RC, and (c) to (e) are UHPC.

### 4.2.3 Steel Shear Studs

The shear test results on the shear studs are presented below. The three studs failed at very similar loads for an average ultimate load of 336 kN and an average shear strength of 332 MPa [Table 4.6]. Due to the high strength and ductility of steel, the shearing surface is not a perfectly clean break, which can be seen in the photographs of Figure 4.6.

Table 4.6 Shear Stud Shear Strength Test Results

Shear Stud	Ultimate Load (kN)	Shear Strength (MPa)	Displacement at Ultimate (mm)	Displacement at Failure (mm)
SS1	340.24	315.27	3.66	7.15
SS2	330.50	329.3	3.71	5.97
SS3	335.57	313.3	3.83	6.78
<b>Average</b>	<b>336.44</b>	<b>331.98</b>	<b>3.73</b>	<b>6.63</b>

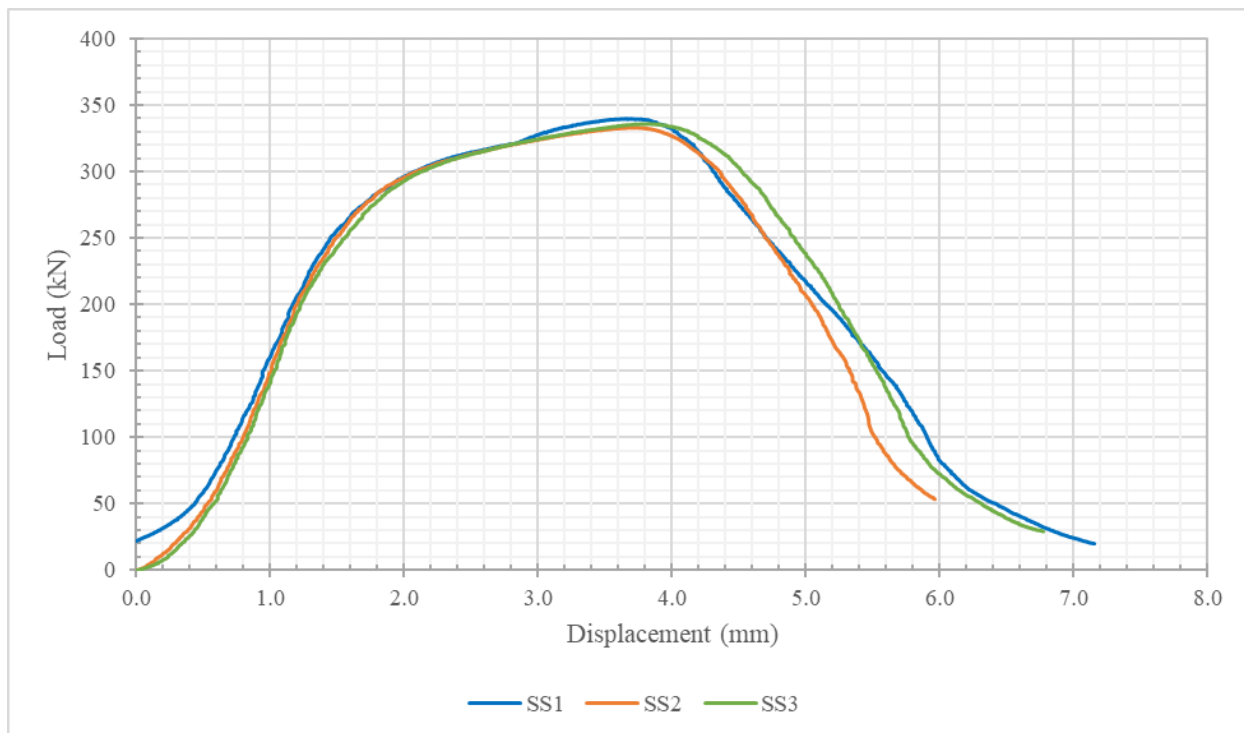


Figure 4.5 Shear stud shear tests displacement development.

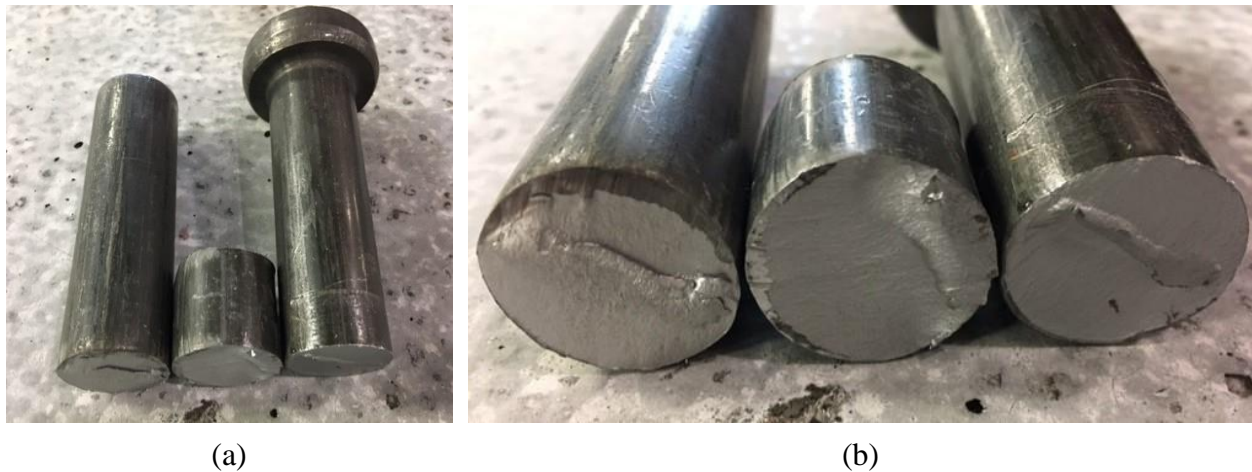


Figure 4.6 Shear stud shear failure.

The shear studs were also tested for their experimental tensile strengths. Five studs were tested in total. The first two had strain gauges at the base of the stud on opposing faces, as described in Section 3.2.2. The strain gauge results were recording strains of opposing signs, which indicates there was bending at the base of the stud. It is very difficult to weld the studs perfectly vertical to the base plates and any angles to the setup, no matter how small, would result in slight bending. Therefore, the strain gauge data was discarded and the strains were calculated by comparing the elongation to the gauge length of the extensometer. The remaining three shear studs were not instrumented with strain gauges and the strains were also calculated as described.

It was also challenging to accurately predict the area along the stud where the necking would occur. Only the TS2 stud failed within the gauge length of the extensometer, and therefore was the only data set that could be used to find the shear stud rupture load of 195 kN with a total elongation of 12 mm. The five studs' ultimate loads were within 5 kN of each other and averaged 263 kN, which gave the tensile strength of 520 MPa. The average strain at the ultimate load was 0.0504. The results for all five tension tests are in Table 4.7.

Table 4.7 Shear Stud Tensile Strength Test Results

Shear Stud	Ultimate Load (kN)	Rupture Load (kN)	Strain at Ultimate	Tensile Strength (MPa)
TS1	263.61	–	0.0532	520.24
TS2	265.84	195.00	0.0630	524.64
TS3	261.10	–	0.0398	515.28
TS4	263.96	–	0.0519	520.93
TS5	261.87	–	0.0439	516.81
<b>Average</b>	<b>263.28</b>	<b>195.00</b>	<b>0.0504</b>	<b>519.58</b>

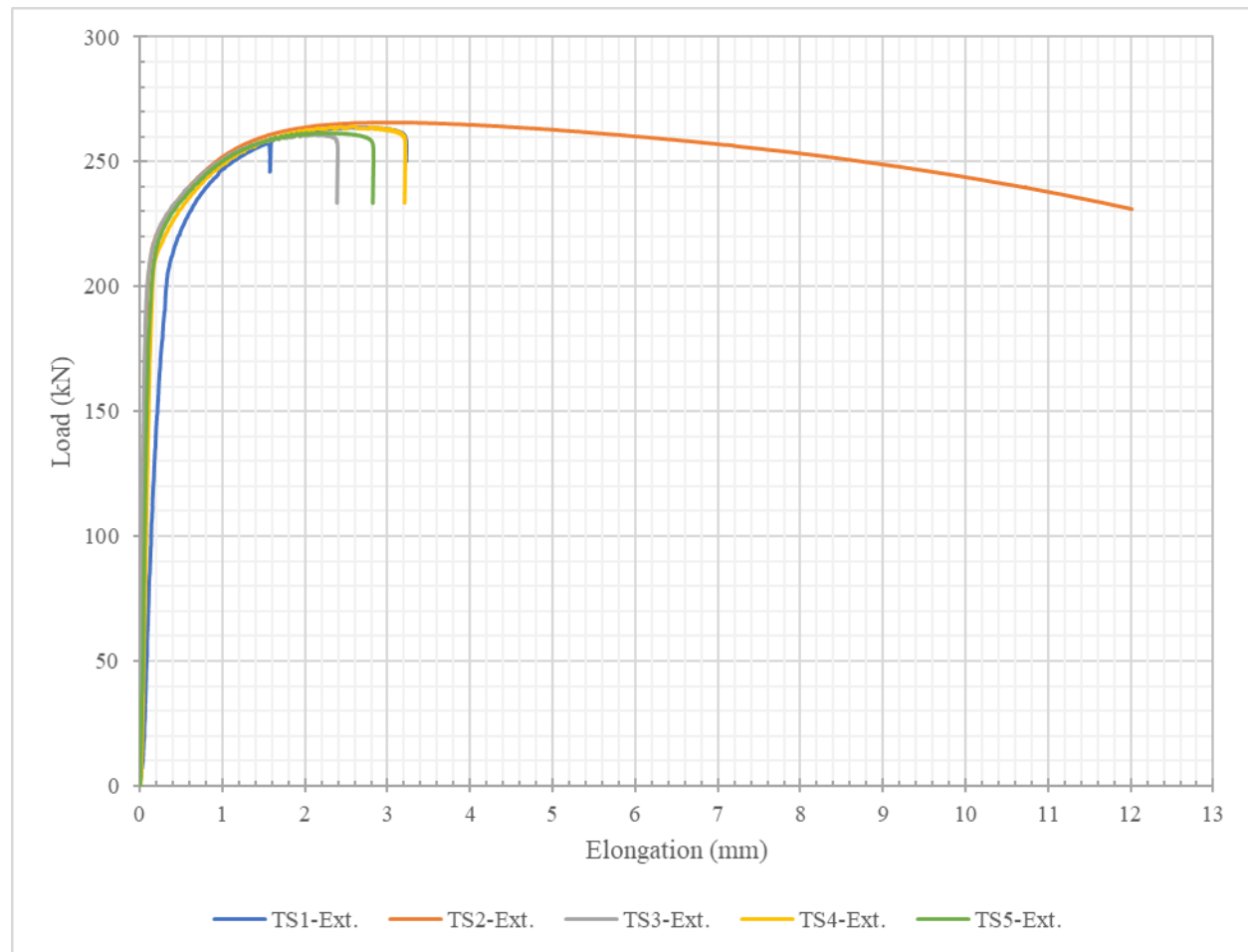


Figure 4.7 Elongation of the shear studs during direct tension testing.

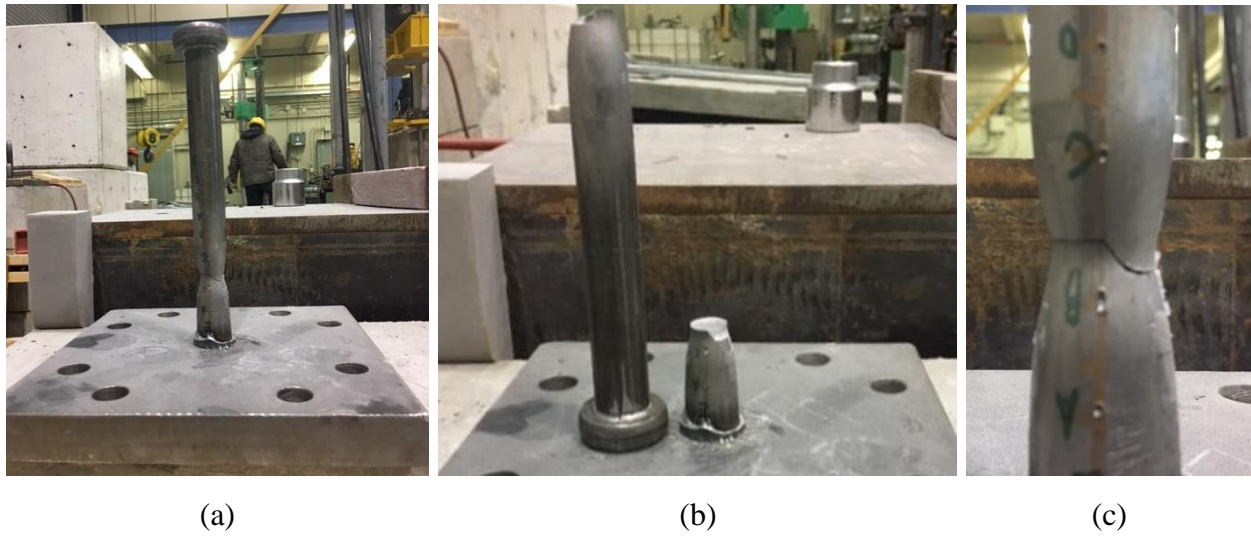


Figure 4.8 Shear stud tension failure.

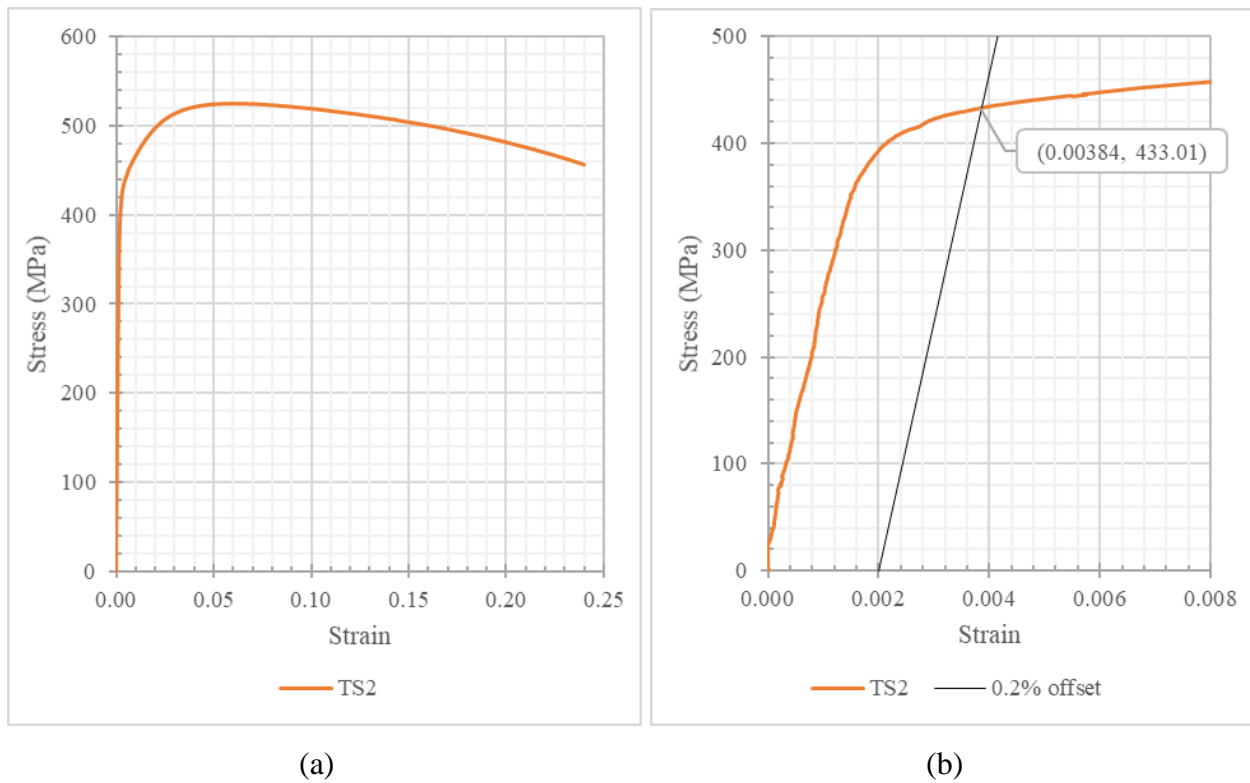


Figure 4.9 Stress-strain curves for shear stud TS2: (a) full data set; (b) 0.2% offset method for shear stud yield strength and modulus of elasticity.

The TS2 data was used to compute the modulus of elasticity of the shear studs. The 0.2% offset method was used to find the yield strength, and subsequently yield strain and the modulus of

elasticity. Figure 4.9 shows the full stress-strain curve for TS2 and a closeup on the first section of the data used to find the yield strength. The resulting yield strength is 433 MPa and the yield strain is 0.00384, at a load of 219 kN.

Therefore, the modulus of elasticity of the shear studs was calculated as follows,

$$E = \frac{\sigma_y}{\varepsilon_y} = \frac{433.01}{0.00384} = 112715 \text{ MPa}$$

The yield properties of the shear studs will be used to determine if the shear studs in the shear pocket specimens and bridge deck yielded, or whether their strength was under-utilized.

### 4.3 Shear Pocket Specimens

The static loading tests on the push-out test shear pocket specimens were completed at various dates throughout the experimental program. The results for the vertical displacement, debonding behaviour, and shear stud strains and behaviour are presented and discussed in this section. The results tables include the data at service load (60% of the ultimate load), 75% and 90% of the ultimate load, and the ultimate load.

The graphical results for the shear pocket specimens present the full loading values, when in reality half the load would have been distributed to both slabs A and B of the overall specimens. Due to the nature of manual construction the shear pocket specimens are not built perfectly and minimal discrepancies will be present, thus the load is not split exactly even between the two slabs for each shear pocket specimen, but will vary minimally. Therefore, vertical displacement and debonding, which were measured with respect to the concrete of each slab, would have been subjected to approximately half the subjected loads. The strains in the shear studs would correspond to approximately half the load divided by the number of studs in each slab (six or three studs).

It is also important to reiterate that the push-out test applies direct shear forces on the shear pocket to isolate the shear behaviour of the composite element. In practice, bridge deck shear pockets do not have direct shear applied since the main loading is live loading along the deck slabs from vehicular traffic.

As aforementioned in Section 3.3.2, the flanges of the built-up steel beam buckled during the first shear pocket specimen testing, which resulted in major crushing at the bottom of the concrete slabs. The push-out test is designed to test the shear pocket connection under direct shear loads; therefore, the steel support cannot fail. As seen in Figure 3.13, a channel was added between the beam flanges to act as an additional stiffener and prevent the steel buckling in the remaining shear pocket tests. Therefore, the SP6-1 data will be reported and discussed with the SP6-2 and SP6-3 specimens, however, will be excluded from comparisons to the test results of the SP3 specimens and the full-scale bridge decks.

#### **4.3.1 Experimental Failure Modes**

The typical ductile versus brittle failure modes does not apply in the same manner for push-out experiments. The loading on a bridge deck is multi-faceted and the entire structure resists the forces collectively. Since the push-out tests apply direct shear to the connection there are two possible failure modes: concrete crushing failure or shear stud failure. If the shear pocket slab fails through concrete crushing, the shear studs remained intact on the built-up beam flange. If the failure is due to the studs, they will have sheared off the beam flange. Table 4.8 summarizes the resulting failure modes and Figure 4.10 and Figure 4.11 are photographs of the two failure modes observed. The test data discussed in the sections below will validate and explain the failure modes the SP6 and SP3 specimens experienced.

Table 4.8 Push-Out Test Failure Modes

Specimen	Failure Mode	
	A	B
SP6-1	<i>Failure initiated by steel beam buckling.</i>	
SP6-2	Stud shearing	Concrete crushing
SP6-3	Concrete crushing	Concrete crushing
SP3-1	Concrete crushing	Stud shearing
SP3-2	Stud shearing	Stud shearing

The 0-stud specimen failure mode is not listed because without studs, the failure occurred when the UHPC debonded from the surface of the built-up steel beam flange. The results of the SP0 specimens will be discussed later.

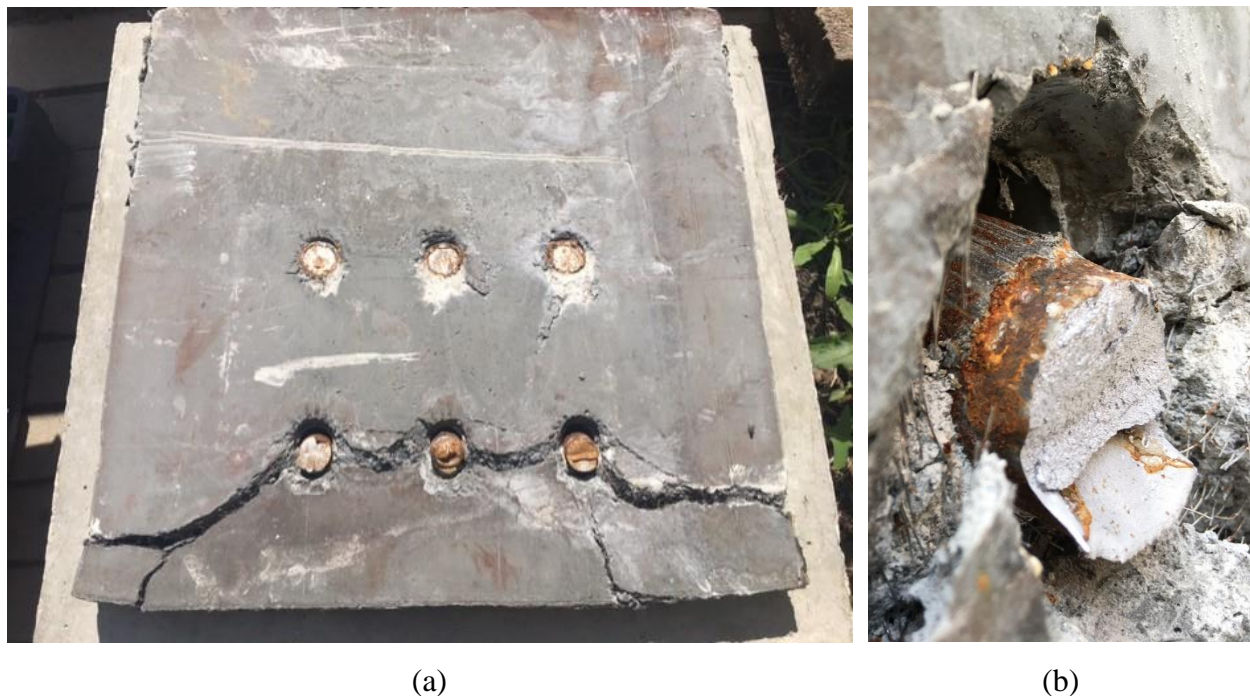


Figure 4.10 SP6-2A stud shearing failure: (a) UHPC haunch with studs still inside, and (b) close-up on bottom left shear stud base.



Figure 4.11 SP6-3A concrete crushing failure.

### 4.3.2 Displacement and Debonding Behaviours

As presented in Chapter 3, the vertical displacement was measured with two LVDTs for each slab of the overall specimen. The measurement point of each LVDT was on the surface of the UHPC haunch, where the “steel” LVDT was mounted on the built-up steel beam and the “concrete” LVDT was mounted on the surface of the RC slab. Increasing readings in the steel-LVDTs indicate the steel beam and studs are experiencing downward displacement, debonding from the UHPC. Increasing readings in the concrete-LVDTs indicate the UHPC is displacing with the steel, debonding from the RC. The peaks in the LVDT data at the ultimate load indicate major concrete cracking and impending specimen failure. The type of failure is indicated by the behaviour between the service load and failure.

The LVDT results for the SP6-1, 2, and 3 specimens are presented below. For the most part, the steel-LVDTs reported greater vertical displacements than the concrete-LVDTs. Specimens SP6-1, 2 and 3 attained an ultimate load of 2642 kN, 3045 kN, and 2892 kN, respectively.

The first specimen's results are similar on sides A and B up to its ultimate load of 2642 kN. The steel-LVDTs recorded 0.50 mm and 0.52 mm of displacement at its service load of 1586 kN for the SP6-1A and 1B, respectively. By the ultimate load the displacements had increased to 2.32 mm and 2.56 mm for SP6-1A and 1B, respectively. The concrete-LVDTs on SP6-1A displaced only 0.13 mm at the service load and reached 0.48 mm by the ultimate load. SP6-1B displaced 0.31 mm at service load and increased to 0.64 mm at the ultimate load [Table 4.9]. Due to the beam buckling, the A side steel-LVDT had a total displacement of 3.66 mm at failure, and the B side steel-LVDT was nearly double that at 6.95 mm [see Figure 4.12].

The SP6-2A concrete-LVDT reported a displacement of 0.11 mm at its service load of 1733 kN and 0.36 mm at its ultimate load of 2892 kN, while the steel-LVDT displaced significantly more with 0.48 mm and 3.57 mm at the service and ultimate loads, respectively. The B side steel had displacements of just less than half the A side values with 0.19 mm at service load and 1.20 mm at ultimate load. The SP6-2B concrete-LVDT increased from 0.22 mm to 0.87 mm of displacement between the service load and ultimate load [Table 4.10].

The SP6-3 specimen also experienced similar displacement values between the concrete-LVDTs and the steel-LVDTs, and both sides experienced concrete crushing failures. Both steel-LVDTs read displacements of 0.55 mm at the service load of 1829 kN. At the ultimate load of 3045 kN, the SP6-3A displaced 3.02 mm and the SP6-3B displaced slightly more with 3.31 mm. The SP6-3A concrete displaced only 0.01 mm at the service load of 1829 kN and 0.12 mm at the ultimate

load of 3045 kN. The SP6-3B concrete displaced 0.15 mm and 0.37 mm at the service and ultimate loads, respectively [Table 4.11].

Table 4.9 SP6-1 LVDT Results

Load (kN)	Vertical Displacement (mm)			
	SP6-1A-Steel	SP6-1A-Concrete	SP6-1B-Steel	SP6-1B-Concrete
1586 (P <sub>S</sub> )	0.50	0.13	0.52	0.31
1981 (75% P <sub>U</sub> )	0.84	0.22	0.82	0.40
2377 (90% P <sub>U</sub> )	1.43	0.35	1.45	0.48
<b>2642 (P<sub>U</sub>)</b>	<b>2.32</b>	<b>0.48</b>	<b>2.56</b>	<b>0.64</b>

Table 4.10 SP6-2 LVDT Results

Load (kN)	Vertical Displacement (mm)			
	SP6-2A-Steel	SP6-2A-Concrete	SP6-2B-Steel	SP6-2B-Concrete
1733 (P <sub>S</sub> )	0.48	0.11	0.19	0.22
2167 (75% P <sub>U</sub> )	0.70	0.21	0.33	0.33
2603 (90% P <sub>U</sub> )	1.25	0.29	0.52	0.52
<b>2892 (P<sub>U</sub>)</b>	<b>3.57</b>	<b>0.36</b>	<b>1.20</b>	<b>0.87</b>

Table 4.11 SP6-3 LVDT Results

Load (kN)	Vertical Displacement (mm)			
	SP6-3A-Steel	SP6-3A-Concrete	SP6-3B-Steel	SP6-3B-Concrete
1829 (P <sub>S</sub> )	0.55	0.01	0.55	0.15
2282 (75% P <sub>U</sub> )	0.85	0.03	0.82	0.19
2740 (90% P <sub>U</sub> )	1.41	0.04	1.37	0.25
<b>3045 (P<sub>U</sub>)</b>	<b>3.02</b>	<b>0.12</b>	<b>3.31</b>	<b>0.37</b>

The LVDT result tables present the vertical displacements at select loads throughout testing, however the shapes of the graphical data presented in the figures below are valuable for analyzing the behaviour of the shear pockets.

Considering Figure 4.12, though the vertical displacements vary in magnitude the similarities in the graphical shapes of the concrete-LVDTs and the steel-LVDTs indicate the same load resistance behaviour for SP6-1A and 1B throughout testing. SP6-1A demonstrated greater cracking and displacement within the RC slab and its shear pocket in comparison to SP6-1B; however, its steel connection had less debonding. The peaks in both concrete and steel results followed the plateaus until failure suggest the overall failure was more ductile than the other specimens since there was nearly 7 mm of displacement.

The SP6-2A results indicate the RC slab and its UHPC shear pocket had slight debonding from one another. The UHPC exhibited significant debonding and displacement from the steel shear studs and beam, which ultimately lead to the specimen's overall failure when its studs sheared off. Meanwhile, up to an approximate load of 2700 kN (just below its ultimate load of 2892 kN) the SP6-2B acted homogeneously, shown through the comparable displacements of the LVDTs; the concrete slab, UHPC pocket, and steel studs and beam debonded from each other at a similar rate. After the ultimate load, the steel and shear pocket plateau while the SP6-2B slab undergoes concrete crushing until SP6-2A's studs shear off [see Figure 4.13].

Figure 4.14 indicates SP6-3A and SP6-3B had similar behaviour and load resistance during testing. The UHPC shear pockets experienced cracking and debonding from the steel shear studs and beam at a similar rate over the full test. The RC slab A and its shear pocket remained intact, resisting loading, it reached its service load of 1829 kN at which point minor cracking commenced and debonding occurred. The B side concrete displayed similar behaviour, though slightly greater

displacements were recorded indicating more cracking and debonding in the concrete slab. The cracking on this side also commenced at approximately 300 kN. Despite the difference in the steel versus concrete displacements, the entire specimen failed through concrete crushing on both sides. Comparing the SP6-2 and SP6-3 results, the ultimate loads only varied by approximately 5% with 2892 kN and 3045 kN, respectively. At failure, the maximum vertical displacement recorded was 4.03 mm for SP6-2 and 4.05 mm for SP6-3.

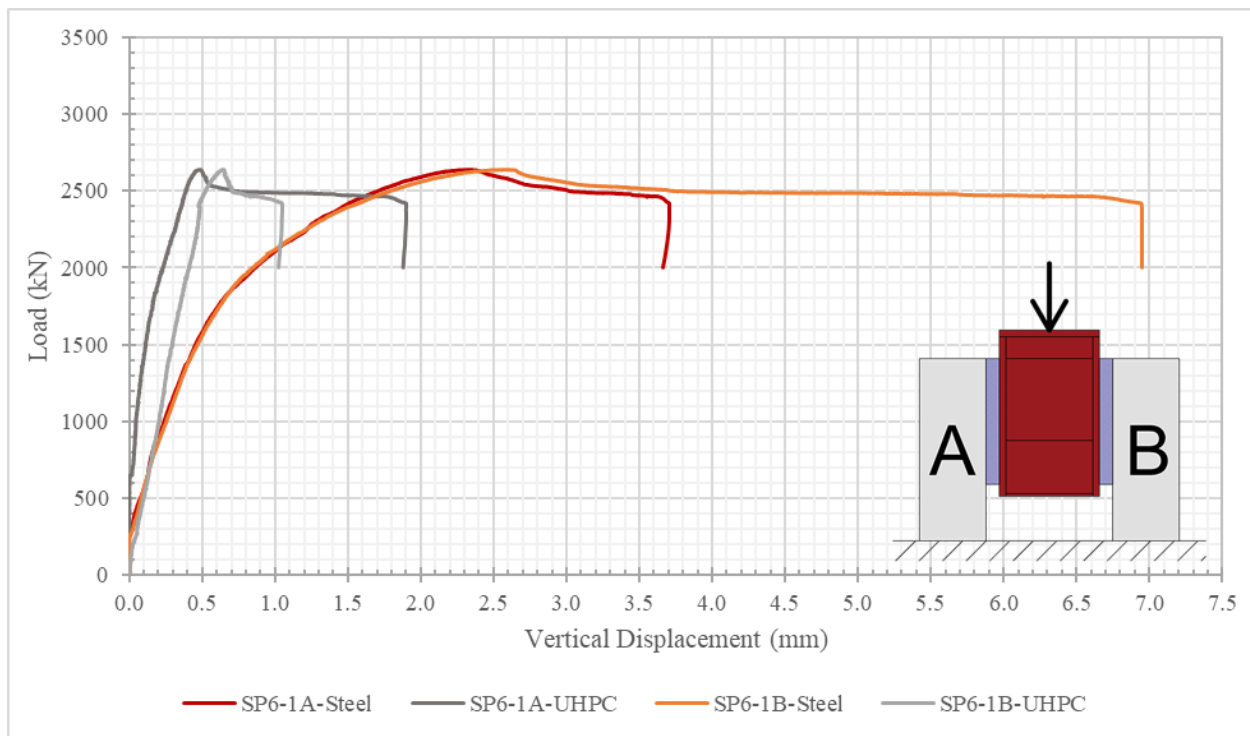


Figure 4.12 SP6-1 vertical displacement development.

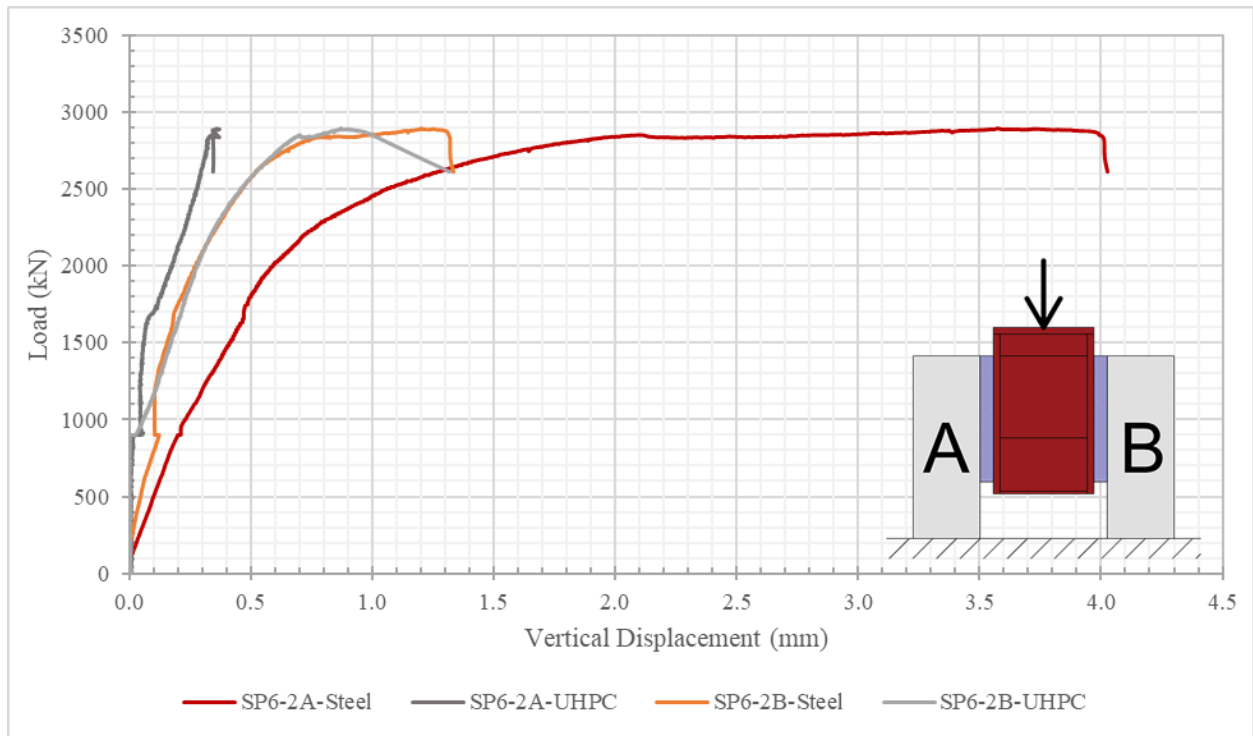


Figure 4.13 SP6-2 vertical displacement development.

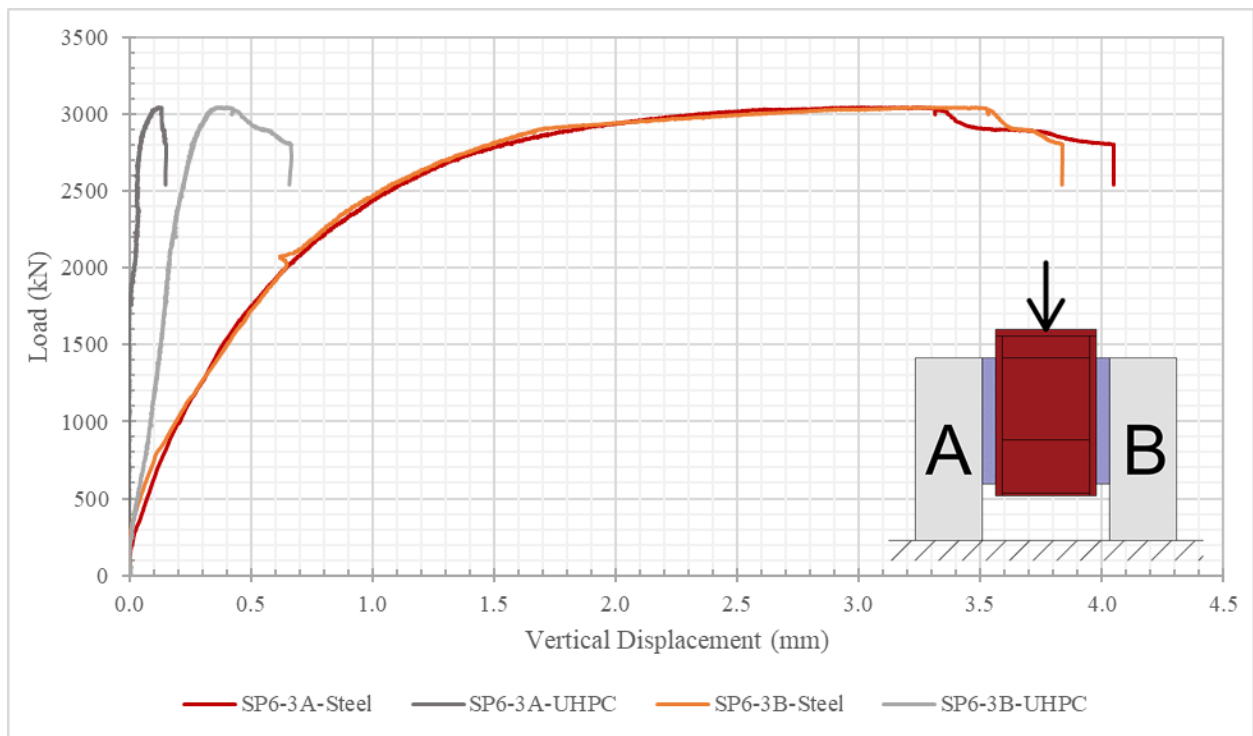


Figure 4.14 SP6-3 vertical displacement development.

The 3-stud shear pocket specimens behave much differently than the 6-stud specimens, visible in comparing the graphical results. The ultimate load of SP3-1 and SP3-2 were 1445 kN and 1674 kN, respectively, which is nearly half the ultimate load of the SP6 specimens.

The SP3-1A steel-LVDT recorded no displacement during testing and the concrete-LVDT only attained displacements of 0.06 mm at its service load of 866 kN and 0.15 mm at its ultimate load of 1445 kN. Meanwhile, for SP3-1B the steel-LVDT recorded displacements of 0.44 mm and 2.90 mm at the service and failure loads, respectively. The SP3-1B concrete-LVDT had the greatest displacement values of 0.93 mm at service load and 5.67 mm at ultimate load [Table 4.12].

The concrete-LVDTs of SP3-2A indicated displacements of 0.37 mm at the service load of 1004 kN and 1.59 mm at the ultimate load of 1674 kN. The displacements of SP3-2B were 0.62 mm and 3.92 mm at the service and ultimate loads respectively [Table 4.13]. Therefore, the concrete in both slabs withheld additional crushing between the ultimate load and failure. Similar to the SP3-1A steel-LVDT, SP3-2A and SP3-2B recorded no displacement along the steel built-up beam, however, both sets of studs sheared off at failure.

Table 4.12 SP3-1 LVDT Results

Load (kN)	Vertical Displacement (mm)			
	SP3-1A-Steel	SP3-1A-Concrete	SP3-1B-Steel	SP3-1B-Concrete
866 (P <sub>S</sub> )	0.00	0.06	0.44	0.93
1084 (75% P <sub>U</sub> )	0.01	0.14	0.52	1.43
1300 (90% P <sub>U</sub> )	0.00	0.10	1.00	2.48
<b>1445 (P<sub>U</sub>)</b>	<b>0.01</b>	<b>0.15</b>	<b>2.90</b>	<b>5.67</b>

Table 4.13 SP3-2 LVDT Results

Load (kN)	Vertical Displacement (mm)			
	SP3-2A-Steel	SP3-2A-Concrete	SP3-2B-Steel	SP3-2B-Concrete
1004 (P <sub>s</sub> )	0.00	0.37	-0.01	0.62
1256 (75% P <sub>U</sub> )	-0.02	0.53	0.00	0.89
1506 (90% P <sub>U</sub> )	0.00	0.98	-0.01	1.54
<b>1674 (P<sub>U</sub>)</b>	<b>0.01</b>	<b>1.59</b>	<b>0.00</b>	<b>3.92</b>

The graphical results of the SP3-1 suggest side A had superior load resistance to side B as neither LVDT recorded significant displacement; the RC slab A, its UHPC shear pocket, and the steel shear studs and beam were all strongly bonded throughout testing. The SP3-1B data indicates debonding of the steel and UHPC pocket, and greater separation between the RC and UHPC within the slab itself. Considering SP3-1A only experienced concrete crushing and SP3-1B studs sheared off at failure, the overall specimen failure was likely due to the B side failure. It is possible the SP3-1A still had loading capacity. The SP3-1B steel-LVDT displayed a sudden displacement to approximately 0.9 mm before the loading reached 100 kN. This reaction is not reflected in the other data for the shear stud strains, nor the specimen pi-gauges of either side of SP3-1. The data recovers to a normal curve by 800 kN. The recorded displacements cannot be explained, but since the displacement increased only 0.9 mm a speculation is that the adhesive affixing the LVDT to the UHPC surface was not fully cured prior to commencing the test.

For specimen SP3-2, the load was resisted more evenly between the slabs. Since the steel mounted LVDTs indicated no displacement occurred, neither UHPC shear pocket debonded from the steel during testing. The specimen's displacements were within the concrete slabs as they cracked and

debonded from their shear pockets. Despite displacement behaviour, both SP3-2A and B failed through the eventual shearing off of the studs.

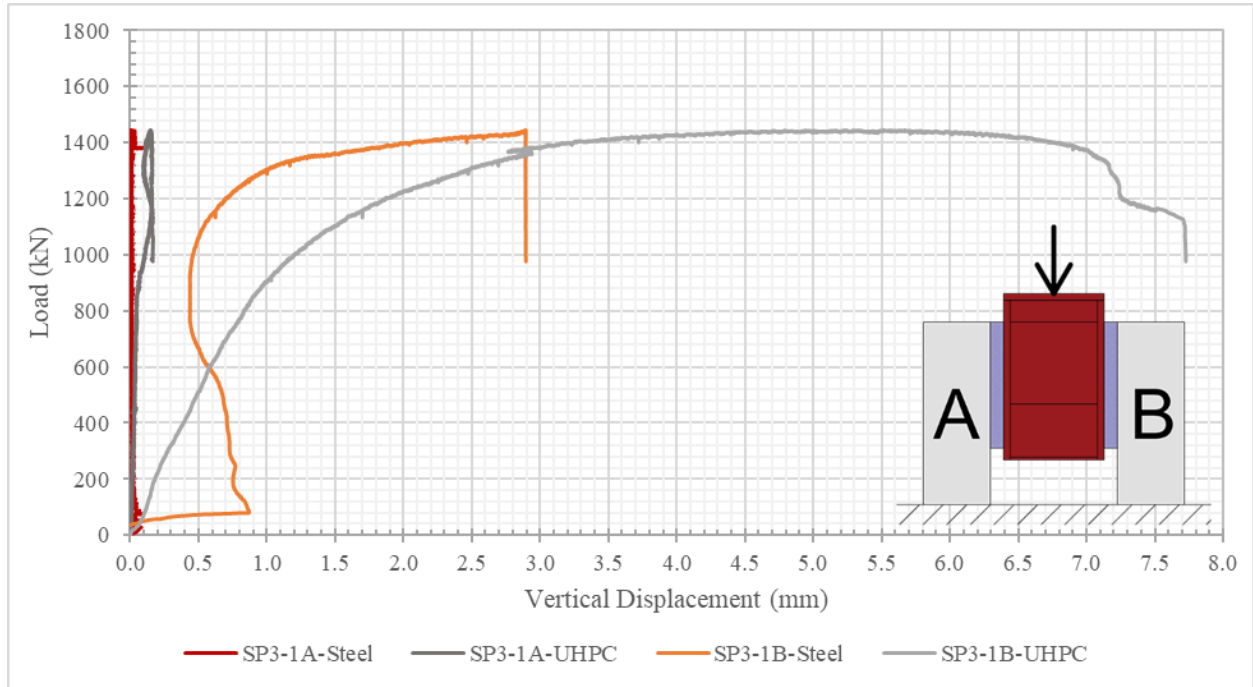


Figure 4.15 SP3-1 vertical displacement development.

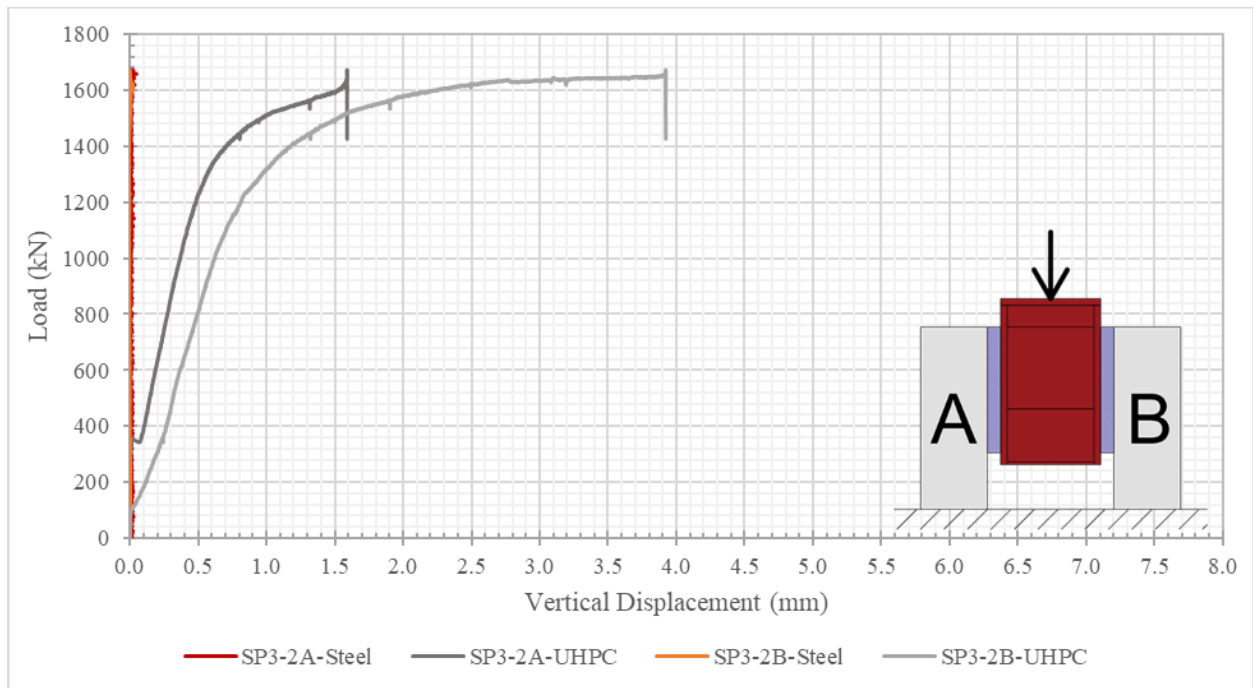


Figure 4.16 P3-2 vertical displacement development.

Comparing the SP6 to the SP3 shear pocket specimens, the results suggest the shear pockets do not require six studs because a strong connection was maintained during testing for the three stud specimens. Though it is true the SP6 specimens resisted greater overall direct shear loads, for an approximate analysis the load to be equally distributed amongst the shear studs by dividing the ultimate load by the total number of studs in the specimens. The resulting resistance per stud can be seen in Table 4.14. The approximate loads each stud would have resisted is very similar between all the specimens, averaging 238 kN/stud for the SP6 specimens and 260 kN/stud for the SP3 specimens. These results are not surprising, since the SP6 specimens had double the studs with nearly double the ultimate load of the SP3 specimens. The displacement results also do not give an indication on the expected failure mode.

The interesting revelation is in the failure mode because though doubling the number of studs will allow the overall specimen to resist greater loads, the failure in the six stud specimens was due to the loss of connection between the steel and the shear pocket, whereas the failure in the three stud specimens was due to the loss of connection within the concrete slab and its shear pocket.

Table 4.14 SP6 and SP3 Result Comparison

Specimen	Total Shear Studs	Ultimate Load (kN)	Approx. Ultimate Load Per Stud (kN/stud)	Max. Vertical Displacement at Ultimate (mm)
SP6-2	12	2892	241	3.57 (steel-LVDT)
SP6-3	12	3045	254	3.31 (steel-LVDT)
SP3-1	6	1445	241	5.67 (concrete-LVDT)
SP3-2	6	1674	279	3.92 (concrete-LVDT)

The pi-gauge results provided information on the horizontal displacements and debonding between the concrete and steel. Negative values indicate the concrete was being pulled inwards and likely

crushed (compression), while positive values indicate the concrete was being pushed outwards (tension). For all the SP6 specimens, the PGTs reported negative values and PGBs reported positive values, which is the expected behaviour. Since the unbonded sections of the concrete are in the bottom half, the base of the concrete wants to rotate outwards during testing, while the top of the concrete is being rotated inwards with the downward movement of the steel beam during loading. The connection between the shear pocket and the steel shear studs and beam resist the moments generated during loading. Figure 4.17 is a sketch of the rotational behaviour discussed.

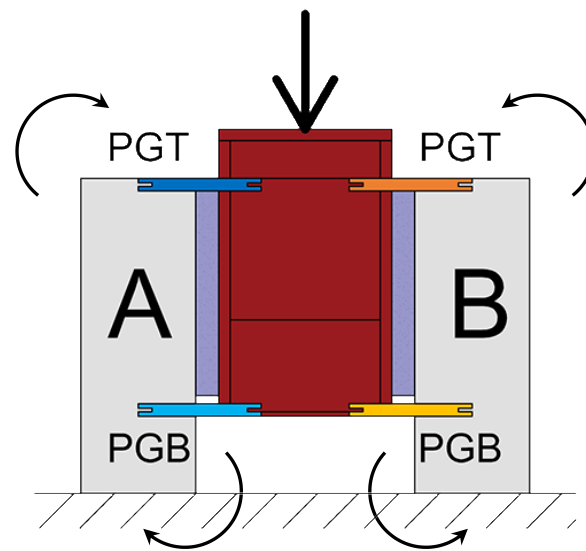


Figure 4.17 Shear pocket specimen rotation.

The pi-gauge results are instrumented to measure horizontal displacements. The displacement represents the debonding and separation between the concrete slabs and the support steel beam. Comparing the data with the LVDT results will indicate whether the horizontal displacement was due to the cracking and debonding between the RC slab and UHPC, and/or the UHPC and the steel shear studs and beam.

Table 4.15, Table 4.16, and Table 4.17 present the pi-gauge results for the SP6 specimens. The PGTs for all three specimens compressed less than 0.5 mm during testing. Based on the values recorded, the load does not appear to directly affect the horizontal displacement measurements.

Rather, the amount of displacement and debonding corresponds to the amount of vertical displacement the specimen endured before failure. The SP6-1 specimen had the greatest horizontal values with 3.62 mm for SP6-1A-PGB and 3.27 mm for SP6-1B-PGB at the ultimate load, due to the steel beam buckling [see Table 4.15]. The SP6-2A and 2B bottom pi-gauges read 0.34 mm and 0.31 mm of horizontal displacement at the service load and increased to 1.54 mm and 1.15 mm at the ultimate load, respectively [Table 4.16]. The SP6-3A and 3B bottom pi-gauges had displacements of 0.72 mm and 0.58 mm at the service load, respectively, but reached similar displacements at the ultimate load to the SP6-2 specimen with 1.54 mm for SP6-3A and 1.57 mm for SP6-B [Table 4.17].

Table 4.15 SP6-1 Pi-Gauge Results

Load (kN)	Horizontal Displacement (mm)			
	SP6-1A-PGT	SP6-1A-PGB	SP6-1B-PGT	SP6-1B-PGB
1586 (P <sub>S</sub> )	-0.09	1.05	-0.13	0.96
1981 (75% P <sub>U</sub> )	-0.08	1.82	-0.16	1.50
2377 (90% P <sub>U</sub> )	-0.07	2.72	-0.17	2.34
<b>2642 (P<sub>U</sub>)</b>	<b>-0.08</b>	<b>3.62</b>	<b>-0.16</b>	<b>3.27</b>

Table 4.16 SP6-2 Pi-Gauge Results

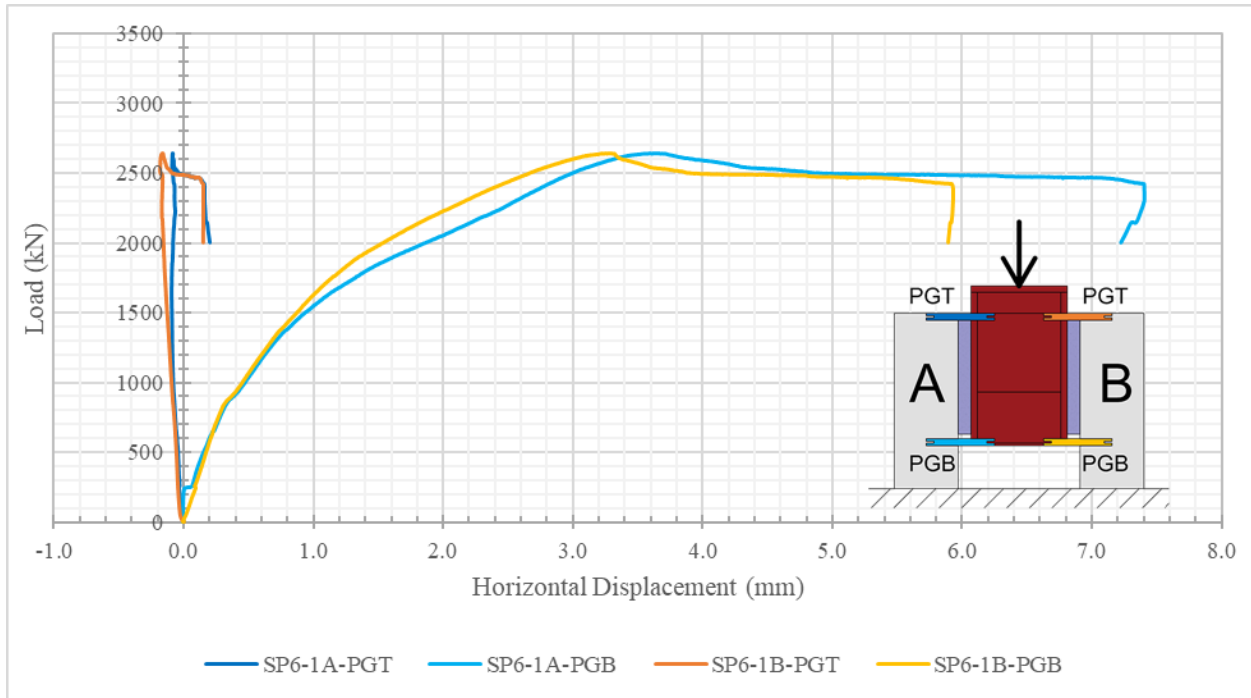
Load (kN)	Horizontal Displacement (mm)			
	SP6-2A-PGT	SP6-2A-PGB	SP6-2B-PGT	SP6-2B-PGB
1733 (P <sub>S</sub> )	-0.20	0.34	-0.35	0.31
2167 (75% P <sub>U</sub> )	-0.21	0.51	-0.38	0.47
2603 (90% P <sub>U</sub> )	-0.21	0.79	-0.41	0.71
<b>2892 (P<sub>U</sub>)</b>	<b>-0.07</b>	<b>1.54</b>	<b>-0.34</b>	<b>1.15</b>

Table 4.17 SP6-3 Pi-Gauge Results

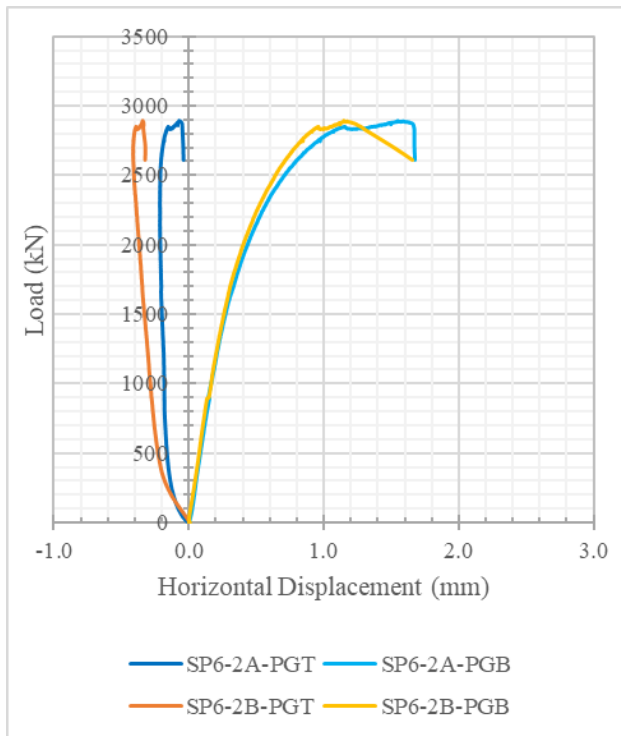
Load (kN)	Horizontal Displacement (mm)			
	SP6-3A-PGT	SP6-3A-PGB	SP6-3B-PGT	SP6-3B-PGB
1829 (P <sub>s</sub> )	-0.13	0.72	-0.42	0.58
2282 (75% P <sub>U</sub> )	-0.15	0.92	-0.45	0.80
2740 (90% P <sub>U</sub> )	-0.17	1.08	-0.49	1.13
<b>3045 (P<sub>U</sub>)</b>	<b>-0.13</b>	<b>1.54</b>	<b>-0.49</b>	<b>1.57</b>

As discussed with the LVDT results, the SP6 specimens experienced the most debonding and movement between the UHPC shear pocket and steel shear studs and beam, therefore the pi-gauge results represent the separation between the UHPC and the beam's flange surface, and the UHPC debonding around the shear studs.

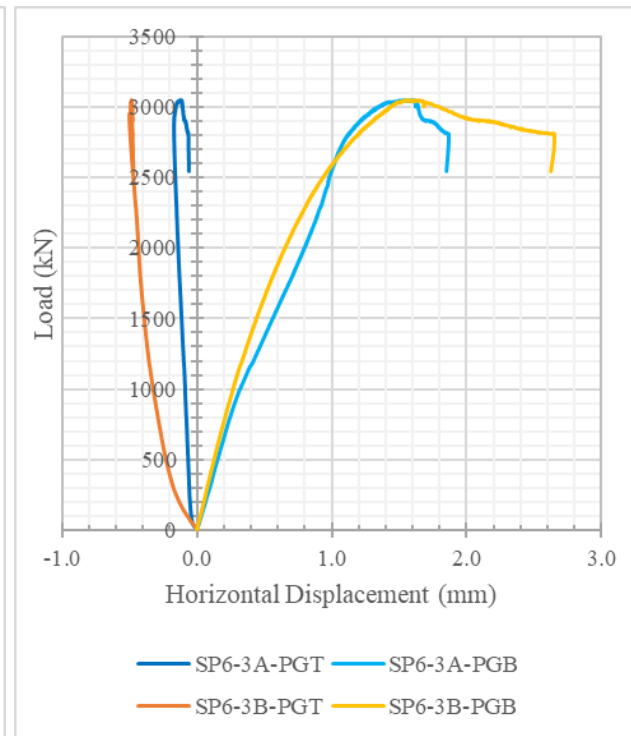
Figure 4.18 presents the development of the horizontal displacement and debonding during testing. The shapes of the graphical data mirror those of the respective SP6 LVDT results. The top of the slabs were subjected to compression and the bottom was in tension. The top pi-gauges measured increasing negative horizontal displacements until the ultimate load was reached and the PGTs indicated the displacements decreased. The decreasing values were likely due to concrete cracking and UHPC debonding from the RC slab and/or the steel beam flange. The bottom pi-gauges measured increasing positive horizontal displacements during the entirety of the testing, due to tensile forces generated during loading.



(a)



(b)



(c)

Figure 4.18 UHPC and steel debonding for specimens (a) SP6-1, (b) SP6-2, and (c) SP6-3.

The results for the SP3 specimens seen in Table 4.18 and Table 4.19 were similar to the SP6-1 and SP6-2 results. All the PGTs compressed inwards less than 0.25 mm during testing. The SP3-1A-PGB recorded 0.25 mm of displacement at the service load and 0.99 mm of displacement upon reaching the ultimate load. The SP3-1B-PGB horizontal displacement values were nearly double those on the A side with 0.45 mm at service and 1.88 mm at ultimate [Table 4.18]. The bottom pi-gauges of SP3-2A and 2B read 0.20 mm and 0.26 mm at service load, and 1.07 mm and 1.16 mm at ultimate load, respectively [Table 4.19].

Table 4.18 SP3-1 Pi-Gauge Results

Load (kN)	Debonding (mm)			
	SP3-1A-PGT	SP3-1A-PGB	SP3-1B-PGT	SP3-1B-PGB
866 (P <sub>S</sub> )	-0.21	0.25	-0.16	0.45
1084 (75% P <sub>U</sub> )	-0.22	0.32	-0.16	0.77
1300 (90% P <sub>U</sub> )	-0.22	0.44	-0.14	1.22
<b>1445 (P<sub>U</sub>)</b>	<b>-0.10</b>	<b>0.99</b>	<b>0.04</b>	<b>1.88</b>

Table 4.19 SP3-2 Pi-Gauge Results

Load (kN)	Horizontal Displacement (mm)			
	SP3-2A-PGT	SP3-2A-PGB	SP3-2B-PGT	SP3-2B-PGB
1004 (P <sub>S</sub> )	-0.06	0.20	-0.08	0.26
1256 (75% P <sub>U</sub> )	-0.07	0.25	-0.09	0.35
1506 (90% P <sub>U</sub> )	-0.07	0.34	-0.11	0.51
<b>1674 (P<sub>U</sub>)</b>	<b>0.11</b>	<b>1.07</b>	<b>-0.10</b>	<b>1.16</b>

The SP3 pi-gauge graphical results do not have comparable shapes to the LVDT results, however, as seen in Table 4.18 and Table 4.19, between 90% of the ultimate load and the specimen failure,

the PGB values experienced the greatest increase in horizontal displacement. These larger increases in displacement are represented by the plateau in Figure 4.19. This behaviour was also seen in the LVDT results for the SP3 specimens [Figure 4.15 and Figure 4.16].

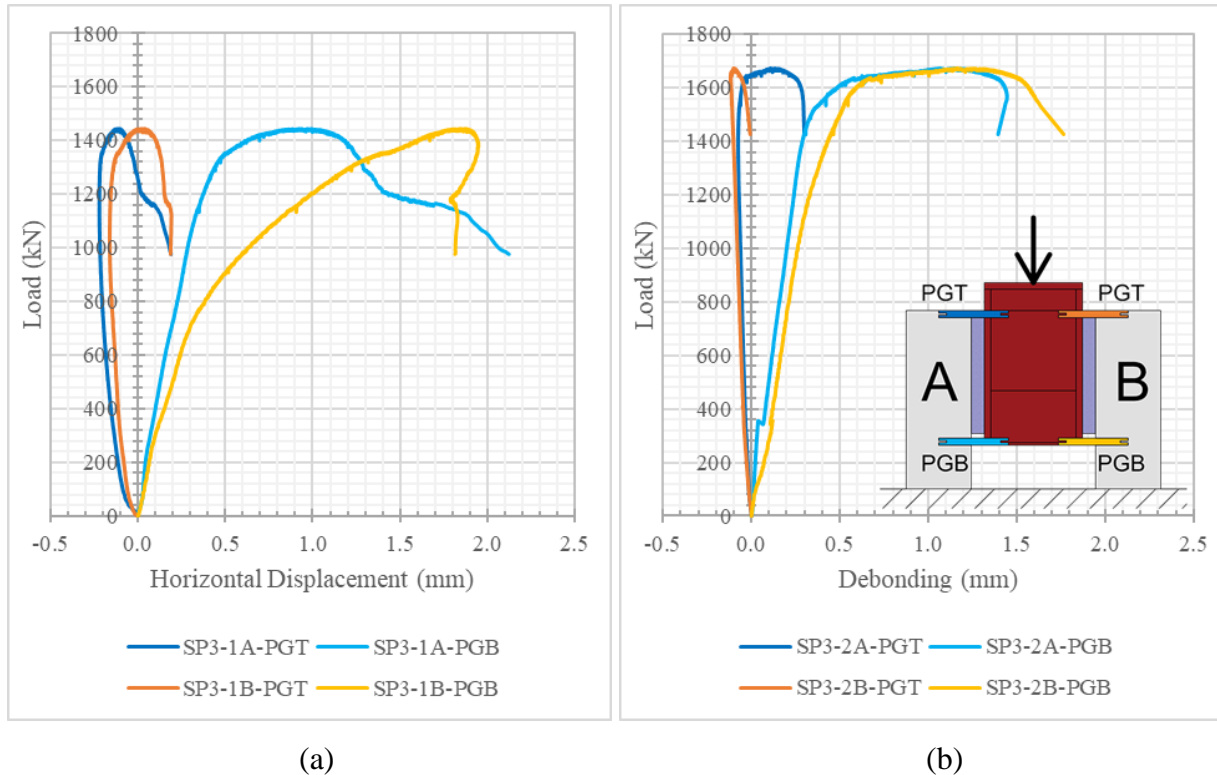


Figure 4.19 UHPC and steel debonding for specimens (a) SP3-1, and (b) SP3-2.

Comparing these results to the SP6 specimens, all three SP6 specimens experienced increasing horizontal displacements more steadily between service loads and the ultimate loads. The SP6 horizontal displacement results were all slightly larger and were approximately 0.5 mm greater at the ultimate load than the SP3 specimens.

The following two figures are an exaggerated visual representation of the horizontal displacement measured by the pi-gauges during testing. Figure 4.20 shows the horizontal displacement of the SP6 and SP3 specimens at 60% of the ultimate load, and Figure 4.21 is at the ultimate load. With the exception of SP6-3, the resulting movement during testing was similar.

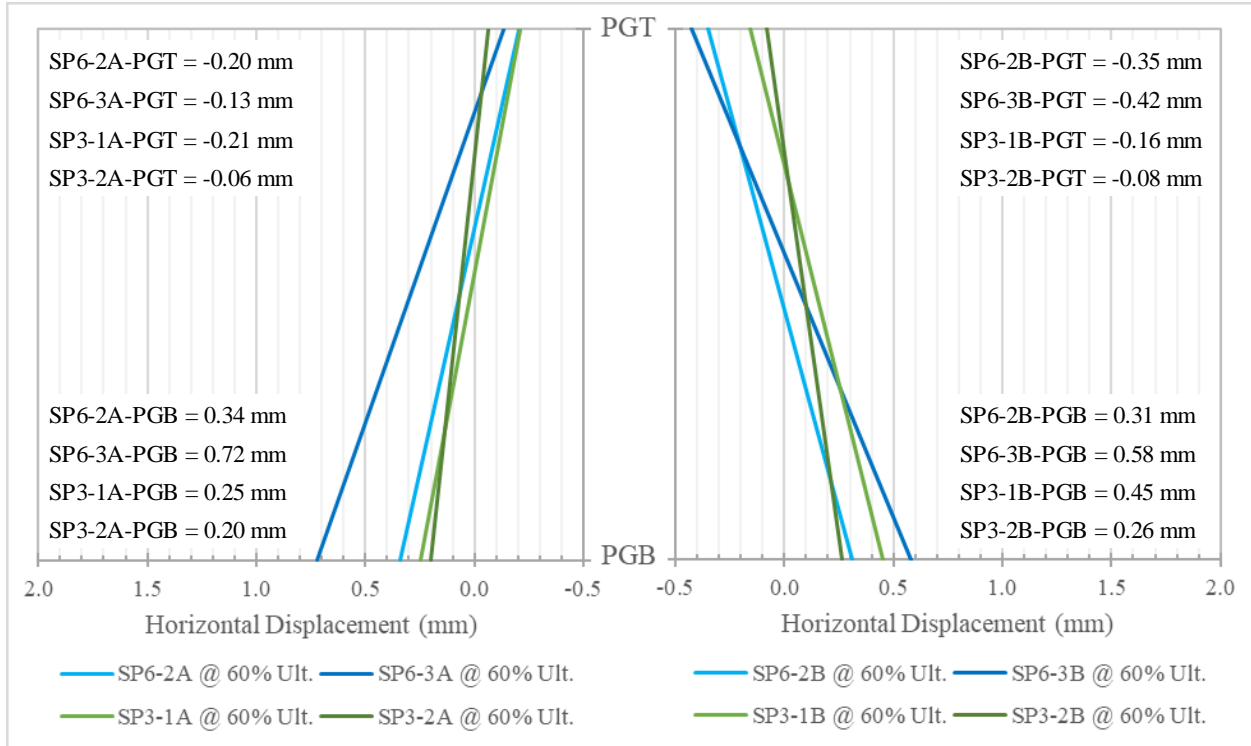


Figure 4.20 Pi-gauge profiles at 60% of the ultimate load for all SP6 and SP3 specimens.

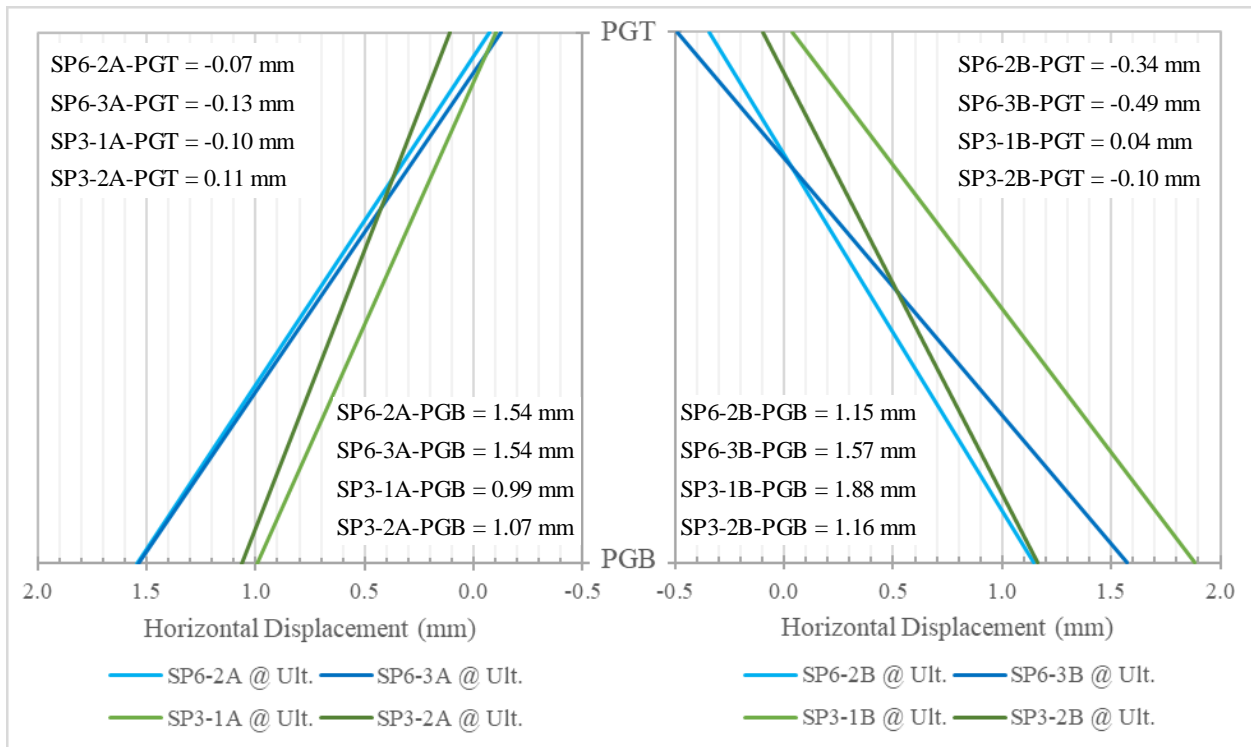


Figure 4.21 Pi-gauge profiles at the ultimate load for all SP6 and SP3 specimens.

The two zero-stud specimens were also tested with LVDT and pi-gauges instrumented to record the debonding and displacement during testing. While lifting SP0-1 into place for testing, the B-side slab debonded from the steel beam's flange. The built-up steel beam was braced to slab B to permit testing of slab A, therefore only SP0-1A was instrumented during testing. Therefore, to avoid this with the second specimen, the SP0-2 specimen was setup below the testing machine and then the UHPC pockets were cast on both sides.

The SP0-1 and SP0-2 specimens only reached ultimate loads of 4.91 kN and 3.44 kN, respectively, before failure. The SP0-1A steel-LVDT recorded negligible displacements, with the data hovering around 0, and the concrete-LVDT recorded a displacement of 0.53 mm at the ultimate load. The steel-LVDT for SP0-2A had its maximum displacement of only 0.08 mm at the ultimate load. The steel-LVDT for SP0-2B and both concrete-LVDTs recorded negligible displacements; all three LVDTs recorded less than 0.01 mm. Based on the exceedingly small vertical displacements and no visible cracking during testing, whether the concrete or steel-LVDT was recording the displacement is deemed irrelevant since the failure was due to slippage between the steel beam and the concrete slabs. There would not have been debonding between the UHPC shear pockets and their RC slabs.

Between the ultimate load and failure, the SP0-1A pi-gauges recorded 0.16 to 0.18 mm at the top of the concrete slab, and 0.11 to 0.12 mm at the bottom of the built-up steel beam. These slight movements are likely a result of the fixity of the bracing that clamped slab B to the beam for testing, because for both sides of SP0-2 the pi-gauges recorded a maximum of only 0.001 mm in horizontal movement.

The SP0-1A had a total test time of 5 minutes and 30 seconds, and SP0-2 only lasted 30 seconds of loading prior to failure. Considering SP0-1B debonded from the steel under its own weight

during the test setup, and since SP0-1A recorded a maximum vertical displacement of 0.58 mm while the greatest displacement in SP0-2 was 0.08 mm, it cannot be concluded whether the SP0-1A slab itself was able to resist the loading or if the manner in which SP0-1B was braced to the beam for testing aided in the specimen's overall strength.

### 4.3.3 Shear Stud Performance

The strain gauges instrumented on the center shear studs were used to measure the strains on the top and bottom surface of the shear studs. Positive strains indicate tension and negative studs indicate compression. Since the steel beam is being loaded downwards, shear forces are generated along the shear stud and UHPC connection bending the ends of the studs. As the studs bend compression was expected on the top of the studs, and tension on the bottom. The microstrains at select loads for the shear studs in the SP6 specimens are tabulated below. Since the load is applied downwards, the strains were expected to be the greatest on the top surface of the shear studs. Recall, the experimental yield strain of the shear studs is 0.00384 (or 3840  $\mu\epsilon$ ), and if the recorded strains surpass it, they will have yielded. Since the specimens are loaded downwards, the top strain gauge indicated if and when the stud yielded during testing. The strains in the bottom gauge may also surpass the yield strain, however this tended to occur after the strain gauges on the top of the stud had recorded the yield strain.

The strains recorded for the SP6-1 specimen were quite erratic since the specimen failed by steel beam buckling. The strains recorded between the service load and failure change rapidly in magnitude and sign due to the load transfer between the shifting steel beam and the cracking concrete. Table 4.20 and Table 4.21, and Figure 4.22 summarize the test data.

The SP6-1A-MS1-ET and EB strains indicate late compressive behaviours in the shear studs with strains of -0.00035 and -0.00015 at ultimate load, respectively. The SP6-1A-MS2 stud has slightly

greater strains at ultimate load of 0.00205 for the ET and 0.00057 for the EB [Table 4.20]. None of the studs in SP6-1A reached the yield strain.

The strain readings of SP6-1B seen in Table 4.21 are less erratic than the A side, and are minimal for most of the test. MS1-ET increases from a strain of 0.00071 at 90% of the ultimate load to a strain of 0.00353 at ultimate. On the underside, MS1-EB reads a strain change of 0.00042 to -0.00085 between 90% of ultimate load and the ultimate load, respectively. The MS2-ET values transition from compression to tension between service and 90% of the ultimate load and reach a strain of 0.00168 at ultimate load. The MS2-EB drops slightly from a strain of 0.00103 to 0.00078 at 90% of the ultimate load and the ultimate load, respectively. The MS1-ET and MS2-ET strain gauges were damaged after the ultimate load, which can be seen in Figure 4.22(b). The last recorded strains for MS1-ET was 0.00403 at a load of 2628 kN, shortly after the ultimate load of 2642 kN was reached. As the specimen neared failure and the sustained load continued to decrease, the last strain for MS2-ET was 0.00399 at 2513 kN. Therefore, the studs in the SP6-1B yielded between the ultimate and failure loads.

Table 4.20 SP6-1A Strain Gauge Results

Load (kN)	SP6-1A Microstrains ( $\mu\epsilon$ )			
	MS1-ET	MS1-EB	MS2-ET	MS2-EB
1586 ( $P_S$ )	585.36	1062.83	574.33	477.41
1981 (75% $P_U$ )	863.96	1331.67	700.84	724.04
2377 (90% $P_U$ )	57.63	1023.93	1389.67	704.45
<b>2642 (<math>P_U</math>)</b>	<b>-352.94</b>	<b>-148.09</b>	<b>2045.58</b>	<b>569.04</b>

Table 4.21 SP6-1B Strain Gauge Results

Load (kN)	SP6-1B Microstrains ( $\mu\epsilon$ )			
	MS1-ET	MS1-EB	MS2-ET	MS2-EB
1586 (P <sub>s</sub> )	51.34	930.50	-230.25	880.76
1981 (75% P <sub>U</sub> )	94.98	888.94	-344.23	1094.30
2377 (90% P <sub>U</sub> )	708.83	421.79	28.73	1032.49
<b>2642 (P<sub>U</sub>)</b>	<b>3532.74</b>	<b>-853.05</b>	<b>1679.73</b>	<b>780.12</b>

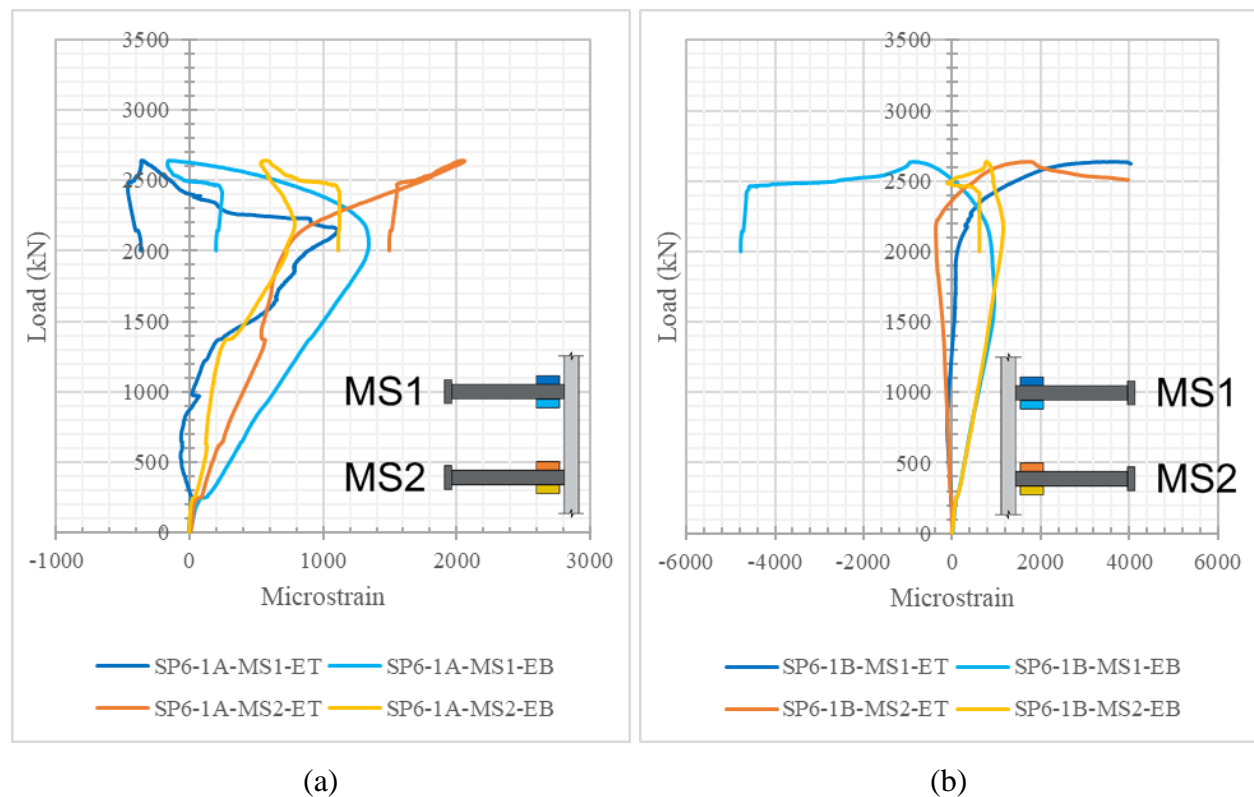


Figure 4.22 SP6-1 shear stud strain development for (a) specimen A, and (b) specimen B.

Table 4.22 and Table 4.23 present the microstrains for the SP6-2 specimens. At service conditions all the strain gauges recorded positive, minimal strains, except for MS1-ET which recorded negligible strains. The SP6-2A studs commenced yielding shortly after the load reached 2712 kN, which is between 90% of the ultimate load and the ultimate load. At the ultimate load, the shear

studs in SP6-2A displayed tension on the top surface and compression on the bottom surface; the MS1-ET and MS2-ET had similar strains at of 0.01434 and 0.01450, respectively, while MS1-EB and MS2-EB were at strains of -0.00634 and -0.00224, respectively. The strains in the SP6-2B studs at the ultimate load of 2892 kN were 0.00234 and 0.00469 for MS1-ET and MS2-ET, respectively. The MS1-EB strain was half that of the top gauge at -0.00122. The MS2 stud did not start yielding until 2863 kN, which was just prior to the ultimate load. The MS2-EB strain gauge was damaged and the last recorded strain in MS2-EB was 0.00081 at a load of 2875 kN. For both SP6-2A and B, the top and bottom surface at the head of the shear studs remained in compression during testing, with strains less than 0.00050. Since the HT and HB strains were negligible, the SP6-3 specimen was not instrumented with strain gauges at the head of the studs.

Table 4.22 SP6-2A Strain Gauge Results

Load (kN)	SP6-2A Microstrains ( $\mu\epsilon$ )					
	MS1-ET	MS1-EB	MS1-HT	MS1-HB	MS2-ET	MS2-EB
1733 (P <sub>S</sub> )	599.21	378.34	242.18	177.58	789.93	476.12
2167 (75% P <sub>U</sub> )	1398.28	-27.83	262.01	213.60	1524.73	354.35
2603 (90% P <sub>U</sub> )	2973.48	-1103.85	287.19	225.48	2855.22	-266.34
<b>2892 (P<sub>U</sub>)</b>	<b>14335.49</b>	<b>-6341.41</b>	<b>304.38</b>	<b>249.03</b>	<b>14501.91</b>	<b>-2238.43</b>

Table 4.23 SP6-2B Strain Gauge Results

Load (kN)	SP6-2B Microstrains ( $\mu\epsilon$ )					
	MS1-ET	MS1-EB	MS1-HT	MS1-HB	MS2-ET	MS2-EB
1733 (P <sub>S</sub> )	-1.01	536.08	87.52	57.07	280.59	662.28
2167 (75% P <sub>U</sub> )	115.82	536.39	114.38	75.60	383.92	840.81
2603 (90% P <sub>U</sub> )	567.17	267.00	132.09	90.17	929.97	1018.68
<b>2892 (P<sub>U</sub>)</b>	<b>2340.47</b>	<b>-1216.73</b>	<b>137.33</b>	<b>96.25</b>	<b>4693.95</b>	–

At the ultimate load of 3045 kN, the SP6-3A shear stud strain gauges recorded were 0.01284 for MS1-ET, -0.00481 for MS1-EB. The MS2-EB strain gauge had a strain of 0.00188 at the ultimate load. The MS2-ET gauge was damaged during testing and the last strain recorded was 0.00342 at a load of 2715 kN, which is approaching the yield strain of 0.00384. For the SP6-3 specimen, 90% of the ultimate load was 2740 kN, and the MS1 stud started yielding shortly after this point at a load of 2760 kN. Therefore, it is highly likely the MS2 stud also yielded during testing given the recorded strains.

On the B-side, the strains in MS1-ET and MS2-ET were very similar at 0.01012 and 0.01055, respectively, at the ultimate load. MS1-EB had positive values during most of the testing, but at ultimate load was under compression and had a strain of -0.00355. The MS2-EB remained in tension, and though it was damaged by the ultimate load it had a strain of 0.00318 recorded at 3039 kN, just below the ultimate load of 3045 kN. The MS2 stud commenced yielding at a load of 2860 kN, and the MS1 stud did not start yielding until a load of 2929 kN.

Table 4.24 SP6-3A Strain Gauge Results

Load (kN)	SP6-3A Microstrains ( $\mu\epsilon$ )			
	MS1-ET	MS1-EB	MS2-ET	MS2-EB
1829 (P <sub>s</sub> )	851.29	624.45	721.01	1052.28
2282 (75% P <sub>U</sub> )	1838.72	250.72	1679.37	1173.34
2740 (90% P <sub>U</sub> )	3716.51	-989.28	–	1235.36
<b>3045 (P<sub>U</sub>)</b>	<b>12841.51</b>	<b>-4807.72</b>	–	<b>1877.69</b>

Table 4.25 SP6-3B Strain Gauge Results

Load (kN)	SP6-3B Microstrains ( $\mu\epsilon$ )			
	MS1-ET	MS1-EB	MS2-ET	MS2-EB
1829 (P <sub>S</sub> )	-151.03	1066.55	66.03	1491.80
2282 (75% P <sub>U</sub> )	94.10	1246.98	730.83	1945.54
2740 (90% P <sub>U</sub> )	1915.60	399.84	2772.46	2451.93
<b>3045 (P<sub>U</sub>)</b>	<b>10117.33</b>	<b>-3546.23</b>	<b>10550.34</b>	–

The strain values are easier to comprehend in their graphical format because of the shift from tension resistance to compression resistance on the bottom surface of some of the shear studs. Figure 4.23 and Figure 4.24 show the strain development for the SP6-2 and SP6-3 specimens, respectively. It has been established that the 6-stud specimens experienced far greater debonding and separation between the UHPC shear pockets and the shear studs, than between the RC slab and the UHPC. The strain values in the shear studs directly reflect the steel-LVDT data, which is evident based on the fact the strain development has the same graphical shape as the displacement developments seen in Figure 4.13 and Figure 4.14.

The SP6-2A experienced the majority of its debonding and separation between the UHPC and the steel shear studs and beam, whereas the SP6-2B had relatively equal debonding and separation within the concrete slab as between the UHPC and steel. The strain gauge results correspond to the UHPC/steel driven displacements of SP6-2, since the displacements and strains were much greater in SP6-2A than SP6-2B.

Recall, the LVDT displacements recorded for the SP6-3 specimens were very similar throughout testing. The steel-LVDT displacement graphical shapes were nearly identical until the ultimate load, at which point the results only varied by a few millimeters [see Figure 4.14]. The MS1-ET,

MS2-ET and MS2-EB all recorded positive strains, and therefore, tension forces on the surfaces of these shear studs throughout testing for both SP6-3A and B. The bottom of the MS1 studs resisted tensile forces during most of the testing, but shortly after service load at approximately 2000 kN the forces started switching to compression, visible by the slope change in the graph.

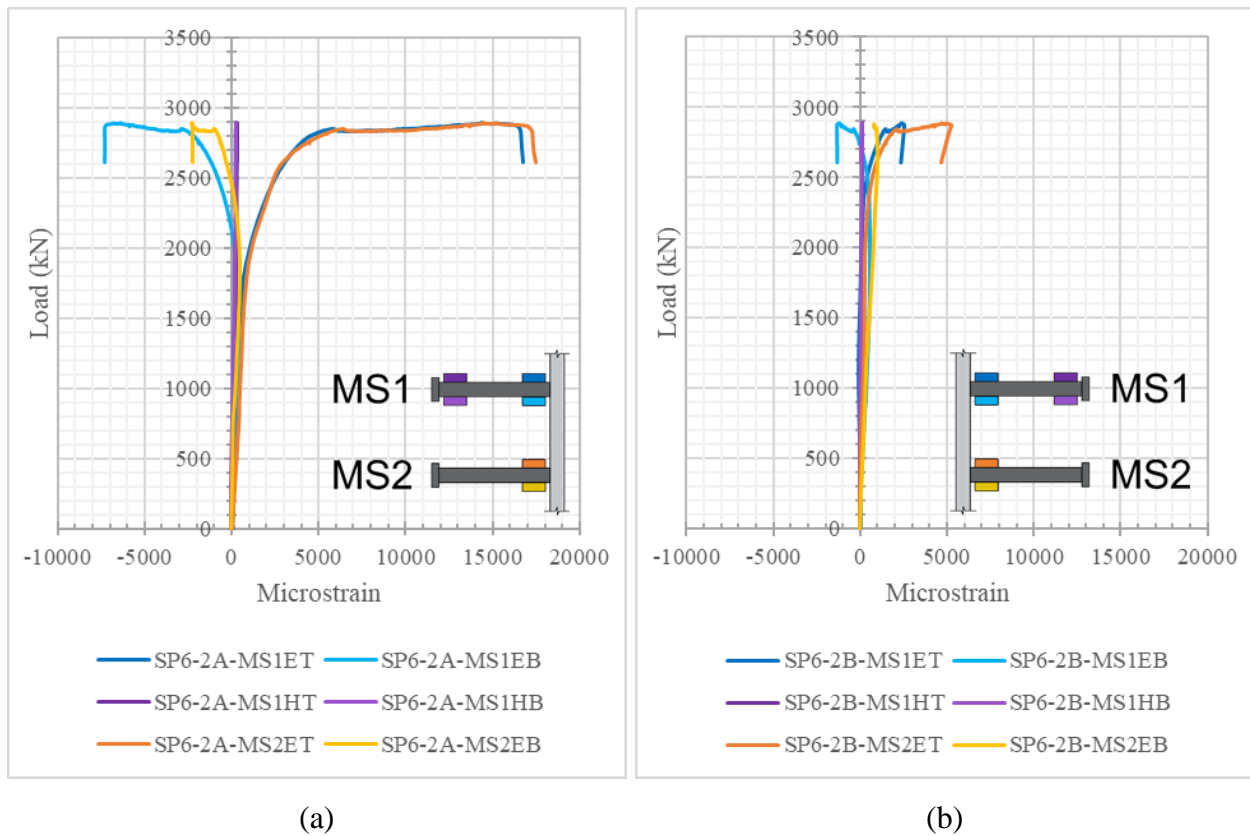


Figure 4.23 SP6-2 shear stud strain development for (a) specimen A, and (b) specimen B.

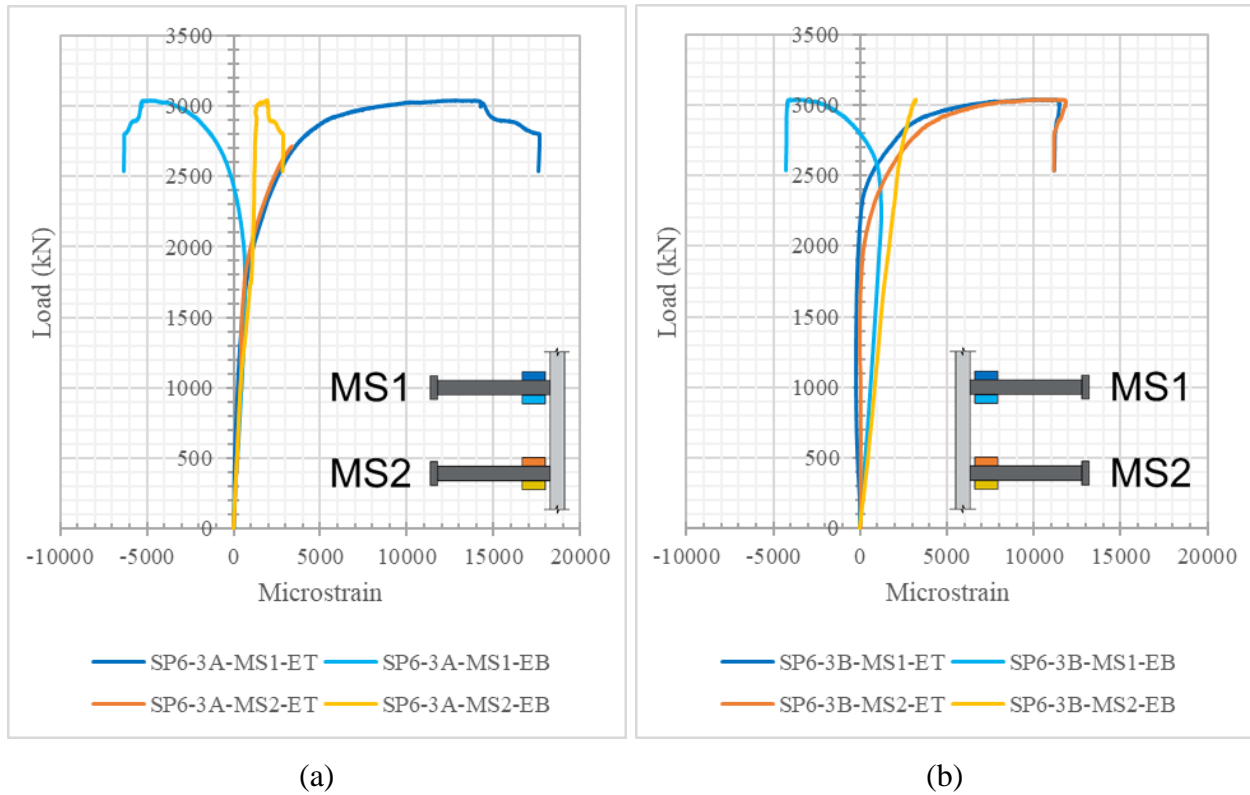


Figure 4.24 SP6-3 shear stud strain development for (a) specimen A, and (b) specimen B.

The center shear stud of in each shear pocket of the SP3 specimens had strain gauges at the base and the head. The MS-EB strain gauges all started with positive strains, but as the loading continued the values switched to negative. The MS-ET strain gauges remained positive during testing, which was to be expected. The results for the SP3 specimens are consistent with the failure modes seen.

The SP3-1A-MS-ET and EB strains at the ultimate load were 0.00237 and -0.00878, respectively, with greater compression below the stud and a concrete crushing failure. The SP3-1B studs sheared off and the strains showed greater tension on this side with strains at the ultimate load of 0.00722 for MS-ET and -0.00499 for MS-EB. The SP3-1A studs started yielding between 75% and 90% of the ultimate load at a load of 1192 kN, and the SP3-1B studs started yielding at a load of 1337 kN, which was shortly after 90% of the ultimate load.

The studs sheared off on both sides of the SP3-2 specimen, and the strains seen in both sides are similar [see Table 4.28 and Table 4.29]. The SP3-2A stud had strains of 0.01281 on the top surface and -0.00368 on the bottom surface, at the ultimate load. The SP3-2B recorded strains of 0.01241 on the top and -0.00187 on the bottom. In this specimen, the studs all yielded between 75% and 90% of the ultimate load at 1403 kN for the SP3-2A-MS and 1490 kN for the SP3-2B-MS.

The strains recorded in the strain gauges at the head of the studs were notably greater than those in the SP6 specimens, however they are still minimal compared to the strains at the base of the stud. The values remained positive, which indicates the heads of the studs were acting in tension the full duration of the test, and the greater strains were sustained on the top surface of the studs. However, at the ultimate load the maximum strains were all less than 0.001.

Table 4.26 SP3-1A Strain Gauge Results

Load (kN)	SP3-1A Microstrains ( $\mu\epsilon$ )			
	MS-ET	MS-EB	MS-HT	MS-HB
866 (P <sub>S</sub> )	902.14	131.67	436.99	27.55
1084 (75% P <sub>U</sub> )	2683.41	-663.94	646.68	97.09
1300 (90% P <sub>U</sub> )	5981.48	-1900.15	882.32	206.92
<b>1445 (P<sub>U</sub>)</b>	<b>2367.12</b>	<b>-8780.70</b>	<b>951.15</b>	<b>386.42</b>

Table 4.27 SP3-1B Strain Gauge Results

Load (kN)	SP3-1B Microstrains ( $\mu\epsilon$ )			
	MS-ET	MS-EB	MS-HT	MS-HB
866 (P <sub>S</sub> )	738.29	-132.72	287.09	98.58
1084 (75% P <sub>U</sub> )	1291.69	-334.98	408.29	153.02
1300 (90% P <sub>U</sub> )	3067.04	-1219.75	541.76	293.78
<b>1445 (P<sub>U</sub>)</b>	<b>7223.08</b>	<b>-4990.75</b>	<b>686.98</b>	<b>569.15</b>

Table 4.28 SP3-2A Strain Gauge Results

Load (kN)	SP3-2A Microstrains ( $\mu\epsilon$ )			
	MS-ET	MS-EB	MS-HT	MS-HB
1004 (P <sub>s</sub> )	1036.84	695.68	438.51	204.17
1256 (75% P <sub>U</sub> )	2101.40	496.92	572.61	284.22
1506 (90% P <sub>U</sub> )	6021.88	-448.99	697.70	414.04
<b>1674 (P<sub>U</sub>)</b>	<b>12812.47</b>	<b>-3687.94</b>	<b>797.63</b>	<b>614.89</b>

Table 4.29 SP3-2B Strain Gauge Results

Load (kN)	SP3-2B Microstrains ( $\mu\epsilon$ )			
	MS-ET	MS-EB	MS-HT	MS-HB
1004 (P <sub>s</sub> )	931.92	1323.29	179.03	186.79
1256 (75% P <sub>U</sub> )	1480.96	1501.75	303.00	275.91
1506 (90% P <sub>U</sub> )	4122.66	1125.54	474.79	414.05
<b>1674 (P<sub>U</sub>)</b>	<b>12409.41</b>	<b>-1872.30</b>	<b>674.73</b>	<b>600.55</b>

Visible in the Figure 4.25 and Figure 4.26, the MS-ET strain gauges within each shear pocket, aside from SP3-2B, show a peak in the strain between 90% of the ultimate load and the actual ultimate load. The maximum strain in MS-ET for the SP3-1A and B specimens was 0.0110 at a load of 1381 kN and 0.0135 at a load of 1435 kN, respectively. The maximum strain in MS-ET for the SP3-2A was 0.0028 at a load of 1652 kN. The MS-ET stud of the SP3-2B slab did not have a distinct peak like the others but shows a cluster of values between the ultimate load and failure. In comparing the graphical shapes of the recorded strains, the overall behaviour of both sets of 3-stud shear pockets was similar with respect to each other.

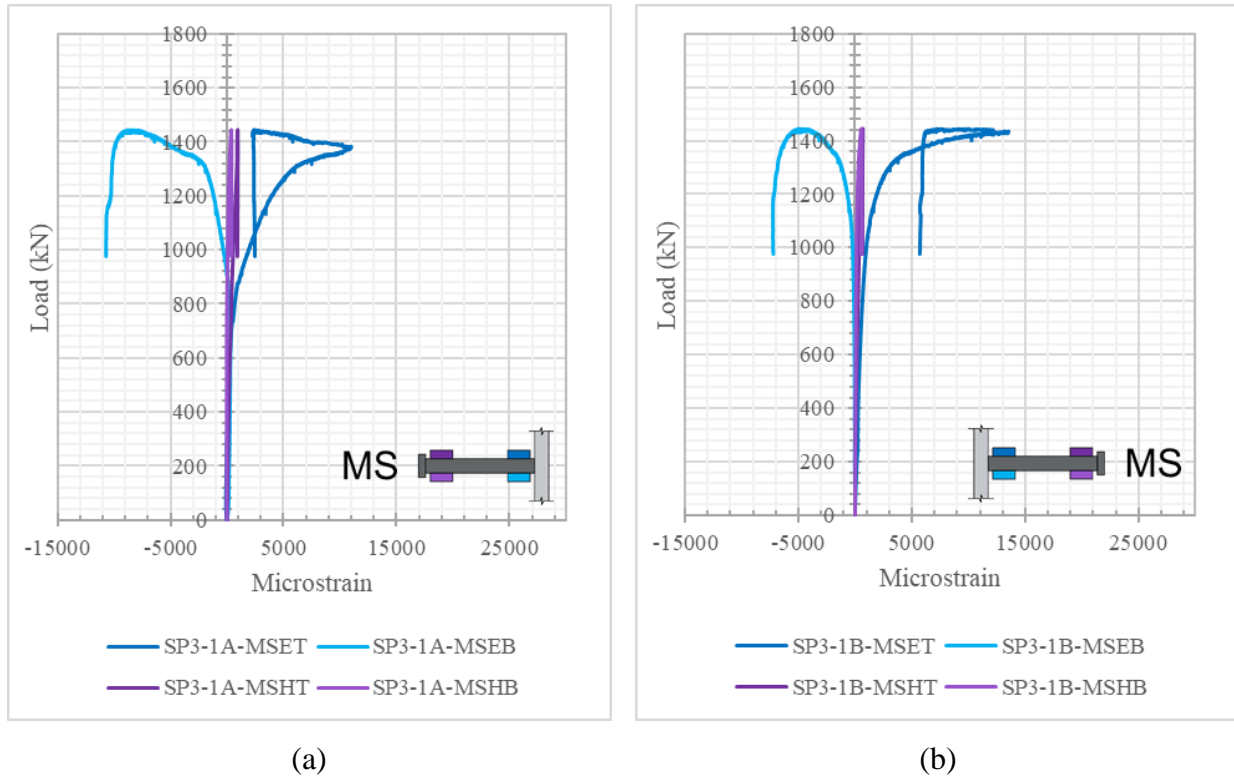


Figure 4.25 SP3-1 shear stud strain development for (a) specimen A, and (b) specimen B.

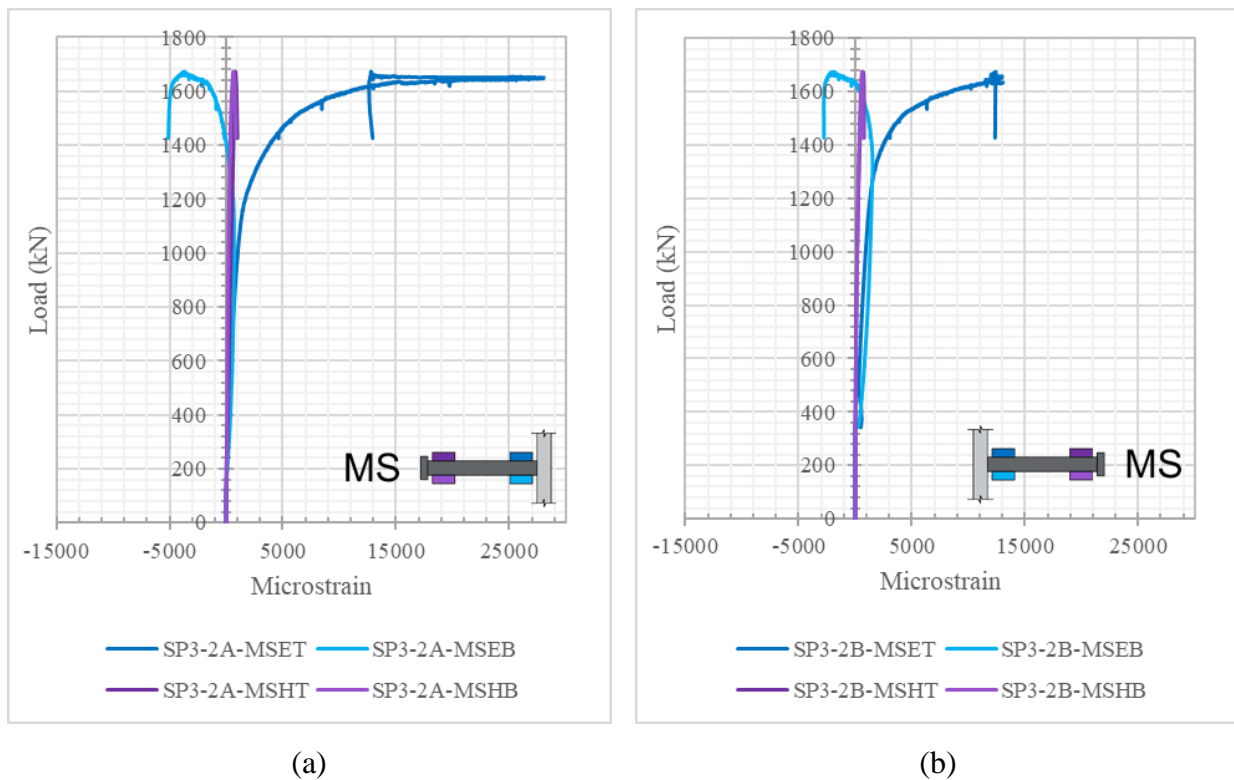


Figure 4.26 SP3-2 shear stud strain development for (a) specimen A, and (b) specimen B.

Comparing the results of the SP6 and SP3 shear stud strains a few assumptions may be made. As the MS1 studs were in the top row and the MS2 studs were in the bottom row relative to the loading in the SP6 specimens, the strain readings indicated the MS1 studs started bending and resisting tensile forces on the top face of the stud, and compression forces on the bottom face. With the exception of SP6-2A-MS2-EB, the MS2 studs all remained in tension and their strength was not fully utilized during testing. As reported, there were a few damaged strain gauges during testing, and they were all on the MS2 studs. The gauge damage was likely due to concrete cracking and crushing around these studs, which further supports that the second row of studs was not fully utilized during testing since there was concrete debonding.

The low strains seen at the heads of the studs in the SP6 and SP3 specimens also suggests that the shear stud length is longer than necessary. The performance also suggests six shear studs are not necessary, and three shear studs may be adequate depending on the application and strength requirements. However, in order to confirm these hypotheses more research and testing would be required.

Table 4.30 is a summary of the push-out test results including the ultimate load, failure mode and the yield load. The approximated ultimate load per stud from Table 4.14 are listed and the yield load is similarly divided by the number of studs to approximate the load in each stud when yielding started. The studs in the SP6 specimens tended to yield between 90% of the ultimate load and the ultimate load, whereas the SP3 studs yielded between 75% and 90% of the ultimate load. There does not appear to be any correlation between the failure mode and the stud yield load, in that, for example, SP3-1A studs reached the yield strain of 0.00384 at a lower load than SP3-1B but the specimen failed from the studs shearing off from the B side while the A side only experienced concrete crushing.

Table 4.30 Push-Out Test Results Summary

Specimen	Ult. Load per Stud (kN/stud)	A			B		
		Failure Mode	Yield Load*		Failure Mode	Yield Load*	
			(kN)	(kN/stud)		(kN)	(kN/stud)
SP6-2 <sup>†</sup>	241	Stud	2712	226	Concrete	2863	239
SP6-3	254	Concrete	2760	230	Concrete	2860	238
SP3-1	241	Concrete	1192	199	Stud	1337	223
SP3-2	279	Stud	1403	234	Stud	1490	249

\*The start of yielding for the studs broken into the overall load and the approximate load per stud. In the SP6 specimens this value is for the first stud that reached the yield point between the two rows of studs.

<sup>†</sup>Recall, only the SP6-2B-MS2 stud showed yielding. The SP6-2B-MS1 stud did not reach the yield strain of 0.00384.

## 4.4 Bridge Decks

The following section presents and discusses the results for the JPD and FPD testing. The results are presented in both graphical and tabulated format. For all charts, the results of the FPD series are presented in oranges and the JPD series are presented in blues, with the exception of the strain results of the FPD shear studs.

### 4.4.1 PUNCH Program Analysis

A computer software called PUNCH was used to estimate the failure loads prior to casting the bridge decks. The supporting structure including the girders and braces was designed to have sufficient capacity in comparison with the tested samples. The load cell capacity was selected to be larger than the estimated load capacity of the deck. The calculated deck failure load was also used to select the hydraulic jack and cylindrical spring piston with the appropriate capacity for testing.

PUNCH was one of several computer programs in a series of bridge analysis tools developed by Dr. John P. Newhook, Dr. Aftab Mufti and Dr. Huma Khalid [10]. It is designed to predict the behaviour and failure load of laterally restrained concrete slab-on-girder bridge decks. The PUNCH program applies truck wheel loads from the Canadian Highway Bridge Design Code (CHBDC) CL-625 design vehicle or the American Association of State Highway Transportation Officials (AASHTO) HSS design vehicle. The geometric properties of the bridge deck, support girders, and design vehicle are input into the program and its algorithm loads the theoretical bridge to failure.

The initial input with 45 MPa concrete compressive strength and a CL-625 design vehicle resulted in a punching failure load of 1530 kN. The PUNCH analysis was run again with 80 MPa concrete compressive strength since the actual compressive strengths from cylinder material testing were between 81 and 84 MPa for both bridge decks [see Table 4.3]. The failure punching load was given as 1536 kN, only slightly higher than the first test.

#### **4.4.2 Experimental Failure Modes**

Both bridge decks failed by punching, but neither had a full punch cone on the underside of the deck. The behaviour during testing was very similar between decks, which is the desired outcome when joining precast elements together with cast-in-place connections. The JPD and FPD both failed in punching of the RC deck concrete; however, a full punch cone was not observed, only large transverse cracks along the underside of the deck, spanning between girders. Figure 4.27 is a section view along the deck centerline to show the main crack of the failure punch cone.

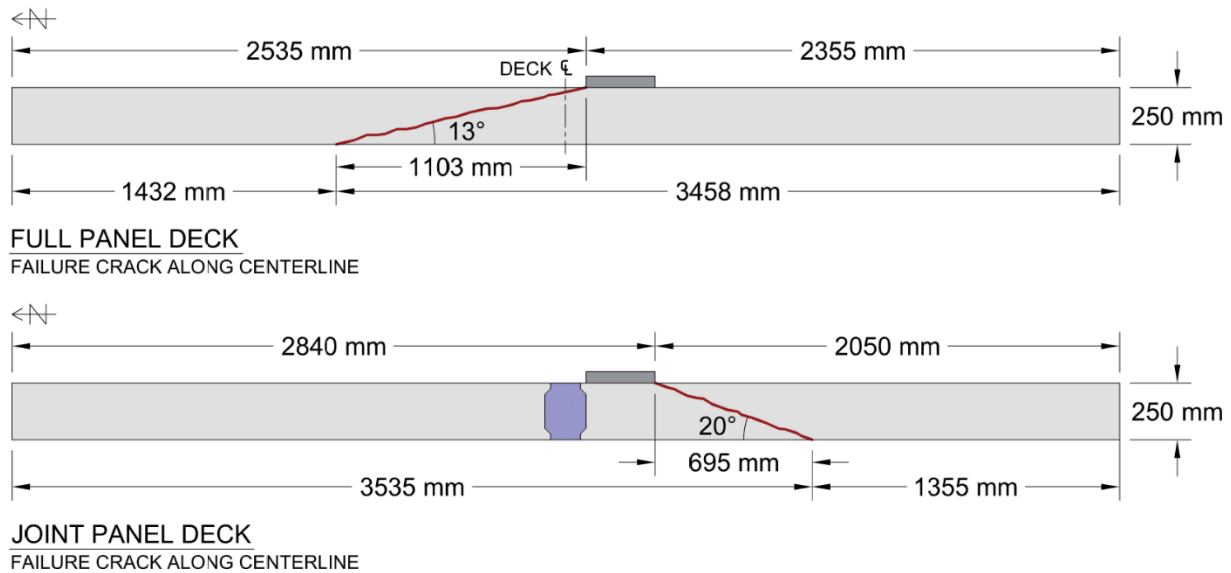


Figure 4.27 Failure crack along longitudinal centerline for FPD and JPD.

The location of the crack was measured and the angle was determined based on the location of the load plate. The FPD failed within the north half of the deck slab and the JPD failed within the south panel. The JPD failure was assumed to occur in the south panel since it was less likely to fail through the much stronger UHPC joint.

#### 4.4.3 Cracking Patterns

During the testing of the JPD the first crack was not visible until a load of approximately 400 kN. As aforementioned, the testing was paused every 200 kN to mark crack progression on the underside of the bridge deck. The pause in cracking in both the JPD and FPD can be seen in the graphical results with vertical dips in the lines. The hydraulic jack was pumped beyond 1200 kN before pausing to mark the cracks and its O-ring failed near 1300 kN, causing an oil spill during testing. Therefore, the JPD was unloaded while the oil spill was cleaned up and a new one installed to continue testing. When testing resumed, the deck was loaded to 1400 kN before pausing to mark the continued crack progression. It was deemed safe to still mark cracking at this load because there were no signs of ultimate failure, and the PUNCH analysis predicted a failure load

of 1530 kN. After this point the JPD was loaded continuously until its ultimate failure load of 1878 kN. This load was just over 20% greater than the estimated failure from the PUNCH analysis. The FPD test had no equipment issues, however, during the trial test, which was run to ensure all instrumentation was working correctly, a spike in the pi-gauges values indicated the first crack had occurred at approximately 180 kN. The first crack was barely visible to the naked-eye and a magnification tool was used to confirm its start and end and measure its width. Cracks typically become visible to the naked-eye at a width of around 0.05 mm, and this crack measured just below at 0.04 mm. The third pi-gauge was therefore installed prior to commencing the actual testing. The first crack occurred below the load plate and thus, the third pi-gauge was installed in a similar location to the third pi-gauge of the JPD, as seen in Figure 3.39. The instrumentation was zeroed after the trial test; therefore, the data was corrected to start the first crack pi-gauge readings at 0.04 mm.

Since the first crack had already occurred, the first pause in the actual FPD testing to mark cracks was at 200 kN. The testing continued, marking cracking at 200 kN intervals, until 1400 kN when the deck was loaded until its ultimate failure load of 1926 kN.

Photographs and measurements were taken to map the cracks in AutoCAD and create diagrams for each 200 kN interval during testing and after failure. The results are shown in Figure 4.28 through Figure 4.31 with the FPD and JPD diagrams adjacent for each load interval. Since the crack progression was captured at 1200 kN in the FPD test, unlike the JPD test, there was no figure to compare and therefore the crack pattern at 1000 kN for the JPD is shown adjacent to the 1200 kN results for the FPD [see Figure 4.30]. The post-failure cracking is shown with red lines to distinguish it from the cracking prior to failure [see Figure 4.31].

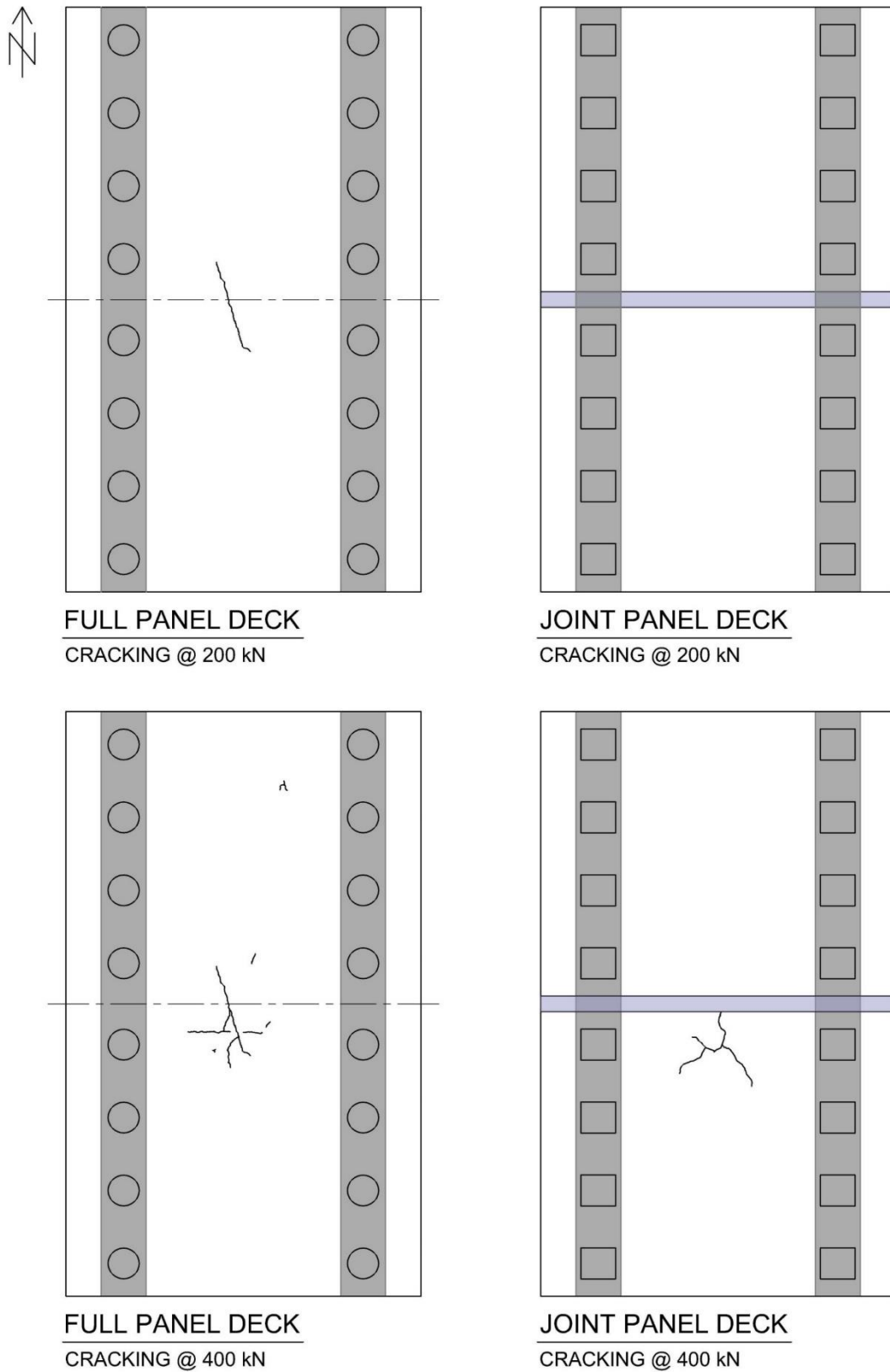


Figure 4.28 Crack development at 200 kN and 400 kN during bridge deck testing.

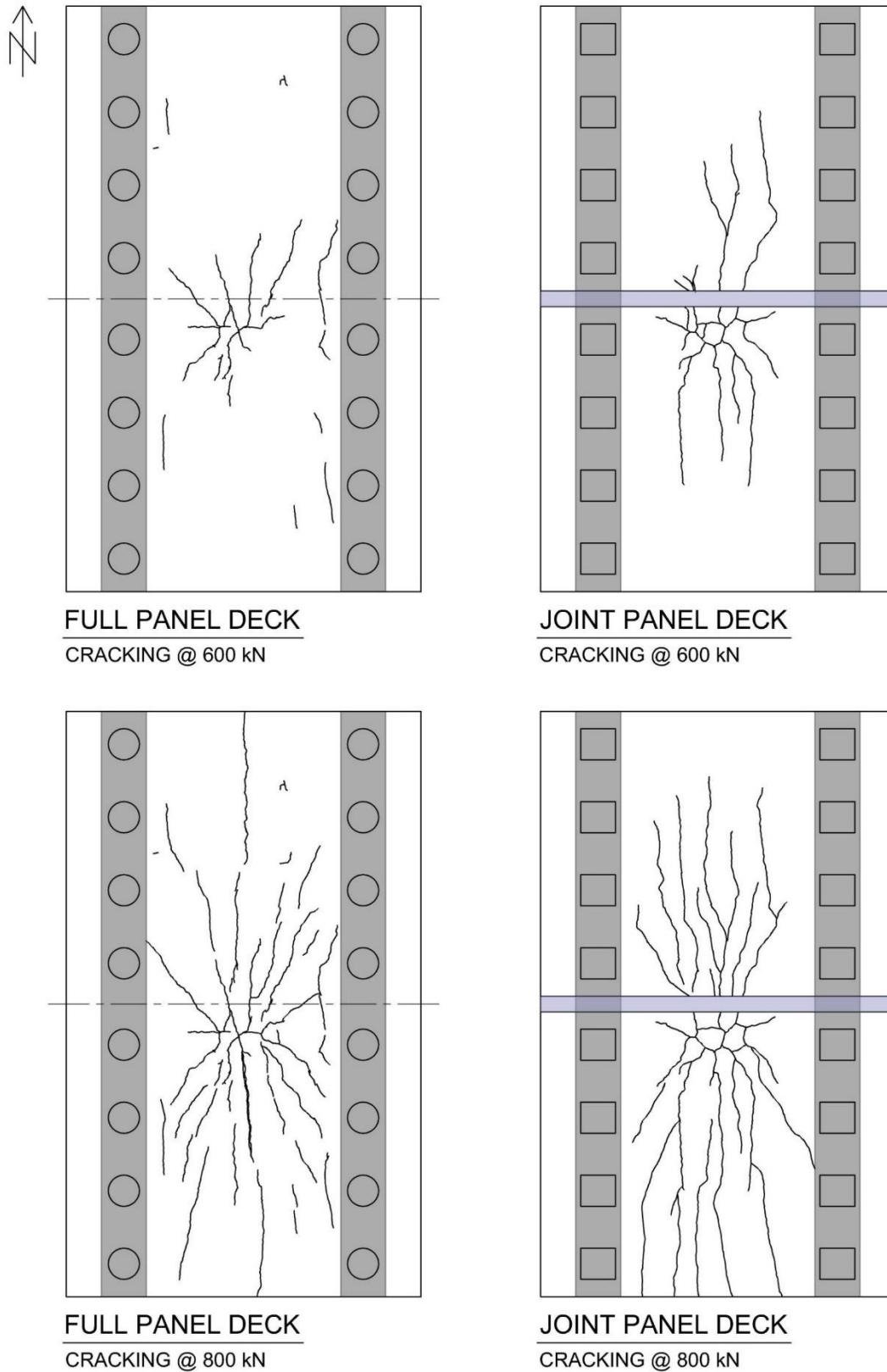


Figure 4.29 Crack development at 600 kN and 800 kN during bridge deck testing.

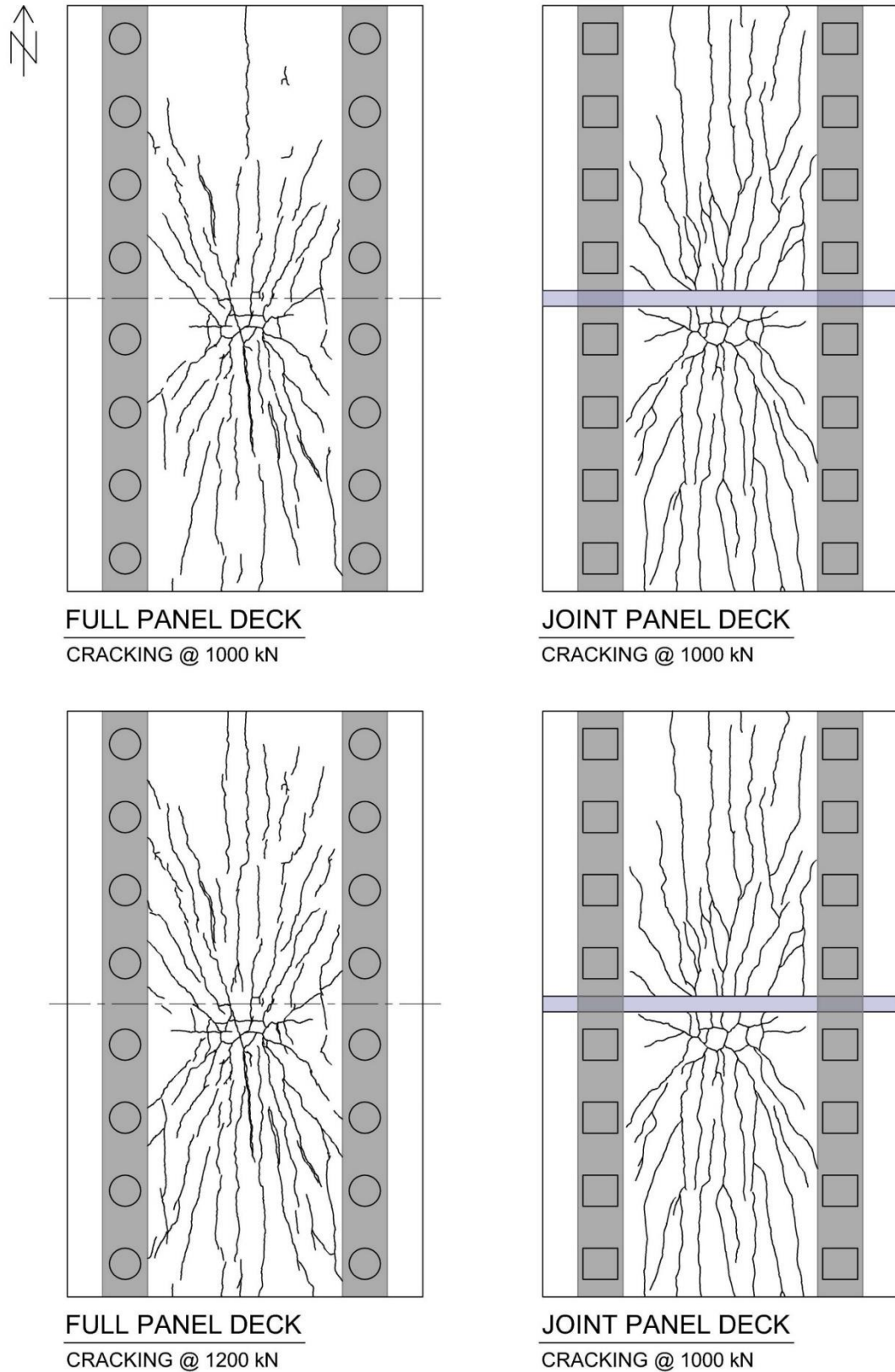


Figure 4.30 Crack development at 1000 kN and 1200 kN during bridge deck testing.

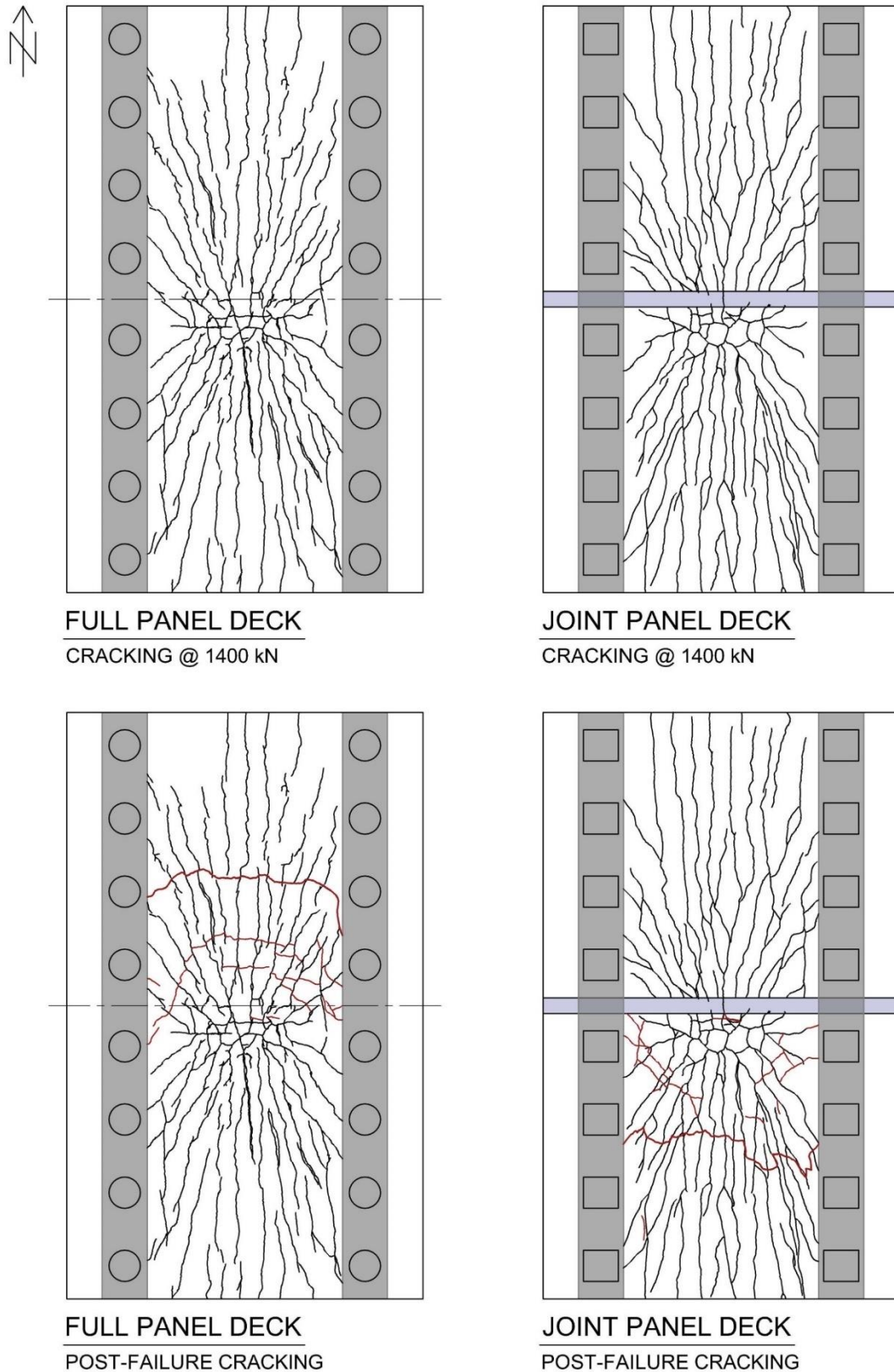


Figure 4.31 Crack development at 1400 kN during bridge deck testing and post-failure cracking.

The crack progression and overall pattern for both bridge decks were very similar, despite the UHPC joint connecting the panels of the JPD. Up to 600 kN, the cracks in the JPD were longer, more interconnected, and all stem from directly beneath the load plate, whereas the FPD cracks were shorter and more sporadic. Not only does the number of cracks in both decks appear to be similar from 800 kN onwards, but there is equal cracking on either half of the decks. Though it is not known when cracking occurred internally in the UHPC joint, it was not visible on the deck surface until 1400 kN.

The top of both bridge decks did not show any cracking during testing. Upon failure, the load plate had sunk into the deck by an average depth of one millimeter for both the FPD and JPD, and otherwise there was no visible cracking [Figure 4.32]. The failure crack of both decks is also seen in the Figure 4.33 and Figure 4.34.



Figure 4.32 Post-failure load plate punch shape in bridge deck surface: (a) JPD with load plate; (b) FPD after load plate removed.



Figure 4.33 FPD failure crack after chiselling away loose pieces of concrete (north half of deck).



Figure 4.34 JPD failure crack after chiselling away loose pieces of concrete (south panel).



Figure 4.35 JPD demolition setup with concrete water saw.

After testing, the bridge decks were cut for safe removal from the structural laboratory. Two longitudinal cuts were made along the inside of each girder, and two transverse cuts were made to separate the deck into three pieces. The transverse cuts were made on either side of the load plate to observe the top of the punching cone.

The cut deck sections of the FPD are shown in Figure 4.36 and Figure 4.37. The section cut around the load plate location clearly shows the shape of the top of the failure cone in the transverse direction [Figure 4.36]. The cracking appears to continue over top of the girders, since the cracking does not terminate at the bottom edge of the section on either face shown in Figure 4.36. However, there was no cracking seen on the bottom face of the deck on the outside of either support girders, thus it is assumed the width of the punching cone ends over top of the girders. Figure 4.37 shows the cracking of the opposite face to Figure 4.36(b) and has more pronounced cracking in the RC

(please note this image was created from merging photographs, which is why the colouring changes across the deck).



(a)



(b)

Figure 4.36 FPD cut section around load plate: (a) northern face adjacent to load plate edge (looking south), and (b) opposite face of section (looking north).



Figure 4.37 FPD deck section of south half (looking south).

The same deck cuts were made to the JPD. The first photograph is through the edge of the UHPC joint along the opening, and thus the 25 mm at the top and bottom are RC, while the rest of the concrete is UHPC [Figure 4.38(a)]. Comparing the opposing faces of the deck section below, there are fewer cracks in the UHPC than the RC, and they generally appear to be shorter and wider, whereas the cracks in the RC are all interconnected.



(a)



(b)

Figure 4.38 JPD cut section around load plate: (a) southern joint-panel interface adjacent to load plate edge (looking south), and (b) opposite face of section south side of load plate (looking north).



Figure 4.39 JPD deck section of north panel, cut through UHP joint (opposite cut of Figure 4.38(a), looking north).

The photographs of Figure 4.40 are of the section cut out of the north half of the JPD including the joint. Consistent with the opposite cut face of the UHPC, there are minimal cracks seen throughout the joint. Seen in photograph (a), there is displacement between the UHPC and RC along the center of the joint-slab interface. This debonding and slippage did not occur until the JPD failure, as the test footage shows the sudden drop at failure. On the west side of the joint, the cracking does not go through to the RC, as seen in photograph (b). In the opposite corner in photograph (c), the minor cracks terminate at the joint interface, however a large crack is seen to continue well into the RC of the JPD north panel along the east edge; this crack was measured to go approximately 855 mm into the deck. Therefore, though the main failure crack was seen in the south panel of the JPD, there was significant cracking through the north panel that contributed to the deck failure.

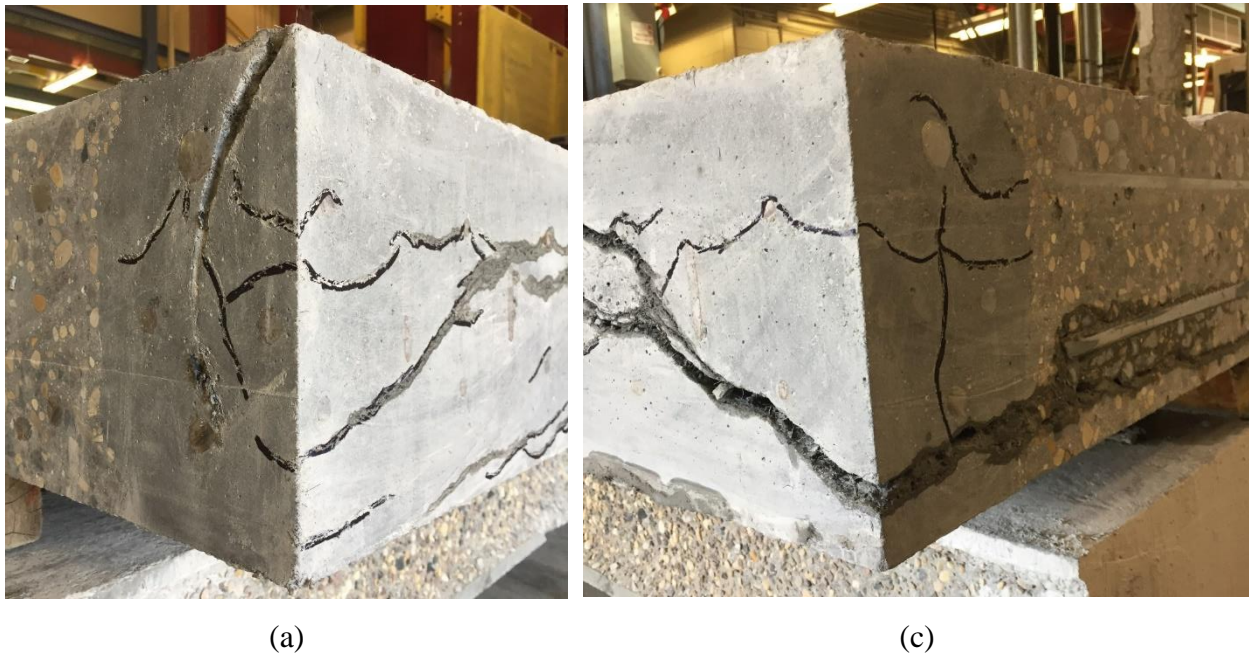


Figure 4.40 South corners of the north JPD section from Figure 4.39: (a) south-west corner, and (b) south-east corner.

The pi-gauge readings are seen in Table 4.31 at various loads throughout testing; the loads after the first crack of each deck, intermittent loads up to the service load, the service load (60% of the ultimate load), 75% and 90% of the ultimate load, and the ultimate load. Negative values indicate concrete crushing, while positive values indicate concrete cracking and/or debonding along the joint interface; however, the latter was less likely. The values in grey are those that are not visible to the naked-eye, because cracks are not usually observed until they are an approximate width of 0.05 mm. Based on the female-female shape of the JPD deck joint debonding and/or cracking was expected to occur at the southern joint-deck interface first since it was adjacent to the edge of the load plate. Depending on the bond strength between the RC and UHPC joint, the northern joint-deck interface would either experience crushing or debonding.

The values of PGS for both decks were less than 0.01 mm until service load. The FPD-PGS read 0.259 mm at 75% of the ultimate load, and 0.637 mm at the ultimate load of 1926 kN. The FPD-PGN indicated minimal crushing with mostly negative readings. At 90% of the ultimate load the gauge measured -0.048 mm and at the ultimate load it measured -0.022 mm. The first crack, which was directly underneath the load place, reached a width of 0.915 mm at the ultimate load.

The JPD had similar pi-gauge readings until surpassing the service load. For this deck, the JPD-PGN across the north joint interface, the values were positive until the ultimate, indicating there was debonding or cracking at this location for the majority of the test duration. The JPD-PGN went from 0.037 mm at 90% of the ultimate load to -0.089 mm at the ultimate load. At the other joint interface, the JPD-PGS recorded 0.535 mm at 75% of the ultimate load and 1.169 mm at the ultimate load. The first crack of the JPD expanded to a width of 1.241 mm at the ultimate load [Table 4.31].

Table 4.31 Pi-gauge measurements for FPD and JPD during testing.

Load (kN)*	UHPC Debonding / Crack Widths (mm)					
	FPD			JPD		
	PGS	PGN	PGFC	PGS	PGN	PGFC
200	0.007	< -0.001	0.076	0.008	0.007	–
400	0.007	< -0.001	0.076	0.013	0.007	0.047
600	0.008	< -0.001	0.177	< 0.001	0.009	0.194
800	0.009	-0.003	0.290	0.005	0.008	0.311
P <sub>s</sub>	0.015	0.004	0.409	0.020	0.004	0.488
75% P <sub>U</sub>	0.259	-0.011	0.559	0.535	0.007	0.634
90% P <sub>U</sub>	0.435	-0.048	0.691	0.986	0.037	0.984
<b>P<sub>U</sub></b>	<b>0.637</b>	<b>-0.022</b>	<b>0.915</b>	<b>1.169</b>	<b>-0.089</b>	<b>1.241</b>

\*For the FPD: P<sub>s</sub> = 1156 kN, 75% P<sub>U</sub> = 1446 kN, 90% P<sub>U</sub> = 1733 kN, P<sub>U</sub> = 1926 kN.

For the JPD: P<sub>s</sub> = 1126 kN, 75% P<sub>U</sub> = 1408 kN, 90% P<sub>U</sub> = 1690 kN, P<sub>U</sub> = 1878 kN.

The pi-gauge results of the FPD and JPD are graphed together in Figure 4.42. To simplify this graph, the portion of JPD data during the unloading and re-loading due to the hydraulic jack O-ring failure was removed because the chart was difficult to interpret with it included.

The graphical data presents a better summary of the pi-gauge results from testing. As seen in the Table 4.31 and confirmed by the graphed data, the FPD-PGN does not indicate notable crushing or cracking until roughly 1200 kN where a sudden negative drop in the data occurs. The drop in data is thought to be a combination of measuring concrete crushing, and the pi-gauge being bumped during crack marking; once testing resumed, the data continued its readings from approximately -0.08 mm (if the gauge reading was only due to human error, it would have rebounded to its readings prior to the loading pause during crack marking). The JPD-PGN exhibited minimal cracking after 1400 kN (less than 0.05 mm) was passed and concrete crushing

after approximately 1750 kN, as its values cross into the negatives until the deck failure [Figure 4.42].

Referring back to the cracking pattern figures, there are no visible cracks near either deck center throughout most of the testing, however there is a crack across the center of the JPD's joint seen at 1400 kN [Figure 4.31]. Close-up photographs of both bridge decks after testing once the pi-gauges were removed show neither FPD-PGN or JPD-PGN have any visible surface cracks passing between the pi-gauges' points of measurement [Figure 4.41]. The photograph (b) shows a crack that narrowly misses passing between the JPD-PGN measurement points.

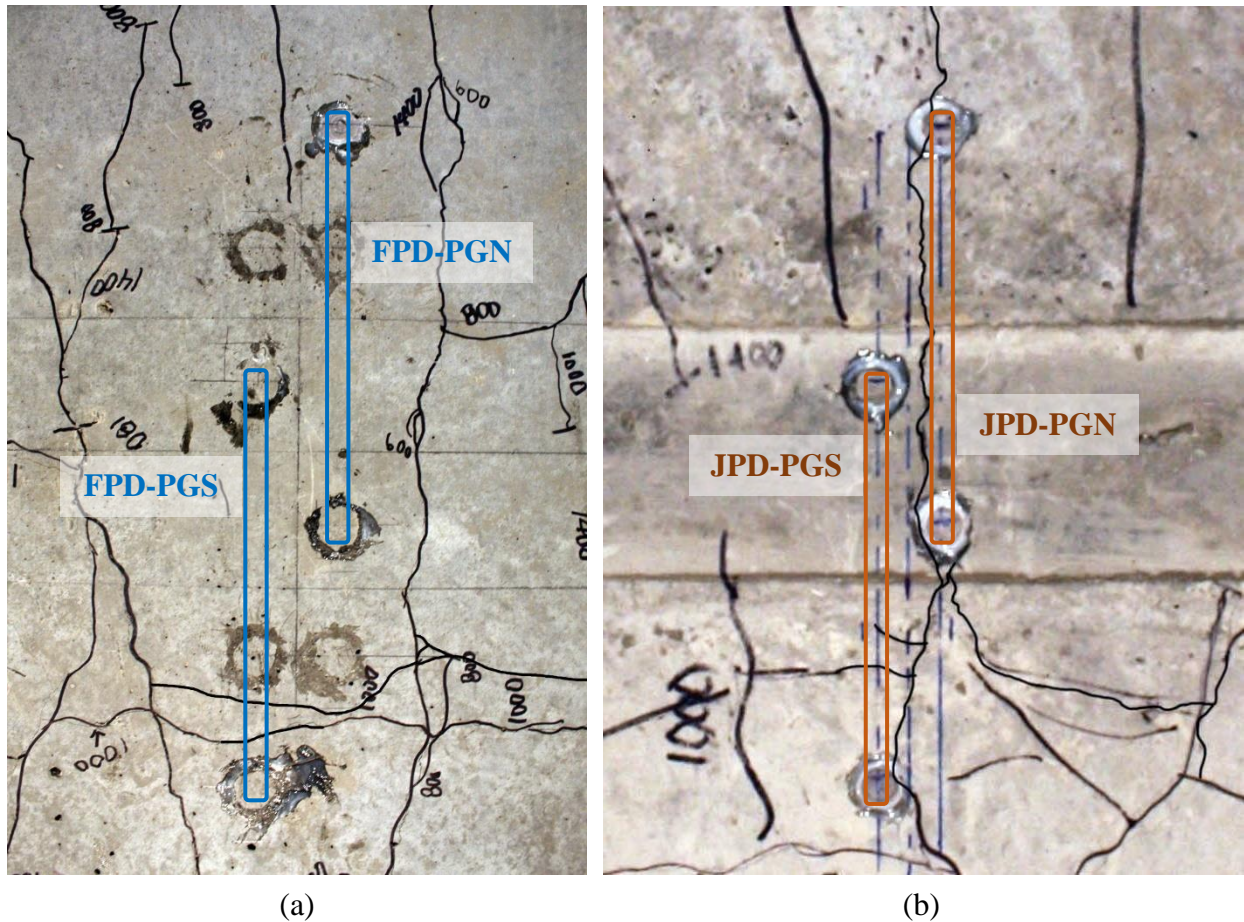


Figure 4.41 Close-up photographs at the deck center post-testing of (a) FPD, and (b) JPD.

The PGS pi-gauges present more interesting results. The FPD-PGS started reading notable crack width around a load of 800 kN, at which point the values increased steadily until failure. Though the JPD-PGS values did not increase until 1300 kN, the measured crack widths increased at a greater rate. In the Figure 4.41 both the FPD and JPD have two cracks that run perpendicular to the PGS. Upon inspection of the JPD, and further examination of the photographs, there was no indication of debonding along the UHPC joint at any point during testing. Therefore, it is assumed the JPD-PGS measured concrete cracking and not debonding between the UHPC joint and RC Panel. Without a joint, the FPD-PGS was evidently only measuring the concrete cracking.

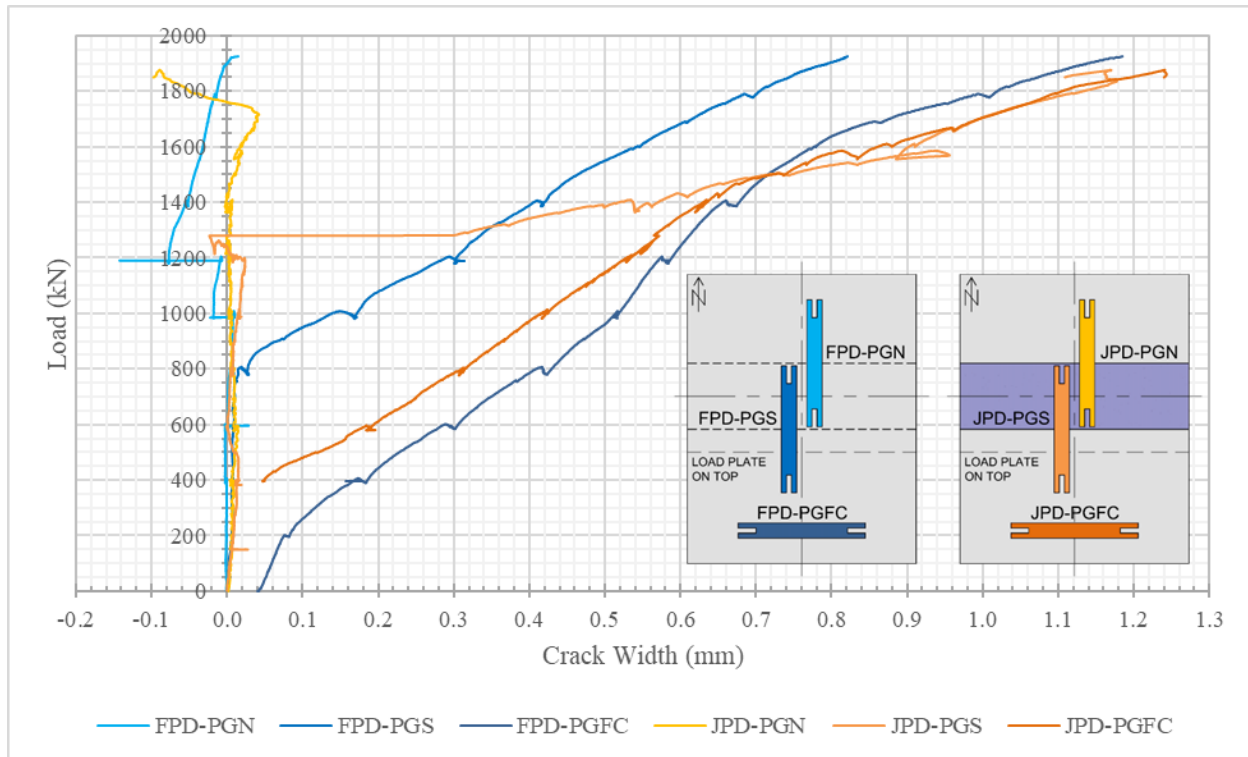


Figure 4.42 Crack width development during bridge deck testing.

As discussed in Chapter 3, the PGN and PGS were placed across the joint-deck interface on the JPD and thus the same location on the FPD for direct result comparison. However, there was no guarantee what the pi-gauge readings would or would not measure cracking or debonding. The

PGFC was glued to the bottom of the deck across the first crack that occurred during testing of both decks. These first cracks were in very similar locations below the load plate [see Figure 3.39 and Figure 4.28]. Since both pi-gauges were definitely measuring a crack width, these results are better for comparison.

The crack widths progressed at similar rates, despite occurring at different loads. Recall the first crack in the FPD was seen during the trial test at 180 kN and measured 0.04 mm, and the first crack in the JPD was not seen until just below 400 kN and measured 0.047 mm. Until after the loading surpassed 1000 kN, the FPD's first crack was approximately 0.1 mm larger than the JPD's first crack. The width of the JPD crack surpassed the FPD's at 1500 kN, and had a width of 1.241 mm at the ultimate load of 1878 kN [Table 4.31]. Approximating from the Figure 4.42, the FPD-PGFC was 1.1 mm at the JPD's ultimate load of 1878 kN, before reaching its ultimate load of 1926 kN with a crack width of 0.915 mm.

#### **4.4.4 Load Deflection Behaviours**

The deflection results are presented in three formats in this section for both bridge decks. The full results are graphed to show the deflection development for the LVDTs along the centerline and transversely across the deck-joint interface. The results at select loads are tabulated and graphed in a profile view to demonstrate the deflected shape. These select loads reflect the conditions at various stages of testing: before or at the first crack, at a few intermittent loads, at 60% of the ultimate load (service load), 75% of ultimate, 90% of ultimate, and the ultimate load. Though the LVDT data is reported in positive values, the deck displacement was in the downward direction.

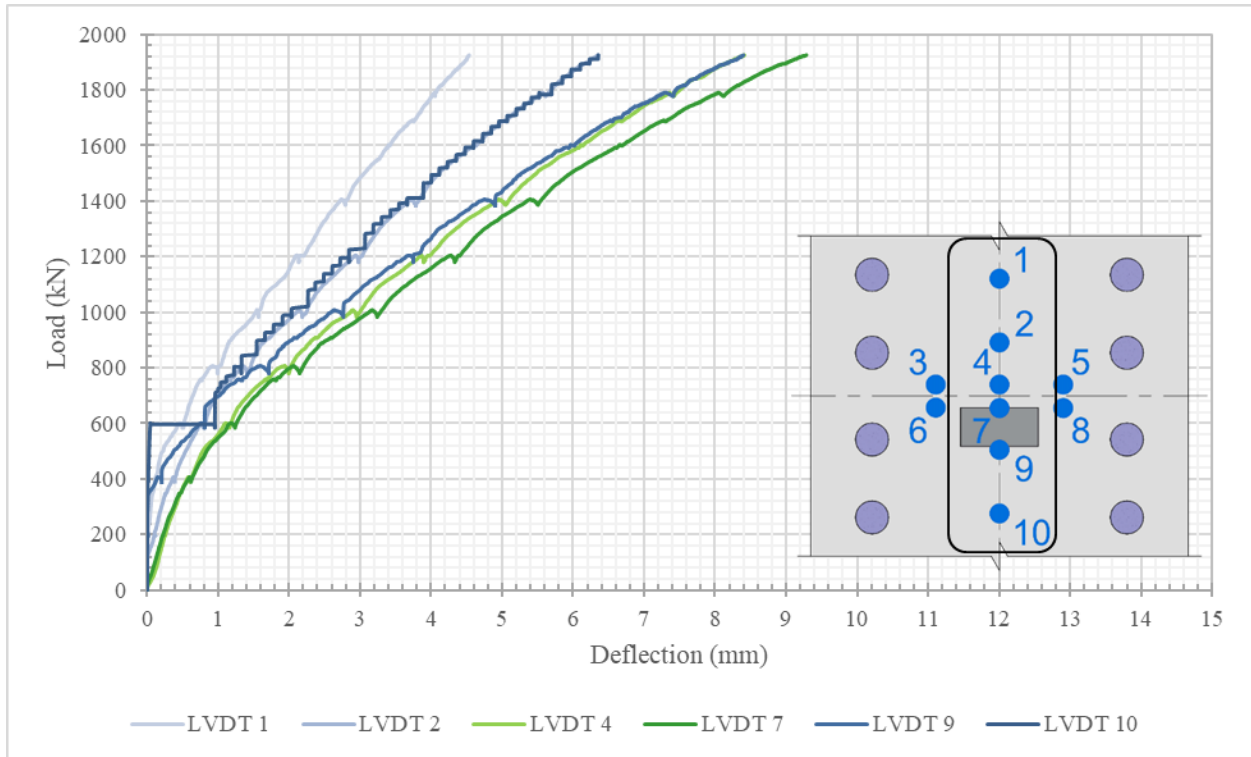


Figure 4.43 FPD longitudinal centerline deflection development during testing.

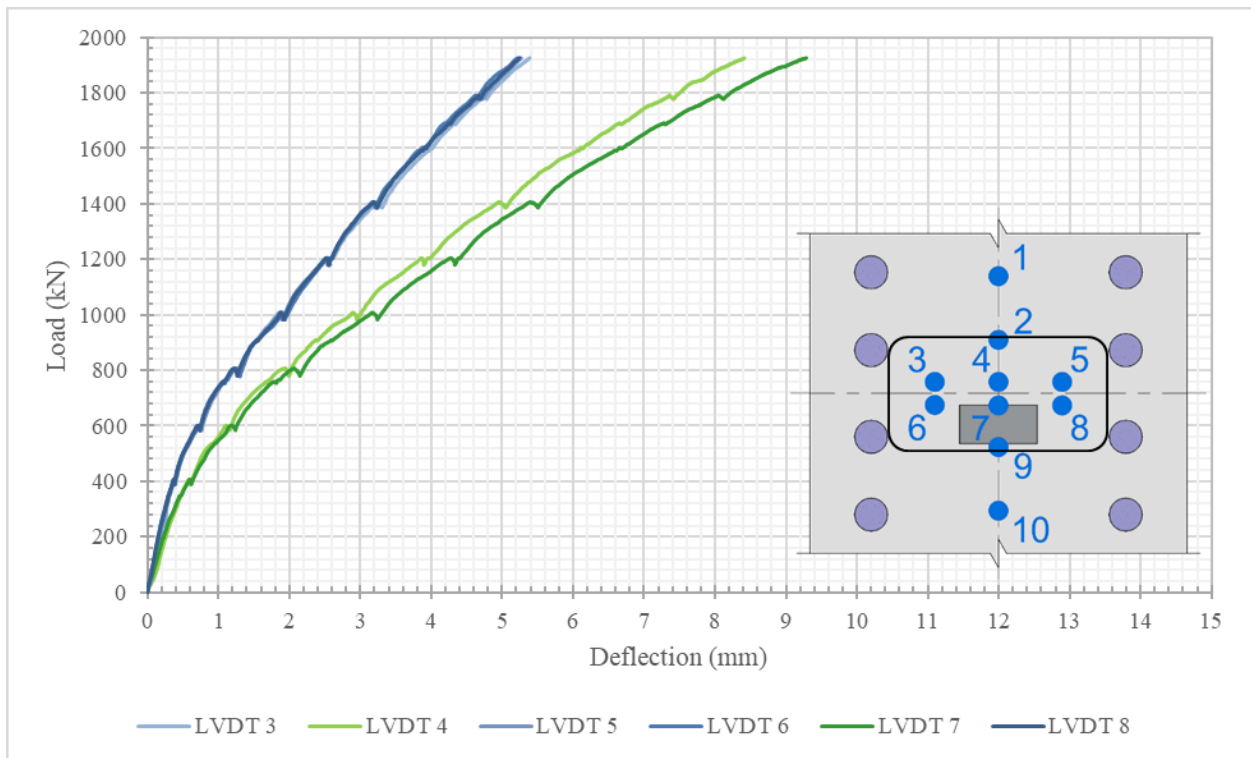


Figure 4.44 FPD transverse deflection development during testing.

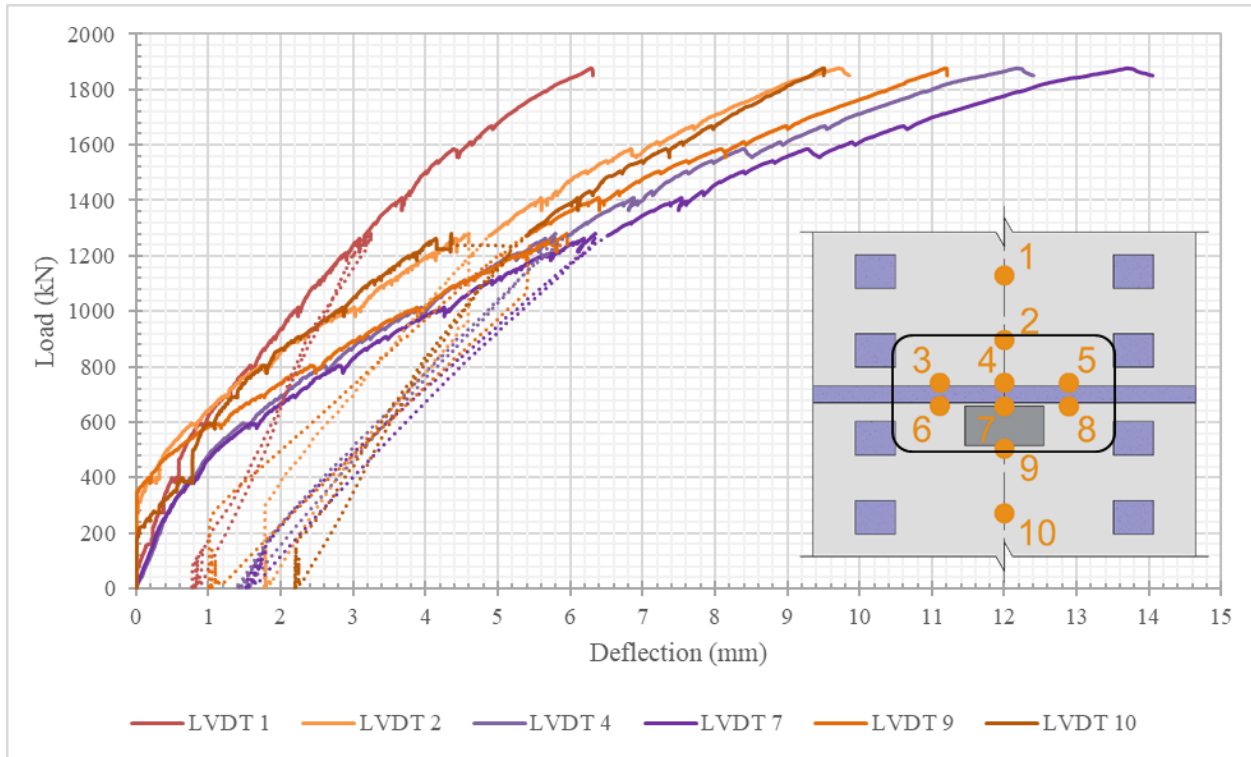


Figure 4.45 JPD longitudinal centerline deflection development during testing.

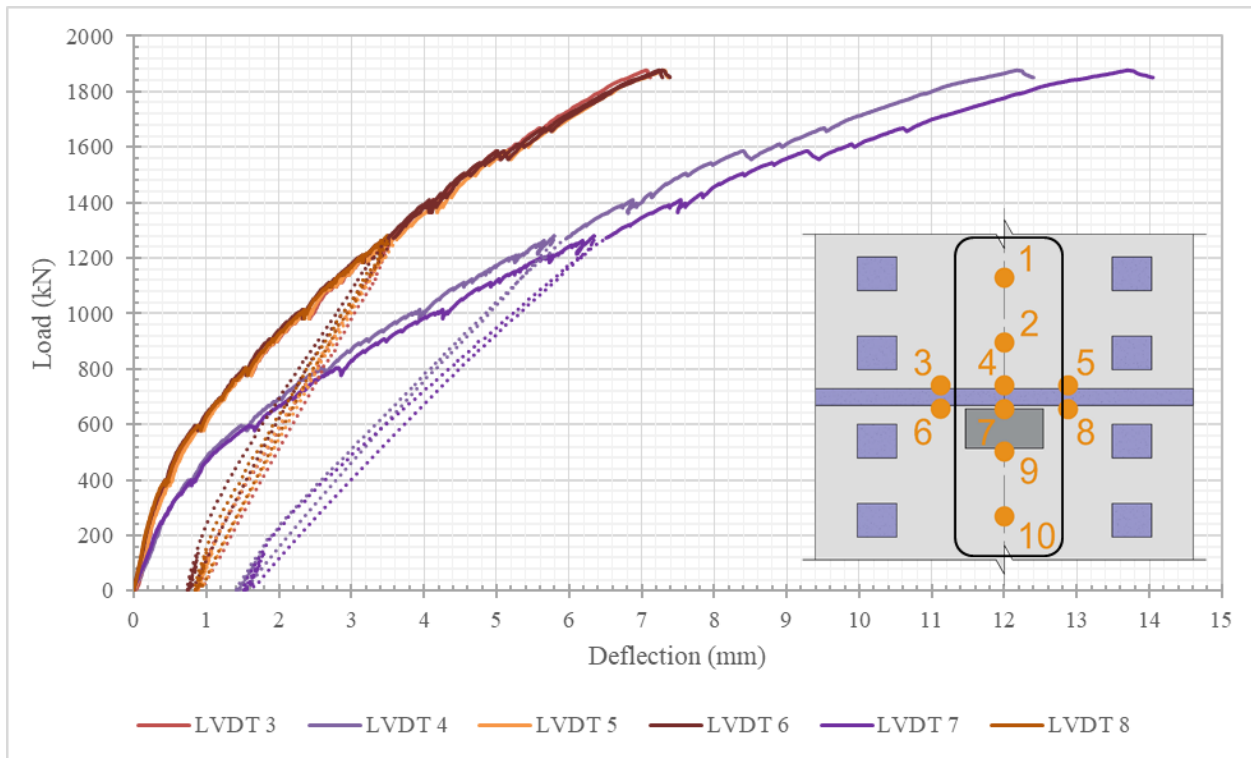


Figure 4.46 JPD transverse deflection development during testing.

The deflection behaviour for both bridge decks are similar; the largest deflections are seen at the center and on the south side of the load plate, at LVDTs 4, 7 and 9. From there the deflections decrease longitudinally along the deck centerline and transversely across the deck-joint interfaces. Since the free ends of the decks are nearly 5 m, whereas the span between the inside edges of the girders is 1625 mm, the decks were quite restricted in the transverse deflections. LVDT 1 was the farthest from the load plate and therefore has the lowest displacement values, followed by LVDTs 2 and 10. Since LVDTs 4 and 7 are reported in the results with the longitudinal and transverse data due to their locations, they have different colours in the displacement development graphs. The FPD deflections were smaller than those recorded in the JPD. The FPD displacements ranged from 4.5 mm to 9.5 mm and the JPD displacements were between 6 mm and 14 mm [see Figure 4.43 to Figure 4.46].

The deflection results are summarized, first for the longitudinal deflections along both deck centerlines, and then for the transverse deflections. They are presented in this order to allow direct comparison between bridge decks. The largest deflection in the FPD at the ultimate load of 1926 kN was 9.29 mm at LVDT 7 at the bridge center, followed by the LVDTs 4 and 9 that measured 8.41 mm and 8.40 mm, respectively [Table 4.32]. The largest deflection in the JPD at its ultimate load of 1878 kN was 13.70 mm at LVDT 7. The deflection on the north joint-deck interface of LVDT 4 was slightly lower at 12.18 mm, and the LVDT 9 on the south side of the load plate measured 11.19 mm [Table 4.33]. The LVDTs 4 and 9 of the FPD had very similar displacements during testing than the JPD much closer in the displacements, varying by less than 0.4 mm throughout the start of testing, and gradually converging to within 0.01 mm. The JPD's LVDTs 4 and 9 varied at random between 0.01 mm and 1 mm throughout testing. The variance between these LVDTs shows the slight differing behaviour of the monolithic full panel cast of the FPD and

the jointed panels of the JPD. Though the UHPC joint is very strong and well bonded to the RC panels, the fact there are two different materials cast at different times still affects the overall behaviour of the deck. However, that being said the variance in the deflections along the deck centerlines at the joint are minimal.

Overall, the FPD deflections were less than the JPD deflections, despite the FPD attaining a greater applied load. At the ultimate load the differences between the FPD and JPD deflections vary by 1.75 mm at LVDT 1 to 4.41 mm at LVDT 7. Considering the deflections and loads at LVDT 7 at the ultimate load, the deflection rate of the FPD was 4.82 mm/N and the JPD deflection rate was 7.30 mm/N. At the point of least deflection, LVDT 1, the FPD and JPD were measuring 2.35 mm/N and 3.35 mm/N at the ultimate load, respectively.

Table 4.32 FPD Centerline Longitudinal Deflection Results

Load (kN)	Deflection (mm)					
	LVDT 1	LVDT 2	LVDT 4	LVDT 7	LVDT 9	LVDT 10
200	0.02	0.10	0.25	0.23	0.00	0.00
400	0.12	0.38	0.59	0.61	0.20	0.02
600	0.47	0.77	1.11	1.19	0.78	0.05
800	0.88	1.31	1.86	2.01	1.53	1.23
1156 (P <sub>s</sub> )	2.00	2.72	3.62	3.99	3.38	2.61
1446 (75% P <sub>U</sub> )	2.89	3.93	5.24	5.69	5.03	3.89
1733 (90% P <sub>U</sub> )	3.88	5.25	6.94	7.58	6.84	5.31
<b>1926 (P<sub>U</sub>)</b>	<b>4.54</b>	<b>6.36</b>	<b>8.41</b>	<b>9.29</b>	<b>8.40</b>	<b>6.35</b>

Table 4.33 JPD Centerline Longitudinal Deflection Results

Load (kN)	Deflection (mm)					
	LVDT 1	LVDT 2	LVDT 4	LVDT 7	LVDT 9	LVDT 10
200	0.23	0.00	0.33	0.28	0.00	0.03
400	0.56	0.28	0.79	0.83	0.19	0.77
600	0.97	0.85	1.60	1.71	1.23	1.08
800	1.56	1.71	2.58	2.78	2.40	1.73
1126 (P <sub>S</sub> )	2.61	3.65	4.72	5.09	4.73	3.40
1408 (75% P <sub>U</sub> )	3.68	5.59	6.88	7.54	6.40	6.10
1690 (90% P <sub>U</sub> )	5.05	7.87	9.77	10.91	9.22	8.12
<b>1878 (P<sub>U</sub>)</b>	<b>6.29</b>	<b>9.71</b>	<b>12.18</b>	<b>13.70</b>	<b>11.19</b>	<b>9.50</b>

Table 4.34 FPD Transverse Deflection Results

Load (kN)	Deflection (mm)					
	LVDT 3	LVDT 4	LVDT 5	LVDT 6	LVDT 7	LVDT 8
200	0.23	0.25	0.18	0.15	0.23	0.15
400	0.38	0.59	0.38	0.37	0.61	0.37
600	0.72	1.11	0.73	0.72	1.19	0.71
800	1.20	1.86	1.21	1.21	2.01	1.18
1156 (P <sub>S</sub> )	2.36	3.62	2.34	2.38	3.99	2.36
1446 (75% P <sub>U</sub> )	3.44	5.24	3.35	3.32	5.69	3.36
1733 (90% P <sub>U</sub> )	4.50	6.94	4.44	4.37	7.58	4.42
<b>1926 (P<sub>U</sub>)</b>	<b>5.39</b>	<b>8.41</b>	<b>5.27</b>	<b>5.22</b>	<b>9.29</b>	<b>5.24</b>

Table 4.35 JPD Transverse Deflection Results

Load (kN)	Deflection (mm)					
	LVDT 3	LVDT 4	LVDT 5	LVDT 6	LVDT 7	LVDT 8
200	0.22	0.33	0.21	0.16	0.28	0.16
400	0.47	0.79	0.51	0.44	0.83	0.46
600	0.96	1.60	0.99	0.92	1.71	0.95
800	1.56	2.58	1.57	1.51	2.78	1.53
1126 (P <sub>s</sub> )	2.89	4.72	2.88	2.79	5.09	2.80
1408 (75% P <sub>U</sub> )	4.12	6.88	4.24	4.07	7.54	4.14
1690 (90% P <sub>U</sub> )	5.74	9.77	5.93	5.82	10.91	5.89
<b>1878 (P<sub>U</sub>)</b>	<b>7.06</b>	<b>12.18</b>	<b>7.30</b>	<b>7.24</b>	<b>13.70</b>	<b>7.28</b>

The transverse deflections are in the Table 4.34 and Table 4.35. Recall, LVDTs 3, 4 and 5 are along the northern joint interface and LVDTs 6, 7, and 8 are along the southern joint interface (and the same location on the FPD). The two rows of transverse LVDTs are thus only 130 mm apart from each other. The FPD transverse deflections were all relatively uniform. The LVDTs 3 and 6 of the FPD measured 5.39 mm and 5.22 mm of deflection at the ultimate load, and on the other side of center the LVDTs 5 and 8 measured 5.27 mm and 5.24 mm, respectively.

For the FPD, the LVDT 3 had the lowest deflection at the ultimate load with 7.06 mm, the adjacent LVDT 6 indicated 7.24 mm of deflection. The LVDT 5 and 8 were very similar with 7.30 mm and 7.28 mm of deflection at the ultimate load. LVDTs on the west side of the deck centerline and are 130 mm apart, on the joint interface. As aforementioned, once the JPD was cut in during demobilization, there did not appear to be internal cracking past the deck joint along the inside face of the west girder. However, the inside face of the east girder had the long 855 mm crack

running through the north panel [see Figure 4.40]. The deflection results therefore reflect the cracking the deck experienced, since the LVDT 3 was 0.24 mm higher than the LVDT 5 on the other half of the deck.

The results indicate that all the deflections in the FPD at its ultimate load of 1878 kN are less than the JPD at 90% of its ultimate load, which was 1690 kN. For example, at LVDT 7, the deflection in the JPD at 1690 kN was 10.91 mm, while it was only 9.29 mm in the FPD at ultimate.

Lastly, the longitudinal deflection profiles are reported in Figure 4.47 and Figure 4.48 at the same loads presented in the LVDT result tables. These graphs are intended to be used as a tool to aid in the visualization of the centerline deflections of both decks during testing. The profiles for the transverse deflections are not included, because there are only three points to each profile and when graphed are not as informative as the longitudinal profiles.

In Figure 4.48 the steeper angle between LVDTs 4 and 7 across the joint is more evident than comparing the numerical values. Despite the fact the load plate is offset from the center of the bridge decks, the largest deflections are still seen on the north side of the plate at center. Though LVDT 9 was 420 mm from the center, since it was immediately after the load plate, it is the third largest deflection location. Outwards from the load plate, LVDTs 2 and 10 are almost equal distances from the load plate with distances of 485 mm and 500 mm, respectively. Therefore, the deflections in both decks are similar throughout testing.

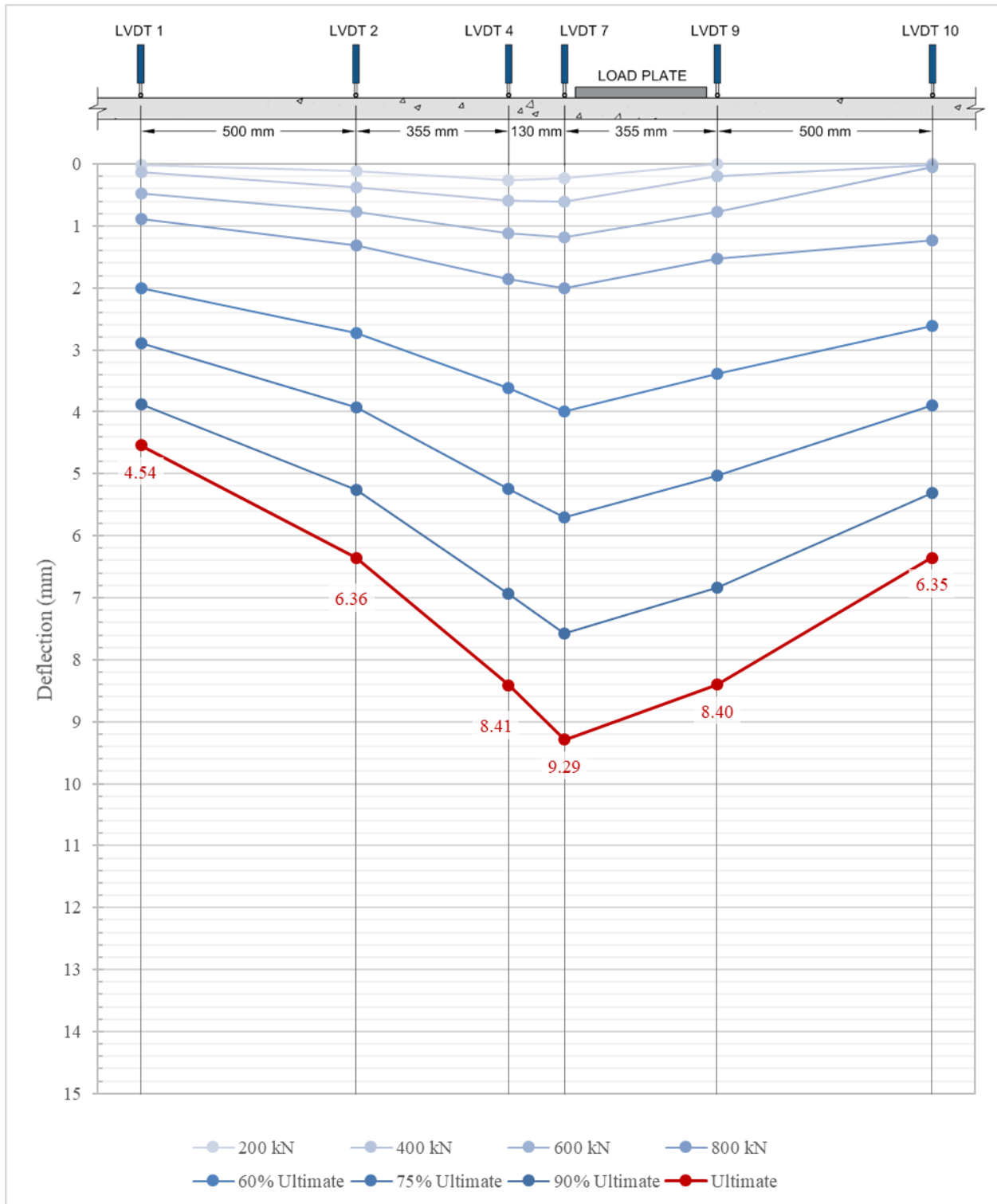


Figure 4.47 FPD centerline longitudinal deflection profiles during testing.

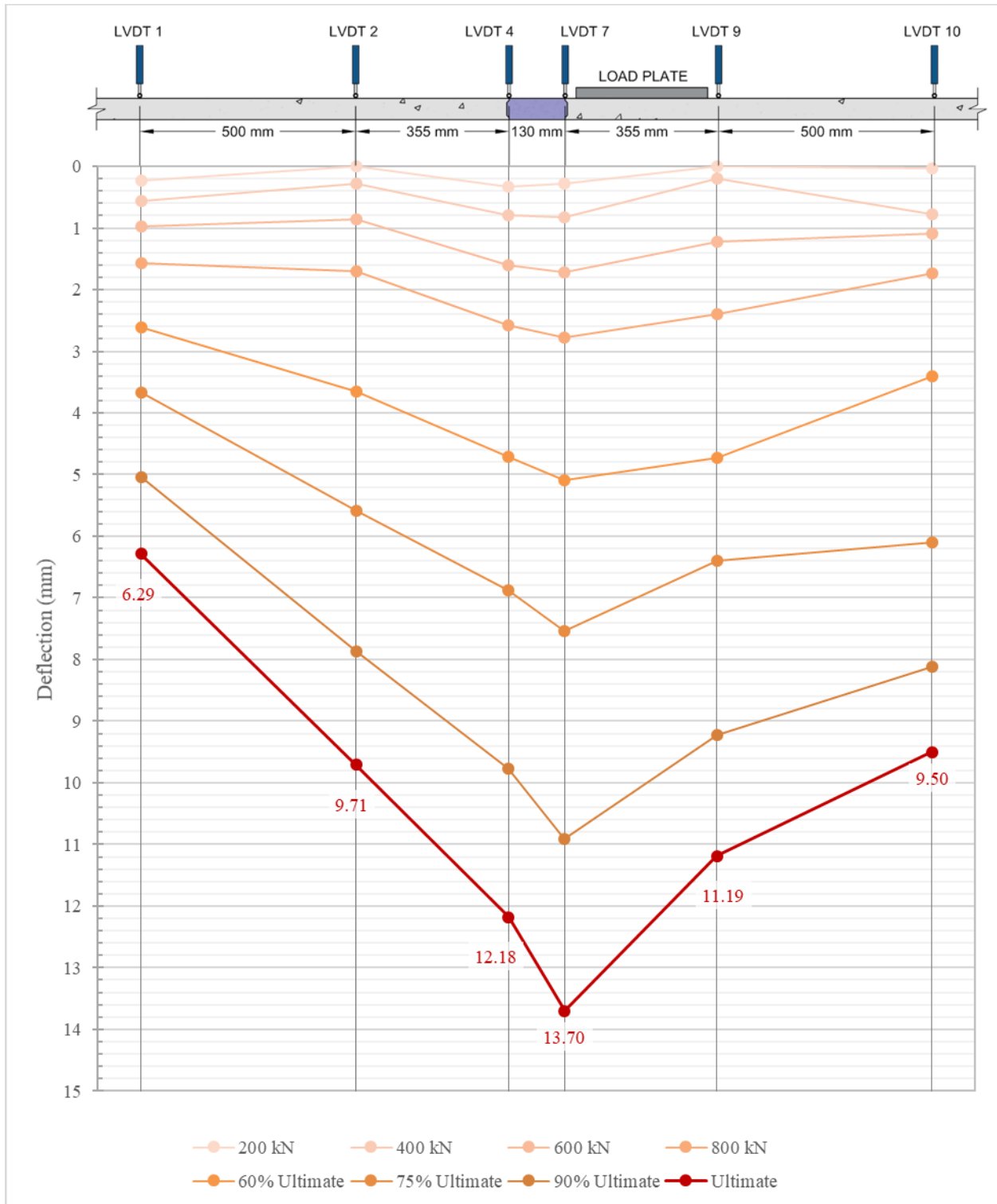


Figure 4.48 JPD centerline longitudinal deflection profiles during testing.

#### 4.4.5 Joint Performance

In this section, the results of the joint instrumentation will be analyzed to determine how well the load transferred across the UHPC joint. The concrete strain results are summarized in Table 4.36. Recall the concrete gauges were adhered to the top surface of the bridge decks. The strains in the FPD are largest in the CM gauge at the center of the deck, followed by the CS gauge and the lowest strains are seen in the CN gauge. Throughout testing the strains between the two decks only vary by less than 0.0002. The strains also do not exceed the ultimate concrete strain of 0.0035, as the greatest strain was 0.00230 in FPD-CM at its ultimate load of 1926 kN. As the FPD went from the ultimate load to its failure, the strains decreased slightly.

The JPD strains were greater than those in the FPD. The largest strains were measured beside the load plate in the south slab with 0.00363 and 0.00377 at the ultimate load of 1878 kN and at the JPD failure, respectively. The JPD-CS reached the ultimate concrete strain of 0.0035 at a load of 1856 kN, just before the ultimate load. The strains in the UHPC, measured by JPD-CM, were the lowest for this deck due to the superior strength of the UHPC compared to the RC. At the ultimate load the JPD-CM measured 0.00260 and reached 0.00269 by failure; 0.0001 less than the CS strains. The JPD-CN recorded strains of 0.00291 and 0.00301 at the ultimate load and failure, respectively. The strain values in the north panel of the JPD were between the CS and CM with 0.00291 at the ultimate load and 0.00301 at failure.

Table 4.36 FPD and JPD Concrete Strain Gauge Results

Load* (kN)	Strains					
	FPD-CS	FPD-CM	FPD-CN	JPD-CS	JPD-CM	JPD-CN
$P_S$	0.00103	0.00107	0.00098	0.00139	0.00110	0.00125
75% $P_U$	0.00140	0.00147	0.00136	0.00201	0.00152	0.00172
90% $P_U$	0.00182	0.00189	0.00174	0.00280	0.00206	0.00234
$P_U$	<b>0.00213</b>	<b>0.00230</b>	<b>0.00207</b>	<b>0.00363</b>	<b>0.00260</b>	<b>0.00291</b>

\*For the FPD:  $P_S = 1156$  kN, 75%  $P_U = 1446$  kN, 90%  $P_U = 1733$  kN,  $P_U = 1926$  kN.

For the JPD:  $P_S = 1126$  kN, 75%  $P_U = 1408$  kN, 90%  $P_U = 1690$  kN,  $P_U = 1878$  kN.

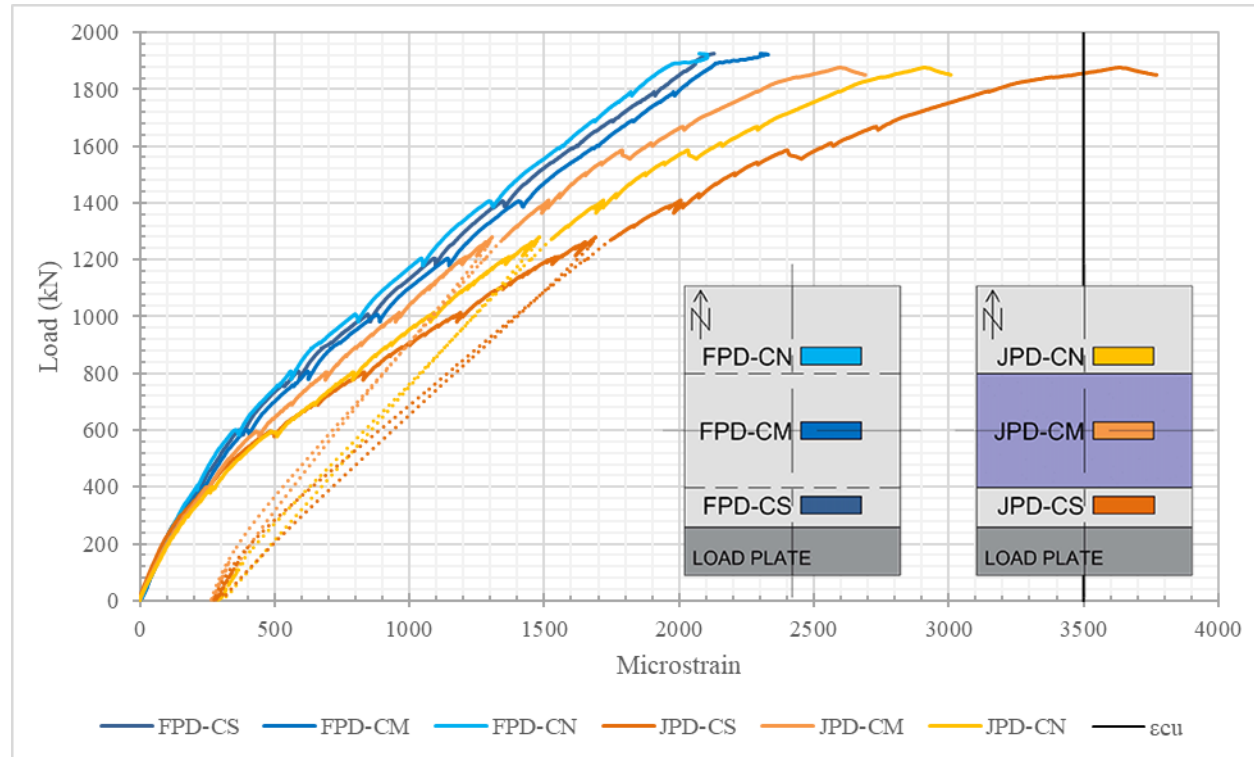


Figure 4.49 Concrete strain development during bridge deck testing.

As discussed in Chapter 3, the strain gauges on the hooked bars in the FPD lost the labels during the storage at the concrete plant and despite efforts to distinguish them, it was not possible to determine which gauge wire corresponded to which strain gauge. Recall, the south grouping

included three strain gauges on the bottom half of the three central 10M hooked bars, and one on the top half of the center 10M hooked bar. The north grouping included the same four strain gauges on the 10M bars, and two gauges on the transverse 15M bars. Only three out of the four south gauges worked, and five out of the six north gauges worked.

Table 4.37 summarizes the microstrain readings from 800 kN to the ultimate load for these gauges in the FPD. The strains at 800 kN were included to show the jump in strain to the service load. At the FPD's ultimate load of 1926 kN, the S1, S2 and S3 strain gauges reported strains of 0.00550, 0.00175, and 0.00706, respectively. The northern gauges recorded 0.00020, 0.00014, 0.00192, 0.00280, and 0.00002 for the N1, N2, N3, N4 and N5 gauges, respectively. The transverse 15M bars in the JPD were not instrumented, and thus no direct strain data comparison may be made. The JPD experienced a significant decrease in the rebar strains north of the deck center, similar to the values seen in N1, N2 and N5, and it is therefore possible the N3 and N4 strain gauges were those on the 15M bars, however, difficult to confirm.

Table 4.37 FPD Internal Strain Gauge Results

Load (kN)	FPD Microstrains ( $\mu\epsilon$ )							
	S1	S2	S3	N1	N2	N3	N4	N5
800	216.33	-23.56	527.81	-44.94	-34.70	430.34	331.65	-28.84
1156 (P <sub>S</sub> )	1366.76	212.59	1733.54	-49.23	10.13	803.94	1070.10	18.81
1446 (75% P <sub>U</sub> )	2170.26	827.68	2380.65	-50.21	30.84	1202.06	1799.65	-6.87
1733 (90% P <sub>U</sub> )	3070.30	1392.77	4659.24	-58.16	72.93	1629.93	2352.34	-34.62
<b>1926 (P<sub>U</sub>)</b>	<b>5498.17</b>	<b>1747.16</b>	<b>7055.49</b>	<b>200.99</b>	<b>136.73</b>	<b>1920.99</b>	<b>2798.35</b>	<b>22.01</b>

Since there were double the amount of strain gauges in the JPD compared to the FPD, the data is split into two tables that present the south panel and north panel separately [Table 4.38 and Table

4.39]. The strain readings in the 10M bars below the load plate experienced lower strains than those in the FPD, with strains of 0.00393, 0.00099, 0.00482, 0.00406 for the SS-WBS, CBS, EBS, and CTS, respectively, at the ultimate load of 1878 kN. At the same load in the FPD, however, the south gauges recorded strains of 0.00498, 0.00168, and 0.00639, which are closer in value to the JPD strains.

Considering the values on the other side of the joint, the SS-WBJ and EBJ lost over half the amount of strain with only 0.00152 and 0.00130, respectively. The center 10M hook strains increased on the bottom and decreased on the top, with SS-CBS reading 0.00206 and SS-CBJ reading only 0.00017.

The strains on the north half of the joint and moving into the north panel continue to decrease as seen in Table 4.39. These gauges, except for NS-WBJ, are all reporting negative strains across the center of the joint, indicating a switch to compression within the deck. Regardless of the sign, the strains in the north panel joint and slab were all less than 0.00035.

Table 4.38 JPD South Panel Internal Strain Gauge Results

Load (kN)	JPD-SS (South Slab) Microstrains ( $\mu\epsilon$ )							
	WBS	CBS	EBS	CTS	WBJ	CBJ	EBJ	CTJ
800	359.18	-173.76	249.85	566.15	308.04	276.19	-28.41	-209.32
P <sub>S</sub>	974.48	-160.86	1285.15	1497.82	627.64	679.98	194.09	-267.00
75% P <sub>U</sub>	2110.70	257.94	3002.88	2892.97	1149.02	1291.96	840.65	-244.23
90% P <sub>U</sub>	3585.34	646.58	4681.30	4077.06	1390.74	1530.01	1162.44	-91.20
<b>P<sub>U</sub></b>	<b>3928.74</b>	<b>986.81</b>	<b>4816.30</b>	<b>4056.23</b>	<b>1519.05</b>	<b>2057.86</b>	<b>1305.66</b>	<b>172.24</b>

\*P<sub>S</sub> = 1126 kN, 75% P<sub>U</sub> = 1408 kN, 90% P<sub>U</sub> = 1690 kN, P<sub>U</sub> = 1878 kN.

Table 4.39 JPD North Panel Internal Strain Gauge Results

Load (kN)	JPD-NS (North Slab) Microstrains ( $\mu\epsilon$ )							
	WBS	CBS	EBS	CTS	WBJ	CBJ	EBJ	CTJ
800	-103.69	-43.89	-36.90	-98.73	8.36	-9.31	24.45	-197.45
P <sub>S</sub>	-158.61	-60.39	-47.96	-130.73	6.37	-63.91	-4.30	-254.44
75% P <sub>U</sub>	-205.27	-103.38	-19.78	-171.63	23.60	-160.24	-80.27	-311.28
90% P <sub>U</sub>	-203.80	-127.84	108.12	-213.35	104.28	-218.63	-134.02	-316.21
<b>P<sub>U</sub></b>	<b>7.84</b>	<b>3.27</b>	<b>123.11</b>	<b>-159.38</b>	<b>229.61</b>	<b>-136.03</b>	<b>-129.63</b>	<b>-160.58</b>

\*P<sub>S</sub> = 1126 kN, 75% P<sub>U</sub> = 1408 kN, 90% P<sub>U</sub> = 1690 kN, P<sub>U</sub> = 1878 kN.

The strains for the FPD are graphed in Figure 4.50 with the purple lines representing the south panel strains, and the blue lines representing the north panel strains. Overall, the shapes of the S1, S3, N3 and N4 are very similar up to 800 kN, at which point all three of the south panel strain gauges experience significant increases until failure. The N3 and N4 strain values continue to increase, just at a lesser rate. As seen in Table 4.37, the rest of the north values are much smaller.

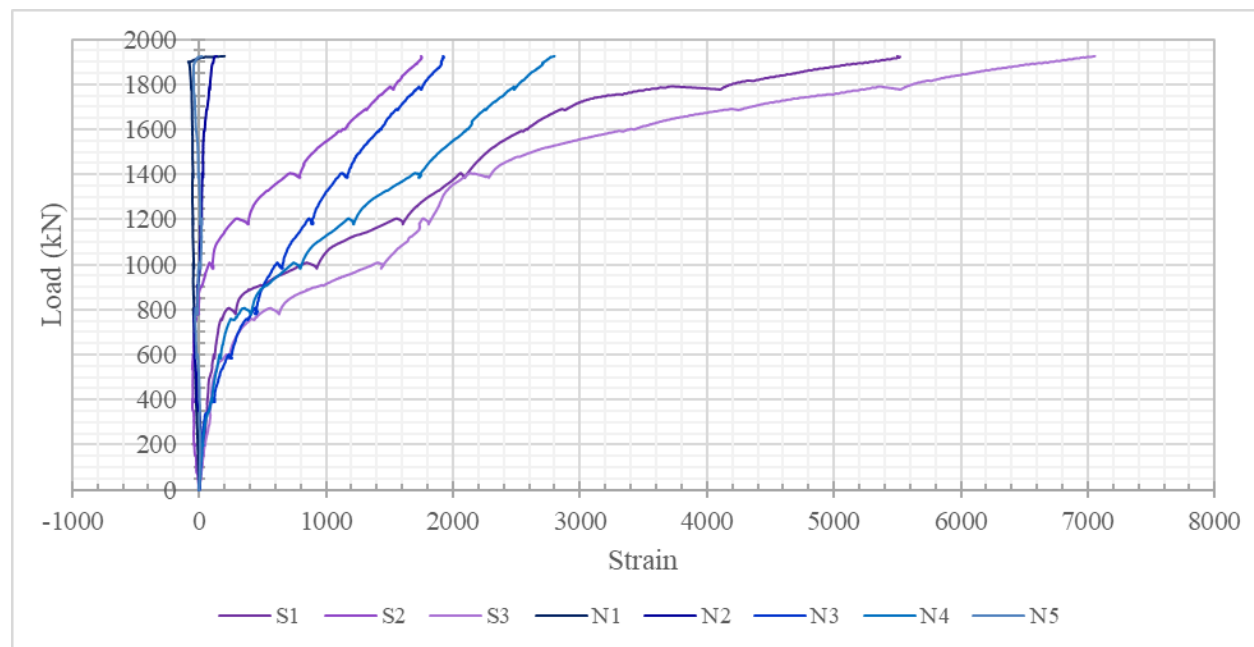


Figure 4.50 FPD internal reinforcing bar strains at deck center.

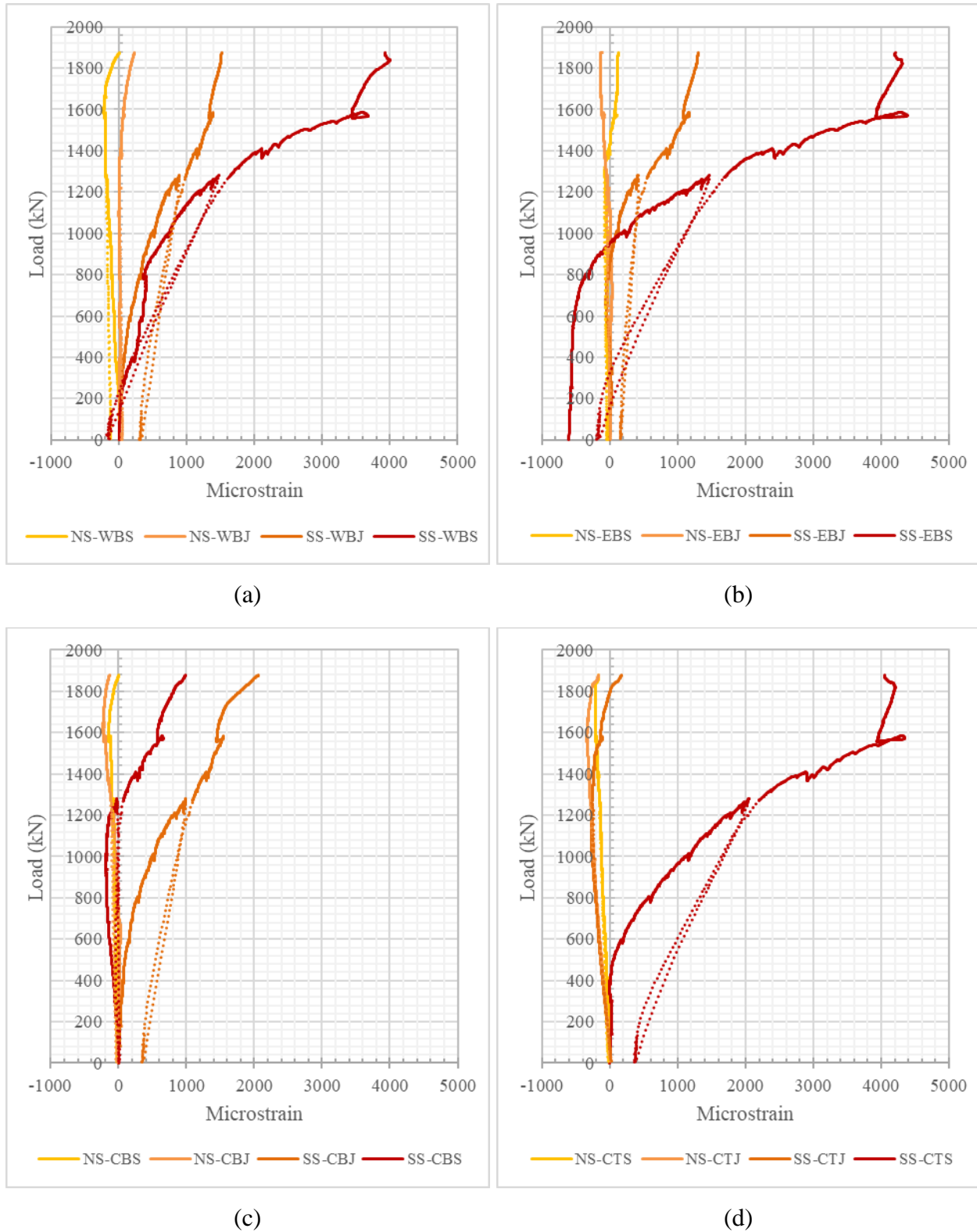


Figure 4.51 JPD strain development of 10M hooked bars on (a) bottom of west bars, (b) bottom of east bars, (c) bottom of center bars, and (d) top of center bars.

The graphed results of the JPD in Figure 4.51 are separated by which set of rears the strain gauges were instrumented on; Figure 4.51(a) is the west 10M hooks, (b) is the east 10M hooks, and (c) and (d) are the strains from the center 10M hooks,. As seen in Table 4.38 and Table 4.39, the north panel slab and joint gauges do not read large strains, whereas the south panel slab and joint gauges show increasing strains throughout testing.

Though the joint rebar is spaced at 150 mm c/c and is not in a direct line as the graphs suggest, the strains are still shown in this profile view for a general understanding of the strain development between panels across the UHPC joint. Since the strain gauges of the FPD could not be distinguished, it was not possible to graph the strain profiles in the same manner.

The strain profiles of the 10M center hooks were graphed separately from the east and west hooks. The strains in the top of the center hook present similar values to the east and west values recorded; the strains are greater in the south panel slab strain gauge and decrease across the joint [see Figure 4.52]. The strains in the center bottom hook are slightly different than the rest of the results. The values recorded by the strain gauge within the south panel slab (SS-CBS) were less than half those in the same bar within the joint (SS-CBJ). At the ultimate load of 1878 kN, the SS-CBS measured a strain of 0.00099 and the SS-CBJ read 0.00206 [see Figure 4.53 and Table 4.38].

Figure 4.54 shows the east and west strain gauge profiles, distinguished by the purple versus green lines as shown in the graphics. The results are very similar for the first 800 kN of loading at all locations, but afterwards the eastern 10M bars recorded greater strains in the south panel slab and joint gauges (SS-EBS and SS-EBJ). Overall, there is a significant drop-off between the south panel slab gauges and the north panel slab gauges. The strains at ultimate load are as high as 0.00482 for the SS-EBS and 0.00393 for the SS-WBS, and decrease to less than 0.00015 in the north panel.

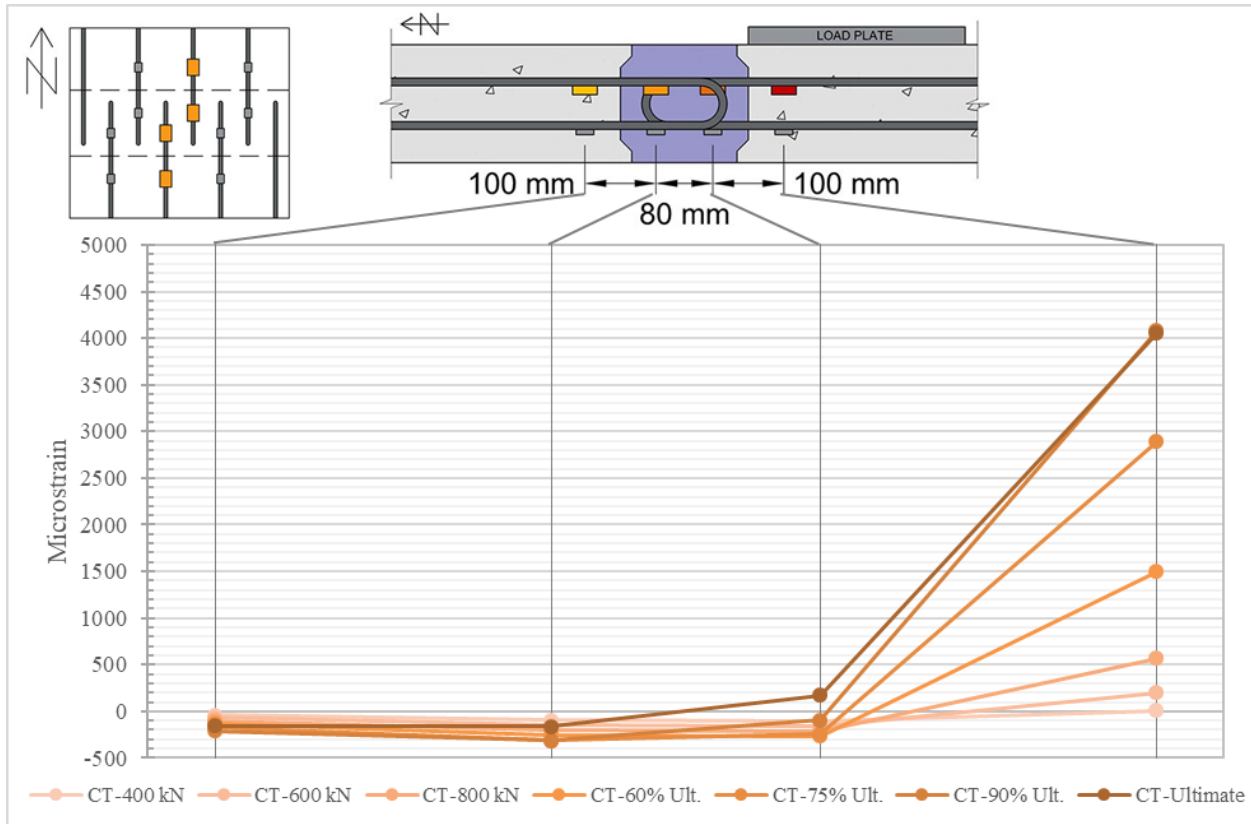


Figure 4.52 JPD strain profiles for the center top internal strain gauges.

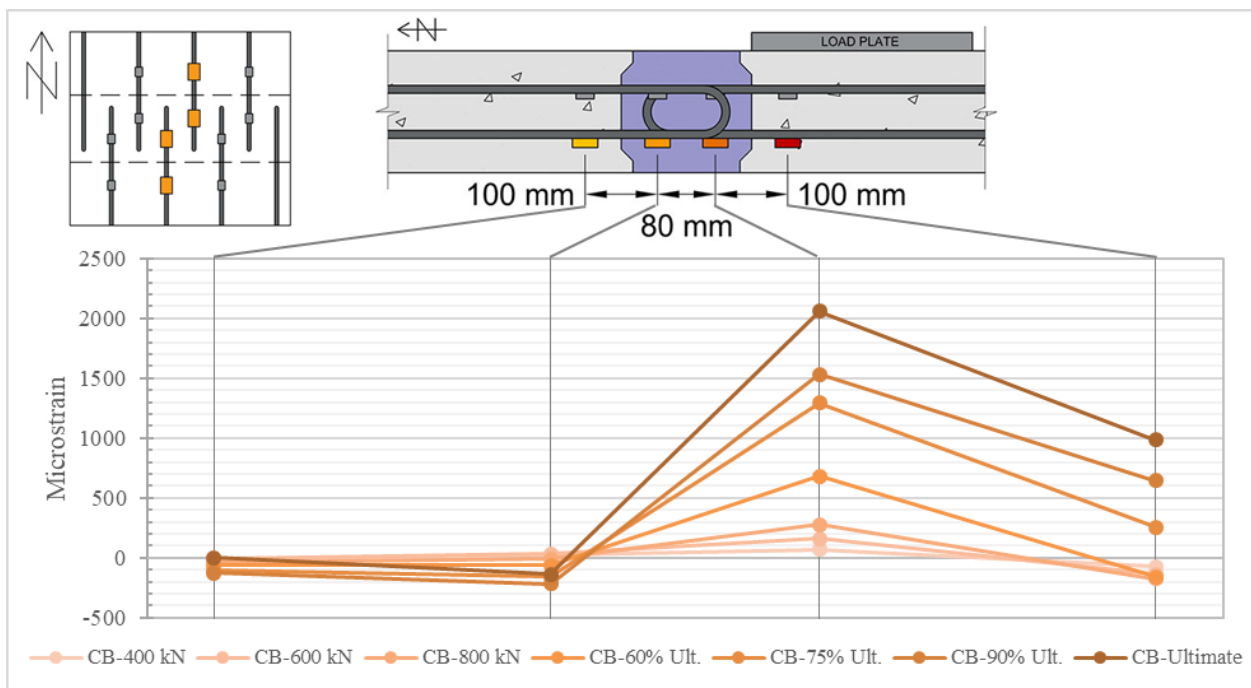


Figure 4.53 JPD strain profiles for the center bottom internal strain gauges.

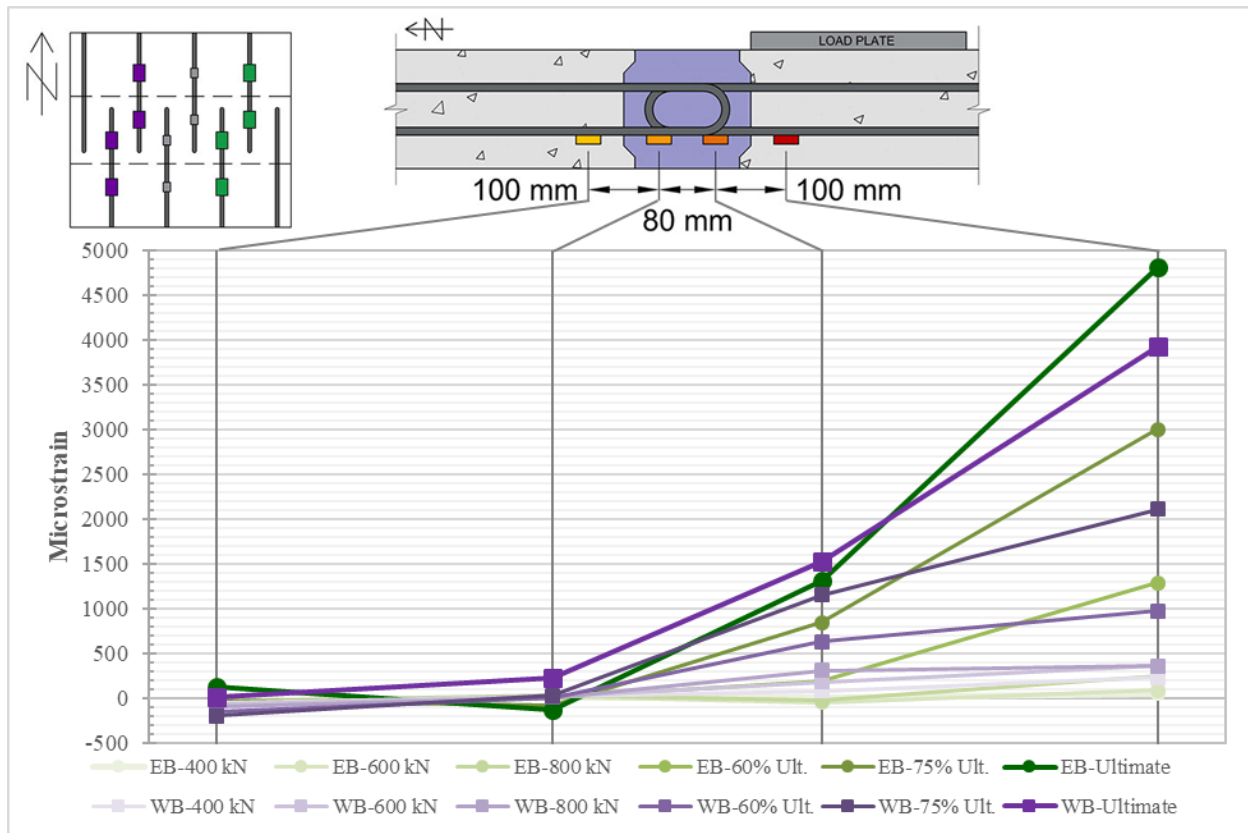


Figure 4.54 JPD strain profiles for easternmost and westernmost internal strain gauges.

Considering the minimal strains seen in the hooked bars of the joint within the JPD and FPD, comparing the strains of the neighbouring bars may not be a practical measure of the overall joint performance. The strains do not appear to transfer to the 10M hooks in the north panel. The concrete strain gauges did not show major decreases in the strains at the deck surface, in comparison to the decreases seen throughout the reinforcing bars. The bulk of the load would be transferred through the concrete, since the downwards force on the load plate causes significant compression to the deck. There were only a few cracks seen on the bottom face of the UHPC joint, and the internal cracking seen after the deck was cut showed a few diagonal cracks outwards from the load plate location. There was no debonding seen at either joint interface, except for along a small section at the north panel interface upon failure.

#### 4.4.6 Shear Stud Performance

The shear studs were expected to show compression in the innermost studs and tension in the outermost studs, due to the load application point and the location of the studs on the girder flanges (i.e. tension in the westernmost studs of pockets P1 and P2, and in the easternmost studs of pockets P3 and P4, and compression in the easternmost studs of pockets P1 and P2, and in the westernmost studs of pockets P3 and P4). Figure 4.55 clarifies the expected forces in each pocket with a sketch, and shows the exaggerated deflected shape expected of the FPD cross-section.

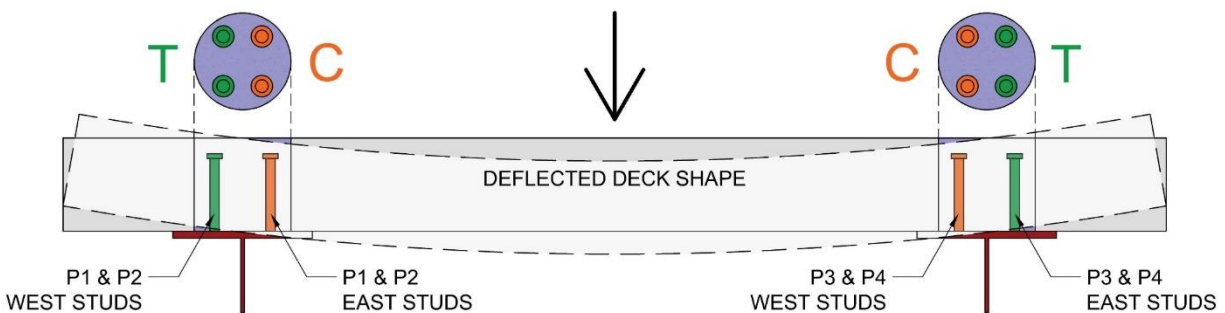


Figure 4.55 Expected shear stud behaviour and deck deflection.

The strain results from the shear studs of the FPD are graphed in Figure 4.56. The charts are arranged in the same order as the shear pockets and the values of the axes are kept the same for result comparison [see Figure 3.44]. The colour scheme for the graphical results is based on the tensile (negative strains) and compressive (positive strains) behaviour, represented by a green line and orange, respectively.

The P2NW and P3SW strain gauges did not work during testing and were represented by the grey lines. These two gauges either did not adhere properly to the studs and/or were accidentally damaged during UHPC casting.

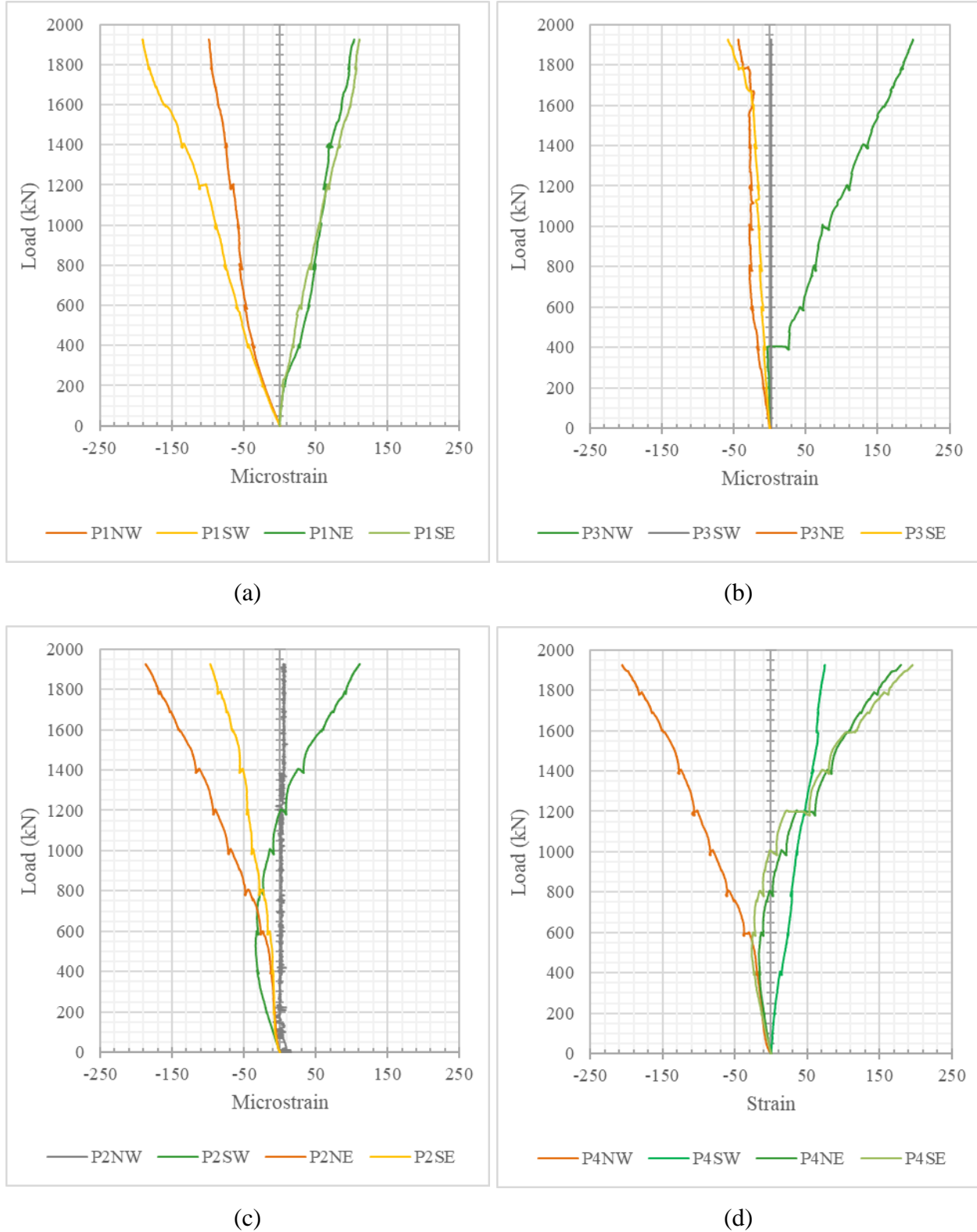


Figure 4.56 FPD shear stud strain development during testing for shear pockets (a) P1, (b) P3, (c) P2, and (d) P4.

The applied loading creates arching action within the concrete deck slab. Arching action is the angled path the load takes from the top of the deck at the load application point, to the bottom of the deck at the support location. This creates an angled compression zone that starts to flatten out as the specimen deflects. The shear pocket and haunch connection resist the resulting moment created that pulls inwards, as seen in Figure 4.57.

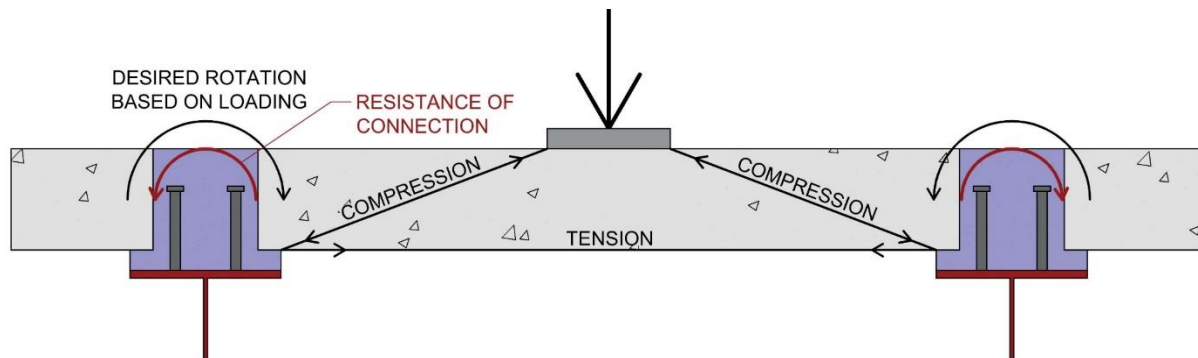


Figure 4.57 Arching action and load resistance.

To understand the difference in load reaction between the shear pockets P1 and P3 compared to P2 and P4, the deck cracking was studied. The results of the arching action can be seen in both bridge decks through the cracking patterns. The bridge deck's resistance of the arching action creates the punch cone shape that eventually leads to the failure. The cracks radiate outwards from the load plate in the resulting cone shape of cracking. Figure 4.58 shows the FPD cracking at 1400 kN with the stud behaviour. Between the load plate the adjacent shear pockets P2 and P4, the cracking is minimal and the stud behaviour is responding in the expected compression and tension from the arching action. The opposite reactions occurred in the shear studs in P1 and P3. The effects of the arching action are resisted differently in these shear pockets since they are not adjacent to the load plate. Since the pockets are north of the deck center and past the lowest deflections, the innermost studs are pulling in tension to resist the deflections.

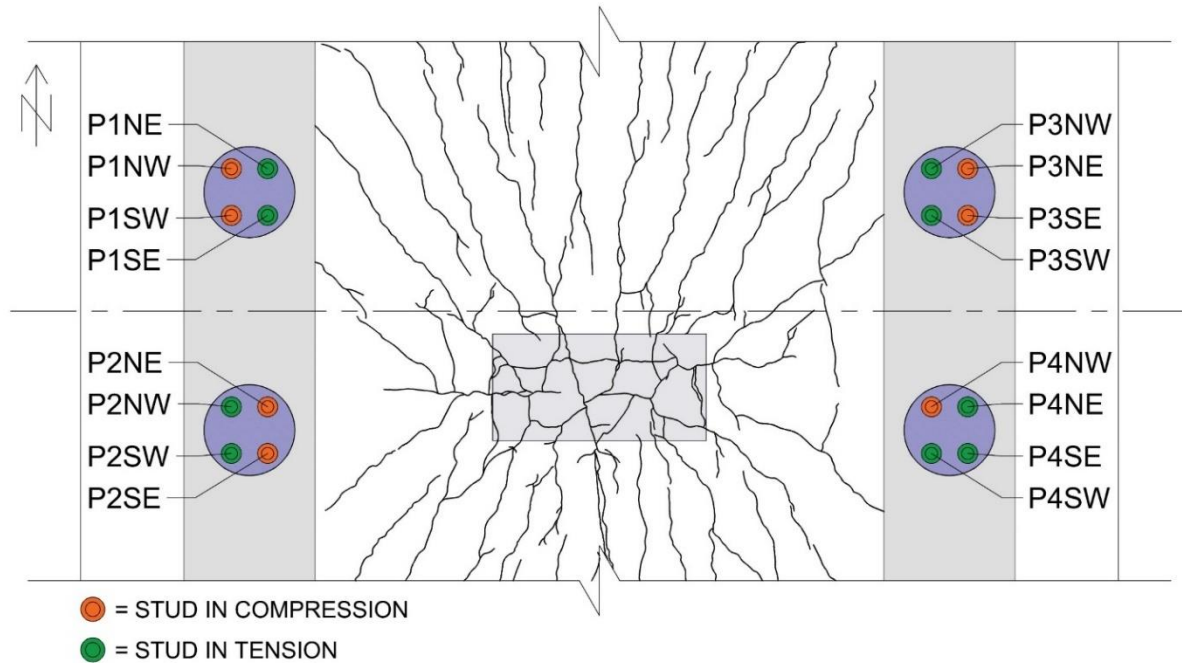


Figure 4.58 FPD 1400 kN cracking and shear stud behaviour.

The resulting microstrains in each shear stud can be seen in Table 4.40 and Table 4.41, presented in the same order as Figure 4.56. It is clear from the microstrains recorded that the shear stud strain was not utilized. The strains are all below 0.0003 and are not remotely close to the experimental yield strain of 0.00384.

Table 4.40 FPD Shear Stud Strain Results for Shear Pockets P1 and P3

Load* (kN)	Microstrains ( $\mu\epsilon$ )							
	P1NW	P1SW	P1NE	P1SE	P3NW	P3SW	P3NE	P3SE
800	-55.09	-75.81	50.01	41.72	60.59	1.79	-28.48	-14.33
$P_s$	-63.37	-99.02	63.49	63.92	100.81	1.79	-26.39	-15.62
75% $P_U$	-76.66	-138.73	74.35	85.24	139.28	1.79	-28.28	-20.59
90% $P_U$	-92.14	-176.50	95.64	105.07	176.34	1.79	-27.98	-34.68
$P_U$	-98.42	-190.52	103.78	111.11	198.83	1.79	-43.83	-58.16

\* $P_s = 1156$  kN, 75%  $P_U = 1446$  kN, 90%  $P_U = 1733$  kN,  $P_U = 1926$  kN.

Table 4.41 FPD Shear Stud Strain Results for Shear Pockets P2 and P4

Load* (kN)	Microstrains ( $\mu\epsilon$ )							
	P2NW	P2SW	P2NE	P2SE	P4NW	P4SW	P4NE	P4SE
800	2.07	-27.30	-42.33	-23.08	-56.56	29.13	-2.56	-16.58
P <sub>S</sub>	4.95	-3.59	-83.83	-42.88	-96.43	44.09	30.16	15.41
75% P <sub>U</sub>	6.32	33.59	-118.60	-55.78	-128.83	59.10	85.24	80.97
90% P <sub>U</sub>	5.60	80.34	-157.84	-76.57	-169.46	66.08	131.40	142.65
P <sub>U</sub>	4.96	111.26	-186.70	-96.76	-205.52	74.69	179.87	195.90

\*P<sub>S</sub> = 1156 kN, 75% P<sub>U</sub> = 1446 kN, 90% P<sub>U</sub> = 1733 kN, P<sub>U</sub> = 1926 kN.

The many differences between the shear pockets of the FPD and the push-out test specimens render a valid comparison of the results difficult; the shear pockets are different shapes, the number of studs is different, and the load resistance is different. However, for a general understanding the strain results from the strain gauges on the ends of the SP6 and SP3 studs will be compared to the FPD shear stud gauges. Recall the ultimate load of the SP6-2 and SP6-3 specimens were 2892 kN and 3045 kN, respectively. The ultimate load of the SP3-1 was 1445 kN, and 1674 kN for SP3-2. The strains in the FPD at the ultimate load of 1926 kN, were surpassed before the SP6 specimens and the SP3 specimens had reached 500 kN in the push-out tests. For a visual representation of the difference in strains, the FPD-P1 results are graphed with the SP3-2 results in Figure 4.59.

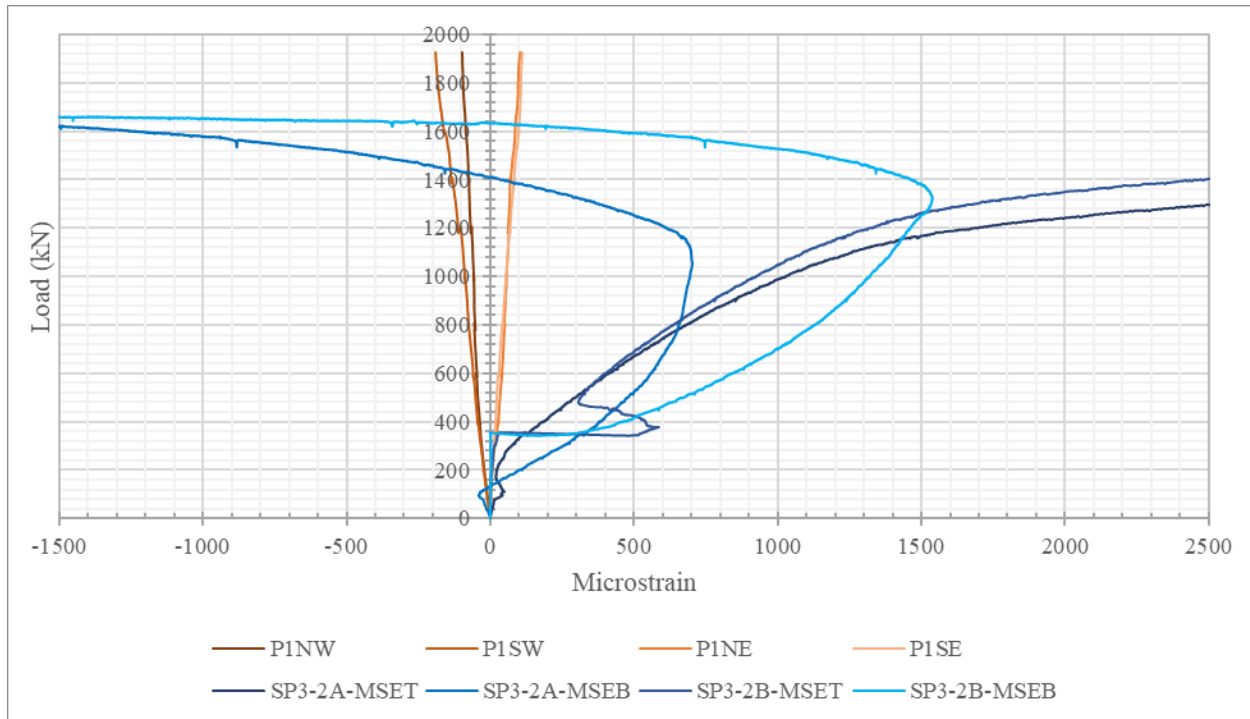


Figure 4.59 FPD P1 shear stud strain development versus the SP3-2 shear strain development.

The shear studs of concrete bridge decks are not subjected to the same magnitude of shear loading since the shear resistance is a small part of the composite bridge deck system of which the majority loads are vertical and not lateral. Considering the underutilization of the shear studs, when UHPC is cast as the connection fill material, the number of shear studs may be minimized.

In Chapter 2, the similar thesis research project completed by David Amorim was summarized. These projects were both completed for MI and though there were many differences between the bridge deck design, there are some points for comparison. There were many cracks seen across the bridge deck joint, similar to the JPD cracking pattern. The negative bending fatigue testing resulted in the failure of the shear studs, however the testing of this thesis program showed minimal strains in the shear studs during the static loading. The results of Amorim's testing suggested larger and/or more shear studs may be required. Recall, the shear studs in this research were

slightly longer at 208 mm in length, compared to the 178 mm length. The bridge deck designs all had a 50 mm haunch and were 250 mm thick, the shear studs had greater penetration in these bridge decks. Since the FPD and JPD were not loaded in fatigue cycles, nor in negative bending, it is unknown whether they would have also failed via the shear studs. It is possible loading the bridge deck in negative bending had different effects on the shear pockets since there are more upwards tensile forces the shear stud groupings are subjected to than with positive bending testing. However, based on this research there can be no conclusions drawn on this matter.

---

## Chapter 5 Conclusions

---

The research program was developed to study the behaviour of UHPC cast bridge shear pockets and panel-to-panel joints. The effects from the number of studs and the load transfer across a UHPC joint was tested. The analysis of the shear pocket specimen results and the full-scale bridge deck testing allowed some conclusions to be drawn.

### 5.1 Shear Pocket Specimens

The push-out specimen tests isolated the shear behaviours of the UHPC shear pocket and steel stud connection. The SP6 specimens failed at double the loads seen in the SP3 specimens, however this was attributed to having double the amount of shear studs in the shear pocket. The average ultimate load per stud was 248 kN/stud for the SP6 specimens and 260 kN/stud for the SP3 specimens. The first SP6 specimen failed via the buckling of the built-up steel beam, and therefore the data cannot be used to draw conclusions since it was not the desired outcome of the test setup. The SP6-2 and SP6-3 specimens had ultimate loads of 2892 kN and 3045 kN. The SP6-2 specimen failed when the studs sheared off of one connection, remaining in the UHPC, which caused the other side to fail by concrete crushing. The SP6-3 specimen failed by concrete crushing on both sides. The SP3-1 specimen had an ultimate load of 1445 kN, with concrete crushing on one side and stud failure on the other. The SP3-2 specimen had an ultimate load of 1674 kN and failed by stud shearing on both sides. The SP0 specimens' UHPC debonded from the surface of the steel beam shortly after loading, indicating there was no significant adhesion between the two smooth surfaces.

The LVDT data indicated the 6-stud groupings resulted in greater debonding between the steel and UHPC shear pocket, whereas the 3-stud groupings experienced more debonding between UHPC

shear pocket and its RC slab. The strain gauges recorded yielding strains at the base of the shear studs (greater than 0.00384 per stud), but negligible strains at the head, regardless of the amount of studs present. Since these experiments isolate the shear behaviour of the shear pocket and stud connection, the results seen are not replicated when the shear pockets are part of a composite bridge deck system. Therefore, despite the greater loads reached by the 6-stud groupings, when used within a UHPC shear pockets the amount and length of the shear studs may be reduced.

## 5.2 Bridge Decks

The FPD reached an ultimate load of 1926 kN prior to its punching shear failure with the main cracking cone breaking through the north half of the bridge deck. The JPD reached an ultimate load of 1878 kN and failed by punching shear the main failure cone breaking the surface of the south deck panel. Both decks experienced similar cracking patterns throughout testing, with cracks reaching the full extents of the deck length. The UHPC joint showed only a few cracks on the bottom surface, but after cutting the deck during demolition cracking was seen radiating out from the load plate along a punch cone shape. The joint did not show debonding until after failure at the deck surface. The FPD experienced deflections up to 9.29 mm at the deck center and despite the lower ultimate load the JPD had greater ultimate load deflections with 13.70 mm at the deck center. The difference in the deck deflections was likely due to the monolithic casting of the FPD and the piece-wise construction of the JPD.

The internal strains recorded on the 10M hooked longitudinal bars were greater in the FPD, whereas the concrete strains on the deck surfaces were greater in the JPD. The strain difference between panels was only 0.00076 for the JPD, and at the same locations, the concrete strain increased in the FPD by 0.00011. The monolithic FPD appears to have carried slightly more load in the steel rebar than the JPD, which is likely due to the superior strength of the UHPC joint.

Therefore, the majority of the load was transferred between panels through the UHPC rather than the reinforcing bars.

The influence of the shear pockets within the composite bridge deck system was far less than the shear capacities shown in the push-out test specimens. The majority of forces in these decks were from their self weight and the downward applied load. The deck was not subjected to any lateral loading that would cause significant shear forces. In reality, the bracing between support girders will pickup lateral loading the bridge is subjected to due to vibrations and wind loading, therefore the shear pockets are mainly designed to transfer the traffic loading down to the support girders and across to the bridge bollards.

The experimental program results indicate that the shear pockets are over reinforced with 6-stud groupings as the strength of the shear studs are not utilized. In addition, the ultimate loads of the SP3 push-out specimens were similar to those of the full-scale bridge decks and the shear studs performed as well as the 6-stud shear pocket specimens. The FPD had only 4-stud groupings within circular pockets and measured very low strains. The results indicate the circular shear pockets with fewer studs had the superior load resistance behaviour. Therefore, the number of shear studs in each shear pocket of composite concrete and steel bridges may be reduced and circular shaped shear pockets are superior.

There is a practicality of using precast concrete panels in bridge deck construction projects. The ability to cast the major concrete elements in controlled laboratory conditions reduces project and schedule risks. The UHPC connections can be designed for minimal site formwork, and the high-early strength reduces the curing time. However, there was no significant advantage seen through the use of UHPC in the deck connections. The general performance of the JPD and its UHPC connected precast panels was similar to the performance of the monolithically cast FPD. Overall,

the FPD performed better with a greater ultimate load, less deflections, circular shear pockets and 4-stud layout, and more evenly distributed concrete strains.

### 5.3 Future Research

Since this research covered small-scale experiments and only two full size bridge decks, there can be no definitive conclusions drawn to the exact number of shear studs appropriate for bridge deck connections. In order to optimize the amount of shear studs within the shear pockets, and the stud lengths, further research is required with more experimental testing. It would be advantageous to complete positive bending fatigue cycle loading to compare to the negative bending results and determine the impact on the length of shear studs. Research has shown that longer shear studs aid in crack reduction, which is critical in precast bridge deck panels for long-term durability. However, this research program demonstrated the full length of the shear studs were not utilized for their strength, as negligible strains were seen at the head of the studs in testing. Further research should focus on the use of shorter studs and alternative methods of crack control reinforcement, such as the continuation of the deck panel reinforcement across the shear pockets.

Another area that could be explored is the shape and size of the shear pockets, as these parameters were not studied in this experimental program. It is likely with the use of UHPC the size of pockets may be reduced. However, as commonly seen in engineering design, the constructability will always be a key factor in the project execution and may limit the minimum size of the shear pockets depending on the scale of the bridge.

## References

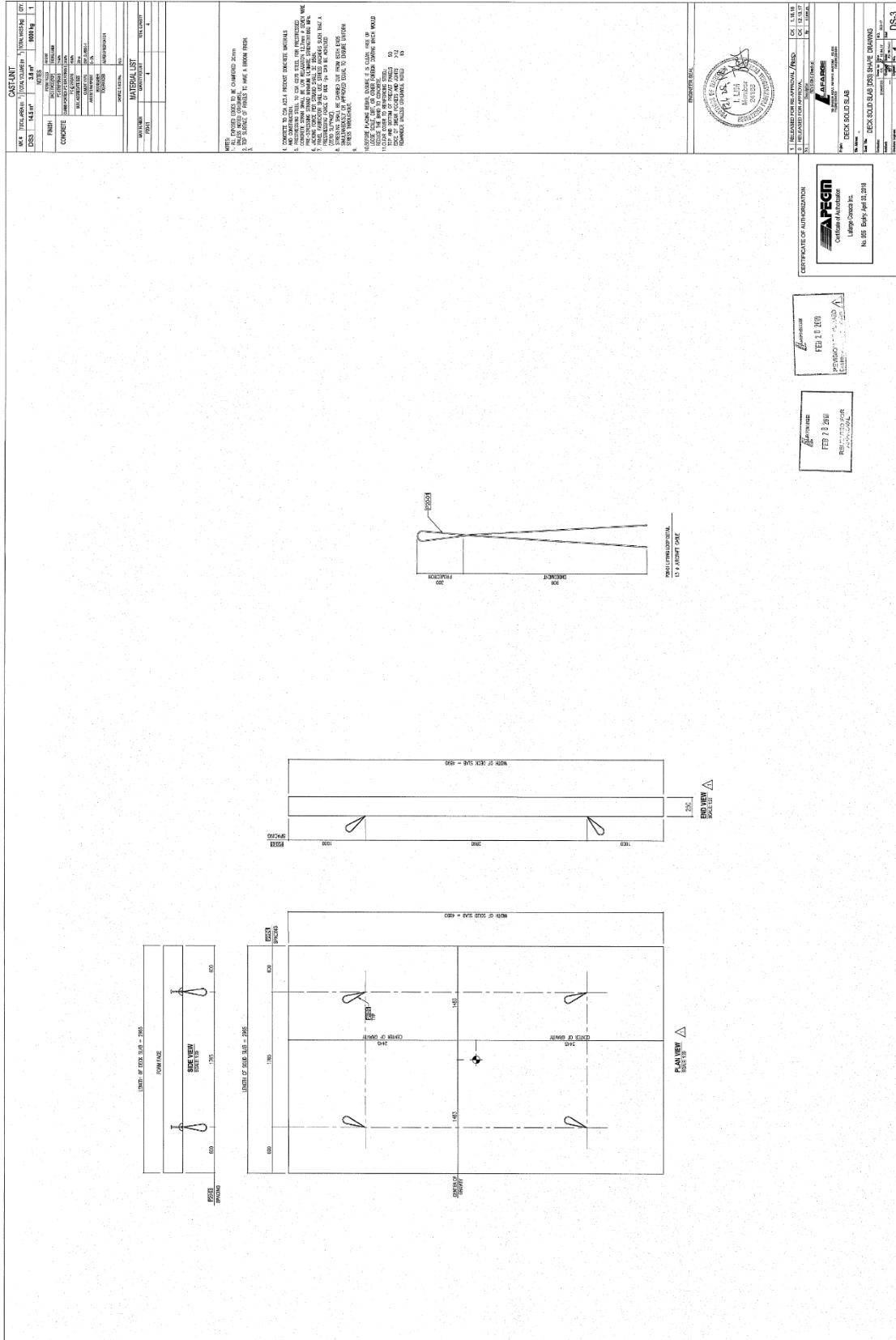
---

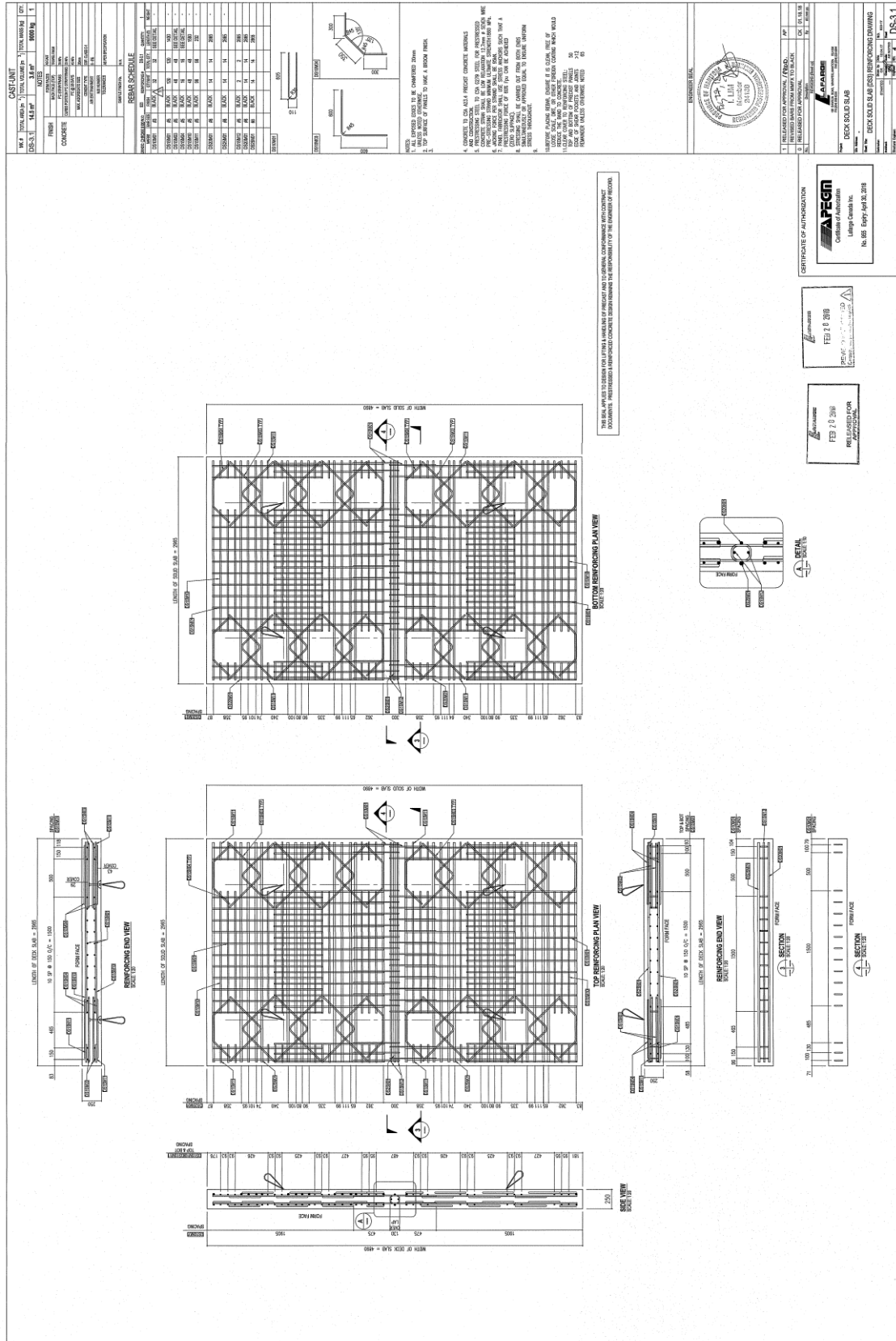
---

- [1] J. S. Kim, S. H. Park, C. Joh, J. D. Kwark and E. S. Choi, "Push-Out Test on Shear Connectors Embedded in UHPC," *Applied Mechanics and Materials*, Vols. 351-352, pp. 50-54, 2013.
- [2] M. Spremic, Z. Markovic, M. Veljkovic and D. Budjevac, "Push-Out Experiments of Headed Shear Studs in Group Arrangements," *Advanced Steel Construction*, vol. 9, no. 2, pp. 139-160, 2013.
- [3] S. D. Porter, J. L. Julander, F. Marvin W. Halling and M. Paul J. Barr, "Shear Testing of Precast Bridge Deck Panel Transverse Connections," *Journal of Performance of Constructed Facilities*, vol. 26, no. 4, pp. 462-468, 1 August 2012.
- [4] S. D. Porter, J. L. Julander, F. Marvin W. Halling, M. Paul J. Barr, H. Boyle and M. Shutao Xing, "Flexural Testing of Precast Bridge Deck Panel Connections," *Journal of Bridge Engineering*, vol. 16, no. 3, pp. 422-430, 2011.
- [5] M. Mostafa Tazarv, L. Bohn and F. Nadim Wehbe, "Rehabilitation of Longitudinal Joints in Double-Tee Girder Bridges," *Journal of Bridge Engineering*, vol. 24, no. 6, p. 14, 2019.
- [6] W. F. Young and J. Boparai, "Whiteman Creek Bridge: A synthesis of accelerated bridge construction, ultra-high-performance concrete, and fiber-reinforced polymer," *PCI Journal*, no. Spring 2013, pp. 37-47, 2013.
- [7] D. Amorim, "Behaviour of Ultra-High Performance Concrete as a Joint-Fill Material for Precast Bridge Deck Panels Subjected to Negative Bending," Department of Civil Engineering, University of Manitoba, Winnipeg, MB, 2015.
- [8] "ASTM C39 / C36M-18, Standard Test Method for Compressive Strength of Cylindrical Concrete Specimens," ASTM International, West Conshohocken, 2018.
- [9] "ASTM C496 / C496M-17, Standard Test Method for Splitting Tensile Strength of Cylindrical Concrete Specimens," ASTM International, West Conshohocken, 2017.
- [10] J. Newhook, M. A and H. Khalid, "PUNCH User Manual," 2016.









## Appendix B: PUNCH Program Analysis

Table B.1 Initial PUNCH Analysis (1/2).

```

*****
*                                     *
*                               PUNCH *
*       Software developed by      *
*       John P. Newhook            *
*       Aftab Mufti                *
*       Huma Khalid                *
*****
UNITS  METRIC  KN,  MM,  SECOND

Clear Span Between Girders          :          2000.000
Diameter of Equivalent Circle for Load :          541.127
Maximum Compressive Stress of Concrete :           45.000
Elastic Axial Stiffness of Strap    :          397.020
Strap to Load Spacing               :              .000
Depth Of Slab                      :          250.000
Beta to Define Rectangular Stress Block :              .700
Concrete Constant used for confinement :           10.000
Area of Load Patch                  :        150000.000
Yield strain                        :          .200E-02

DELTA      ALPHA      P      STRN
0.00      0.00      0      0.00000
0.50      27.91     104    0.00012
1.00      26.79     204    0.00024
1.50      25.91     301    0.00036
2.00      25.18     395    0.00048
2.50      24.57     486    0.00059
3.00      24.05     576    0.00070
3.50      23.60     663    0.00082
4.00      23.20     749    0.00093
4.50      22.84     833    0.00104
5.00      22.52     915    0.00115
5.50      22.23     996    0.00125
6.00      21.96    1076    0.00136
6.50      21.72    1155    0.00147
7.00      21.49    1232    0.00158

```

7.50	21.29	1308	0.00168
8.00	21.09	1383	0.00179
8.50	20.91	1457	0.00189
9.00	20.73	1530	0.00200
***** Punch Load-Yield Strain in Strap *****			

Table B.2 Initial PUNCH Analysis (2/2)

```

*****
*
*
*           PUNCH
*       Software developed by
*           John P. Newhook
*           Aftab Mufti
*           Huma Khalid
*
*****
UNITS  METRIC  KN,  MM,  SECOND

Clear Span Between Girders           :      2000.000
Diameter of Equivalent Circle for Load :      541.127
Maximum Compressive Stress of Concrete :      45.000
Elastic Axial Stiffness of Strap      :      397.020
Strap to Load Spacing                :      51.000
Depth Of Slab                        :      250.000
Beta to Define Rectangular Stress Block :      .700
Concrete Constant used for confinement :      10.000
Area of Load Patch                    :      150000.000
Yield strain                          :      .200E-02

```

DELTA	ALPHA	P	STRN
0.00	0.00	0	0.00000
0.50	27.91	104	0.00012
1.00	26.79	204	0.00024
1.50	25.91	301	0.00036
2.00	25.18	395	0.00048
2.50	24.57	486	0.00059
3.00	24.05	576	0.00070
3.50	23.60	663	0.00081
4.00	23.20	749	0.00092
4.50	22.84	833	0.00103

5.00	22.52	915	0.00114
5.50	22.23	996	0.00125
6.00	21.96	1076	0.00136
6.50	21.72	1155	0.00147
7.00	21.49	1232	0.00157
7.50	21.29	1308	0.00168
8.00	21.09	1383	0.00178
8.50	20.91	1457	0.00189
9.00	20.73	1530	0.00199
***** Punch Load-Yield Strain in Strap *****			

Table B.3 Final PUNCH Analysis (1/2)

```

*****
*                                     *
*                               PUNCH *
*                   Software developed by *
*                   John P. Newhook *
*                   Aftab Mufti *
*                   Huma Khalid *
*****
UNITS  METRIC  KN,  MM,  SECOND

Clear Span Between Girders                :          2000.000
Diameter of Equivalent Circle for Load    :          541.127
Maximum Compressive Stress of Concrete    :           80.000
Elastic Axial Stiffness of Strap          :          397.020
Strap to Load Spacing                    :              .000
Depth Of Slab                             :          250.000
Beta to Define Rectangular Stress Block   :              .700
Concrete Constant used for confinement    :           10.000
Area of Load Patch                         :        150000.000
Yield strain                              :          .200E-02

```

DELTA	ALPHA	P	STRN
0.00	0.00	0	0.00000
0.50	26.62	105	0.00012
1.00	26.00	207	0.00025
1.50	25.47	307	0.00037
2.00	25.00	405	0.00048

2.50	24.59	500	0.00060
3.00	24.22	594	0.00072
3.50	23.89	686	0.00083
4.00	23.59	777	0.00095
4.50	23.32	866	0.00106
5.00	23.07	954	0.00117
5.50	22.83	1040	0.00128
6.00	22.62	1125	0.00139
6.50	22.42	1210	0.00151
7.00	22.23	1293	0.00162
7.50	22.06	1375	0.00173
8.00	21.89	1456	0.00183
8.50	21.74	1536	0.00194

\*\*\*\*\* Punch Load-Yield Strain in Strap \*\*\*\*\*

Table B.4 Final PUNCH Analysis (2/2)

```

*****
*
*           PUNCH
*       Software developed by
*           John P. Newhook
*           Aftab Mufti
*           Huma Khalid
*****
UNITS  METRIC  KN,  MM,  SECOND

Clear Span Between Girders          :          2000.000
Diameter of Equivalent Circle for Load :          541.127
Maximum Compressive Stress of Concrete :           80.000
Elastic Axial Stiffness of Strap     :          397.020
Strap to Load Spacing                :           51.000
Depth Of Slab                       :          250.000
Beta to Define Rectangular Stress Block :             .700
Concrete Constant used for confinement :           10.000
Area of Load Patch                   :        150000.000
Yield strain                          :           .200E-02

DELTA      ALPHA      P      STRN
0.00      0.00      0      0.00000

```

---

0.50	26.62	105	0.00012
1.00	26.00	207	0.00024
1.50	25.47	307	0.00036
2.00	25.00	405	0.00048
2.50	24.59	500	0.00060
3.00	24.22	594	0.00072
3.50	23.89	686	0.00083
4.00	23.59	777	0.00094
4.50	23.32	866	0.00106
5.00	23.07	954	0.00117
5.50	22.83	1040	0.00128
6.00	22.62	1125	0.00139
6.50	22.42	1210	0.00150
7.00	22.23	1293	0.00161
7.50	22.06	1375	0.00172
8.00	21.89	1456	0.00183
8.50	21.74	1536	0.00194

\*\*\*\*\* Punch Load-Yield Strain in Strap \*\*\*\*\*